Investigation of Topology and Integration for Multi-Element Resonant Converters

Daocheng Huang

Dissertation submitted to the faculty of the
Virginia Polytechnic Institute and State University
in partial fulfillment of the requirements for the degree of

Doctor of Philosophy
in
Electrical Engineering

Fred C. Lee, Chair
Dushan Boroyevich
Paolo Mattavelli
Jaime De La Ree
Dwight Viehland

December 6th, 2013
Blacksburg, Virginia

Keywords: Integration, Topology, LLC resonant converter

Investigation of Topology and Integration for Multi-Element Resonant Converters

Daocheng Huang

ABSTRACT

With the fast development of communication systems, computers and consumer electronics, the power supplies for telecoms, servers, desktops, laptops, flat-panel TVs, LED lighting, etc. are required for more efficient power delivery with smaller spaces. The LLC resonant converter has been widely adopted for these applications due to the advantages in high efficiency, high power density and holdup time operation capability.

However, LLC resonant converter meets some issues, especially in high output current applications. Those issues include magnetic design, start-up, short-circuit protection, synchronous rectifier drive, EMI noise and integration, etc.

To solve those issues, like start-up and short-circuit protection, SR driving and EMI, etc., a synthesis method is proposed to find the similar resonant topologies like LLC. Based on this method, lots of multi-element resonant converters are found to solve the issues that LLC resonant converter cannot handle.

To evaluate the performance of found numerous valuable topologies. Thus, a general evaluation system is required. State-plane analysis with new normalization factors is utilized. Based on it, the voltage stress, current stresses and apparent power of resonant converters are easy to compare. This method can help select suitable circuit topology for

certain applications. Meanwhile, it also can help resonant converters' design. The important performance factors, like start-up, short-circuit protection, SR driving, integration and EMI performance, are also taken into account for the whole evaluation system.

The high switching frequency is needed recently for high power density requirement. However, LLC resonant converter suffers high transformer loss. Matrix transformer is introduced to reduce winding loss and total volume. Flux cancellation method is utilized to reduce core size and loss. Synchronous Rectifier (SR) devices and output capacitors are integrated into secondary windings to eliminate termination related winding losses, via loss and reduce leakage inductance.

The passive integration is necessary for high power density resonant converter, especially for high order system. Based on stress, suitable passive components are chosen for integration. Then, the magnetic integration method is shown based on multi-winding transformer structure. The passive integration principles are discussed. A novel passive integration method is proposed for multi-elements resonant converters.

In conclusion, this work is focus on the topology analysis and integration of resonant converters. Searching the suitable topologies for certain application, and evaluate the performance of them. Then, improve the system power density by integration techniques.

To My Family:

My parents: Liugen Huang

Fengling Luo

Acknowledgments

First I would like to express my sincere gratitude to my advisor, Dr. Fred C. Lee. It is him who shows me how to climb the mountain of research and see the beautiful scenery of power electronics. It is his depths of knowledge and experience that gave me the power to break the rock blocking my research path. Besides his board knowledge, his rigorous research attitude and logical way of thinking have been a great value for me.

I would like to thank Dr. Dushan Boroyevich for his valuable guidance during my research. I am also grateful to his enthusiastic help during the CPES annual conference when I was the fresh chairman. I also want to acknowledge the other members of my advisory committee, Dr. Paolo Mattavelli, Dr. Jaime De La Ree and Dr. Dwight Viehland for their support, comments, and suggestions.

I am especially indebted to my colleagues in the Power Management Mini-Consortium Group. It has been a great pleasure to work with the talented, creative, helpful and dedicated colleagues. I would like to thank all the members of our teams: Dr. Ming Xu, Dr. Shuo Wang, Dr. Julu Sun, Dr. Authur Ball, Dr. Yan Jiang, Dr. Jian Li, Dr. Yan Dong, Dr. Chuanyun Wang, Dr. Dianbo Fu, Dr. Pengju Kong, Dr. David Reusch, Dr. Qiang Li, Dr. Zheng Zhao, Dr. Mingkai Mu, Dr. Yingyi Yan, Dr. Weiyi Feng, Mr. Doug Sterk, Mr. Bin Huang, Mr. Yucheng Ying, Mr. Yi Sun, Mr. Ya Liu, Mr. Clark Person, Mr. Zheng Luo, Mr. Pengjie Lai, Mr. Zijian Wang, Mr. Qian Li, Ms. Yin Lu, Mr. Chanwit Prasantanakorn, Mr. Shu Ji, Mr. Feng Yu, Mr. Haoran Wu, Mr. Yipeng Su, Mr. Wei Zhang, Mr. Li Jiang, Mr. Shuilin Tian, Mr. Pei-Hsin Liu, Dr. Dongbin Hou, Mr.

Zhiqiang Wang, Mr. Xiucheng Huang, Mr. Zhengyang Liu, Mr. Yucheng Yang, Mr. Yang Jiao, Mr. Sizhao Lu, Mr. Chao Fei, Mr. Xuebing Chen, Ms. Yincan Mao, Mr. Zhongsheng Cao, Mr. Syed Bari. Dr. Marcos Alonso, Dr. Fang Luo, Dr. Ke Jin, Dr. Xiaoyong Ren, Dr. Fanghua Zhang, Dr. Yuling Li, Dr. Shaojun Xie, Dr. Xinke Wu, Dr. Brian Cheng, Dr. Feng Wang, Dr Xin Ming, Dr. Feng Zheng.

My thanks also go to all of the other students I have met in CPES, especially to Dr. Jing Xu, Dr. Michele Lim, Dr. Yan Liang, Dr. Rixi Lai, Dr. Honggang Sheng, Dr. Di Zhang, Dr Puqi Ning, Dr. Tim Thacker, Dr. Carson Baisden, Dr. Xiao Cao, Dr. Zhiyu Shen, Dr. Ruxi Wang, Dr. Dong Jiang, Dr. Dong Dong, Dr. Hemant Bishnoi, Dr. Zhen Chen, Ms. Yiying Yao, Mr. Jing Xue, Ms. Zhuxian Xu, Mr. Zheyuan Tan, Mr. Xuning Zhang, Mr. Bo Wen, Mr. Lingxiao Xue, Mr. Zhemin Zhang, Mr. Bo Zhou, Mr. Ying Wang, Mr. Li Jiang, Mr. Marko Jaksic, Ms. Han Cui.

I would also like to thank all the wonderful staffs in CPES: Ms. Linda Gallagher, Ms. Teresa Rose, Ms. Marianne Hawthorne, Ms. Linda Long, Mr. Robert Martin, Mr. Jamie Evans, Mr. Dan Huff, Dr. Wenli Zhang and Mr. David Gilham for their support and help over the past six years. I also hope give my special thanks to Ms. Teresa Shaw for her sincere help during the CPES annual conference.

With much love and gratitude, I want to thank my parents: my mother Fengling Luo and my father Liugen Huang for their endless love, encouragement, and support throughout more than twenty years of school.

Special thanks go out to the CPES PMC mini-consortium members for the funding of my research: Chicony Power, CSR Zhuzhou Institute Co., Ltd., Delta

Electronics, Huawei Technologies, Infineon Technologies, International Rectifier, Linear Technology, Murata Manufacturing Co., Ltd., NEC TOKIN Corporation, NXP Semiconductors, Richtek Technology, Texas Instruments.

Table of Contents

List of Figures

List of Tables

Chapter 1. Introduction

This chapter presents the motivations, objectives and overview of this dissertation. The advantages of LLC resonant converters and its wide applications are investigated. The challenges in LLC resonant converter are described. A review in this field is provided, followed by the dissertation outline and the scope of research.

1.1 Background and Motivation

Over the past decade energy efficiency and power density have become the top concerns for power conversions. Rising energy intensity leads to a higher cost for delivering power. Meanwhile, the demand for compact power supplies grows significantly. It requires power supplies with high efficiency, low profile and high power density.

With the explosive development of information technology, the communication and computing systems, such as data centers, telecoms, servers, desktops, laptops and notebooks have become a large market for the power supply industry. For the advance of the integrated circuit technology, the density and functionality of computer systems are continually increasing, which requires more efficient power delivery while smaller size on power suppliers [A.1]-[A.11]. For consumer electronics, such as flat-panel TVs and LED lighting, high reliability, low cost and high efficiency power supplies are demanded [A.12]-[A.15]. More ever, for the prosperousness of the cloud computing and online service, energy saving and cost reduction become major concerns.

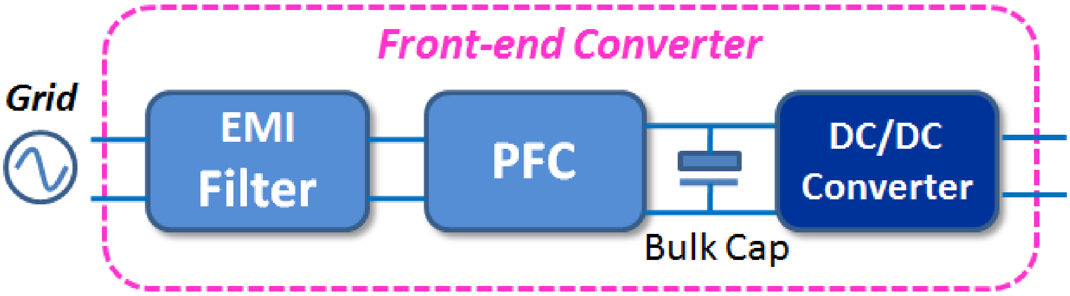

Fig. 1.1 Ac-dc front-end converter

Ac-dc front-end converters as shown in Fig. 1.1 are widely adopted by these applications. Driven strongly by economic and environmental concerns, high efficiency is becoming more and more desired for ac-dc front-end converters. The 80 PLUS programs provide a class of efficiency requirements as shown in Fig. 1.2[A.9]. Take the 80 PLUS TITANIUM program as an example, it provides the highest efficiency requirement for the front-end converters nowadays. The certified power supplies are expected to achieve 91% efficiency at 100% load, 96% efficiency at 50% load, 94% efficiency at 20% load, and 90% efficiency at 10% load when converting 230V ac power from electric utilities to dc power used in most electronics. Right now, some industry benchmarks are beyond TITANIUM. The efficiency requirement at the dc-dc stage is even higher to meet the overall efficiency from ac input to the load.

In addition to the efficiency requirement, the power density of front-end converters is continuously increasing as well [A.5]. Higher power density will eventually reduce the converter cost and allow for accommodating more equipment in the existing infrastructures. As shown in Fig. 1.3, in the past years, the power density of front-end commercial converters has increased by more than twenty times. This will continuously increase in the future because of the fast developments in new devices, magnetic materials and so on [A.16]-[A.19].

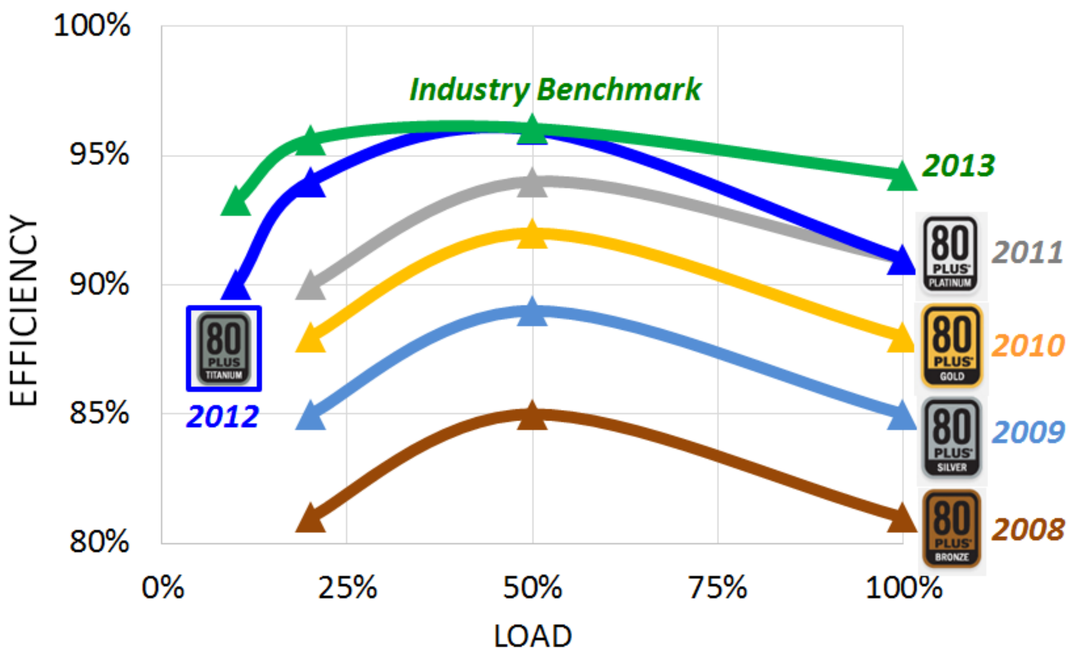

Fig. 1.2 Efficiency trend for ac-dc front-end converters of redundant, datacenter applications

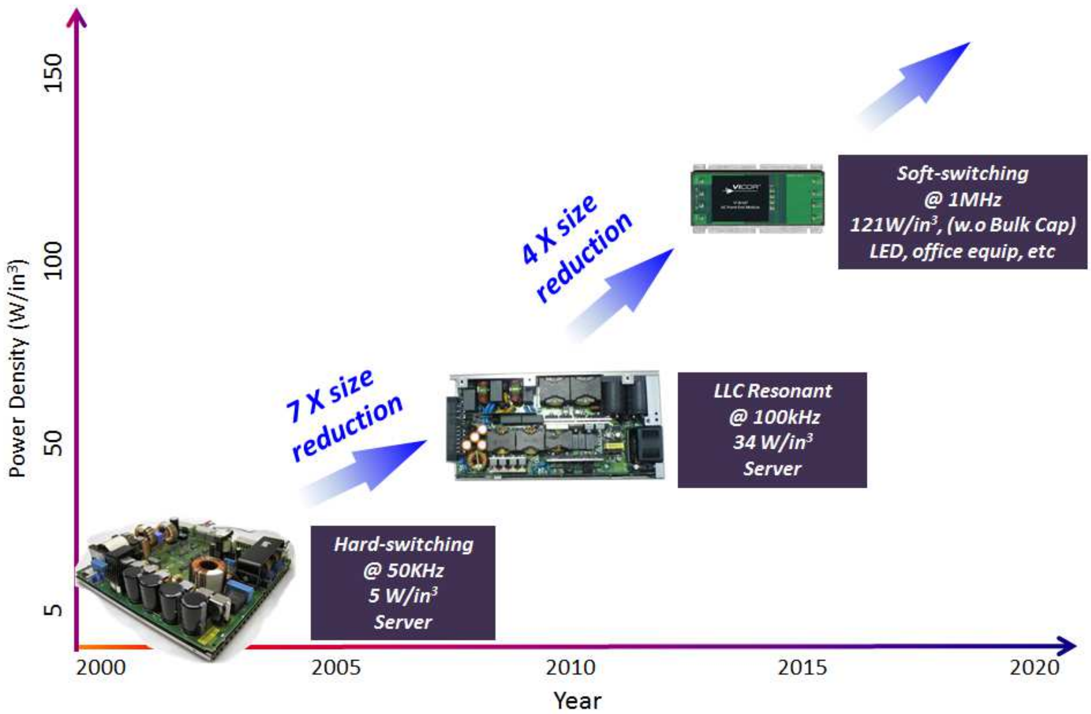

Fig. 1.3 Power density trend for ac-dc front-end converters

1.2 Issues of PWM DC-DC Power Conversions

1.2.1 Pros and Cons of Soft-switching PWM DC-DC Converter

Hard switching pulse-width-modulation (PWM) converters are common in power supplies, however, they suffer high switching losses. Soft switching techniques can help the PWM circuit achieve zero-voltage-switching (ZVS) so that lower switching loss and higher frequency can be accomplished. Soft-switching PWM circuits, such as the phase-shift full-bridge PWM converter (PSFB)[A.20]-[A.23]and the asymmetrical half-bridge PWM converter (AHB)[A.24]-[A.28], are widely used for front-end dc-dc conversion. These topologies are plotted in Fig. 1.4, respectively.

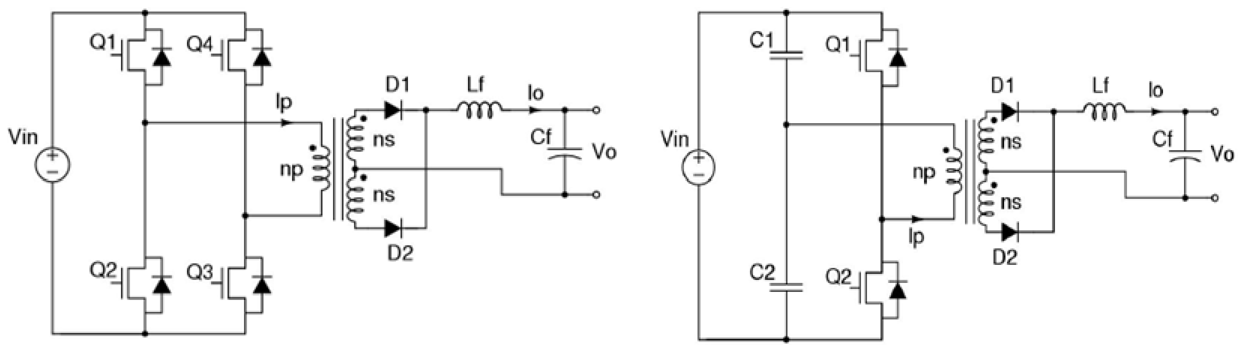

(a) Phase shift full bridge PWM converter (b) Asymmetry half bridge PWM converter

Fig. 1.4 Typical Soft-switching PWM converters

ZVS lost at light load is one drawback of soft-switching PWM converters. For PSFB, large leakage inductance is needed to achieve ZVS. With large leakage inductance, the duty cycle loss due to charge and discharge leakage inductance will be significant. This will limit the choice of transformer turns ratio, which will affect the performance of whole converter. Even with large leakage inductance, still ZVS cannot be achieved at light load. There are many different methods to expend ZVS region for phase shift full bridge[A.29], but they are not been widely adopted due to complexity. Since AHB also utilizes leakage inductance to achieve soft switching, there is similar problem as discussed for PSFB, which lost ZVS during light load condition.

High turnoff loss for primary devices is another drawback. As dash circled in Fig. 1.5, the turnoff current of primary devices is around the highest point due to the trapezoid or square shape primary current.

No ZCS for synchronous rectifier (SR) generates large reverse recovery loss. As circled in Fig. 1.5, the turnoff current of SR device is around the highest point due to the trapezoid or square shape current.

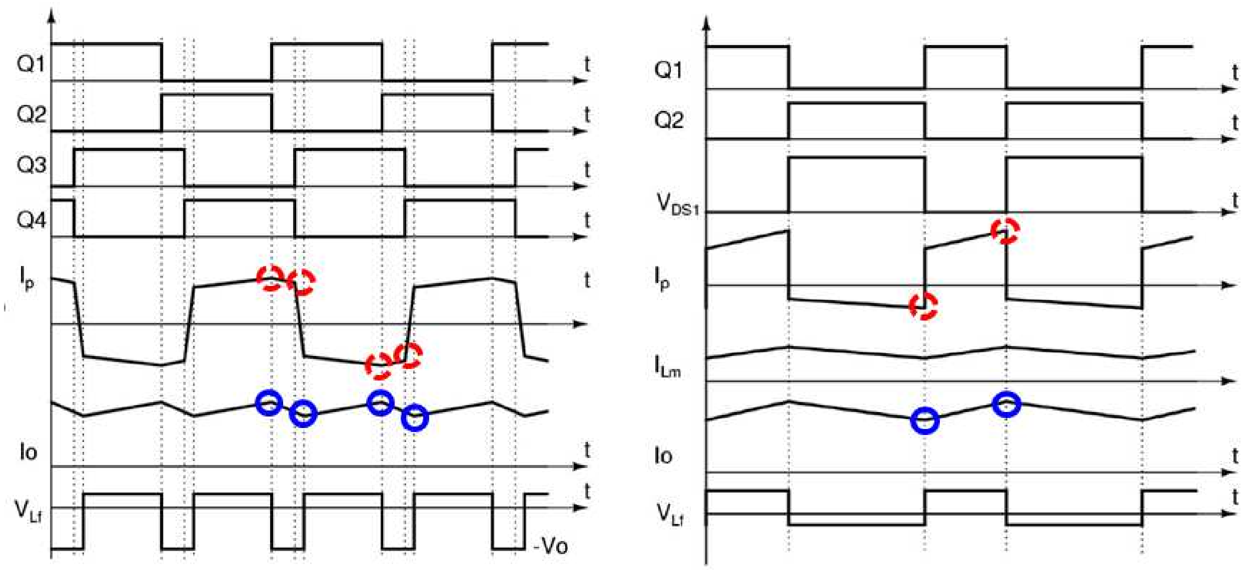

(a) Phase shift full bridge PWM converter (b) Asymmetry half bridge PWM converter

Fig. 1.5 Waveforms of typical Soft-switching PWM converters

Passive components are hard to reduce volume. As mentioned above, the switching loss of soft-switching PWM converters is not small, which limit the switching frequency increasing. That means passive components are not easy to reduce volume. On the other hand, there are usually two individual magnetic components in the circuit, the transformer and the output inductor. Sometimes, an extra inductor is in series with transformer to help achieving ZVS. It is very challenge to integrate them all to shrink the volume.

1.2.2 Limitation of PWM DC-DC Converter with Hold-up Time Requirement

The holdup time operation poses a major design challenge in front-end converters. As shown in Fig. 1.6, the front-end ac-dc converters are required to maintain the regulated output voltage for about 20ms when the input ac line is lost[A.30].As shown in Fig. 1.1, during the holdup time, all the energy transported to the load comes from the bulk capacitor. The requirement of this capacitor is determined by the system power level and the input voltage range of the dc-dc converter. The relationship between holdup time capacitor requirement and minimum dc-dc stage input voltage for 1kW front-end converter is shown in Fig. 1.7.Apparently, the wider the dc-dc stage input voltage range is, the fewer bulky holdup time capacitors are required, and the higher power density will be. Therefore, to meet the holdup time operation requirement, the capability of operating within a wide input voltage range is required for the dc-dc stage in front-end converters.

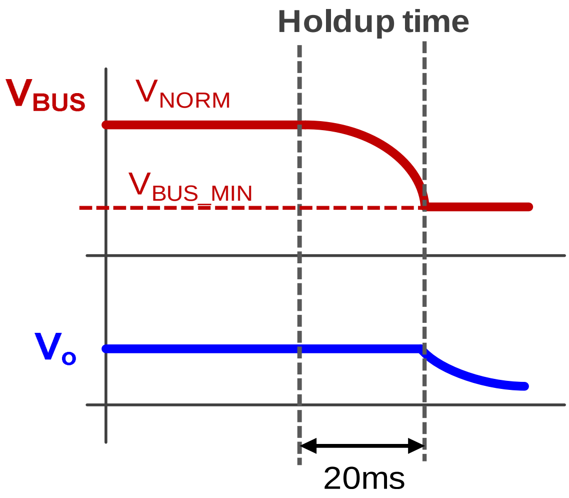

Fig. 1.6 Holdup time operation of ac-dc front-end converters

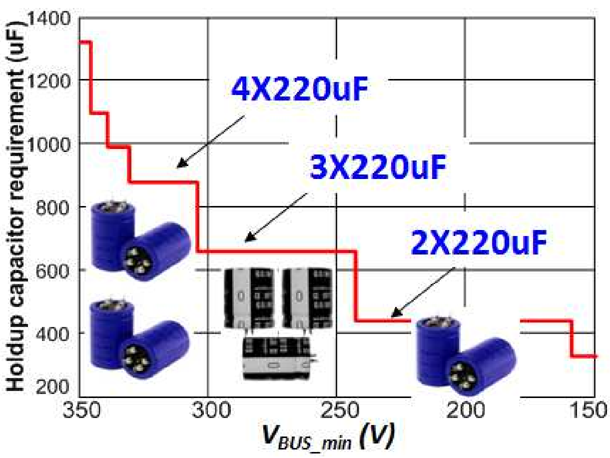

Fig. 1.7 Holdup time capacitance vs. input voltage range for dc-dc converters of the front-end converter

However, conventional PWM converters have to sacrifice normal operation efficiency to extend their operation range. It is difficult to design a wide-operation-range PWM converter with high efficiency. Normally, the duty cycle is designed to be as high as possible to handle the holdup time operation, shown in Fig. 1.8. Thus, at normal conditions, the duty cycle is much smaller. The primary side to secondary side transformer turns ratio is small, which leads to high primary side current, as equation (1.1) and (1.2) indicated. Both conduction loss and switching loss increase. Consequently, efficiency suffers at normal operation conditions.

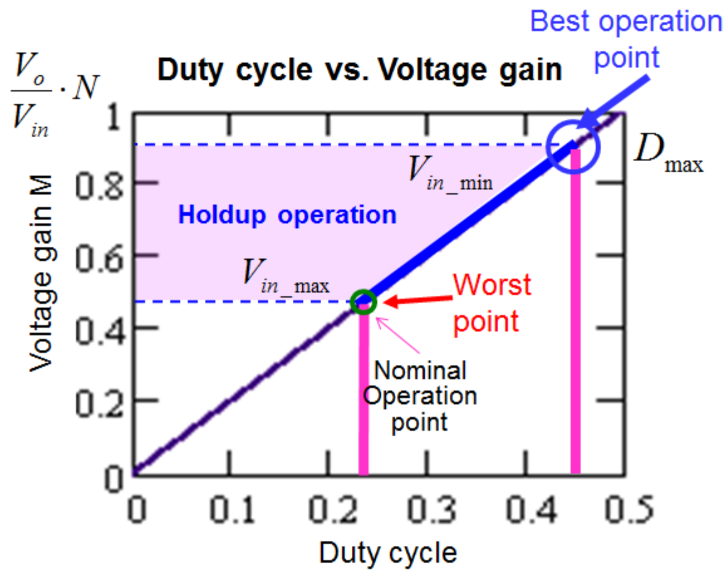

Fig. 1.8 Duty cycle range for PWM converter with hold up requirement.

$$N = \frac{n_p}{n_s} = \frac{V_{in\_min}}{V_o} D_{max} \qquad \text{(Full bridge)} \qquad (1.1)$$

$$N = \frac{n_p}{n_s} = \frac{V_{in\_min}}{2V_o} D_{max} \qquad \text{(Half bridge)} \qquad (1.2)$$

1.3 Opportunity of Resonant DC-DC Converters

1.3.1 Basic Concepts of PWM Converter and Resonant Converters

Conceptually, PWM converters control the power flow by controlling the duty circle of switches. When switch is on, the power flows from the source to the load. When switch is off, the power flow is blocked. The output filter of PWM converters is for switching frequency and higher order harmonics, as shown in Fig. 1.9.

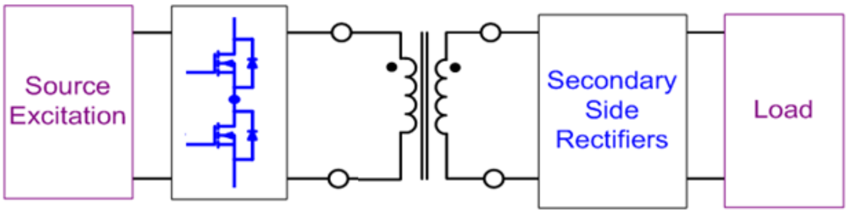

Fig. 1.9 Simplified general isolated dc/dc PWM converter block diagram

Different with PWM converter, resonant converters have quite different way to control power flow. In general, resonant converters can be presented in a simplified block diagram form as shown inFig. 1.10. The input can be either voltage or current source. The output sink is implemented by rectifier circuits. The output circuit consists of either a series inductor or a parallel capacitor with the load resistance in order to give current sink or voltage sink, respectively. The basic resonant cell consists of frequency selective network whose function is to transfer the energy from the source to the load. In other words, it works like a band-pass filter.

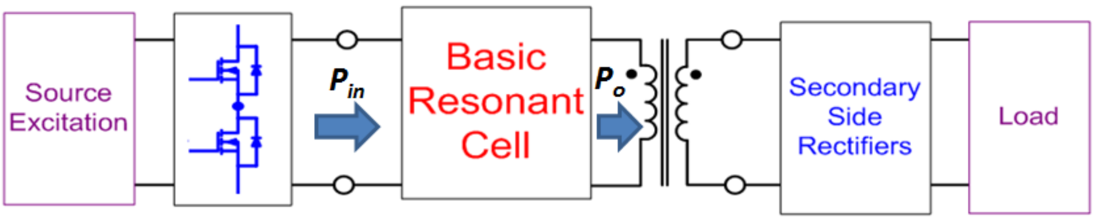

Fig. 1.10 Simplified general isolated dc/dc resonant converter block diagram

As shown in Fig. 1.11, resonant converter controls the power flow by adjusting the switching frequency. When the switching frequency is around the resonant frequency, most of the input power pass through the band-pass filter. When the switching frequency deviates from the resonant frequency, the input power is attenuated by the filter, thus, only part of it flow to the load. This mechanism is quite different from PWM converter.

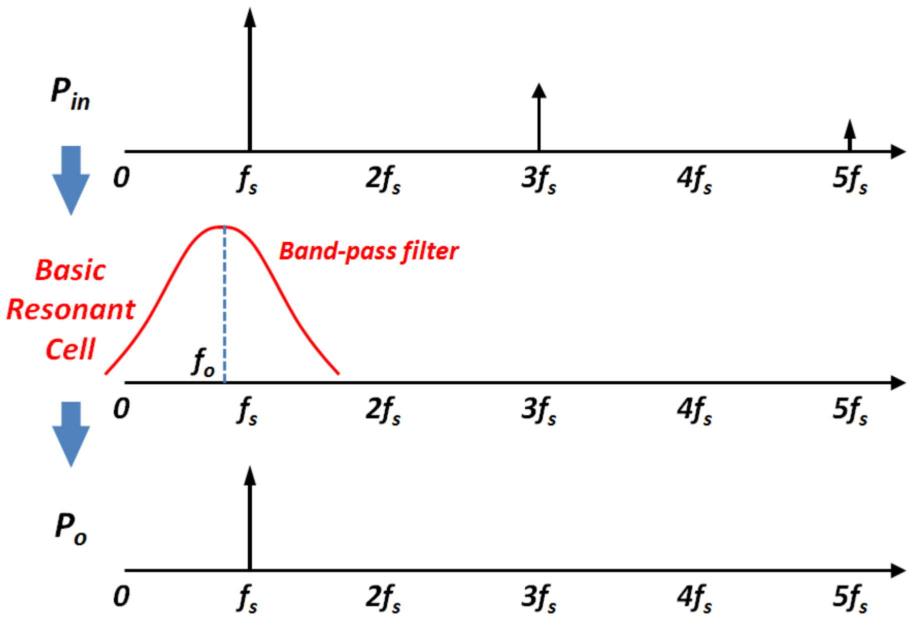

Fig. 1.11 Band-pass filter concept for resonant converters

A good band-pass filter is desirable for efficient energy delivery. Here, good band-pass filter means the least circulating energy in the converter. Nevertheless, which resonant cell contributes good band-pass filter?

a. Series Resonant Converter (SRC)

Series resonant converter (SRC) is one of the basic resonant converters[A.31]-[A.36]. The schematic of series resonant converter is Fig. 1.12. The voltage gain curves of the SRC is shown in Fig. 1.13. The benefits are ZVS achievable above resonant frequency, ZCS achievable below resonant frequency. The operating region is on the right side of resonant frequency owing to preferred ZVS operation.

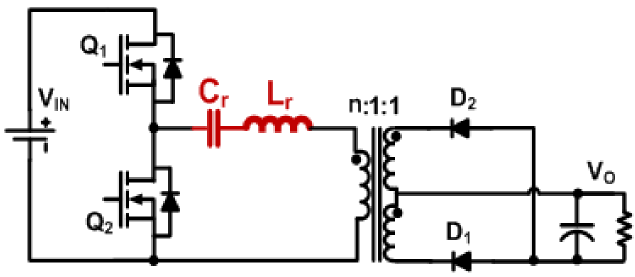

Fig. 1.12 Series resonant converter

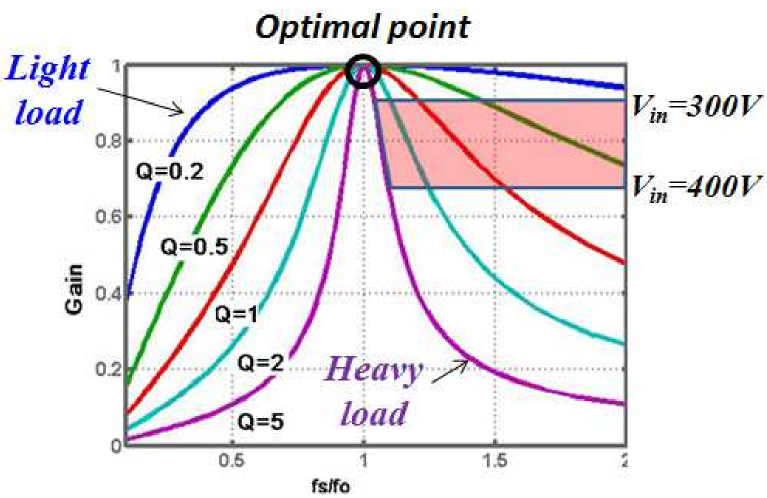

Fig. 1.13 Gain curves of series resonant converter

Series resonant frequency is most efficient point. From the gain curves, we can see the gain equals one at resonant frequency. The total energy from the source is delivered to the load. However, the resonant frequency is the boundary of ZVS and ZCS region. It is very risky to operate at this point. Due to the holdup time requirement, the operation point is far away from resonant point at nominal input voltage (V_{in}=400V), and the voltage gain is much smaller than one. Meanwhile, the turn-off current increases significantly due to large phase shift between excitation voltage and current of the resonant tank. The switching loss will be high.

Light load regulation is bad for SRC. It can be seen from the operating region that at light load, the switching frequency needs to increase to a very high value to keep the output voltage regulated due to the flat voltage gain beyond resonant frequency.

SRC is not a good candidate for front end DC-DC converter. The major problems are: light load regulation, high circulating energy and turn off current at nominal input voltage condition.

b. Parallel Resonant Converter (PRC)

Parallel resonant converter is another basic resonant converter[A.37]-[A.40]. The schematic of parallel resonant converter is Fig. 1.14. The voltage gain curves of the SRC is shown in Fig. 1.15. The operating region of the PRC is shown inFig. 1.15as shaded area. Similar to SRC, the operating region is also designed on the right hand side of resonant frequency to achieve ZVS.

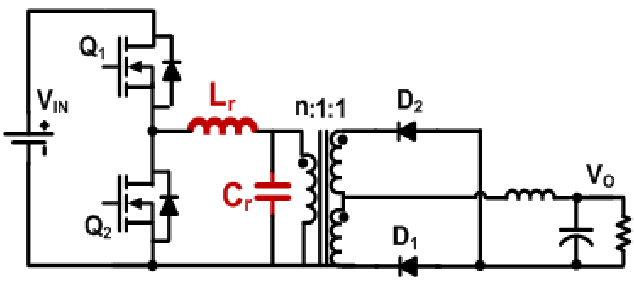

Fig. 1.14 Parallel resonant converter

Compared with SRC, the voltage gain of PRC can be larger than one. That means PRC can boost voltage. Meanwhile, the operating region of PRC is much narrower. At light load, the frequency doesn't need to change too much to keep output voltage regulated.

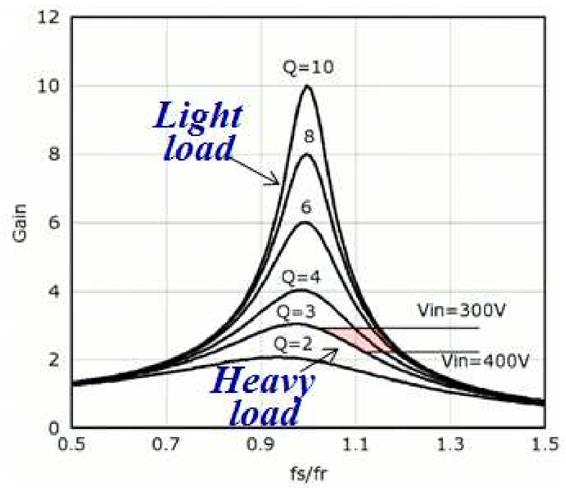

Fig. 1.15 Gain curves of parallel resonant converter

However, ***the circulating energy is very high for PRC***, even at light load. For PRC, since the load is in parallel with the resonant capacitor, even at a no-load condition the input still sees a pretty small impedance of the series resonant tank. This will induce pretty high circulating energy, even when the load is zero.

The major problems of PRC are: high circulating energy, high turn off current at high input voltage condition.

In sum, to deal with a wide input voltage range, all these traditional resonant converters encounter some problems. To achieve higher efficiency, other resonant topologies should be considered.

1.3.2 Advantages of LLC Resonant Converter (LLC) with Hold-up Time Requirement

LLC resonant converters (LLC) is drawn a lot of attention since 1990 [A.41]-[A.48].The half bridge LLC resonant converter is illustrated in Fig. 1.16. The voltage gain of the LLC resonant converter is drawn in Fig. 1.17. When switching frequency lower than resonant frequency (fs<fo), the voltage gain is more like parallel resonant converter. When switching frequency higher than resonant frequency (fs>fo), the voltage gain is more like series resonant converter. With variable frequency control, the voltage gain of LLC resonant converter can be controlled as boost mode or buck mode. Based on the combination of two resonant frequencies, LLC resonant converter has more advantages than previous introduced converters.

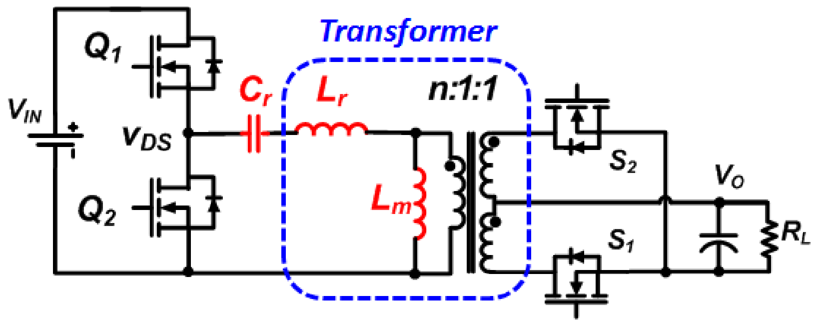

Fig. 1.16 LLC resonant converter

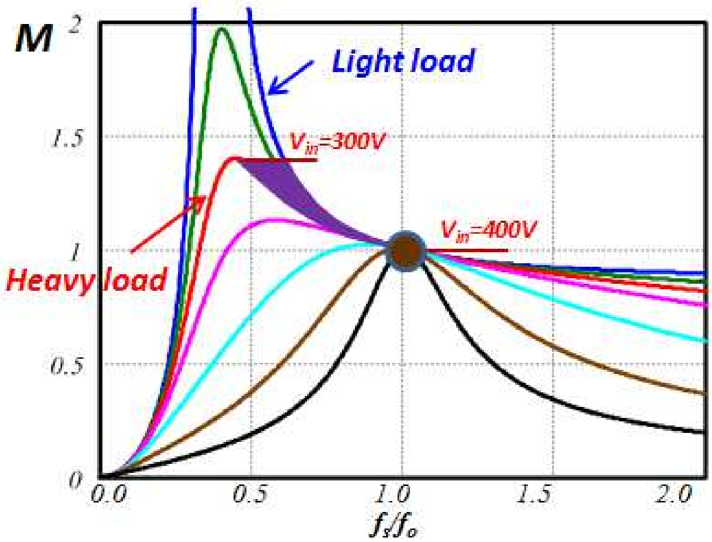

Fig. 1.17Voltage gain of LLC resonant converter

ZVS is achievable from no load to full load. With the help of parallel resonant frequency, LLC can operate around series resonant frequency without the risk falling into ZCS region. In addition, voltage gains of different Q converge at this point. Thus, the LLC would not change frequency too much as load changes. The voltage second on L_m, which determines the turnoff current, is relatively constant. And this current independent of load helps primary devices charge and discharge junction capacitance to achieve ZVS. In other words, ZVS is independent of load.

Low turnoff loss is achievable for primary devices due to low turnoff current. The turnoff current could be controlled by L_m to be as low as just fulfill ZVS requirement.

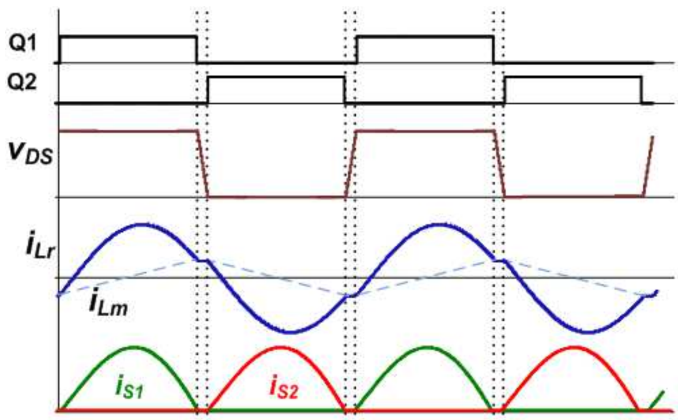

Fig. 1.18 Waveforms of LLC resonant converter at resonant frequency

ZCS for synchronous rectifier (SR) is naturally achieved if it operates at or below series resonant frequency. When switching period equals the series resonant period, the primary current (i_{Lr}) resonances to touch magnetizing current (i_{Lm}). Meanwhile, secondary side current reaches zero. When switching period becomes larger, the discontinuous period of secondary current extends.

Magnetic integration is easily achieved for LLC. Because of soft-switching for primary and secondary devices, LLC can increase switching frequency to push power density. On the other hand, high switching frequency introduces small magnetic component, which makes them easy integration. For LLC, L_r could be the leakage inductance of transformer, while L_m is the magnetizing inductance, as shown in Fig. 1.16. Naturally, LLC has the potential to integrate all the magnetic components into transformer, which continue push power density.

The holdup time extension capability is accomplished without sacrificing the efficiency under the nominal operating condition. As mentioned before, series resonant frequency is the optimal operation point for LLC. By reducing the LLC switching frequency, high voltage gain is achievable, which is desired for the holdup time operation. Therefore, the LLC resonant converter has been a very popular topology for the front-end power supplies in computing systems and consumer electronics systems.

Soft-switching diminish most of switching loss, thus, LLC can reach high efficiency and be easy to push high frequency. High frequency and easy integration structure give LLC the potential to reach high power density. Fig. 1.19 shows the volume and efficiency comparison of two commercial front-end products. It is obvious that the front-end converter with LLC has better power density and efficiency than the one with PWM converter.

For the benefits of LLC resonant converter as mentioned above, firstly it is adapted by flat-panel display. Then, telecom quickly accepts it as main stream solution. Right now, LLC gradually takes the markets of LED lighting, server and datacenter, etc.

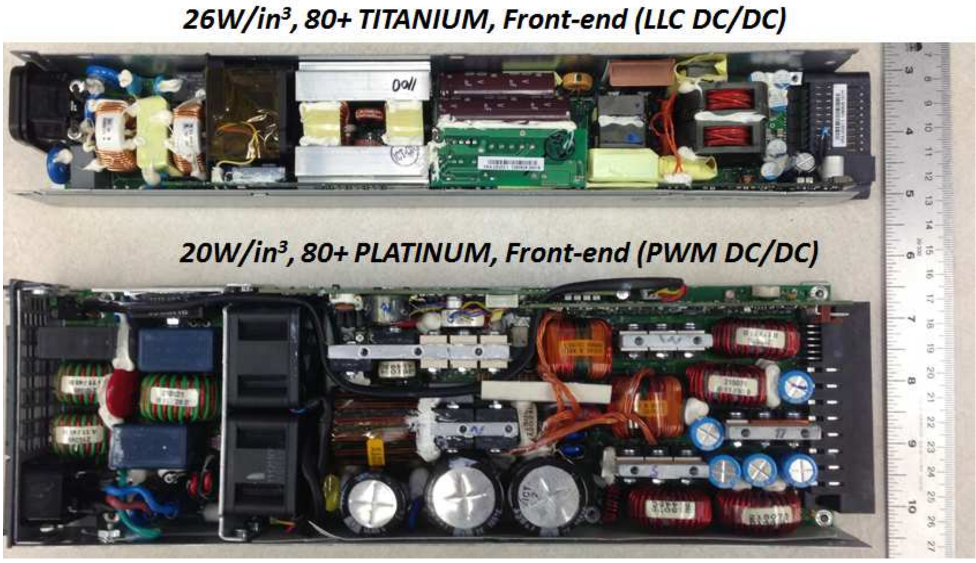

Fig. 1.19 Commercial products comparison with LLC DC/DC and PWM DC/DC

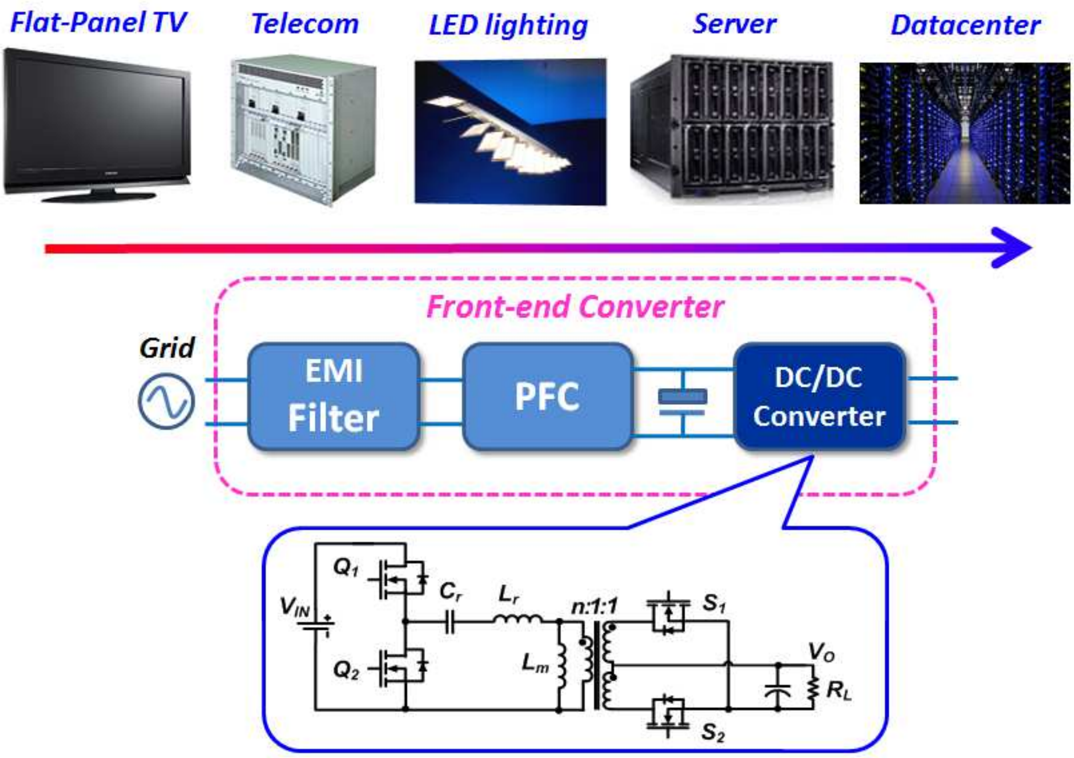

Fig. 1.20 Market trend for LLC resonant Converter

1.4 Challenges of LLC Resonant Converter

However, there are many issues for the LLC resonant converter to deal with, like start-up, short-circuit protection, SR driving method, EMI noise reduction and magnetic design, etc.

1.4.1 Start-Up and Short Circuit Protection

The first issue is start-up process. Although LLC has parallel resonant frequency to help achieve holdup requirement, the voltage gain above resonant frequency is very flat due to the characteristics of series resonant frequency, as shown in Fig. 1.21.

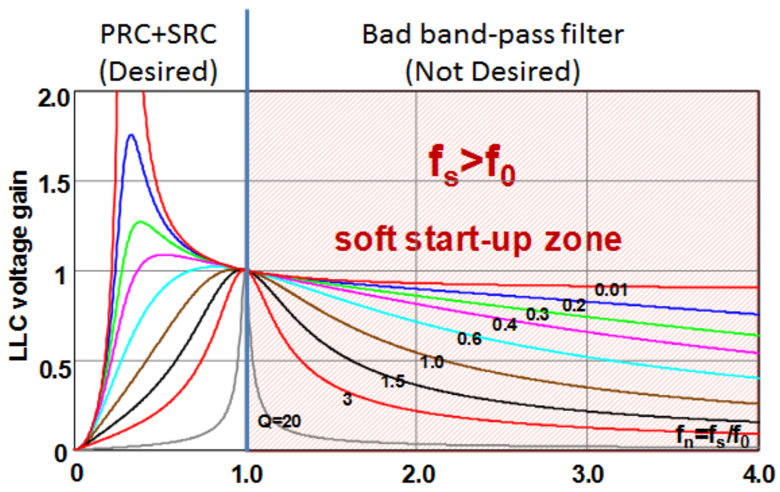

Fig. 1.21 LLC soft start-up in above resonant frequency region

During the soft start-up process, the switching frequency needs to be pushed to a high value ($f_s > f_0$), and then decreased step by step, in order to minimize the voltage and current stress in the resonant tank, meanwhile building up the output voltage[A.49]-[A.55].

If the start-up frequency (f_{max}) is not high enough, there will be large voltage and current stress in the resonant tank at the start-up moment. Fig. 1.22shows the experimental test of [A.49] where the voltage and current stress is large in the resonant tank if starting-up with 1.6 times of resonant frequency.

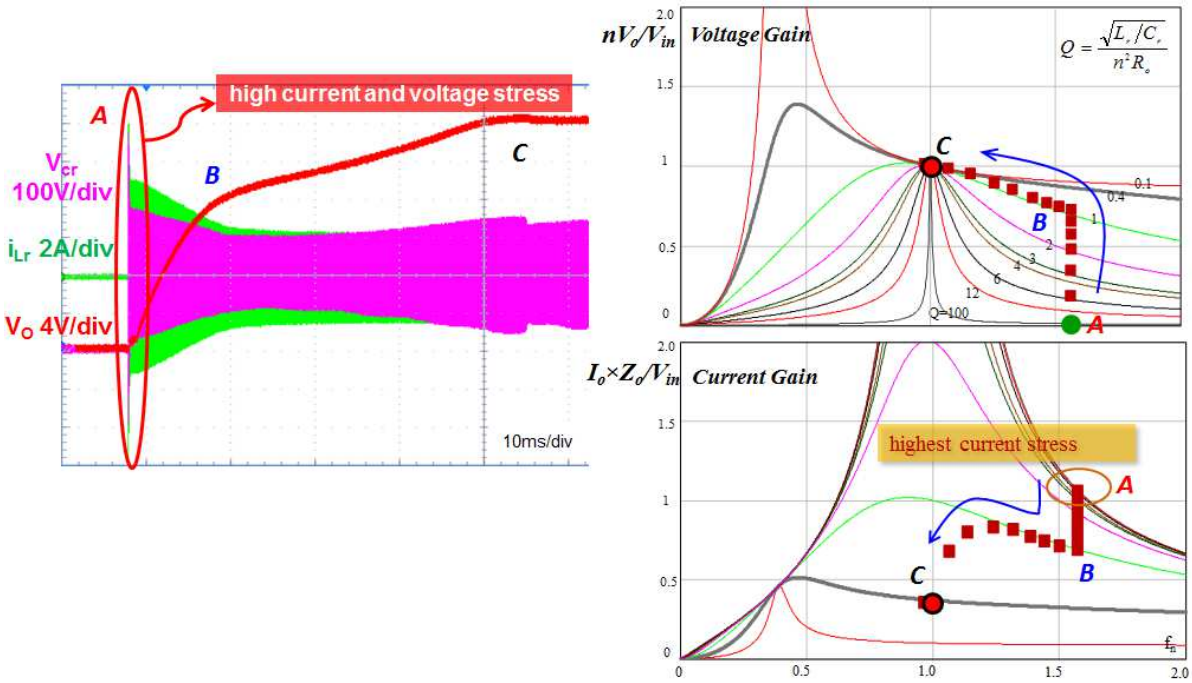

Fig. 1.22 LLC soft starts process by commercial IC chip

Thus, start-up is an inherent issue for LLC resonant converter.

1.4.2 Synchronous Rectifiers (SR) Driving Scheme

For isolated dc/dc converter, synchronous rectifier is necessary to improve the efficiency of DC/DC converter. The SR driving signals for PWM dc/dc converter are very easy to get from primary side device signal. Take phase shift full bridge converter as example[A.56], the circuit is shown in Fig. 1.23. The driving signal of SR2 is the same as SA, and the driving signal of SR1 is the same as SB.

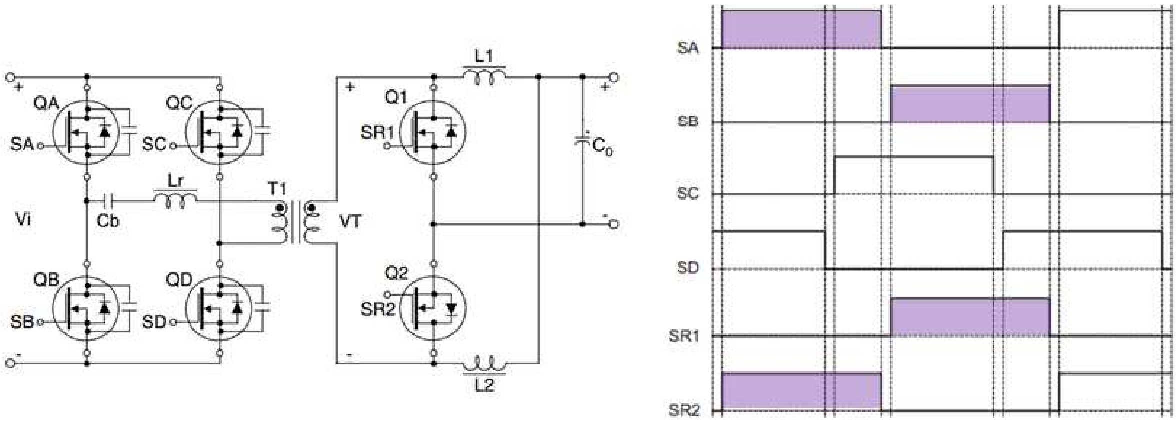

Fig. 1.23 PSFB circuit and devices' driving signals

LLC resonant converter is quite different with PWM converter for SR driving scheme. The driving signal of primary side and secondary side devices are not in phase, as shown in Fig. 1.24.

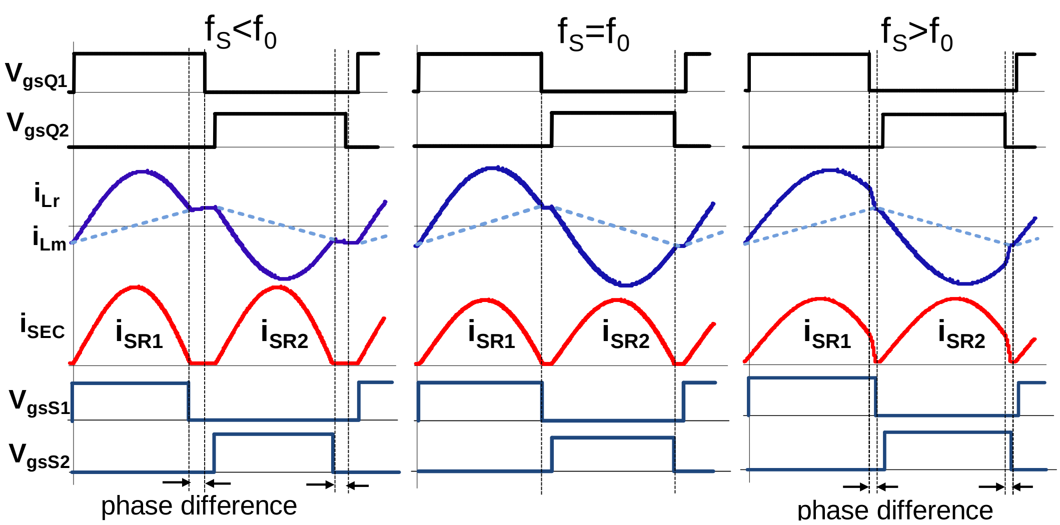

Fig. 1.24 Desired SR gate driving signals in different switching frequency regions

When $f_s<f_0$, the SR should be turned off earlier than the main switch. Otherwise, the SR would conduct circulating energy, namely a reverse current from the load to the source, thus causing a greater increase in the RMS currents and turn-off current, and causing efficiency to deteriorate dramatically. When $f_s>f_0$, the SR should be turned off a bit later than the main switch. Otherwise, the sharply decreased current would go through the paralleled body diode, resulting in a serious reverse recovery. Therefore, the driving signals of SRs and main switches cannot derive from the same PWM signal for control of the conduction times as those in the isolated PWM converters.

One solution [A.57] is based on the SR current i_{SR}sensing by transformers to generate SR driving signal. The method is precise, but due to the large current on the secondary side, it requires a large size current transformer and it presents a lower efficiency due to the extra resistance of the transformer windings.

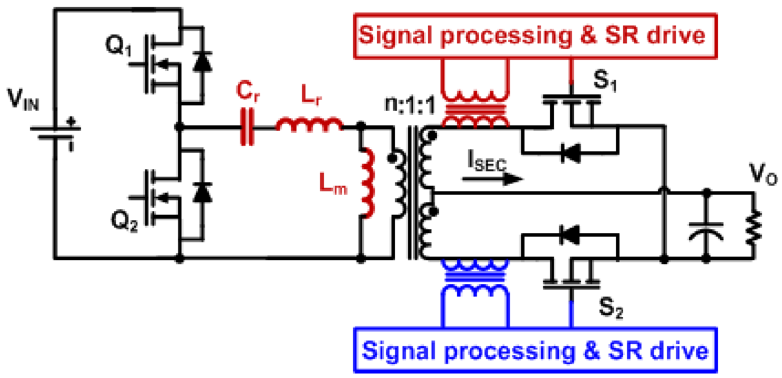

Fig. 1.25 SR gate driving signals by secondary current sensing

An alternative solution [A.58] is sensing current through the transformer's primary side winding. The primary side current is a precise replica of the secondary side current. Although a smaller loss could be achieved when compared to the secondary side current sensing, three magnetic components are needed, losing the integration of leakage, magnetizing inductors and transformer in a single element.

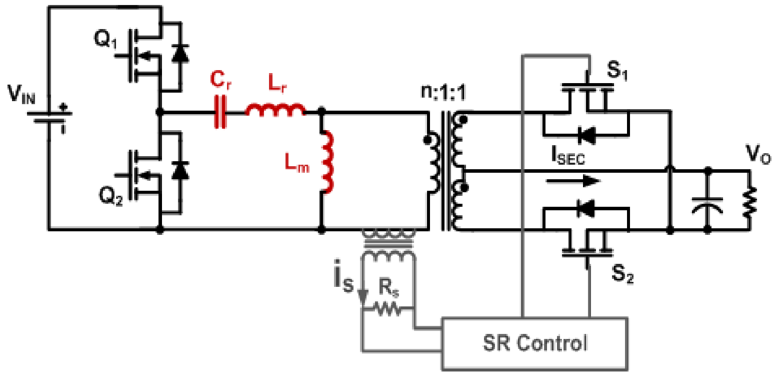

Fig. 1.26 SR gate driving signals by primary current sensing

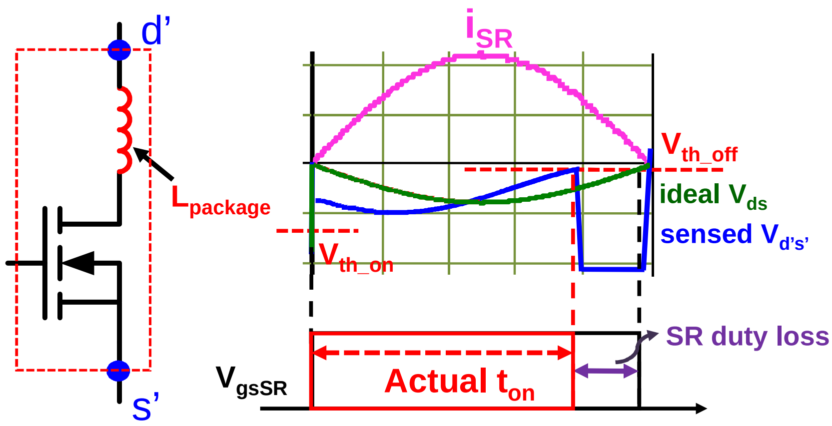

Fig. 1.27 The influence of package inductance

A promising driving method is based on the SR drain to source voltage. The sensed SR V_{ds} is processed by the control circuits as [A.59]. However, the accuracy of this driving scheme is highly affected by the SR package [A.60]. Due to the inevitable package inductance, the sensed terminal drain to source voltage of the SR is actually the sum of the MOSFET's on status resistive voltage drop and the package inductive voltage drop. Fig. 1.27shows that the sensed $V_{d's'}$ of the SR terminal deviates greatly from the purely resistive voltage drop V_{ds} of the MOSFET. Thus, the actual SR drive signal V_{gsSR} is significantly shorter than the expected value.

Therefore, an accurate SR driving scheme under high frequency is required, which can control the SR gate driving signal in the whole switching frequency regions with simple implementation. This method should not increase the volume of whole system too.

1.4.3 Chanllenges for High Output CurrentApplication

Isolated high output current dc/dc converter may suffer very high conduction loss at secondary side even synchronous rectifier is applied [A.52] [A.53].

High conduction loss of secondary windings and SR devices is the first issue for low-voltage high-current applications. To deal with this issue, a paralleled winding structure with paralleled SR devices is a common practice. However, this structure is not good enough. The conventional circuit schematic of the transformer and SR structure is shown in Fig. 1.28. The conventional planar transformer and the secondary side structure are depicted in Fig. 1.29.

The current sharing among secondary windings and SR devices becomes an issue for this parallel structure**.** The current distribution through secondary side is determined by many aspects, including the resistance and leakage inductance of windings, the package inductance and resistance of SR devices, the trace and connection inductance and resistance, etc. Thus, it is hard to keep even current distribution by traditional transformer structure.

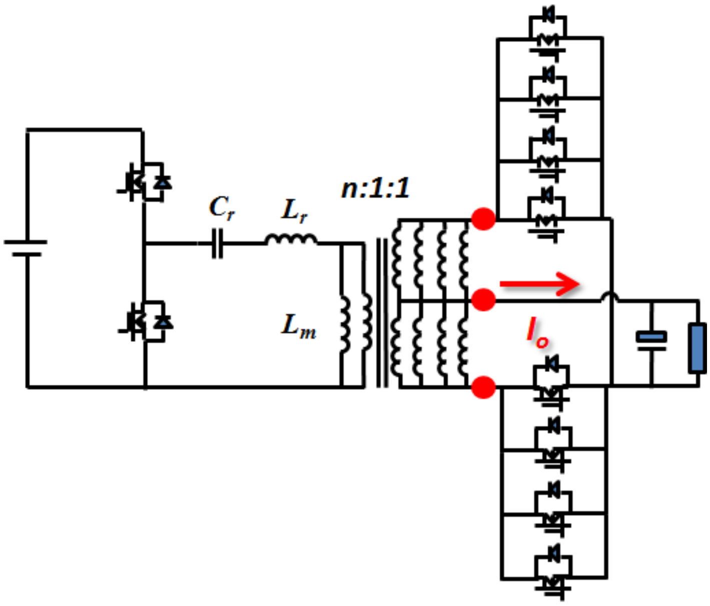

Fig. 1.28 Circuit schematic of the conventional transformer and SR structure.

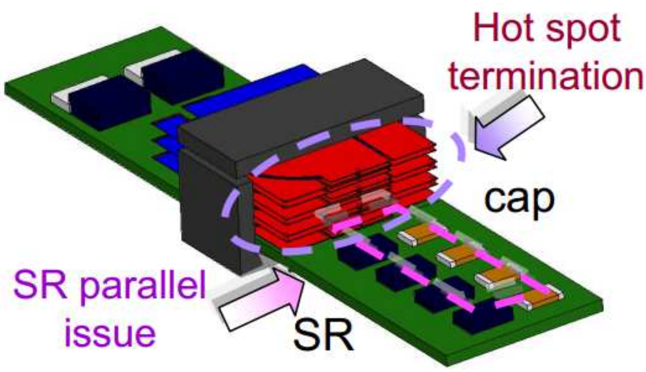

Fig. 1.29 Conventional transformer and the secondary side structure.

High termination losses is the another issue. Due to the proximity effect and skin effect, the currents in adjacent terminals with opposite directions attract each other. Thus, very high losses and hot spots are generated. This termination loss deteriorates efficiency significantly. For the conventional design, all SR devices are placed on the motherboard. Physically speaking, a large loop of the secondary side rectifiers is inevitable. Consequently, a large distribution loss will be generated. In addition, for large number of SR devices, it is extremely difficult toachieve a symmetrical layout for each SR. Hence, current-sharing of the SR is a severe problem.

Thus, how to improve the efficiency and power density of high step-down dc/dc converter is a key issue.

1.4.4 EMI Performance of LLC Resonant Converter

In EMC standards, such as FCC part 15 in the United States and EN55022, CISPR 22 in Europe, the conducted EMI noise emissions of devices are limited. It is required to meet the EMI standard for front-end converters.

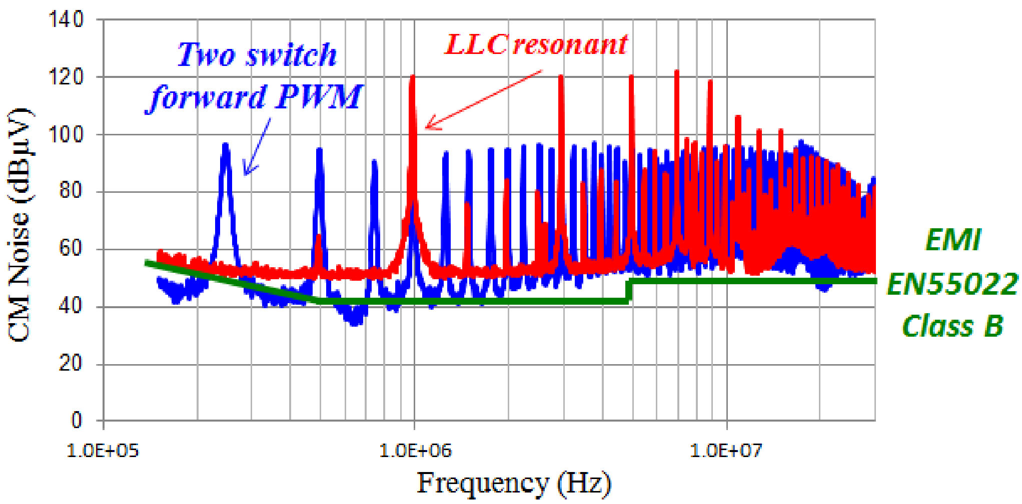

Fig. 1.30 CM noise spectrum comparison of PWM and LLC resonant converters.

Because of the bulk capacitor between PFC and dc-dc converter, only common mode noise of dc-dc converter will influence the grid and EMI filter. The measured common mode EMI noise spectrum of LLC resonant converters is shown in Fig. 1.30. Compare with PWM converter, it is a stringent challenge to reduce the EMI noise due to the EMI standard requirement [A.61].

1.5 Multi-Element Resonant Converters

Since LLC resonant converter has so many issues, how to deal those issues but still keep the merits of LLC is a challenge. Some issues come from the fundamental characteristics of LLC resonant converter. How to overcome them remains a problem. As mentioned in [A.62]-[A.64], there are more than hundreds multi-element resonant topologies. Is there any resonant topology similar or better than LLC resonant converter?

Based on the previous sections, the merits of LLC come from the combination of two resonant frequencies. Thus, we want to keep the characteristics below series resonant frequency of LLC gain curves in Fig. 1.17. However, we do want to change the gain curves of LLC resonant converter above resonant frequency.

For the start-up and short-circuit protection issue, the fundamental reason is the flat voltage gain above resonant frequency. To deal with this issue, the resonant topology has sharp gain above resonant frequency is desired as presented in Fig. 1.31[A.64].

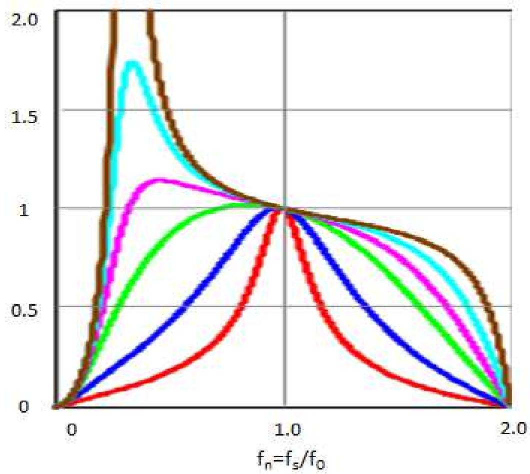

Fig. 1.31 Desired voltage gain for LLC start-up.

For the SR driving scheme, the resonant topology, which can simply utilize primary side current information to drive SR without suffering the benefit of integration, is desirable.

Low EMI noise by nature is also desired for resonant topology.

The question is if there is any resonant topology having those benefits among the ocean of resonant topologies. How to find it and how to compare them with LLC is very challenging.

1.6 Opportunity of Emerging Technologies

The exponential rise in "Big Data" generation, processing and storage highlights the growing demand for datacenter and cloud computing power worldwide. The subsequent task is to maximize energy efficiency, thus saving money and natural energy resource, minimizing pollution and meeting the US Department of Energy's "Exascale" challenge.

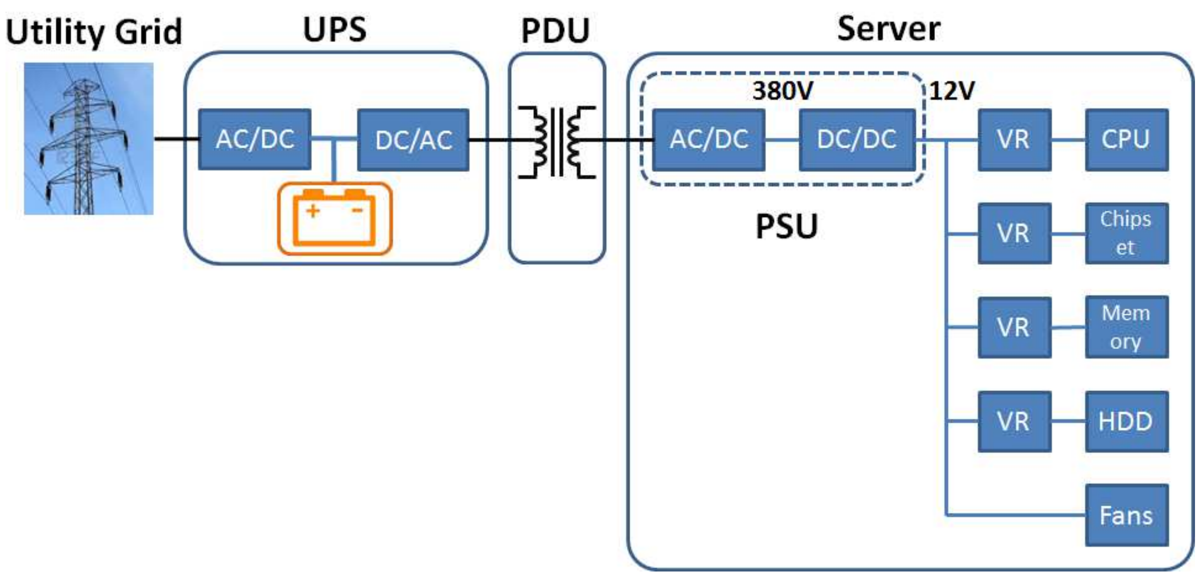

Fig. 1.32 Traditional AC distribution system for data center

For the power semiconductor industry, the challenge is to provide efficient and high quality power conversion from 480V 3-phase AC power entering the datacenter, all the way to 1V, 100A+ processors. Fig. 1.32 shows the typical AC distribution system structure for data center.

1.6.1 New System Architectures

The ever-present trend for datacenter distributed power systems is the pursuit of higher efficiency and power density. Existing solutions within the AC-DC conversion-system topology are struggling to provide even a fewpercentage points of large-scale improvement despite localized improvements in performance.

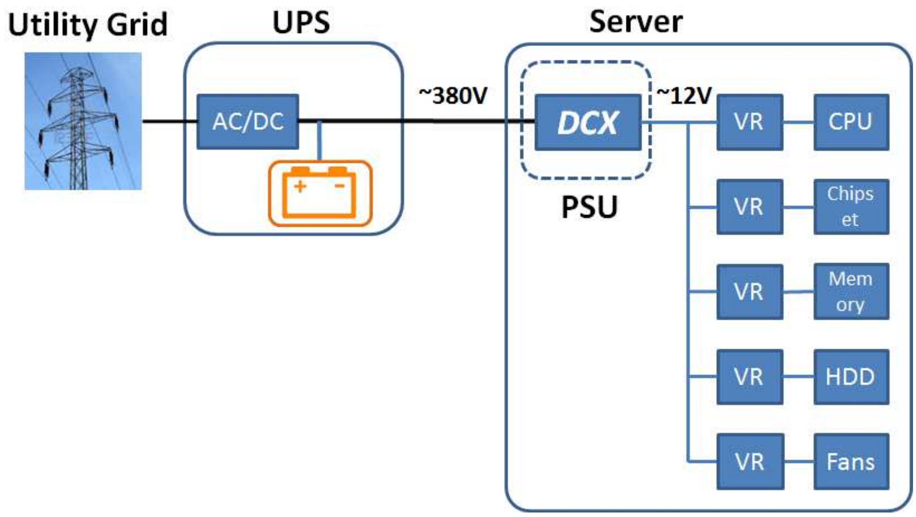

Fig. 1.33 380V DC distribution system for data center

The answer may be to look instead to a very different AC-DC structure, based on new approaches rather than merely incremental ones. Using high-voltage DC for power transmission, in conjunction with new conversion approaches, offers tangible and significant benefits for both sourcing options and system end-to-end performance. Recently, Intel proposed a 400 Vdc direct-distribution bus for data center applications in order to reduce the number of power conversion stages and the power loss in the power distribution path, as shown in Fig. 1.33. By eliminating an AC uninterruptible power supply (UPS) and a transformer in the power distribution unit (PDU), the overall efficiency can be improved. In fact, some work from France Telecom and China Mobile estimate that between 8% and 10% across the board can be saved by going to DC distribution[A.7]-[A.8], [A.65]-[A.67].

Continue pushing whole system efficiency, one effective way is to reduce the regulated DC/DC stage. For new DC distribution system, the holdup requirement is not valid due to the battery connecting to 380V bus. IBM supercomputer utilizes the DC system illustrated in Fig. 1.34. The efficiency of each module is also given in each box. There is only one regulation stage: PRM (Pre-Regulated Module) regulator. Bus converter and VTM (Voltage Transformer Module) are both unregulated DC/DC converter. The efficiency of the power train can be as high as 87%.

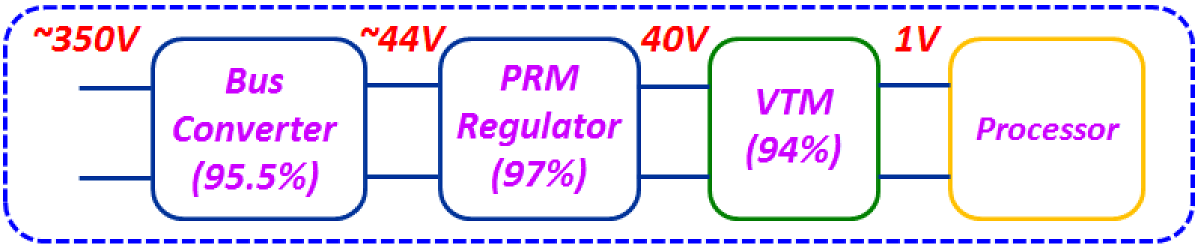

Fig. 1.34 DC power-train for IBM Supercomputer

Another possible power train structure is shown in Fig. 1.35. The DC/DC converter from 400V to 12V only needs to deal with small ripple on the bus, which can be easily deal with next regulated stage (VR). It is obvious that two regulated stages are less efficient than one regulated stage with one unregulated stage.

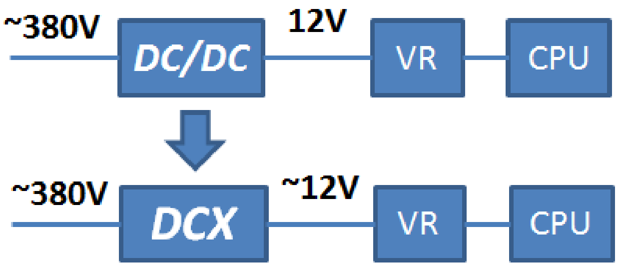

Fig. 1.35 Improved DC power-train for 400V to CPU

Thus, how to improve the efficiency and power density of high ratio step-down DCX is one of the key issues for the whole performance of datacenter.

1.6.2 Benefits and Chanllenges of LLC-DCX

Compared with regulated LLC-D2D, LLC-DCX has better performance and less issues especially at high switching frequency.

Firstly, its switching frequency is fixed exactly at the resonant frequency point (f_s=f_0) to achieve the best efficiency[A.68]. Meanwhile, the SR current is in phase with primary side driving signal just like PWM converter. It is very easy to achieve SR driving by utilizing primary side driving signal. Due to new system architecture, LLC-DCX do not need to worry about start-up problem, the regulator before or after LLC-DCX can help.

Thus, start-up, short-circuit protection and SR driving are not issues for LLC-DCX anymore.

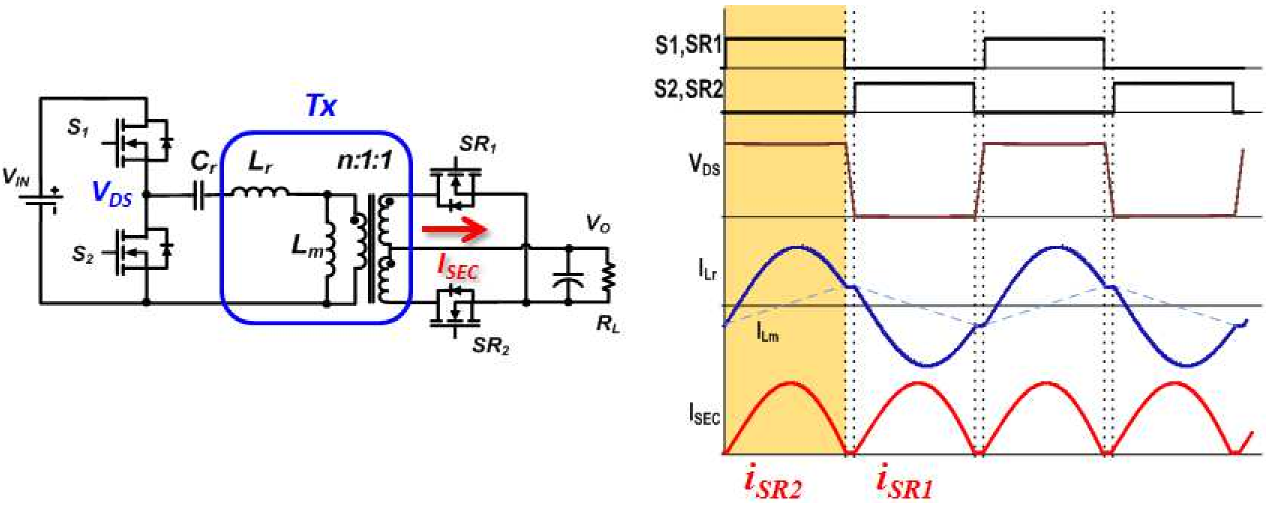

Fig. 1.36 LLC resonant converter as DCX

Usually, large L_r is designed for LLC-D2D to help achieve holdup time and regulation requirement, while LLC-DCX does not have that. Mostly large L_r needs extra inductor in series with leakage inductance of transformer, which increases the volume and loss of whole system. For LLC-DCX, L_r is only the leakage inductance of transformer, and can be as small as possible.

LLC-DCX has potential to be high efficiency and high power density. For high efficiency and easy magnetic integration, LLC-DCX could operate at high switching frequency. ***Meanwhile, the high frequency transformer design and EMI are still issues for LLC-DCX.***

1.6.3 Wide Band Gap Devices —GaN HEMT

High performance active devices have been the first force to increase power density to meet the requirements of modern systems including datacenter. Silicon devices have dominated for power management since the late 1950s. However, due to continuous device optimization and improvements in the production process, material properties of Si are increasingly becoming the limiting factor.

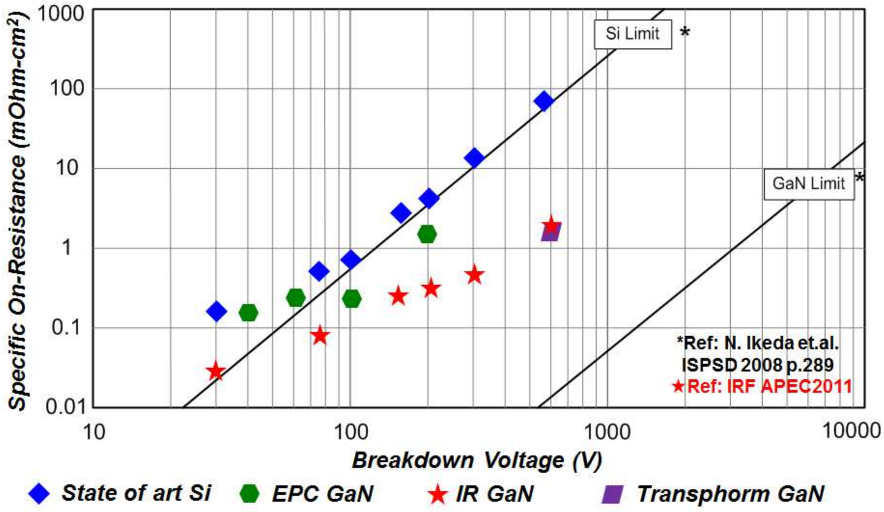

Fig. 1.37 Specific on-resistance versus breakdown voltage for GaN and Si

In recent years, the GaN HEMT has emerged as a promising device for high frequency, high efficiency, high density power conversion due to a better figure of merit than comparable Si and SiC transistors [A.69]-[A.71]. A progressively larger number of GaN devices have been manufactured for in field applications ranging from low power voltage regulators to high power infrastructure base-stations[A.72]-[A.80]. The switching frequency has been continuously pushed up to several MHz to both reduce passive components size and increase power density.

1.7 Dissertation Outline

Taking into account the challenges raised during the review of the existing literature on the LLC resonant converters, several issues have been addressed in this dissertation.

Chapter 1:

Research background, motivation, and literature review.

The advantages of LLC resonant converter over PWM converter and traditional resonant converters are presented, especially under hold up time requirement. However, LLC has its own issues, like startup, short-circuit protection, SR driving, transformer design and EMI performance. Multi-element resonant converters are one possible way to deal with them. Meanwhile, with the new system architecture of datacenter, there is opportunity to use unregulated LLC, which has less issues and better performance than regulated LLC resonant converter. This new structure and emerging GaN HEMT promote the requirement of high frequency high efficiency transformer design. To be more advanced, passive integration for multi-element resonant converter is also achievable.

Chapter 2:

One effective way to solve the fundamental issues of LLC resonant converter is to find alternative resonant converters.

The resonant tank acts like band-pass filter in resonant converters. The four type basic resonant cells are studied. A synthesis of resonant topology based on basic resonant cells is proposed. Every two basic resonant cells are combined to form a new resonant cell. Three three-element LLC-like resonant converters are discovered.

For four-element resonant converters, a notch filter is introduced to LLC-like resonant converters helping limit the inrush current during startup or short-circuit protection period.Eight LLC-like resonant converters with notch filter are discovered based on previous synthesis.

To enhance power delivery efficiency, an extra element is added to four-element resonant tank for 3^{rd} harmonics band-pass filter. Twenty five-element resonant converters with 3^{rd} harmonics band-pass filter are gotten.

Chapter 3:

Lots of LLC-like resonant converters are discovered based on the method in chapter 2. How to evaluate each topology still remains an issue. To find out if new resonant topologies have similar or better performance than LLC, an evaluation system is necessary.

To utilize state-plane for evaluation, traditional normalization factors are not good enough. The new normalization factors are proposed based on the apparent power of converter. Utilizing the state-plane with new normalization factors, the apparent power, voltage and current stresses of each multi-element resonant converter can be easily compared.

Current limit capability, SR driving scheme, magnetic integration and EMI noise are very important to resonant converters. All of them are taken into account to evaluate the performance of resonant converters.

Based on the pros and cons of each LLC-like resonant converter, several possible application examples are proposed as reference.

Chapter 4:

To deal the high output current conduction loss, the resonant topology can hardly help. The circuit topology can help. To alleviate the heavy output current, the matrix transformer instead of the traditional transformer is proposed. Matrix transformer can help split transformer secondary current to reduce conduction loss. With the matrix transformer winding structure, series at primary side and parallel at secondary side, the current sharing problem among windings and SR devices can be solved.

The price is the multiple cores of matrix transformer. With the concept of flux cancellation, the number of core reduces into half. In other words, the core loss and core volume are greatly reduced without suffering conduction loss.

Meanwhile, a system method is proposed to integrate transformer winding with SR devices to eliminate termination loss. After that, the tradeoff of termination loss and interleaving is discussed. Then, the optimal winding structure is figured out.

Finally, a detail design procedure for transformer dimensions is given.

Chapter 5:

To be more advance integration, magnetic integration method for multi-element resonant converter is proposed based on transformer cantilever model. A measuring method is given to identify the parasitic inductance value in complex cantilever model.

For better power density, passive integration is necessary. However, capacitance integration is risky due to life time constraint. An evaluation criteria is proposed to determine which components integrated in the system based on lowest voltage and current stress.

A passive integration method is given to integrate all the magnetic components and capacitor with lowest stresses.

Chapter 6:

Conclusion and future work.

Chapter 2. Synthesis of Multi-Element Resonant Converters

In this chapter, a general and systematic method to explore the characteristics of multi-element resonant converters is proposed. Each resonant converter is synthesized by basic resonant cells. The resonant converter inherits the characteristics of parental resonant cells. LLC resonant converter is one of the most popular topologies in DC/DC converters. The LLC-like resonant converters are found by the synthesis of basic resonant cells. Furthermore, the LLC-like resonant converters are improved by synthesizing more resonant cells.

2.1Fundamental Concept of Resonant Converters

As mentioned in chapter one, dc-dc resonant converters can be presented in a simplified block diagram form as shown in Fig. 2.1.

The input DC voltage or DC current source is converted into square waveform by primary switches. The output sink is implemented by rectifier circuits. The output circuit consists of either a series inductor or a parallel capacitor with the load resistance in order to give current sink or voltage sink, respectively.

The basic resonant cell consists of frequency selective network whose function is to transfer the energy from the source to the load, in other words, band-pass filter. The passing-through energy is controlled by changing the switching frequency. The band-pass filter characteristic of each resonant tank could be represented by its voltage transfer functions [B.1], [B.2].

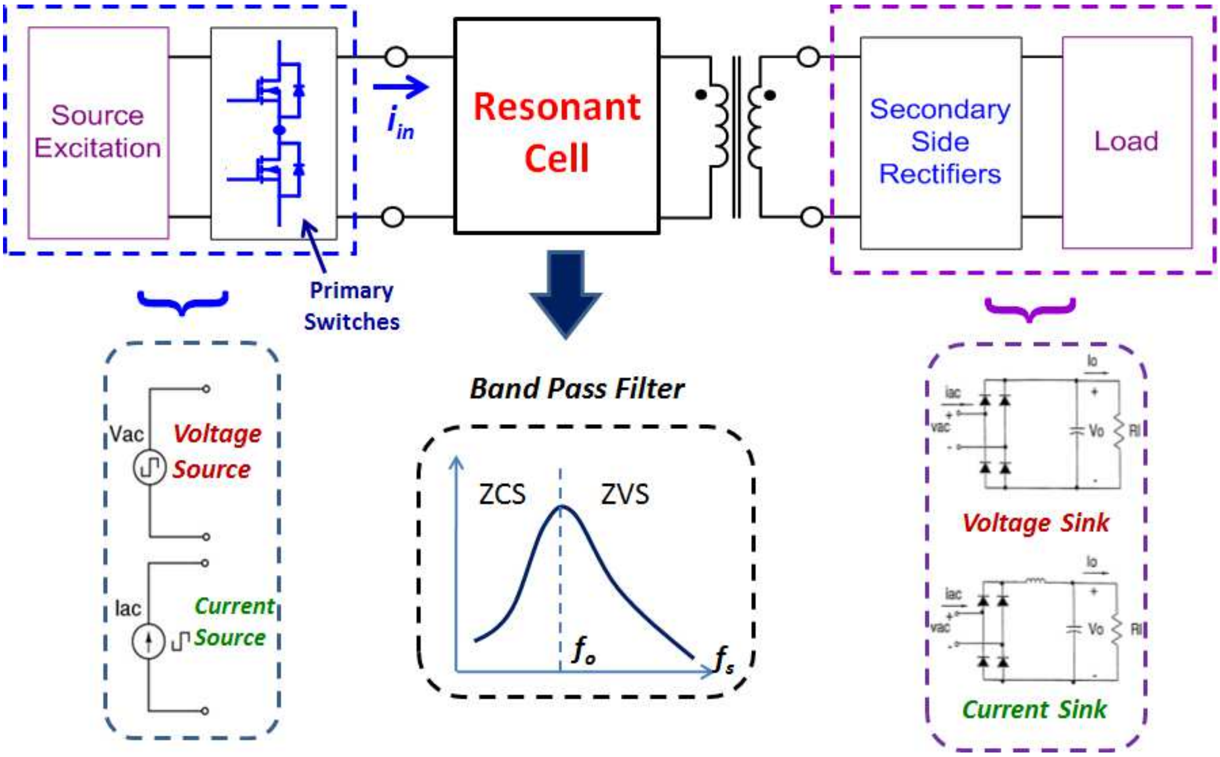

Fig. 2.1Simple Block diagram for the basic concept of resonant converter

Most of dc-dc applications are voltage source, like front-end dc-dc converters. Thus, the voltage source is taken into account in the following analysis. The similar concept can also be applied to current source application.

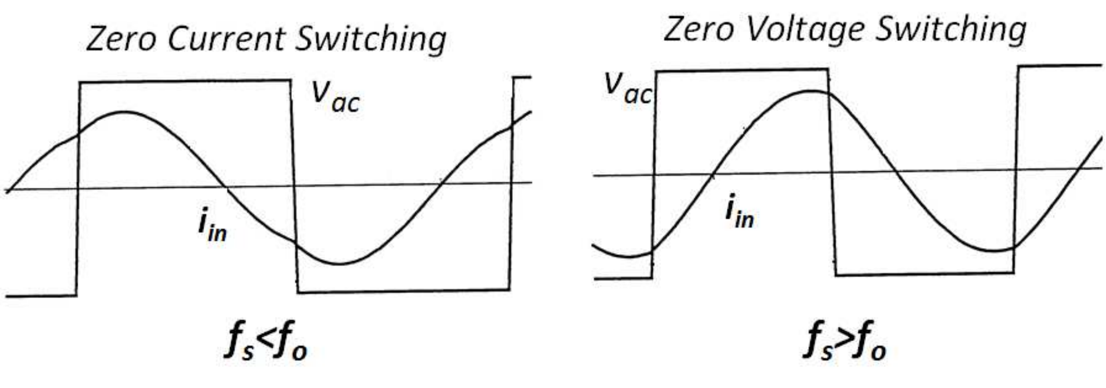

Fig. 2.2Zero current switching and zero voltage switching principles

When the operation point at resonant frequency (f_o, in Fig. 2.1), the input voltage (V_{ac}) is in phase with input current (i_{in}). The output power reaches its maximum value if input power is fixed. All of the input power is directly delivered to the load. When operation below f_o, the voltage is leading the current, so the tank is capacitive. The up slop of voltage gain indicate ZCS operation, as shown in Fig. 2.2.When operation above f_o, the current is leading the voltage, so the tank is inductive. The down slop of voltage gain indicates ZVS operation.

2.1.1 Basic Resonant Cells (Two-Element Resonant Tanks)

Two-element resonant tanks are basic resonant cells of multi-element resonant converters. For two energy storage elements, there are totally eight resonant tank configurations as shown in Fig. 2.3. Tank A, B, C and D are suitable for voltage source, and Tank E, F, G and H are suitable for current source. Here, not "suitable" means no regulation capability (like Tank E to voltage source), and/or no resonance (like Tank F to voltage source).

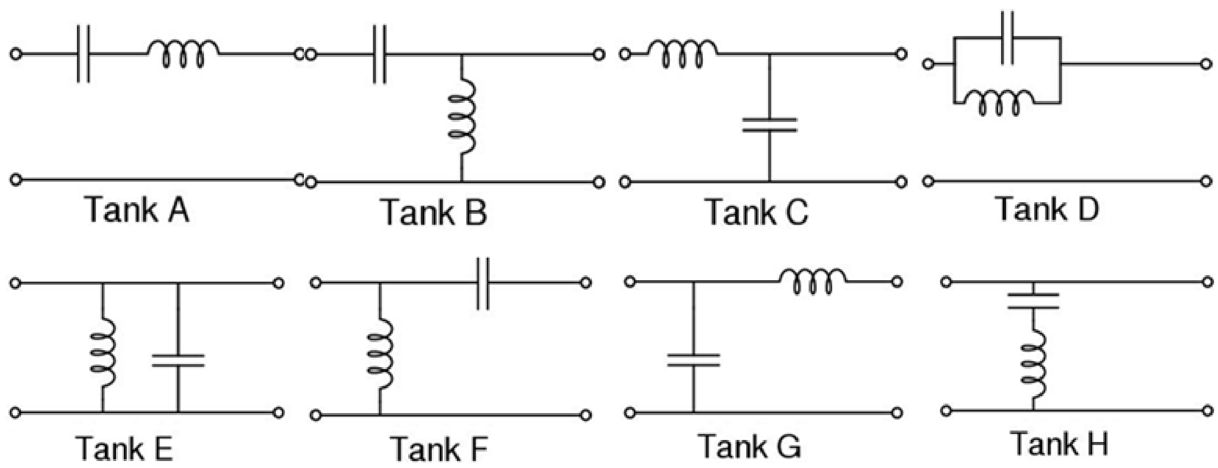

Fig. 2.3 Two-element resonant tanks

Tank A is series resonant tank, which is the resonant tank of series resonant converter (SRC). It behaves like band-pass filter. The resonant frequency in Fig. 2.4 (a) is named series resonant frequency (SRF). When the frequency of input energy is the same as SRF, the whole energy will pass through it, while the energy of other frequencies is attenuated. However, this band-pass filter is not good at light load. The voltage gain becomes flat. Hence, a very high switching frequency is required for series resonant converter light load regulation.

The resonant frequency in Fig. 2.4 (b) is named parallel resonant frequency 1 (PRF1). It is not good band-pass filter either. The high frequency input energy will pass through it, but low frequency energy will be blocked. Thus, it performs more like high-pass filter.

The resonant frequency in Fig. 2.4 (c) is named parallel resonant frequency 2 (PRF2). It is the resonant tank of parallel resonant converter (PRC). It is not good band-pass filter either. The low frequency input energy will pass through it, but high frequency energy will be blocked. Thus, tank C performs more like low-pass filter.

Both of two PRFs have high gains at light load around resonant frequency. Steep slope close to resonant frequency come with this.

The resonant frequency in Fig. 2.4 (d) is named notch resonant frequency (NRF). This tank is quite different from previous tanks. It behaves like a band-stop filter. When the frequency of input energy is the same as NRF, the tank impedance is infinite high, the whole energy will be blocked. Meanwhile, the energy of high order harmonics pass through the whole tank. Thus, Tank D alone can hardly form a resonant converter.

All of basic resonant cells are only have one resonant frequency. The resonant frequency is the most efficient point for the resonant tank except band-stop filter, because all the fundamental of input power is delivered to the load. Otherwise, part of it is attenuated by the tank. However, they cannot operate at resonant frequency in fear of falling into different soft-switching region, like from ZVS into ZCS or from ZCS into ZCS, which is detrimental to devices.

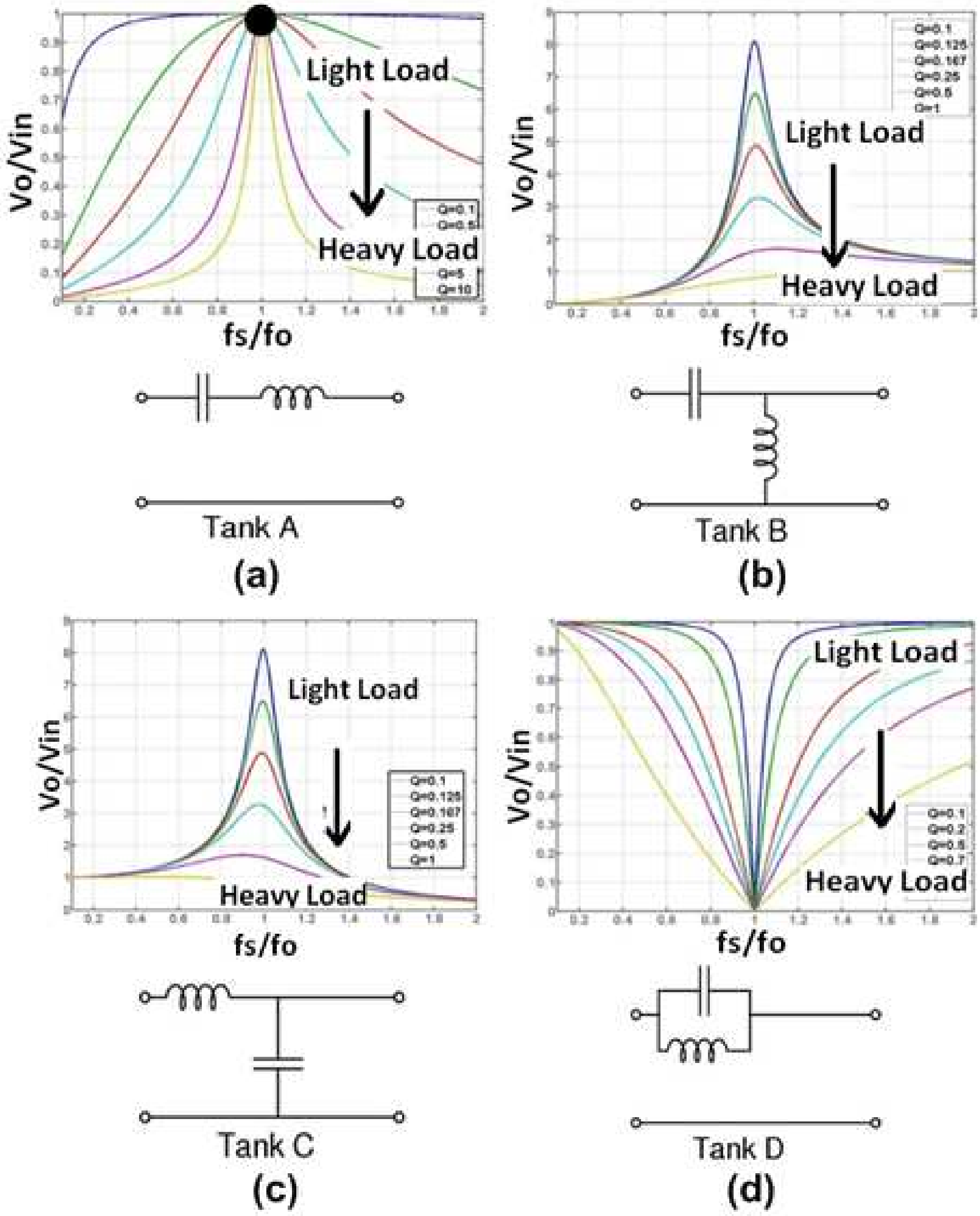

Fig. 2.4 Voltage gains of two-element resonant tanks

2.1.2 Synthesis of Basic Resonant Cells

From the discussion above, two-elements resonant converters have their inherent limitations. Because each resonant frequency has its own characteristics, the synthesis of two or more resonant frequencies may give resonant converter more merits.

LCC resonant converter (LCC) and LLC resonant converter (LLC) are very good examples to illustrate the concept of resonant converter synthesis.

LCC resonant converter (LCC) is a popular resonant converter in many applications. It is the combination of series resonant converter (tank A) and parallel resonant converter (tank C). SRF is at the left side of PRF2, in other words, ZCS region of PRC. Around SRF, most region is ZCS region, which is not preferred. Series resonant frequency (SRF) (black dot in Fig. 2.5 (a)) helps in operation; however, the operation region (shadow in Fig. 2.5 (a)) is away from SRF. Thus, LCC is still dominated by parallel resonant frequency (PRF), and have similar pros and cons as PRC. It cannot operate at resonant frequency either.

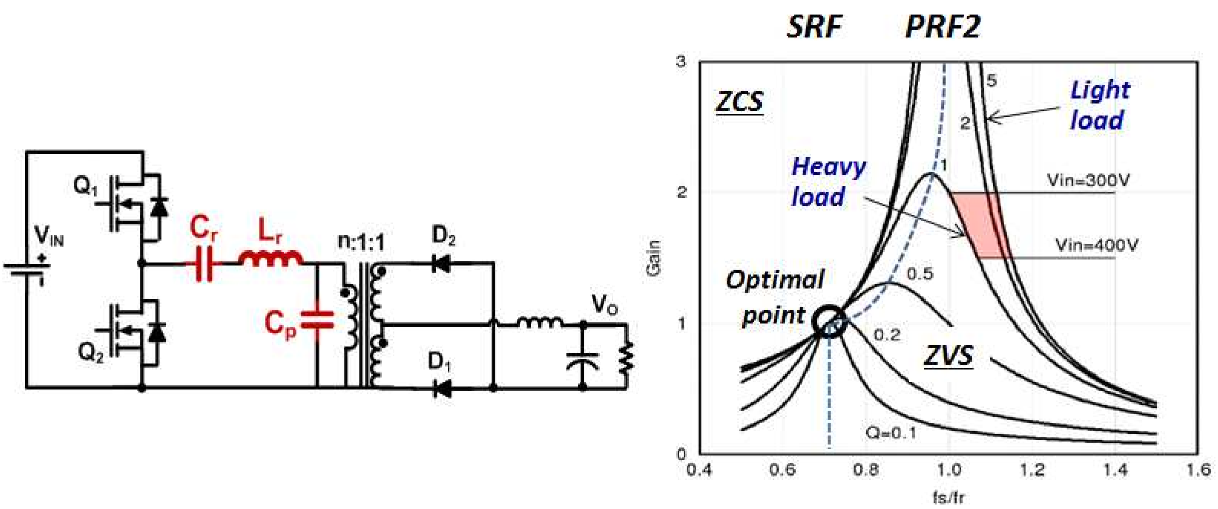

Fig. 2.5 Circuit and voltage gains of LCC resonant converter

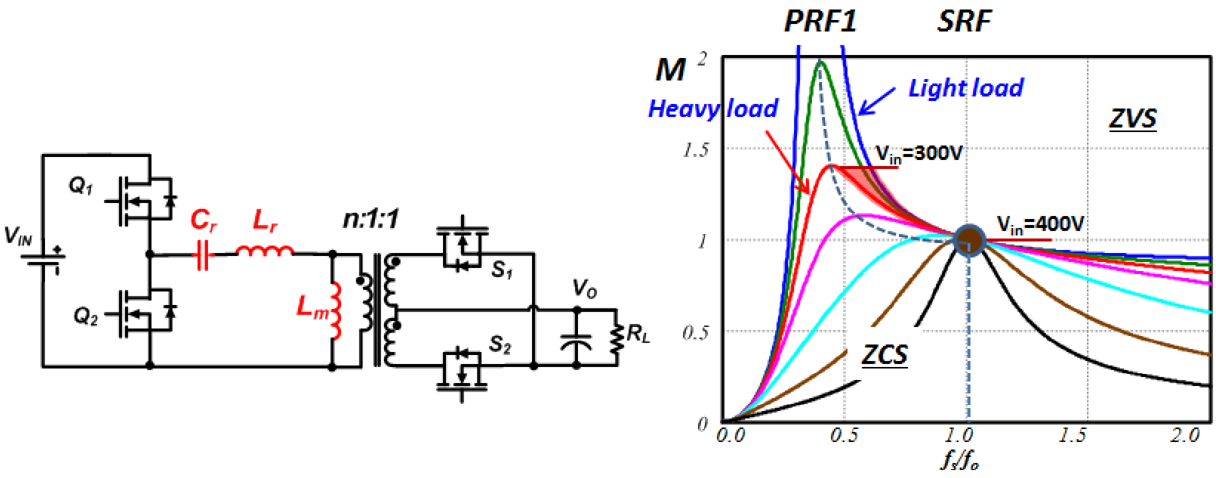

Fig. 2.6 Circuit and voltage gains of LLC resonant converter

LLC is the combination of tank A and tank B. It is different from LCC due to the different order of two resonant frequencies. PRF2 is at the left side of SRF, in other words, the ZCS region of SRF. PRF2 improves part of this region into ZVS region. Thus, it is safe to operate around SRF, where is the optimal point. However, the right side of SRF is still flat [B.3]-[B.10].

The synthesis of SRF and PRF1 generates many merits : (1) ZVS capability for zero to full load range; (2) low turn off current for primary side switches; (3) Zero-current-switching (ZCS) for synchronous rectifier devices; (4) voltage gain boost capability without deterioration of efficiency at normal condition.

Three-element resonant converters have more resonant frequencies than two-element. The synthesis of resonant frequencies could provide extra benefits to the resonant converter. However, the synthesis should be the right types and the right order of resonant frequencies to improve the performance, or the improvement could be very little or worse.

2.3 Synthesis of Three-Element Resonant Converters

As mentioned before, LLC has many advantages due to the synthesis of resonant frequencies. A systematic analysis is given below to search LLC-like resonant converters.

All the three-element resonant topology networks are given in Fig. 2.7 [B.11]. The topology networks 15, 16, 17 are degraded to two-elements if the blocks replaced by an inductor or capacitor.

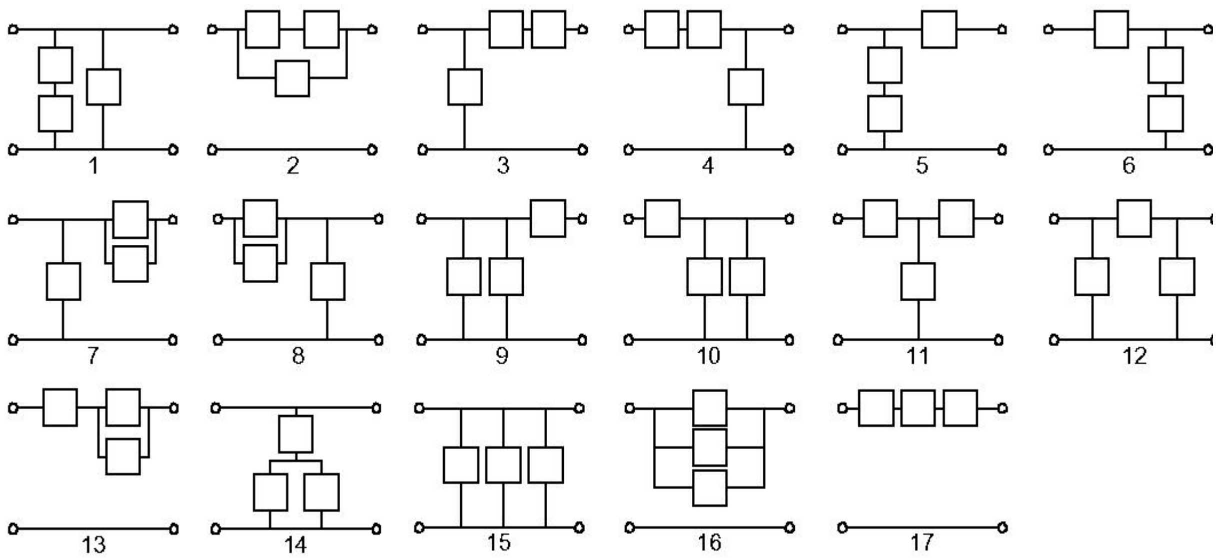

Fig. 2.7 Three-element resonant topology networks

Replacing each block of networks with an inductor or capacitor, 36 topology candidates are gotten in Fig. 2.8.

If the input source types are taken into account, there are some tanks are not suitable. Firstly, if one or more elements are clamped to input voltage source, the whole resonant tank will be degraded to less order system. Secondly, capacitors cannot be in parallel with voltage source. Based on these two criteria, there are only 13 topologies left, shown in Fig. 2.9.

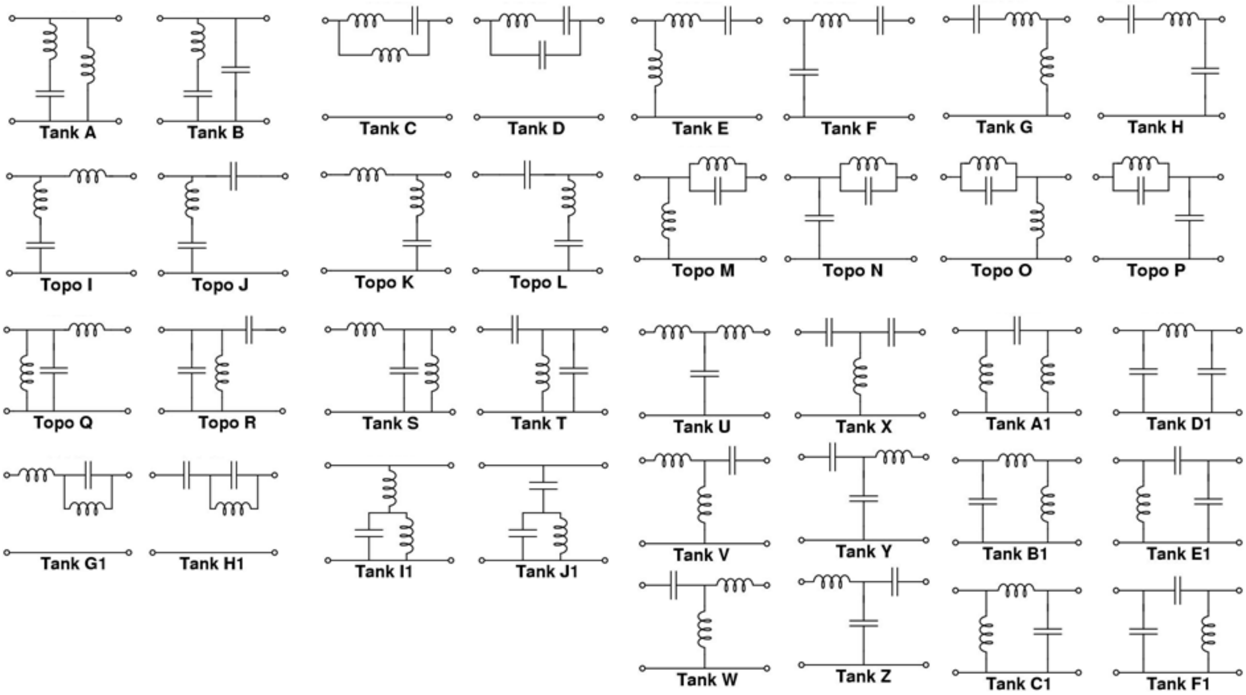

Fig. 2.8 Three-element resonant tanks

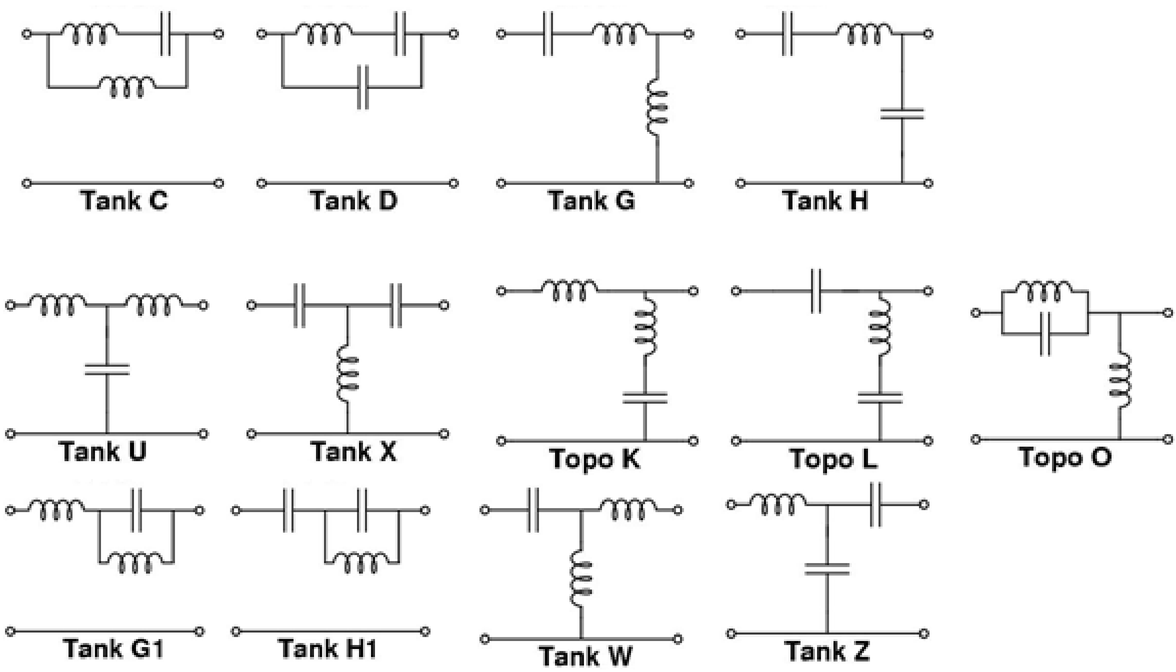

Fig. 2.9 Three-element resonant tanks for voltage source

The tanks in Fig. 2.9 are classified by combination of the resonant frequencies defined in section 2.1.1.

From Fig. 2.10 to Fig. 2.14, the dot lines show the boundaries of ZVS and ZCS regions.

As shown in Fig. 2.10, Tank D and Tank H1 are the synthesis of SRF and NRF. Thus, this group has similar characteristics like SRC. NRF sharps flat voltage gains above SRF, so ZVS region of SRC is improved. Voltage regulation is achievable in a narrow frequency range. However, resonant frequencies are the boundaries of ZVS and ZCS regions. Operation at resonant frequency is still not achievable in this topology group.

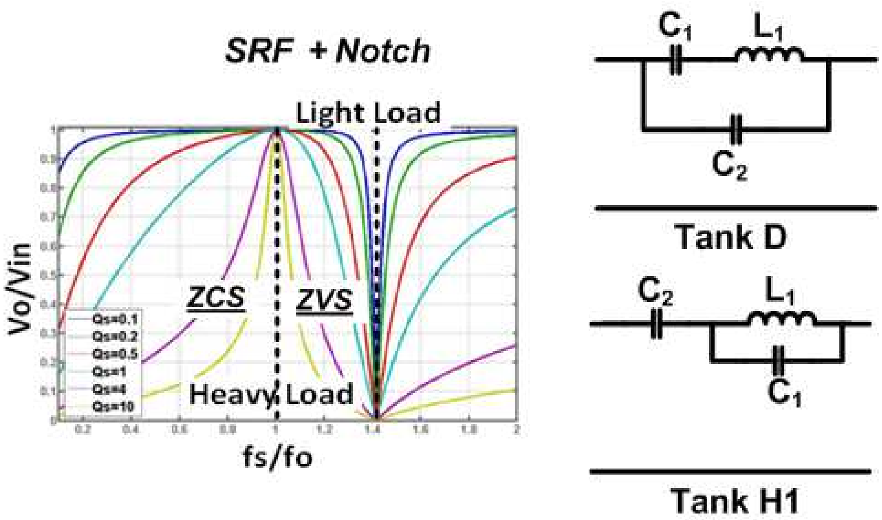

Fig. 2.10 Voltage gains and tanks of SRF+Notch

As shown in Fig. 2.11, Tank C and Tank G1 are the synthesis of SRF and NRF. Thus, this group has similar characteristics like SRC. In this group, NRF sharps flat voltage gains below SRF, so ZCS region of SRC is improved.

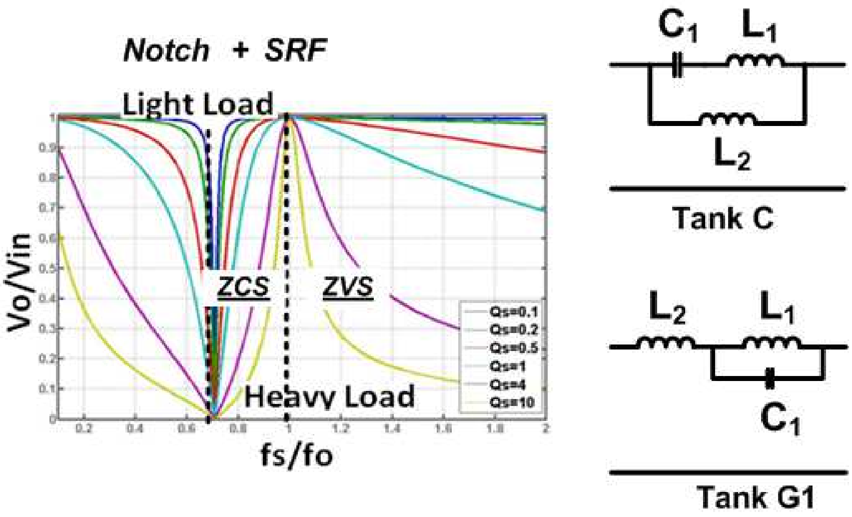

Fig. 2.11 Voltage gains and tanks of Notch+SRF

As shown in Fig. 2.12, Tank K is the synthesis of PRF and NRF. Thus, this group has similar characteristics like PRC. NRF sharps voltage gains above PRF, so ZVS region of PRC is improved. However, the ZVS region of PRC is sharp before. Thus, the improvement is limited. Meanwhile, PRF and Notch filter are the boundaries of ZVS and ZCS regions. Operation at resonant frequency is still not achievable in this topology group either.

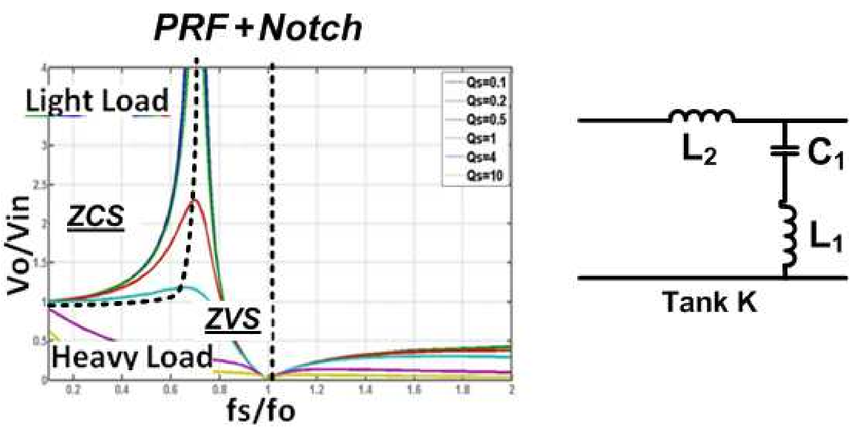

Fig. 2.12 Voltage gains and tanks of PRF+Notch

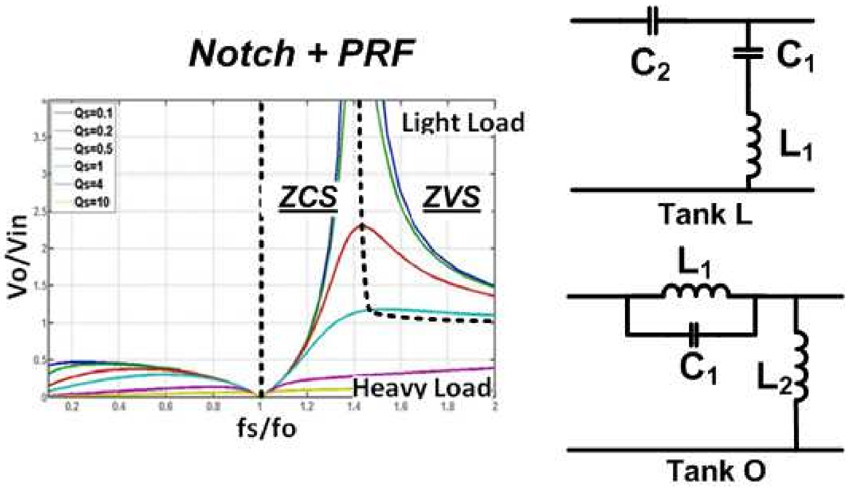

Fig. 2.13 Voltage gains and tanks of Notch+PRF

As shown in Fig. 2.13, Tank L and Tank O are the synthesis of PRF and NRF. Thus, this group has similar characteristics like PRC. Similarly, NRF sharps voltage gains below PRF, so ZCS region of PRC is improved. Operation at resonant frequency is still not achievable in this topology group either.

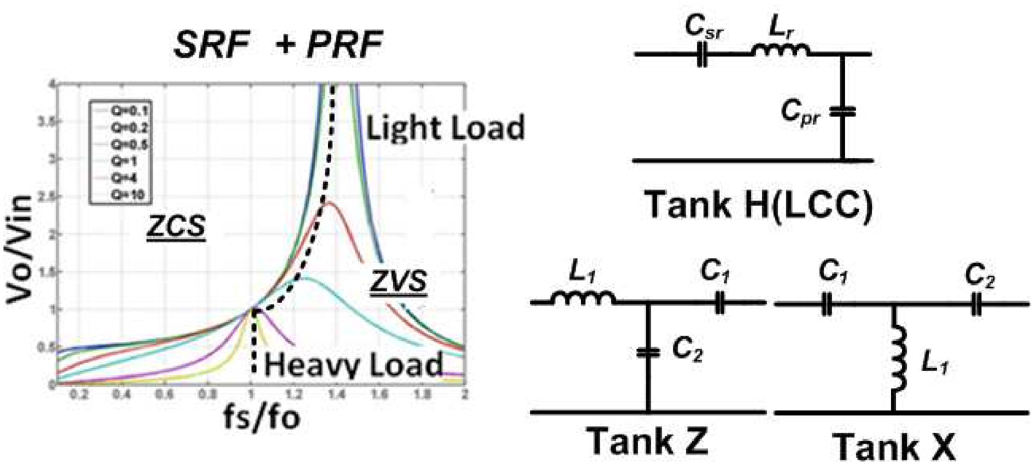

Fig. 2.14 Voltage gains and tanks of SRF+PRF (LCC-like)

As shown in Fig. 2.14, Tank H, Tank Z and Tank X are the synthesis of SRF and PRF. Thus, this group has both characteristics of SRC and PRC.PRF locates at higher frequency and SRF at lower frequency. Tank H in this group is the resonant tank of LCC resonant converter. The typical voltage gain curves are very similar as LCC resonant converter. Thus, this group is named LCC-like resonant converters.

As shown in Fig. 2.15, Tank G, Tank W and Tank U are the synthesis of SRF and PRF, like LCC. The difference is PRF locates at lower frequency and SRF at higher frequency. Tank G in this group is the resonant tank of LLC resonant converter. The typical voltage gain curves are very similar as LLC resonant converter. In this group, operation at resonant frequency is durable due to the help of PRF. The resonant converter in this group can operate around series resonant frequency without the concern falling into the ZCS region under given load condition. Furthermore, they have the similar merits of LLC, like low loss at nominal conditions, ZVS for whole load range, ZCS for output rectifier, etc. They can also achieve good efficiency at high input voltage, where the front-end dc-dc works for 99% time, with wide input range. Thus, this group is named LLC-like resonant converters [B.12].

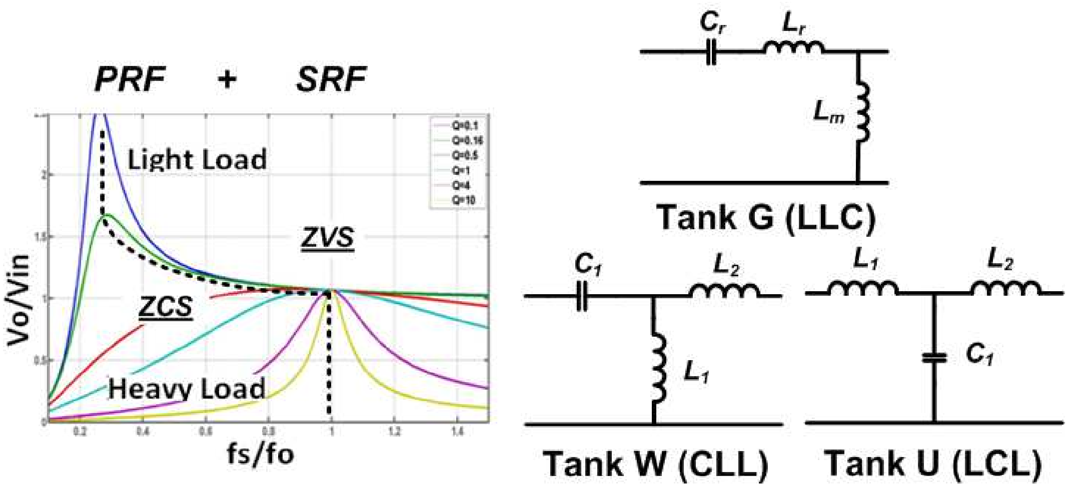

Fig. 2.15 Voltage gains and tanks of PRF+SRF (LLC-like)

For the inherent problem from SRF, the startup and short-circuit protection of LLC are still an issue due to the flat voltage gains above SRF.

2.4 Inherent Issues of LLC Resonant Converter

Fig. 2.16 shows the DC characteristic of the LLC resonant converter. Normally, the LLC operates near the resonant frequency point ($f_s=f_0$) to keep the best efficiency. During the hold-up time operation, the input voltage decreases while the output voltage should stay constant, thus the switching frequency decreases ($f_s<f_0$) to boost the voltage-gain. Under the soft start-up condition, the output voltage needs be built up from zero to the steady-state value, in order to prevent from entering the zero-current-switching (ZCS) zone, the LLC should work in above resonant frequency region ($f_s>f_0$).

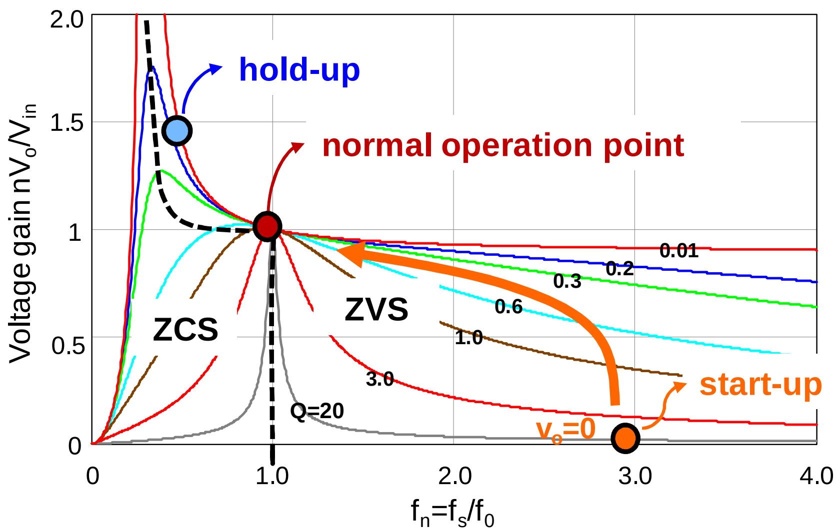

Fig. 2.16 DC characteristic of the LLC resonant converter

However, as shown in Fig. 2.17, if the start-up switching frequency (f_s) is not high enough, large voltage and current stress can be observed at the start-up moment [A.49]-[A.54].

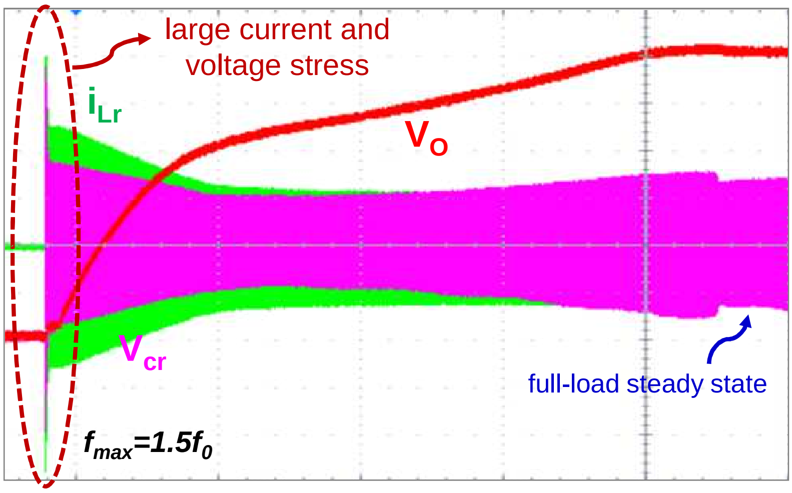

(a) Voltage and current stress of resonant tank during soft start-up

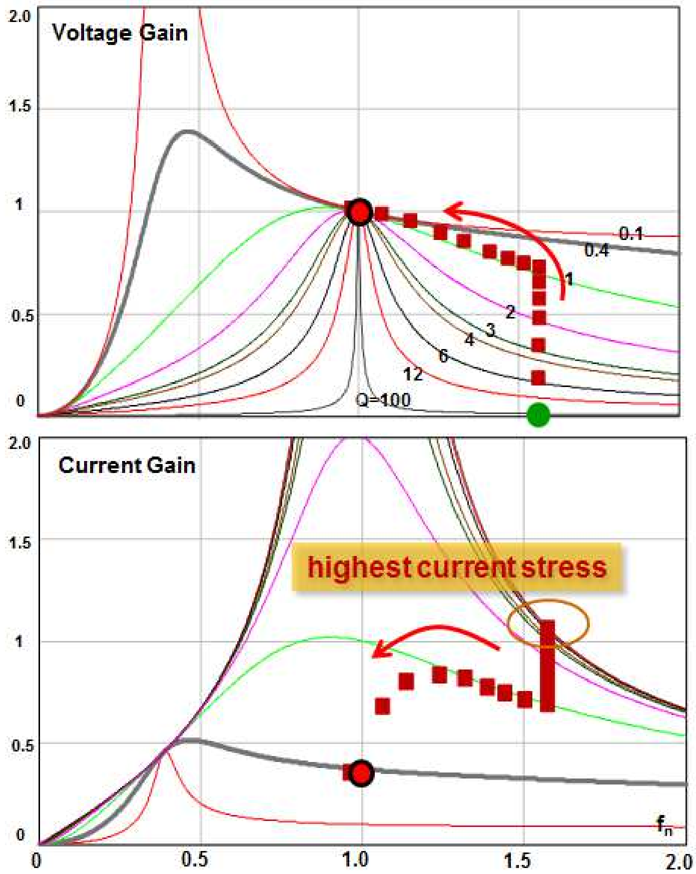

(b) Output current and voltage during soft start-up

Fig. 2.17 Soft start-up with low switching frequency

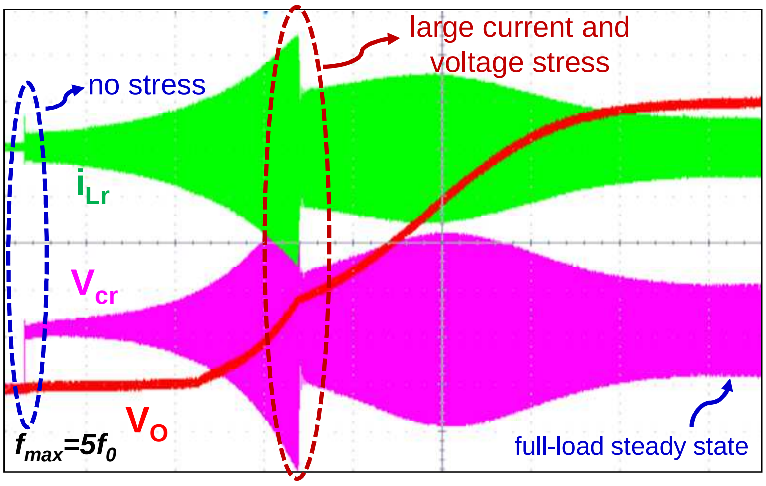

(a) Voltage and current stress of resonant tank during soft start-up

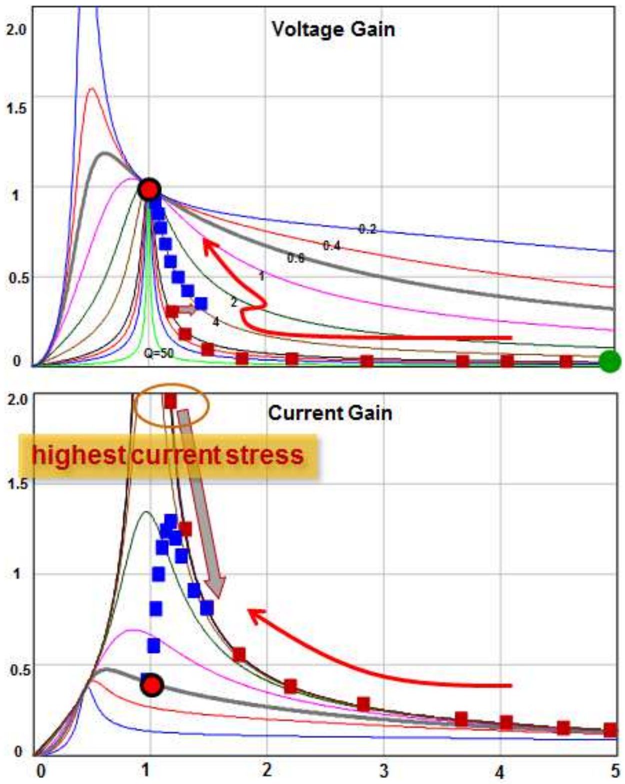

(b) Output current and voltage during soft start-up

Fig. 2.18 Soft start-up with a high switching frequency

Otherwise, as shown in Fig. 2.18, if the LLC starts up with a very higher, this is about 5 times of normal operation frequency. At the beginning, the voltage and current stress will be not large. However, during the soft start-up process, if f_s decreases too quickly, large voltage and current stress can still happen, which will trigger the over-current-protection. As a result, f_s will increase a bit to limit the stress, and then decreases smoothly to finish the soft start process. If f_s decreases slowly, the stress will stay small, but the output voltage will build up slowly, which means, the soft start-up process will take much longer.

Thus, if frequency control is applied start-up process, the operation frequency of LLC resonant converter should be very high to attenuate the voltage and current stress at the beginning of start-up. Even start up at high frequency, the high voltage and current stresses still high.

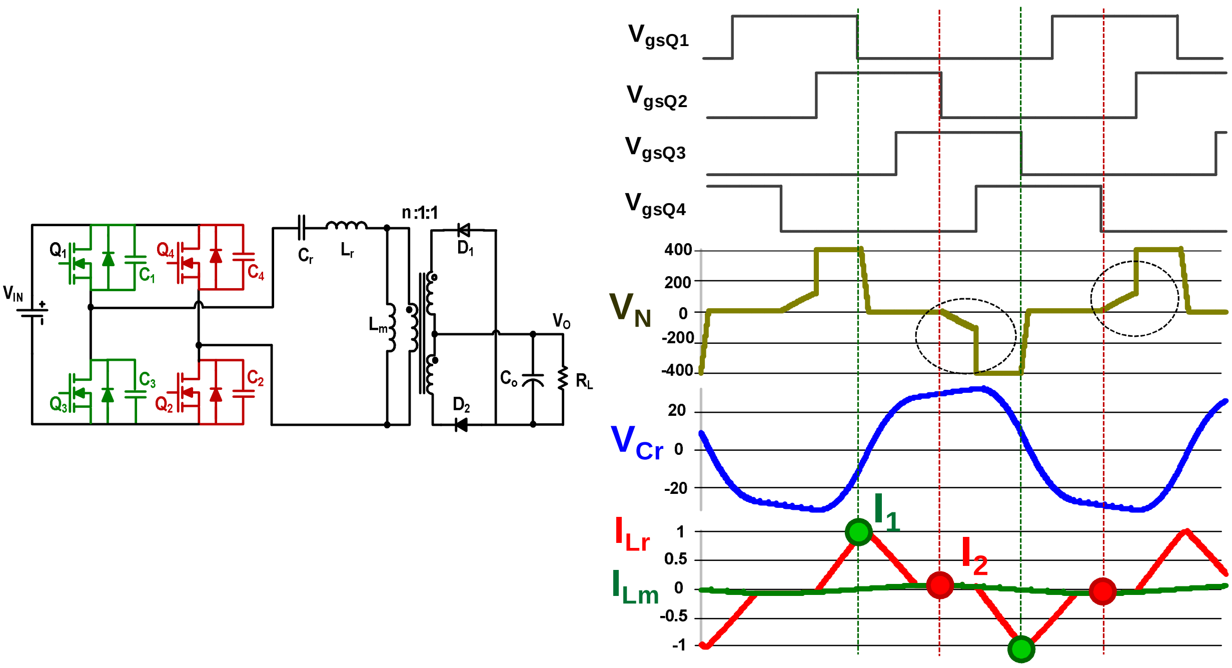

Fig. 2.19 Phase-shifted control in full-bridge LLC (f_s=2f_0, Φ=π/2)

Besides the frequency control, phase-shifted control can be used in full-bridge LLC to limit the voltage and current stress during the soft start process. Fig. 2.19 shows steady state waveforms when $f_s=2f_0$ with $\pi/2$ phase shift. For the leading leg (Q_1 and Q_3), it is easy to realize ZVS, since the resonant current is large at the turn-off moment. However, for the lagging leg (Q_2 and Q_4), it is hard to achieve ZVS due to the lower current to charge the junction capacitors at the turn-off instant.

Based on frequency control and phase-shift control, [B.13] proposed an optimal trajectory control for the LLC soft start-up. The resonant voltage and current stress can be limited, the output voltage should be built up quickly and smoothly, and the ZVS of all switches can be guaranteed.

Fig. 2.20 shows the experiment results. The start-up frequency is more than 2 times of normal operation frequency.

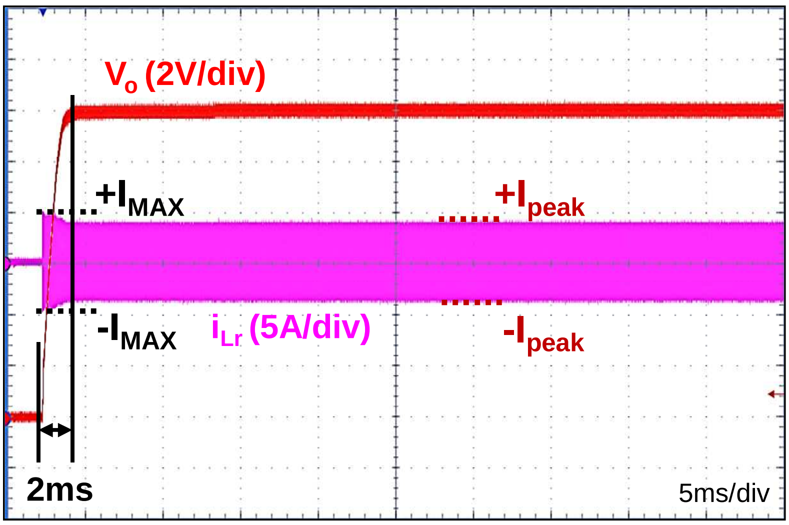

Fig. 2.20 Optimal trajectory soft start-up

However, all above control methods need very high switching frequency to attenuate the voltage and current stress during the process of start-up. This issue comes from the inherent problem of series resonant converter.

2.5 LLC-like Resonant Converters with Notch Filter

As discussed in previous sections, three-element topologies have more merits than two-elements, but three-element topologies still have their own limitations. With poor frequency selectivity, namely, very wide bandwidth, the frequency has to be increased very high to achieve enough damping effect.

To improve the flat voltage gain above series resonant frequency of LLC-like resonant converters, additional resonant elements are needed to create sharp gain. The desirable voltage gain curves are plotted in Fig. 2.21. One possible way building sharp voltage gains is making a notch filter.

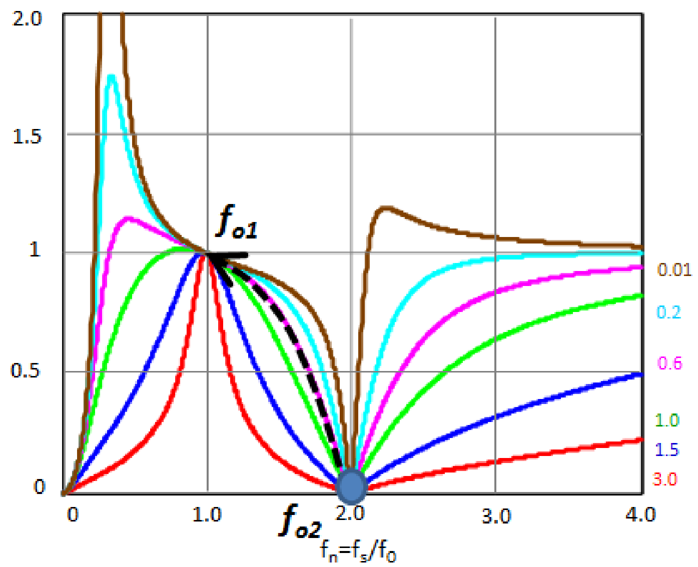

Fig. 2.21 Desirable Gain Curves for LLC-like resonant converters

The resonant tank with notch filter characteristic can create zero voltage gain. Conceptually, infinite impedance can be created when frequency operates at the resonant frequency f_{02} of the notch filter. As a result, if overload or even shorted output condition occurs, the current can be limited inherently by the resonant tank characteristic. The notch filter center frequency f_{02} can be designed to achieve the over load protection.

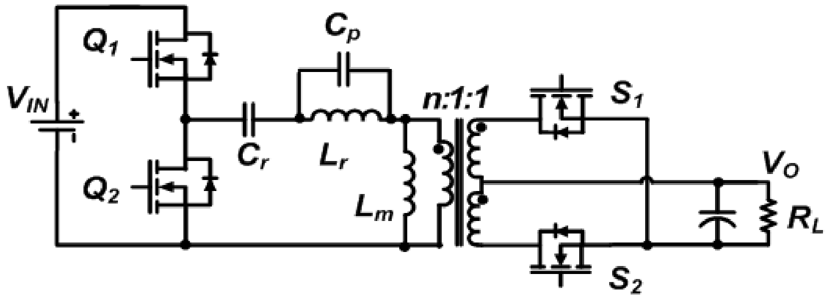

Fig. 2.22 One example of selected 4-elements resonant converters

One of these resonant converters is depicted in Fig. 2.22. The notch filter section is created with L_p and C_p. The band pass filter section consists of L_p, C_r and C_p.

In general, with variable frequency control, the resonant tank input voltage is excited as a square waveform. According to the Fourier analysis, the voltage excitation only consists of odd harmonics. Therefore, to avoid circulating energy at nominal condition, notch filter resonant frequency f_{02}should be designed at even times of nominal resonantfrequencyf_{01}. Meanwhile, f_{02} is preferred close to f_{01}.Thus, $f_{02} = 2f_{01}$ is a good choice.

When converter operates at f_{01}, the notch filter represents inductive. The impedance of C_p is much larger than L_p. The major part of primary side current flows through L_p, not C_p. The current stress on C_p is much less than C_r.

However, the number of four-element resonant topologies is numerous. A systematic way for classification and selection can save a lot effort and energy to find desired topologies.

All four-element networks are listed in [B.14], [B.15], as shown in Fig. 2.23. Each square block represents one energy storage element. The networks in the dot line pane in Fig. 2.23 are not suitable for voltage source, for they cannot regulate voltage.

Fig. 2.24 shows the relationship between resonant frequency types and topology networks. Each square block in Fig. 2.24 represents one or more energy storage elements. The rectangle block indicates input source or output sink or other energy storage elements. If the resonant characteristics shown in Fig. 2.24 are wanted, the network below gain curves should be part of resonant tanks.

As discussed before, series resonant frequency (SRF) is needed to achieve low switching loss and low circulating energy at nominal conditions where the operation point is close to it. Parallel resonant frequency is required for wide range voltage regulation. With the combination of these two resonant frequencies, zero-current switching (ZCS) is achieved for the output rectifiers, and no reverse recovery appears. A notch filter is also needed for startup and short-circuits protection. Thus, the candidate topology should include PRF, SRF and NRF. The desired gain curves should be similar as Fig. 2.21.

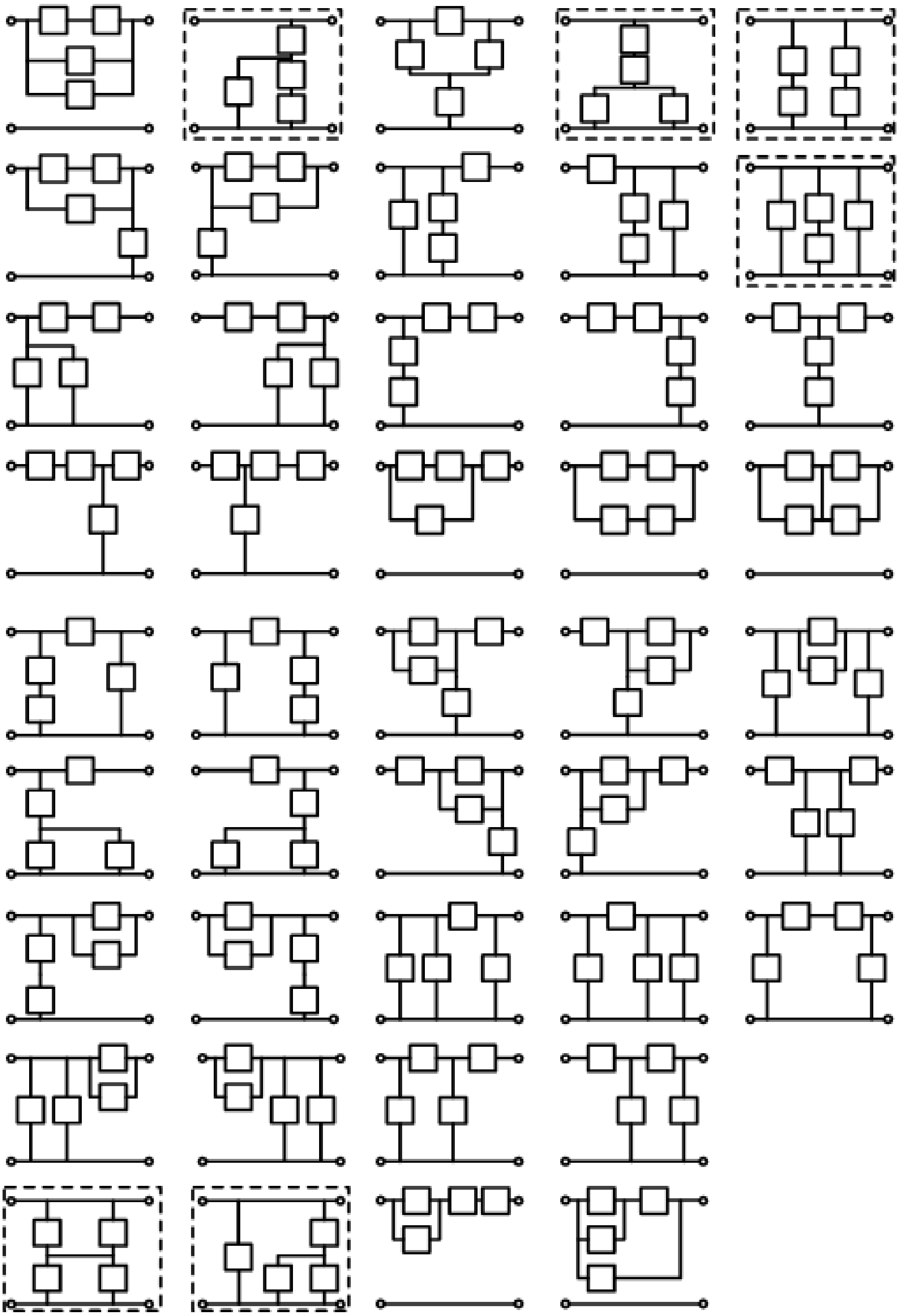

Fig. 2.23Four-element resonant topology networks

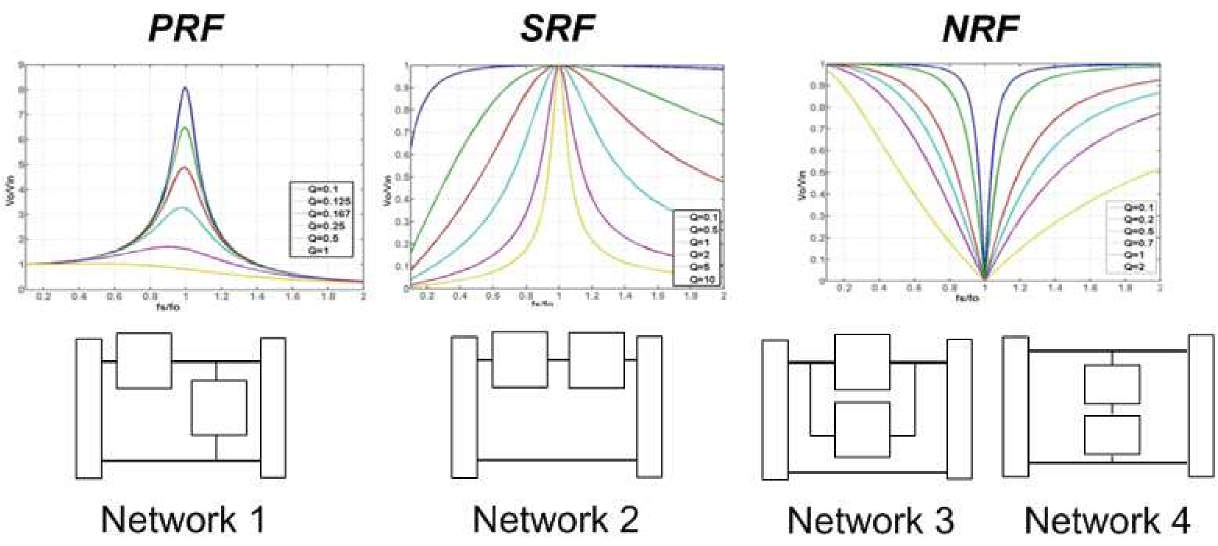

Fig. 2.24 Gain curve characteristics vs. networks

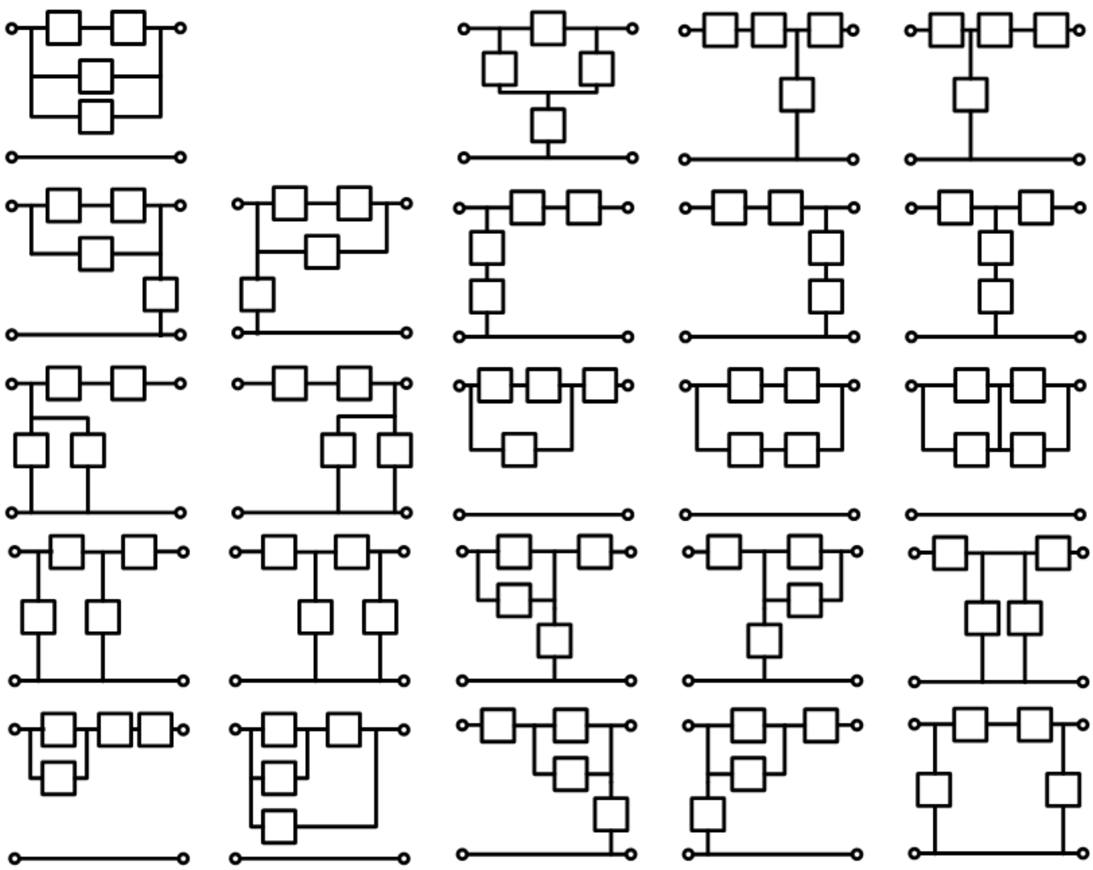

Fig. 2.25 Four-element resonant topology networks including Network 2(SRF)

Fig. 2.25 shows the topology networks including network 2 structure based on Fig. 2.23 and Fig. 2.24. The number is 24.

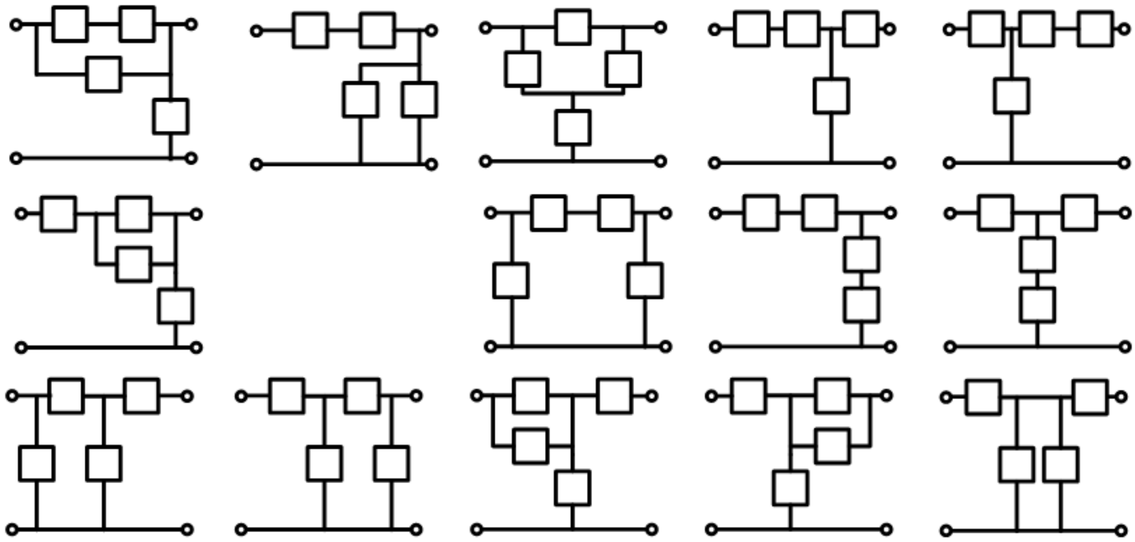

Fig. 2.26 Four-element resonant topology networks including Network 2(SRC) and Network 1(PRF)

Fig. 2.26 shows the topology networks including network 1 and network 2 structures based on Fig. 2.24 and Fig. 2.25. The number is 14.

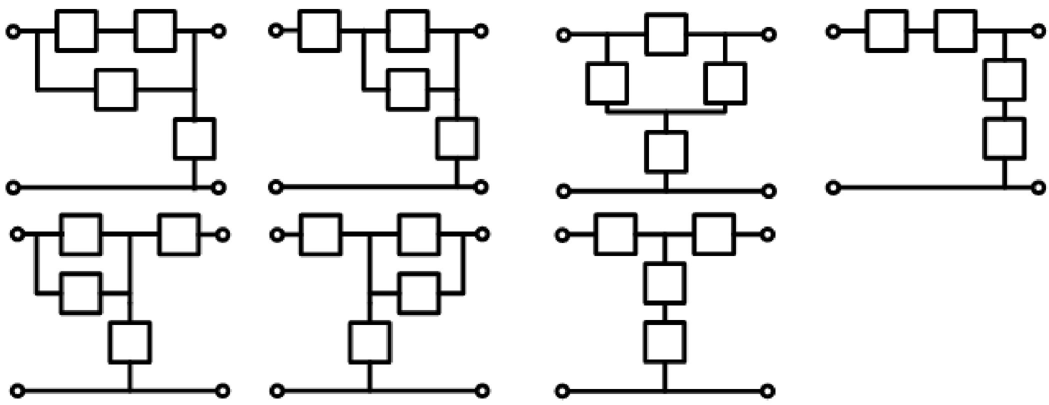

Fig. 2.27 Four-element resonant topology networks including Network 2(SRC), Network 1(PRF) and Network 3 or 4 (NRF)

Fig. 2.27 shows the topology networks including network 1, network 2 and network 3 (or network 4) structures based on Fig. 2.26 and Fig. 2.24. The number is 7.

In topology network shown in Fig. 2.27, each energy storage element can be replaced with inductor or capacitor. The result is shown in Fig. 2.28, ignoring which are not suitable for voltage source.

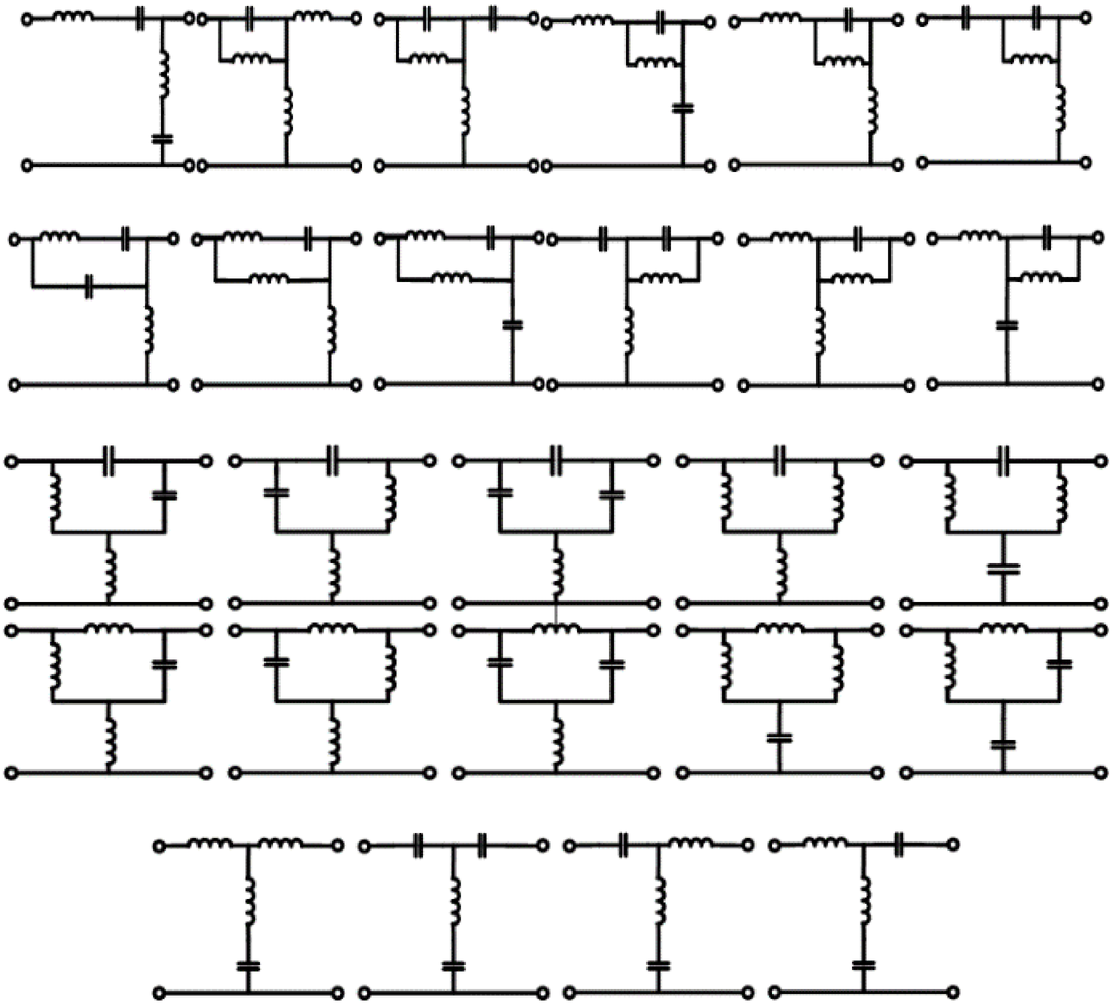

Fig. 2.28 Four-element resonant topologies including Network 2 (SRC), Network 1(PRF) and Network 3 or 4 (NRF)

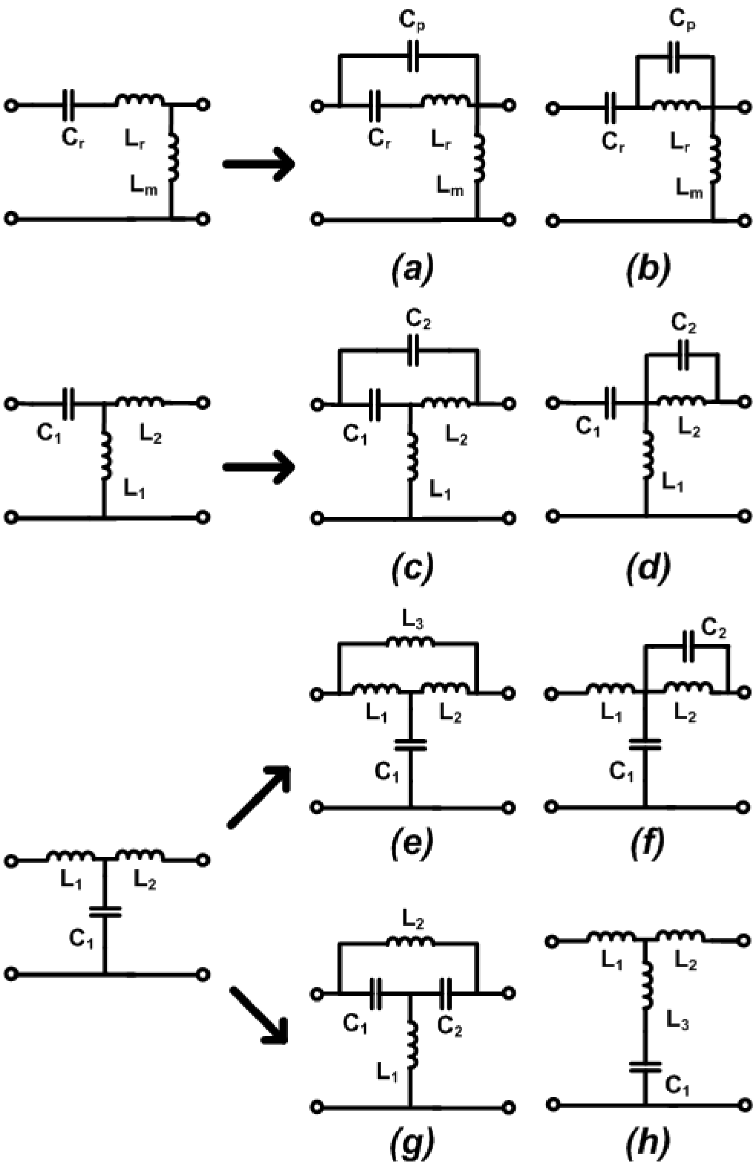

Fig. 2.29 Four-element resonant topologies with desired resonant frequencies

Three different resonant frequencies should be arranged in order. Operation point is near series resonant frequency (SRF) to achieve low switching loss and low circulating energy. Parallel resonant frequency (PRF) should locate at lower frequency for wide range voltage regulation. Notch resonant frequency (NRF) should be placed at higher frequency for start-up and short-circuit protection. Thus, the order of resonant frequencies is PRF, SRF and NRF from low frequency to high frequency (shown in Fig. 2.29). Eight topologies are gotten based on this rule shown in Fig. 2.29. We can see that they also can be deduced from three-element LLC-like resonant converters.

Similarly, the synthesis method based on resonant frequencies can be utilized in three, four, five, or higher elements resonant converters.

2.6 LLC-like Resonant Converters with Notch Filter and Two Band-pass Filters

With leakage inductance L_r, a second band pass filter is created. A 5-elements resonant tank is given as an example, shown in Fig. 2.30. The second band pass filter is designed at the three times of the nominal frequency. The third order harmonics energy of primary side can be delivered through this band pass filter as shown in Fig. 2.31. Obviously, the power delivery is more efficient.

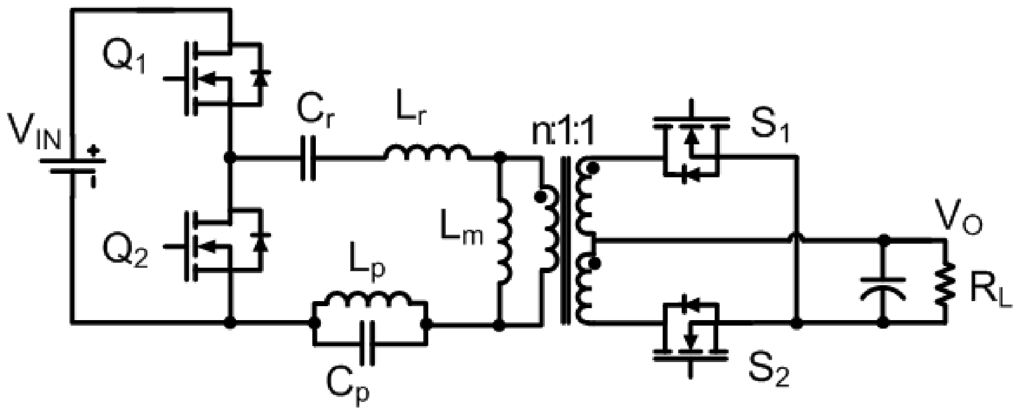

Fig. 2.30 One example of 5-element resonant converters

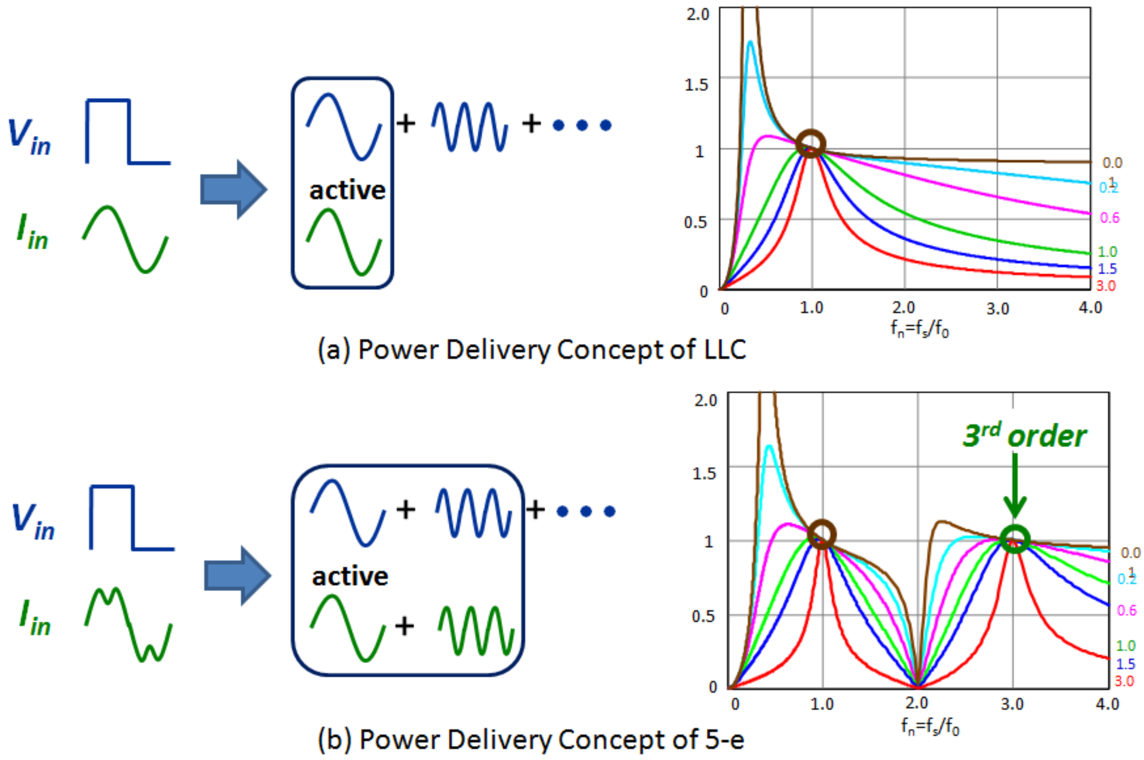

Fig. 2.31 Power Delivery Difference between LLC & 5-e

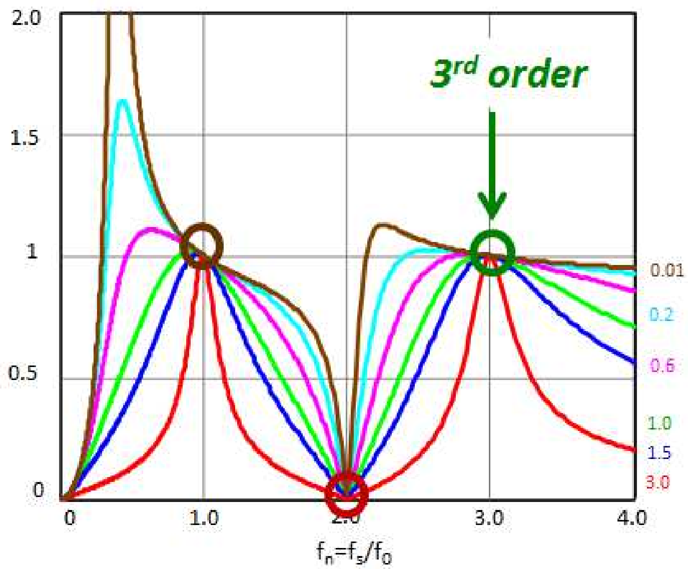

Fig. 2.32 Gain Curves of selected 5-elements resonant converter

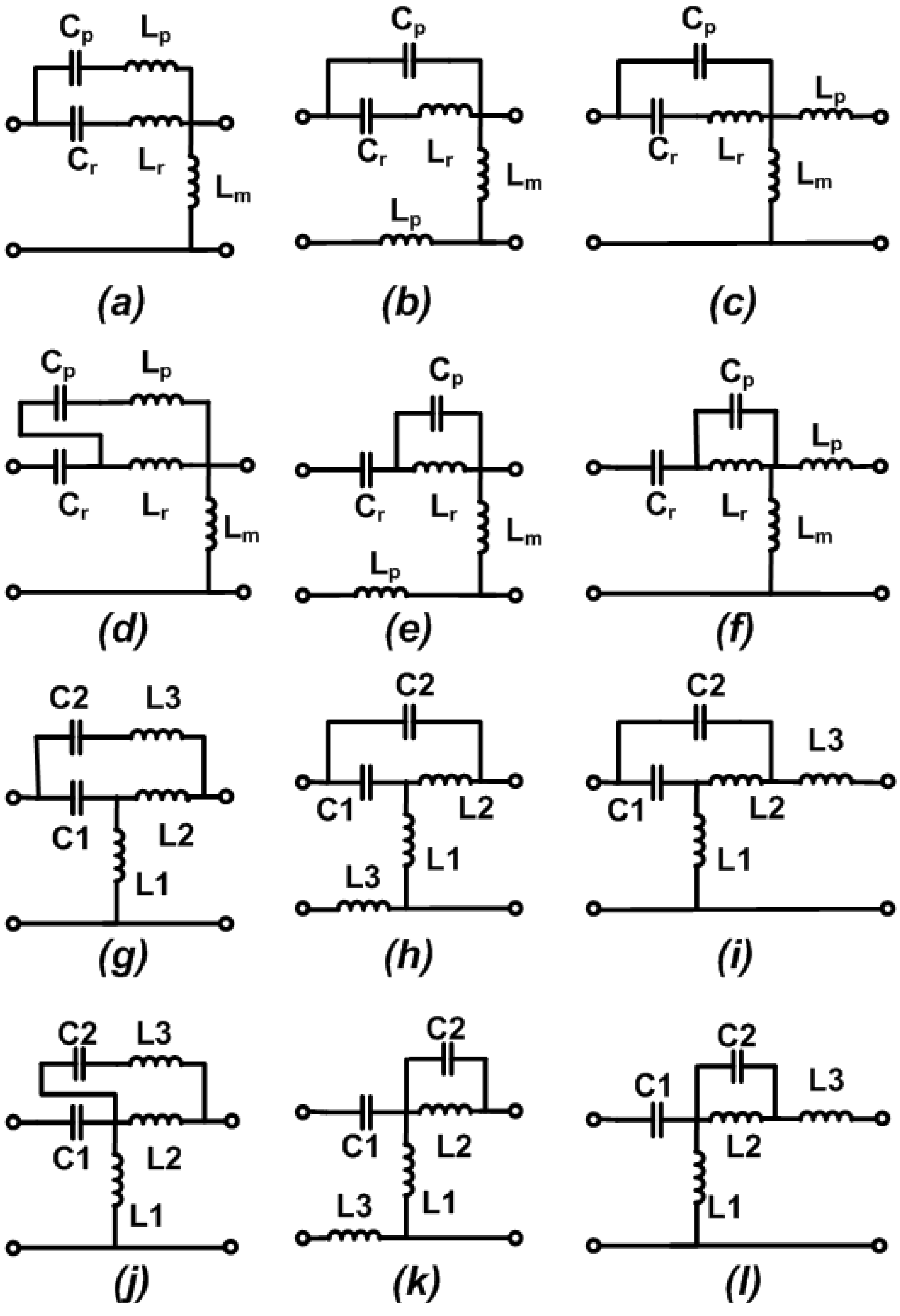

Fig. 2.33Five element resonant tank cell based on LLC with notch filter and 3rd harmonics band filter

However, the number of five-element resonant topologies is even much more than four-element resonant converters. A same systematic way is used for searching resonant topologies with similar gain curves like Fig. 2.32.

Based on the searching results of previous section, one more inductor should be added into resonant tanks in Fig. 2.29. Fig. 2.33 shows the searching results of 5-element resonant converters with desired voltage gain curves.

Each resonant frequency expression is shown in equation (3.1), (3.2) and (3.3) for the example circuit is shown in Fig. 2.30.

When switching frequency is very low, the effect of C_p is weak, L_r and L_p are in series to resonance with C_r. L_p resonances with C_p to get notch filter. If switching frequency reach very high, the impedance of L_p is very high. Thus, only C_r and C_p are in series to resonance with L_r.

$$f_{o1} = \frac{1}{2\pi}\sqrt{\frac{L_rC_r+L_pC_p+L_pC_r-\sqrt{\left(L_rC_r+L_pC_p+L_pC_r\right)^2-4L_rC_rL_pC_p}}{2L_rC_rL_pC_p}} \approx \frac{1}{2\pi}\sqrt{\left(L_r+L_p\right)C_r} \qquad (2.1)$$

$$f_{o2} = \frac{1}{2\pi}\sqrt{\frac{1}{L_pC_p}} \qquad (2.2)$$

$$f_{o3} = \frac{1}{2\pi}\sqrt{\frac{L_rC_r+L_pC_p+L_pC_r+\sqrt{\left(L_rC_r+L_pC_p+L_pC_r\right)^2-4L_rC_rL_pC_p}}{2L_rC_rL_pC_p}} \approx \frac{1}{2\pi}\sqrt{L_r\frac{C_rC_p}{(C_r+C_p)}} \qquad (2.3)$$

Fig. 2.34shows the waveforms of under full load condition. The tank current is more like square waveform which combines fundamental and 3^{rd} harmonics. Fig. 2.35 shows the tank waveforms under short-circuit condition. The output current is limited to less than half load.

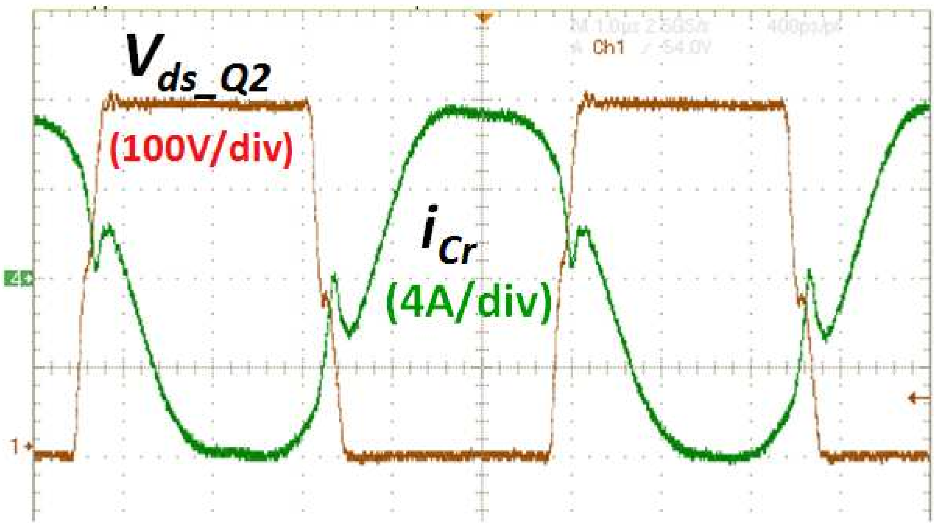

Fig. 2.34 Experimental results for 5-element resonant converters under full load

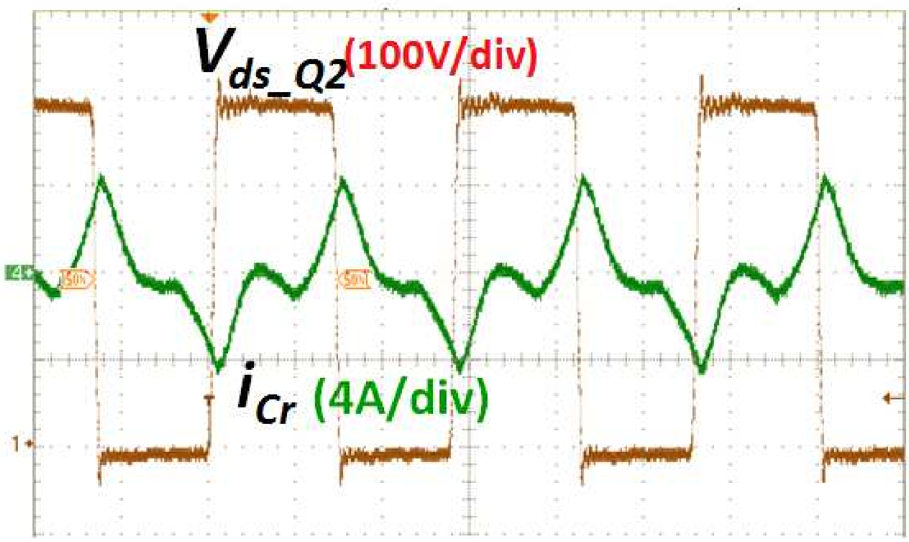

Fig. 2.35 Experimental results of 5-element resonant converters under short-circuit condition

2.7 Conclusion

A systematic method to classify and select resonant tanks is proposed. Three-element, four-element and five-element resonant tanks are analyzed based on the proposed principle.

Chapter 3. Evaluation of LLC-like Resonant Converters

In this chapter, a general evaluation system is proposed to help evaluate the performance of resonant converters. State-plane analysis with new normalization is proposed to evaluate the resonant converter performance. Based on it, the voltage stress, current stresses and apparent power of resonant converters are easy to compare. This method can help select suitable circuit topology for certain application. Meanwhile, it also can help resonant converters' design. The important performance factors, like start-up, short-circuit protection, SR driving and EMI, are also taken into account for the whole evaluation system.

3.1 Introduction

There are still many candidate topologies which fits required characteristics based on previous selection methodology. It is not enough to choose resonant topologies based on the combination of resonant frequencies. Thus, several evaluation methods are proposed. First, the current stress of primary devices is major concern, because it will determine the conduction of primary side. Secondly, the voltage stress on resonant capacitor is still important due to the life time of capacitor. Then, the integration is taken into consideration, which includes the ease of magnetic integration and the impacts of integration, including synchronous rectifier drive, EMI noise, transformer loss, etc.

3.2 State-Trajectory Analysis of LLC Resonant Converter

In order to determine the optimal trajectory under transition conditions, the state-plane analysis is introduced. In [C.1]-[C.3], the state plane is presented to analyze the SRC steady state and transient behavior. In this section, we extend this approach to the LLC resonant converter.

To simplify the analysis, it is assumed that the output capacitor is large enough that the output voltage (V_o) can be approximated to be constant. A second assumption is that the circuit losses, including the resonant tank, switch, and filter losses, are negligible.

Under these conditions, the LLC resonant converter can be viewed as a piecewise linear system switching among six possible linear stages.

- **Operation stage I**

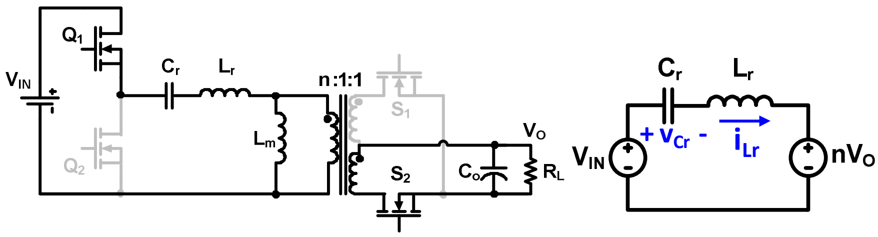

Fig. 3.1 Equivalent circuit of stage I

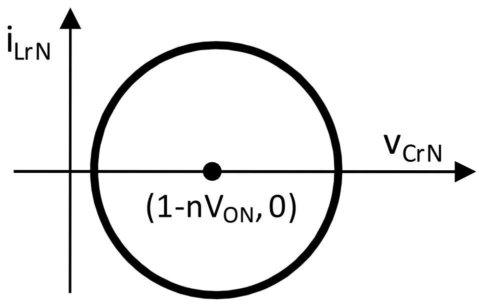

Fig.3.2 State-trajectory of stage I

The primary main switch Q_1 turns on, and the resonant current flows through the secondary-side synchronous rectifier S_2. In this stage, the magnetizing inductor L_m is clamped by the output voltage. The equivalent circuit is shown in Fig. 3.1, where the resonant capacitor C_r and the resonant inductor L_r form the series resonant tank. The source voltage across the resonant tank is V_{in}-nV_o. Thus, we can write:

$$\dot{v}_{Cr} = \frac{1}{C_r} i_{Lr} \tag{3.1}$$

$$\dot{i}_{Lr} = -\frac{1}{L_r} v_{Cr} + \frac{1}{L_r}\left(V_{in} - nV_o\right) \tag{3.2}$$

Wherev$_{Cr}$ and i_{Lr} are the resonant capacitor voltage and resonant inductor current. Combining (5.1) and (5.2), v_{Cr} and i_{Lr} can be expressed as:

$$v_{Cr} - \left(V_{in} - nV_o\right) = I_{Lr0} \cdot Z_0 \cdot \sin\left[\omega_0\left(t - t_0\right)\right] + \left[V_{Cr0} - \left(V_{in} - nV_o\right)\right] \cdot \cos\left[\omega_0\left(t - t_0\right)\right] \tag{3.3}$$

$$i_{Lr} = I_{Lr0} \cdot \cos\left[\omega_0\left(t - t_0\right)\right] - \frac{V_{Cr0} - \left(V_{in} - nV_o\right)}{Z_0} \cdot \sin\left[\omega_0\left(t - t_0\right)\right]. \tag{3.4}$$

where V_{Cr0} and I_{Lr0}, are the initial conditions at time t=t_0, $Z_0 = \sqrt{L_r/C_r}$ is the characteristic impedance, and $\omega_0 = 1\big/\sqrt{L_r C_r}$ is the resonant frequency.

By normalizing all voltages with the voltage factor V_{in}, and all currents with the current factor V_{in}/Z_0 in (5.3) and (5.4), the following expressions are derived:

$$v_{CrN}-(1-nV_{oN})=I_{Lr0N}\cdot\sin[\omega_0(t-t_0)]+[V_{Cr0N}-(1-nV_{oN})]\cdot\cos[\omega_0(t-t_0)] \tag{3.5}$$

$$i_{LrN}=I_{Lr0N}\cdot\cos[\omega_0(t-t_0)]-[V_{Cr0N}-(1-nV_{oN})]\cdot\sin[\omega_0(t-t_0)]. \tag{3.6}$$

The subscript N in (5.5) and (5.6) refers to normalized circuit variables.

From (5.5) and (5.6), the trajectory equation is given by:

$$[v_{CrN}-(1-nV_{oN})]^2+i_{LrN}{}^2=[V_{Cr0N}-(1-nV_{oN})]^2+I_{Lr0N}{}^2, \tag{3.7}$$

which behaves as a circle as shown in Fig. 5.2, whose center (1-nV_{oN}, 0) is determined by the source voltage across the tank, and radius depends on the initial conditions: V_{Cr0} and I_{Lr0}.

- **Operation stage II**

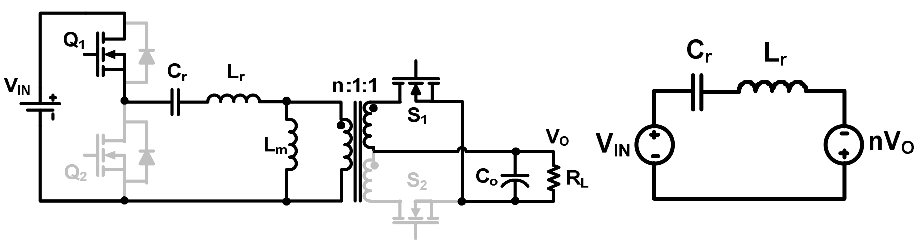

Fig. 3.3 Equivalent circuit of stage II

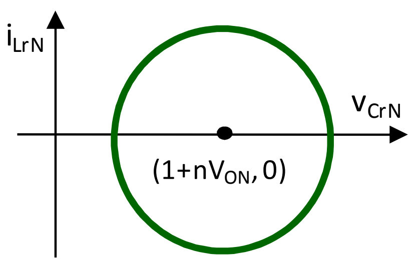

Fig. 3.4State-trajectory of stage II

In operation stage II, Q_1 is on, but the current flowing through the secondary side changes its direction as shown in Fig. 3.3. This occurs when the switching frequency is larger than the resonant frequency (i.e. $f_s>f_0$). This stage is similar to Stage I, but the source voltage across the resonant tank changes to $V_{in}+nV_o$.

Similar to Stage I, the trajectory expression is given by:

$$[v_{CrN}-(1+nV_{oN})]^2+i_{LrN}{}^2=[V_{Cr0N}-(1+nV_{oN})]^2+I_{Lr0N}{}^2, \tag{3.8}$$

which behaves as a circle as well, but the center changes to $(1+nV_{oN}, 0)$ as shown in Fig. 3.4.

- **Operation stage III:**

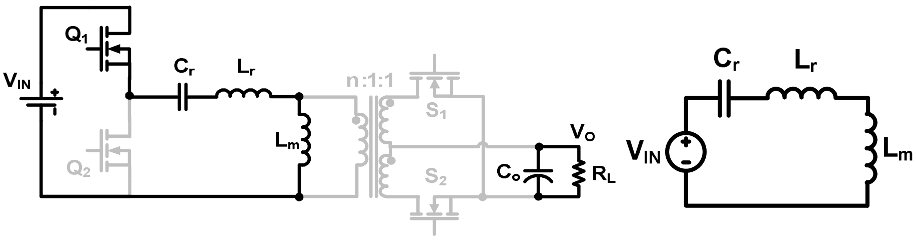

Fig. 3.5Equivalent circuit of stage III

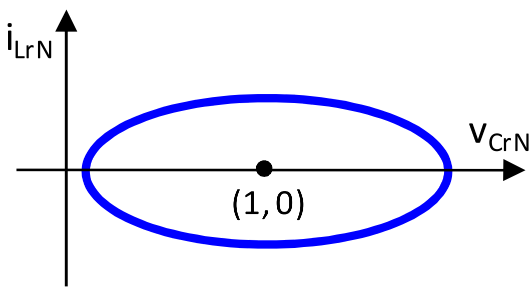

Fig. 3.6 State-trajectory of stage III

In operation stage III, Q_1 is on, but there is no current flowing through the secondary side. This stage occurs when $f_s<f_0$. In this stage, the magnetizing inductor L_m joins the resonance. The equivalent circuit is shown in Fig. 3.5, where C_r, L_r, and L_m form the series resonant tank. The source voltage across the resonant tank is V_{in}, and:

$$\dot{v}_{Cr} = \frac{1}{C_r} i_{Lr} \tag{3.9}$$

$$\dot{i}_{Lr} = -\frac{1}{L_r + L_m} v_{Cr} + \frac{1}{L_r + L_m} V_{in} \tag{3.10}$$

From (5.9) and (5.10), v_{Cr} and i_{Lr} in Stage III are given by:

$$v_{Cr} - V_{in} = I_{Lr0} \cdot Z_1 \cdot \sin[\omega_1 (t - t_0)] + (V_{Cr0} - V_{in}) \cdot \cos[\omega_1 (t - t_0)] \tag{3.11}$$

$$i_{Lr} = I_{Lr0} \cdot \cos[\omega_1 (t - t_0)] - \frac{V_{Cr0} - V_{in}}{Z_1} \cdot \sin[\omega_1 (t - t_0)], \tag{3.12}$$

where $Z_1 = \sqrt{(L_r + L_m)/C_r}$ is the characteristic impedance, and $\omega_1 = 1/\sqrt{(L_r + L_m)C_r}$ is the resonant frequency when L_m is in the resonance.

With the same normalization factors, the normalized forms of v_{Cr} and i_{Lr} are

$$v_{CrN} - 1 = \frac{I_{Lr0N}}{Z_0/Z_1} \cdot \sin[\omega_1 (t - t_0)] + (V_{Cr0N} - 1) \cdot \cos[\omega_1 (t - t_0)] \tag{3.13}$$

$$\frac{i_{LrN}}{Z_0/Z_1} = \frac{I_{Lr0N}}{Z_0/Z_1}\cdot\cos[\omega_1(t-t_0)] - (V_{Cr0N}-1)\cdot\sin[\omega_1(t-t_0)]. \tag{3.14}$$

The trajectory is obtained from (4.13) and (4.14):

$$(v_{CrN}-1)^2 + \left(\frac{i_{LrN}}{Z_0/Z_1}\right)^2 = (V_{Cr0N}-1)^2 + \left(\frac{i_{Lr0N}}{Z_0/Z_1}\right)^2, \tag{3.15}$$

which behaves as an ellipse with a center (1,0) as shown in Fig. 3.6. Since L_m participates in the resonance, the characteristic impedance Z_1 becomes large ($Z_1>Z_0$). If it is normalized with the same current factor V_{in}/Z_0, the trajectory will be an ellipse.

If switch Q_1 is off and Q_2 turns on, there are another three operation stages:

- **Operation stage IV**

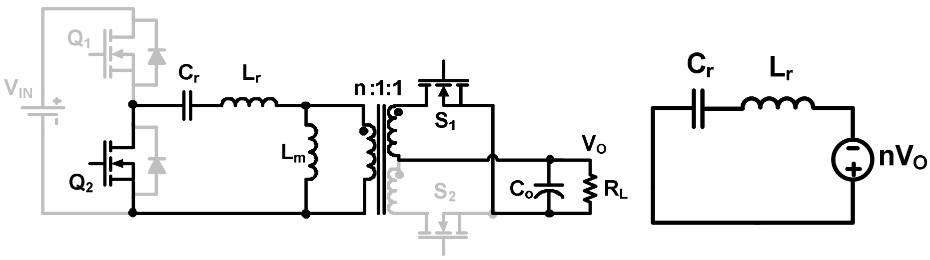

Fig. 3.7 Equivalent circuit of stage IV

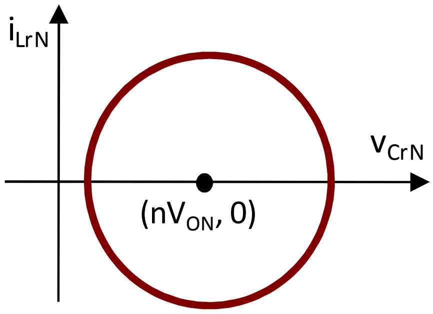

Fig. 3.8 State-trajectory of stage IV

In operation stage IV, the primary-side main switch Q_2 turns on, and the resonant current flows through the secondary-side SR S_1 as shown in Fig. 3.7. The only difference from Stage I is the source voltage across resonant tank becomes nV_o. Deriving the normalized equation for the state trajectory, we get:

$$(v_{CrN} - nV_{oN})^2 + i_{LrN}{}^2 = (V_{Cr0N} - nV_{oN})^2 + I_{Lr0N}{}^2 , \tag{3.16}$$

and thus, the circle center changes to (nV_{oN}, 0) as shown in Fig. 3.8.

- **Operation stage V**

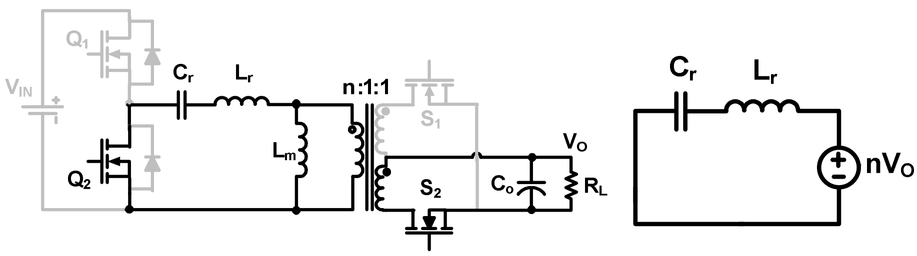

Fig. 3.9 Equivalent circuit of stage V

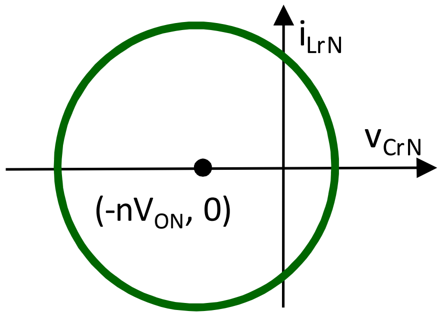

Fig. 3.10State-trajectory of stage V

In operation stage V, Q_2 is on, but the current on the secondary side changes its direction, flowing through S_2, as shown in Fig. 3.9. This occurs when $f_s>f_0$, similar to stage II. The normalized expression for the trajectory is:

$$(v_{CrN}+nV_{oN})^2+i_{LrN}{}^2=(V_{Cr0N}+nV_{oN})^2+I_{Lr0N}{}^2 \; . \tag{3.17}$$

Now the circle center changes to $(-nV_{oN}, 0)$ as shown in Fig. 3.10.

- **Operation stage VI**

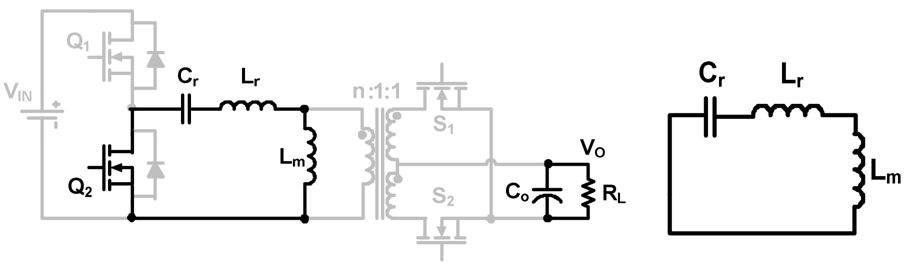

Fig. 3.11Equivalent circuit of stage VI

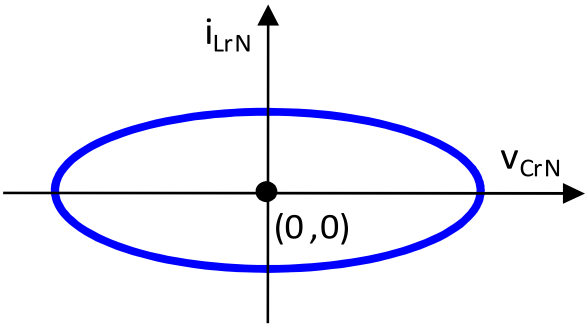

Fig. 3.12State- trajectory of stage VI

In operation stage VI, Q_2 is on, but there is no current flowing through the secondary side. This stage happens when $f_s<f_0$. Like in stage III, C_r, L_r and L_m form the series resonant tank. But the source voltage across the resonant tank changes to 0. The trajectory after normalization is:

$$v_{CrN}{}^2 + \left(\frac{i_{LrN}}{Z_0/Z_1}\right)^2 = V_{Cr0N}{}^2 + \left(\frac{I_{Lr0N}}{Z_0/Z_1}\right)^2, \tag{3.18}$$

which is an ellipse as in stage III, but with a center (0, 0) shown in Fig. 3.12.

The LLC steady-state trajectory is the combination of the above six operation stages. Fig. 3.13 shows the time-domain waveforms when the LLC operates at the resonant frequency point ($f_s=f_0$). Fig. 3.14shows the corresponding trajectory locus when mapping the normalized resonant current i_{LrN} and resonant voltage v_{CrN} to the state plane. To the half-bridge LLC resonant converter, when $f_s=f_0$, the voltage gain is one; that is, $nV_{oN}=0.5$. Therefore, the two half circles of Stage I and Stage IV have the same center (0.5, 0), which combine to form one whole circle.

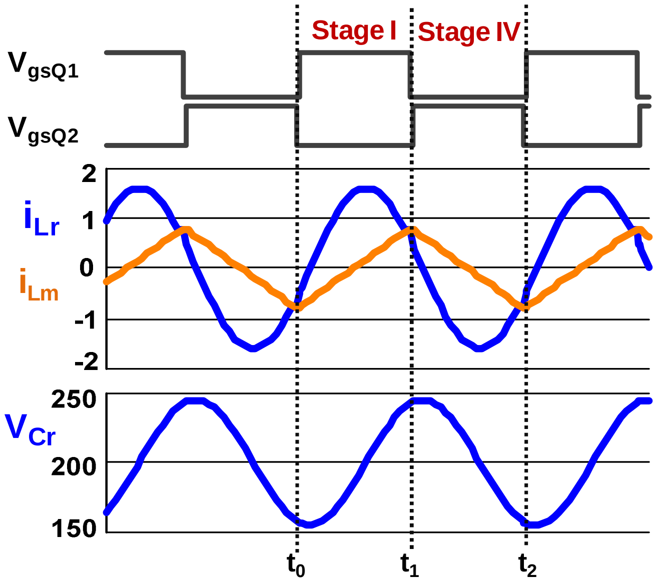

Fig. 3.13Steady-state time-domain waveforms when $f_s=f_0$

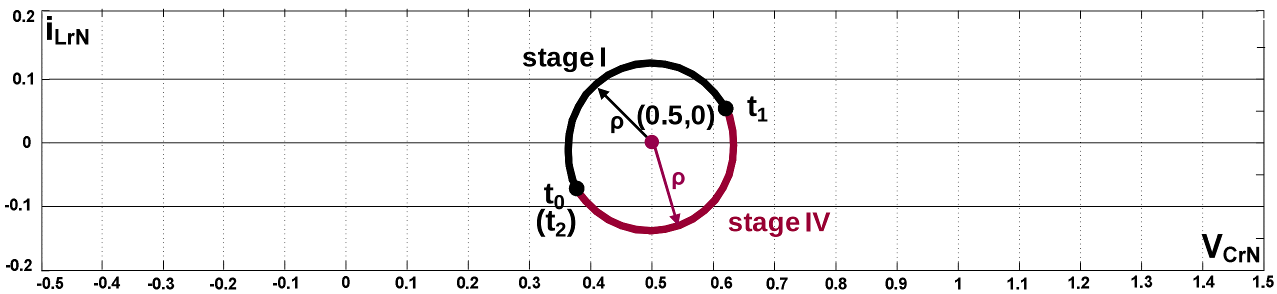

Fig. 3.14Steady-state trajectory when $f_s=f_0$

When the LLC operates below the resonant frequency region ($f_s<f_0$), the magnetizing inductor L_m participates in the resonance from times t_1 to t_2 and from t_3 to t_4, as shown in Fig. 3.15. When mapping to the state plane in Fig. 3.16, there are two partial ellipse trajectory loci of Stage III and Stage VI, connecting two half circles of Stage I and Stage IV with split centers. In fact, when $f_s<f_0$, the voltage gain is larger than one (i.e., $nV_{oN}>0.5$), and the circle center of

StageI is on the left of (0.5, 0), since $1\text{-}nV_{oN}<0.5$; and the circle center of Stage IV is on the right of (0.5, 0), since $nV_{oN}>0.5$.

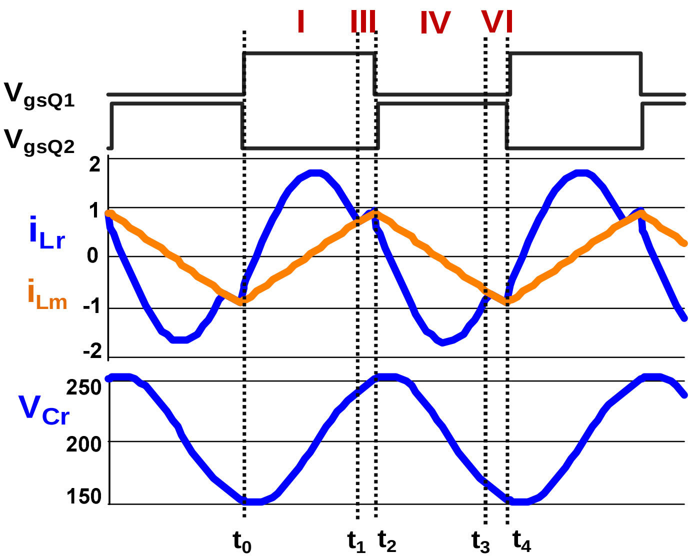

Fig. 3.15 Steady-state time-domain waveforms when $f_s<f_0$

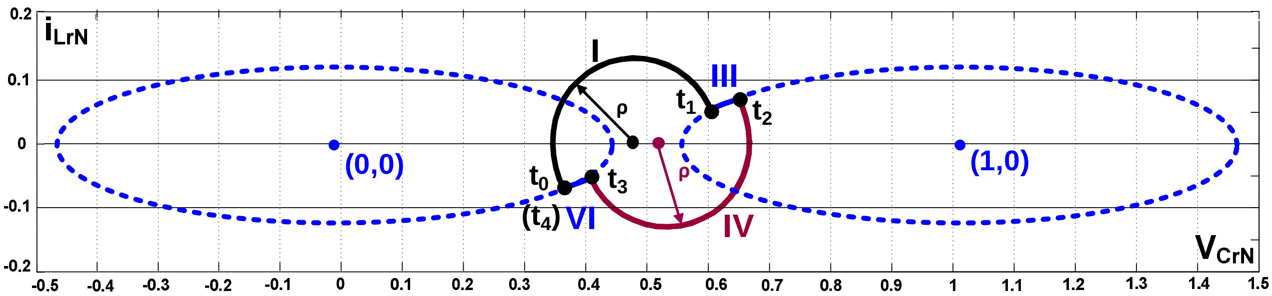

Fig. 3.16 Steady-state trajectory when $f_s<f_0$

In Fig. 3.17and Fig. 3.18, the LLC operates above the resonant frequency region ($f_s>f_0$). From time t_1 to t_2, it operates in Stage V, which corresponds to the partial locus of the large circle, whose center is located near (-0.5, 0). Similarly, from times t_3 to t_4, it operates in Stage II, corresponding to the partial locus of another large circle whose center is located near (1.5, 0).

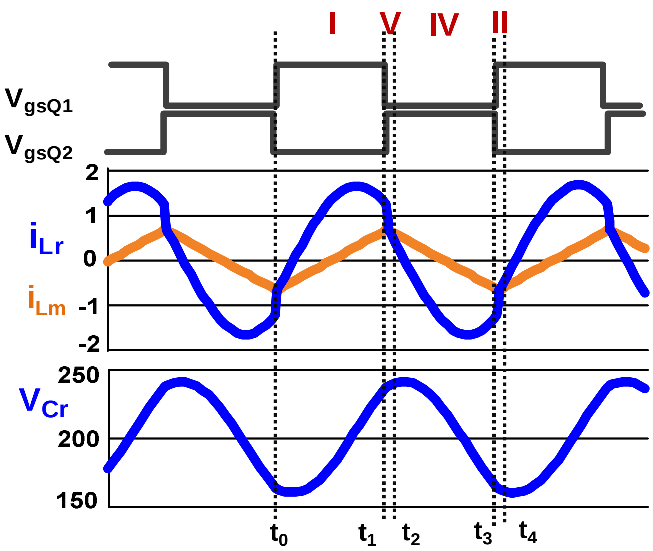

Fig. 3.17 Steady-state time-domain waveforms when $f_s>f_0$

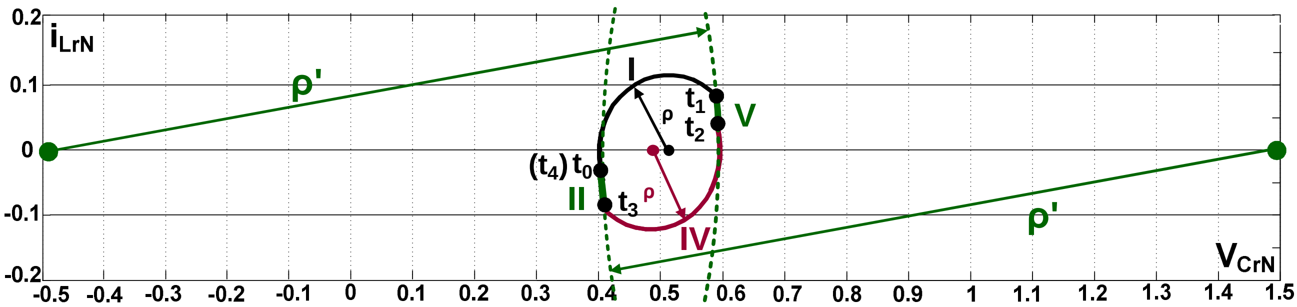

Fig. 3.18 Steady-state trajectory when $f_s>f_0$

3.3 New Normalization for State-plane

State-plane analysis was found to be a simple, yet powerful method which can clearly portray the steady-state and transient operation of resonant converters. Also, the current stress and voltage stress of resonant components can be observed in one single figure. Significantly the state plane directly indicates the resonant tank energy level at which the system is operating.

As stated above, state plane of resonant converters is good tool to analyze the performance of whole converter. However, if we want to compare different design of same topologies or different topologies, there are some revisions needed. Previous state-plane analysis is based on same normalize factors, which are V_{in} for voltage, $\boldsymbol{V_{in}/Z_o}$ for current, as shown in Equation (3.19). Z_o is the characteristic impedance of resonant converter.

$$V_N = V_{in} \quad \mathrm{I_N} = \mathrm{V_{in}/Z_o} \tag{3.19}$$

However, Z_o is varied in different designs or different topologies. For resonant converters having two or more resonant frequencies, Z_o is even varied at different time period. It is hard to compare the performance based on $\boldsymbol{V_{in}/Z_o}$.

Fig. 3.19 gives a comparison example of LLC and CLL resonant converters. Both converters work at same condition: V_{in}/V_o=400V/12V, output power P_o=250W, switching frequency f_s=1Mhz. The input current waveforms of two converters are the same. However, the normalized currents do not represent the real current value due to the different characteristic impedance Z_o. In this example, $Z_0 = \sqrt{L_r/C_r} = 88$ for LLC, and $Z_0 = \sqrt{L_1 \cdot L_2/(L_1 + L_2)/C_r} = 131$ for CLL.

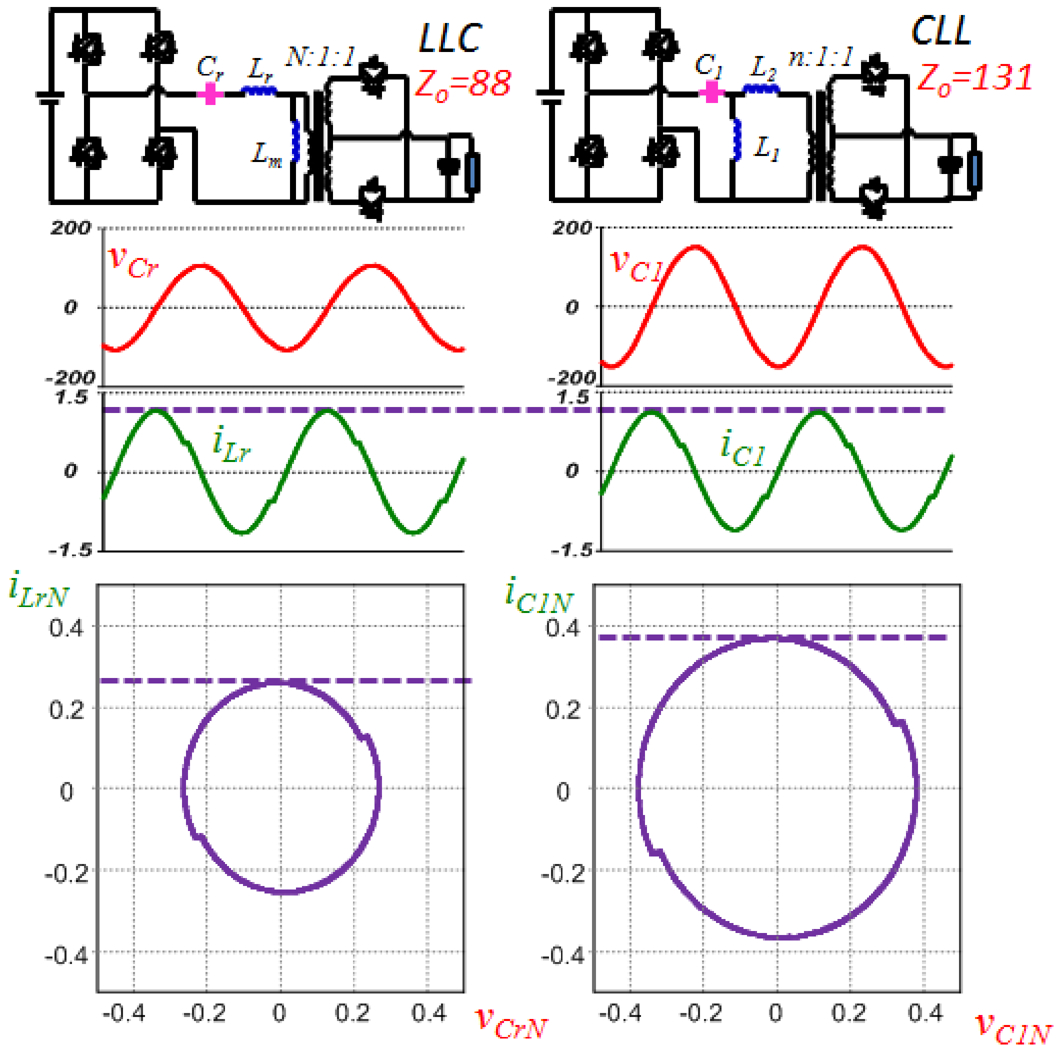

Fig. 3.19LLC and CLL state-plane comparison based on conventional normalization

For given application, the output power P_o and input voltage $\boldsymbol{V_{in}}$ are fixed. These two values are independent with resonant topology. $\boldsymbol{P_o/V_{in}}$ also means the average input current assuming no loss in the converter. ***Thus, P_o/V_{in} is an ideal normalized factor for current.*** Meanwhile, $\boldsymbol{V_{in}}$ is the voltage normalizing factor, as shown in Equation (3.20). In the resonant converters, primary side current represents the conduction loss of primary side devices, and the voltage cross capacitor express the life time of it. Thus, the state-plane of them can illustrate those key performances.

$$\mathrm{V_N} = \mathrm{V_{in}} \quad \mathrm{I_N} = \mathrm{P_o}/\mathrm{V_{in}} \tag{3.20}$$

Because of full bridge structure, the rms value of input voltage equals its average value. At the same time, normalized input current $\boldsymbol{I_{inNRMS}}$ equals the apparent power $\boldsymbol{P_{appr}}$ over output power $\boldsymbol{P_o}$.as shown in Equation (3.21).

$$\mathrm{I_{inNRMS}} = \mathrm{I_{inRMS}}/(\mathrm{P_o}/\mathrm{V_{in}}) = \mathrm{I_{inRMS}} \times \mathrm{V_{in}}/\mathrm{P_o} = \mathrm{P_{appr}}/\mathrm{P_o} \tag{3.21}$$

Series resonant converter is taken as an example to illustrate how to utilize the new normalization factors.

When SRC operates at resonant frequency, the tank impedance is zero. The input voltage of resonant tank is square waveform, while the input current is sinusoidal waveform, as shown in Fig. 3.20. Only fundamental of input voltage contributes real power, while high order harmonics of input voltage do not. The RMS value for fundamental of input voltage is shown in Equation (3.22).

$$V_{1\_\mathrm{inRMS}} = \frac{2\sqrt{2}}{\pi} \cdot \mathrm{V_E} \tag{3.22}$$

The apparent power of whole converter with new normalization factors is

$$\mathrm{P}_{appr\_N} = \frac{\mathrm{P_{appr}}}{\mathrm{P_o}} = \frac{\mathrm{V_E} \cdot \mathrm{I_{inRMS}}}{\frac{2\sqrt{2}}{\pi} \cdot \mathrm{V_E} \cdot \mathrm{I_{inRMS}}} = \frac{1}{\frac{2\sqrt{2}}{\pi}} \approx 1.11 = \mathrm{I_{inNRMS}} \tag{3.23}$$

That means 11% extra power is the minimal value for resonant converter operation.

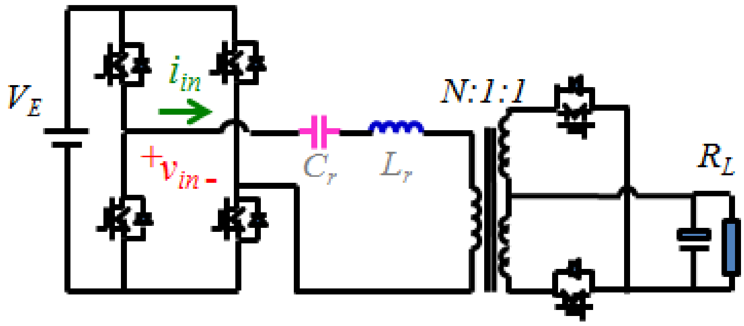

(a) Series Resonant Converter

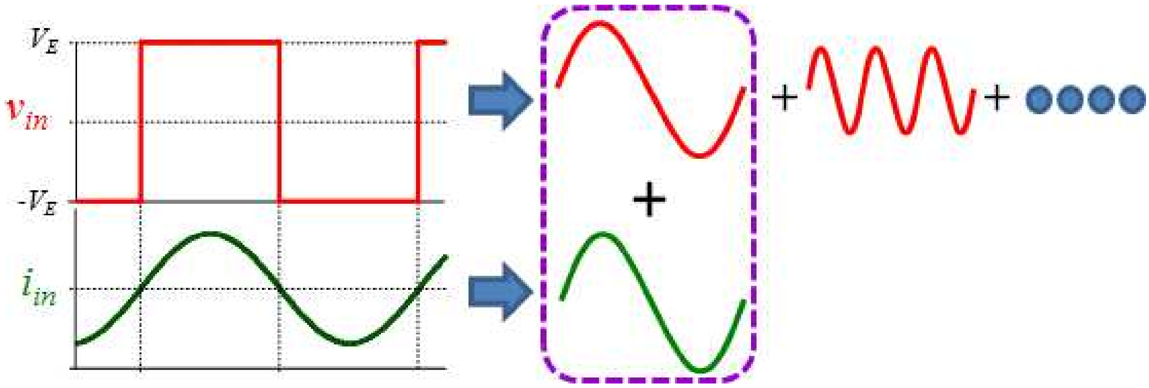

(b) Fourier transform of input voltage v_{in} and input current i_{in}

Fig. 3.20Series resonant converter operates at resonant frequency

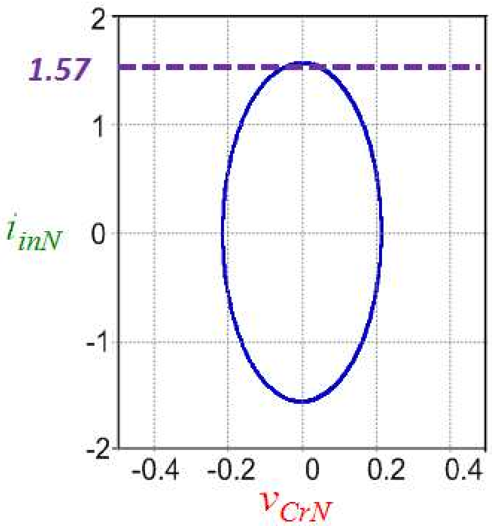

Fig. 3.21State-plane of SRC operates at resonant frequency

Fig. 3.21 shows the state-plane of SRC at resonant frequency. The amplitude of normalized current is $1.57 = 1.11 \times \sqrt{2}$, which is the minimal value of normalized current.

Design factors for LLC are shown in Equation (3.24). L_n is the ratio of magnetizing inductance L_m and resonant inductor L_r. Q is the quality factor. C_r is the resonant capacitor. R_L represents the full load. n is the transformer turns ratio.

$$L_n = L_m/L_r \qquad Q = \sqrt{L_r/C_r}/(n^2 R_L) \qquad f_o = 1/\left(2\pi\sqrt{L_r/C_r}\right) \tag{3.24}$$

Fig. 3.22(a) is the voltage gain curves of LLC, when L_n=12.5. Fig. 3.22(b) plots the steady state-plane under new normalized factor for different Q and same L_n under full load. The voltage and current stresses of different design can be easily compared in one coordinate system.

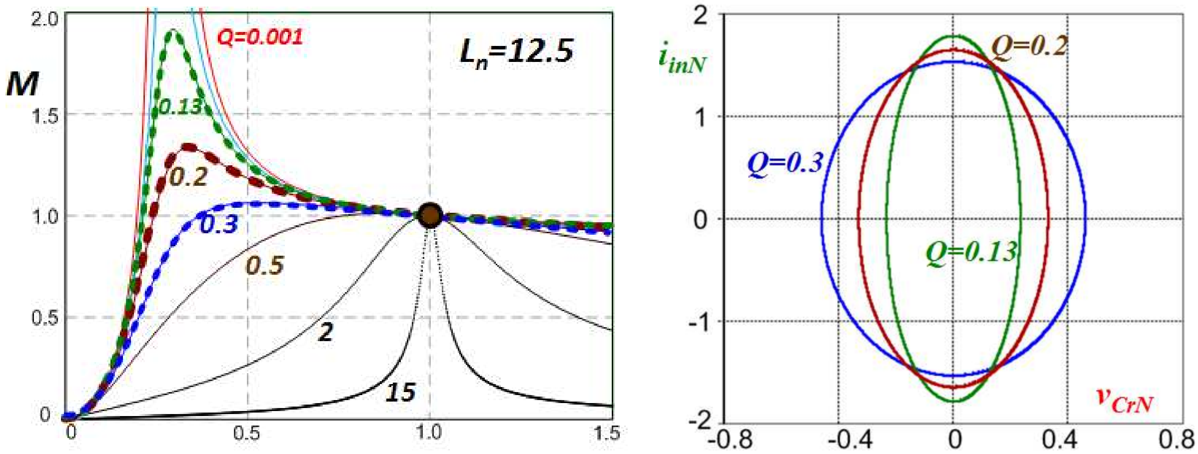

(a) Voltage gain curves of LLC (b) State-plane of given design @full load

Fig. 3.22 Steady-state trajectory when $f_s=f_0$

Fig. 3.23plots the steady state-plane under new normalized factor for different Q and same L_n under full load. The voltage and current stresses of different design can be easily compared in one coordinate system.

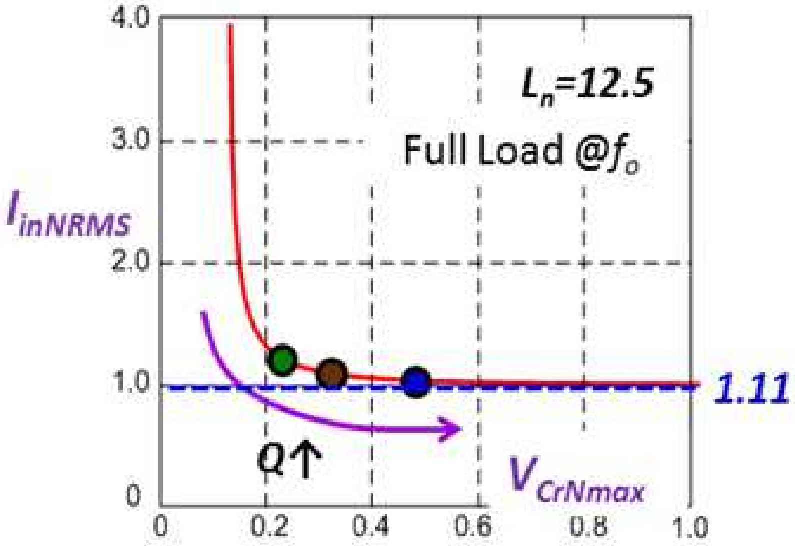

Fig. 3.23V-I stresses of LLC resonant converters for L_n=12.5

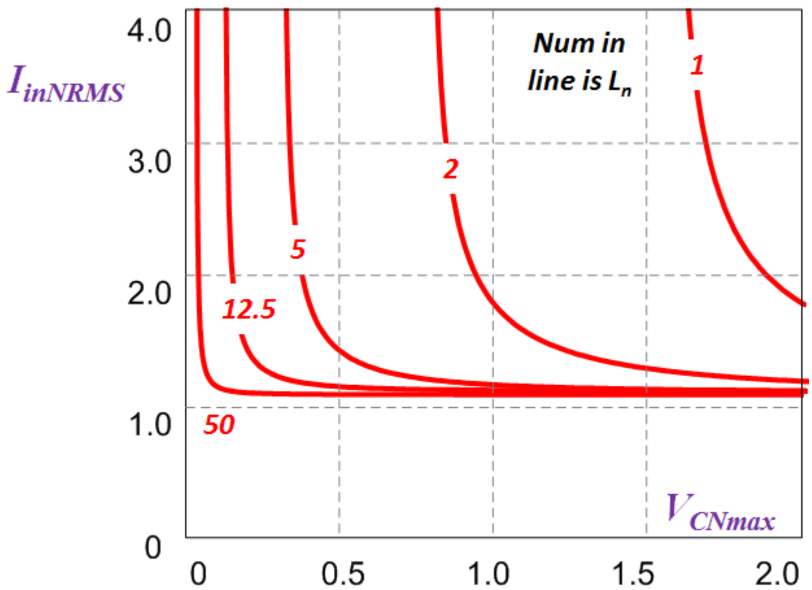

Fig. 3.24V-I stresses of LLC resonant converters for different L_n

Fig. 3.24depicts the voltage and current stress of LLC for different L_n and *Q*. Each line in Fig. 3.24means those designs sweep *Q* for one L_n. As *Q* increases, the current stress decrease, and the voltage stress rises. The optimal design for each L_n should be around knee point of according line. It is also known that the large the L_n is, the smaller voltage and current stresses the knee point locates. And it is also known that the minimal apparent power of LLC is 1.11 times of output power.

Based on chapter 4, there are three good candidates in three-element resonant topologies. The V-I stress figure is easily drawn for other two resonant topologies.

Fig. 3.25gives the LCL resonant converter. Fig. 3.26shows the whole picture of LCL resonant converter V-I stress.

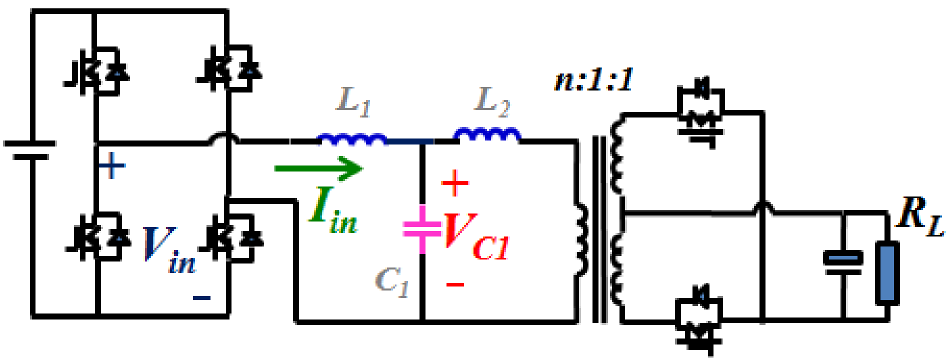

Fig. 3.25LCL Resonant Converter

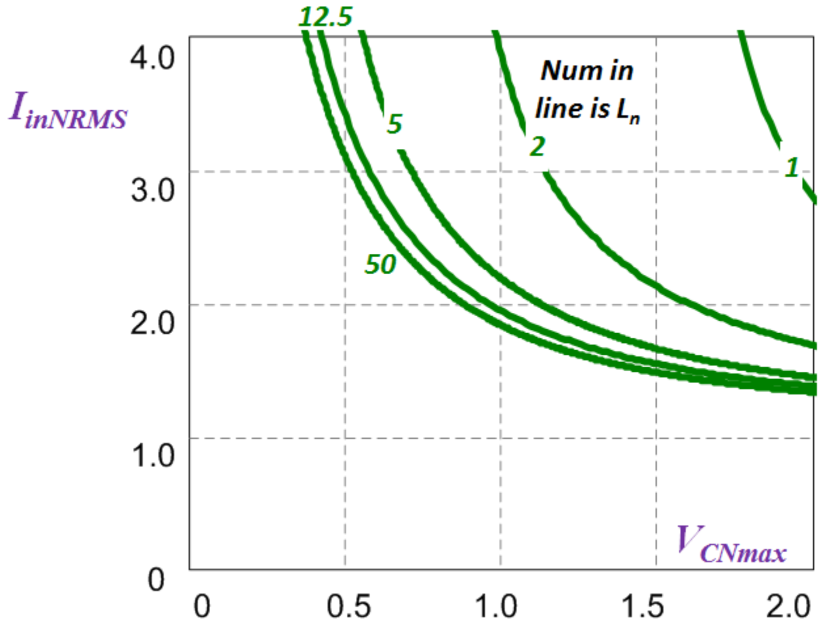

Fig. 3.26V-I stresses of LCL resonant converters for different L_n

Fig. 3.27gives the CLL resonant converter. Fig. 3.28shows the whole picture of LCL resonant converter V-I stress.

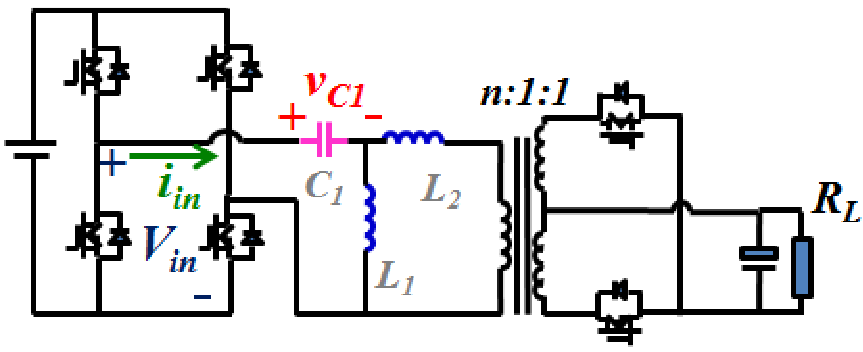

Fig. 3.27CLL Resonant Converter

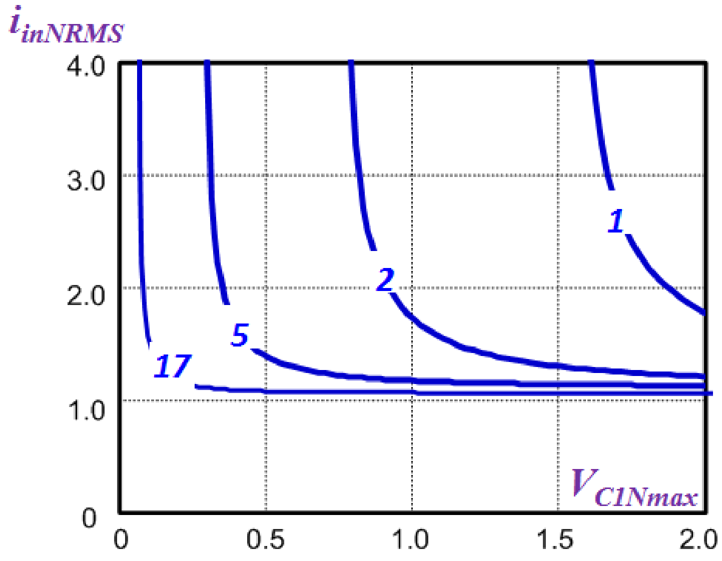

Fig. 3.28V-I stresses ofCLL resonant converters for different L_n

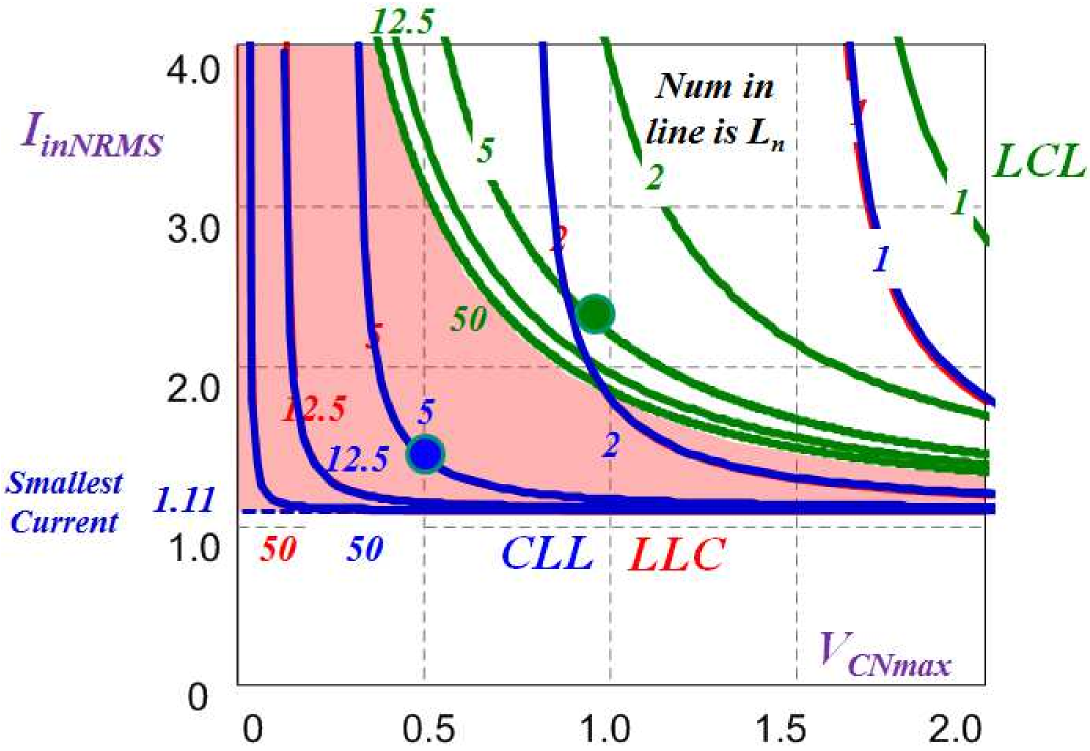

Fig. 3.29V-I stresses ofthree-element resonant converters for different L_n

Fig. 3.29 gives the V-I stress comparison of all three 3-element resonant converters. It is obvious that LCL resonant converter have larger voltage and current stress than CLL and LLC resonant converters. The shadow area shows the difference.

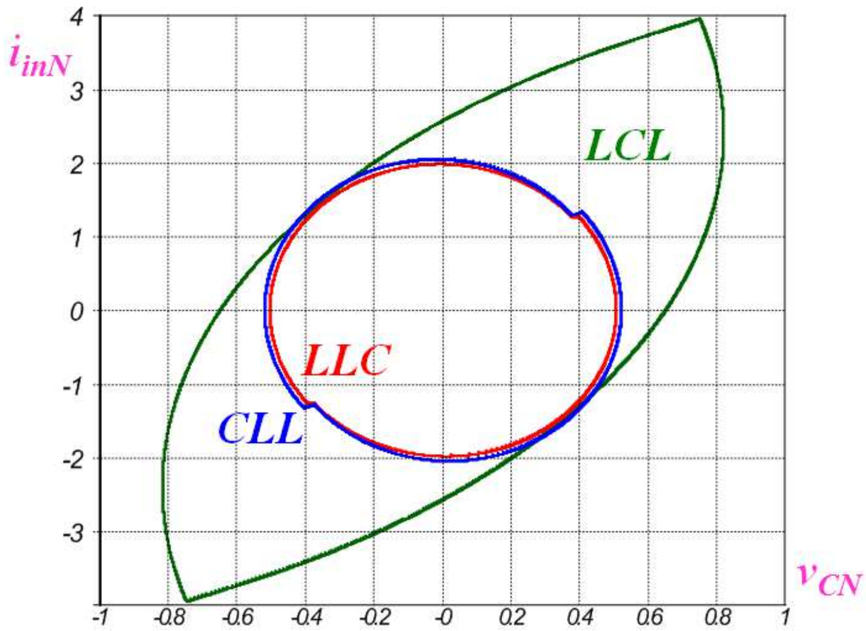

Fig. 3.30 V-I stresses of three-element resonant converters for different L_n

One design for each topology is chosen to depict in state-plane based on proposed normalized factor in Fig. 3.30. Each design is one dot shown in Fig. 3.29.

3.4 Evaluation based on Startup, Synchronous Rectifier and EMI

Startup and short-circuit protection are not good in LLC resonant converter. Fig. 3.31gives one example of LLC resonant converter startup procedure. The LLC resonant converter starts up at one higher frequency than resonant frequency, where current stress depends on current gain. The output voltage gradually increases at this frequency. When it reaches one preset voltage, the switching frequency slowly decrease to resonant frequency. The whole start up progress is shown as dot line in Fig. 3.31.

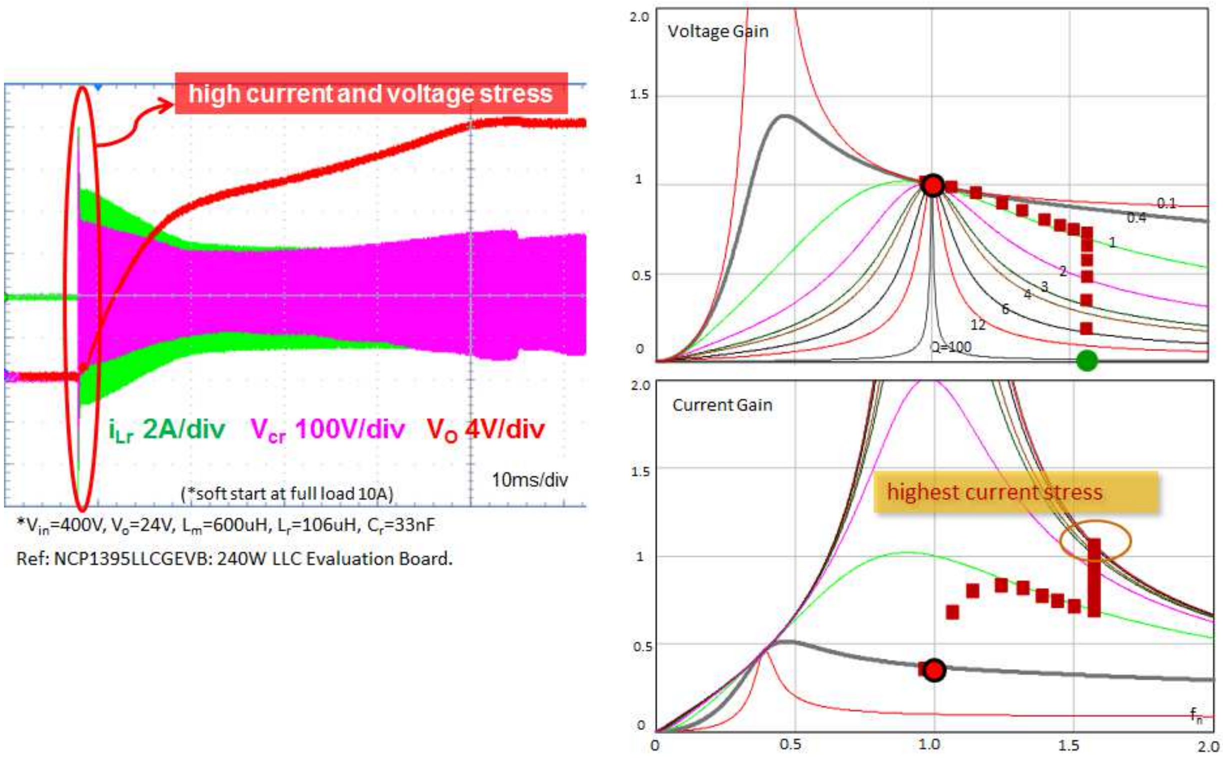

Fig. 3.31Startup example of LLC Resonant Converter

The key problem in LLC startup is the current stress is very high.

Fig. 3.32presents the voltage gain and current gain curves comparison of three-element resonant converters. It is clear that CLL resonant converter has the same problem as LLC. However, the LCL resonant converter is quite different. The startup current of LCL resonant converter is small compare with the full load current.

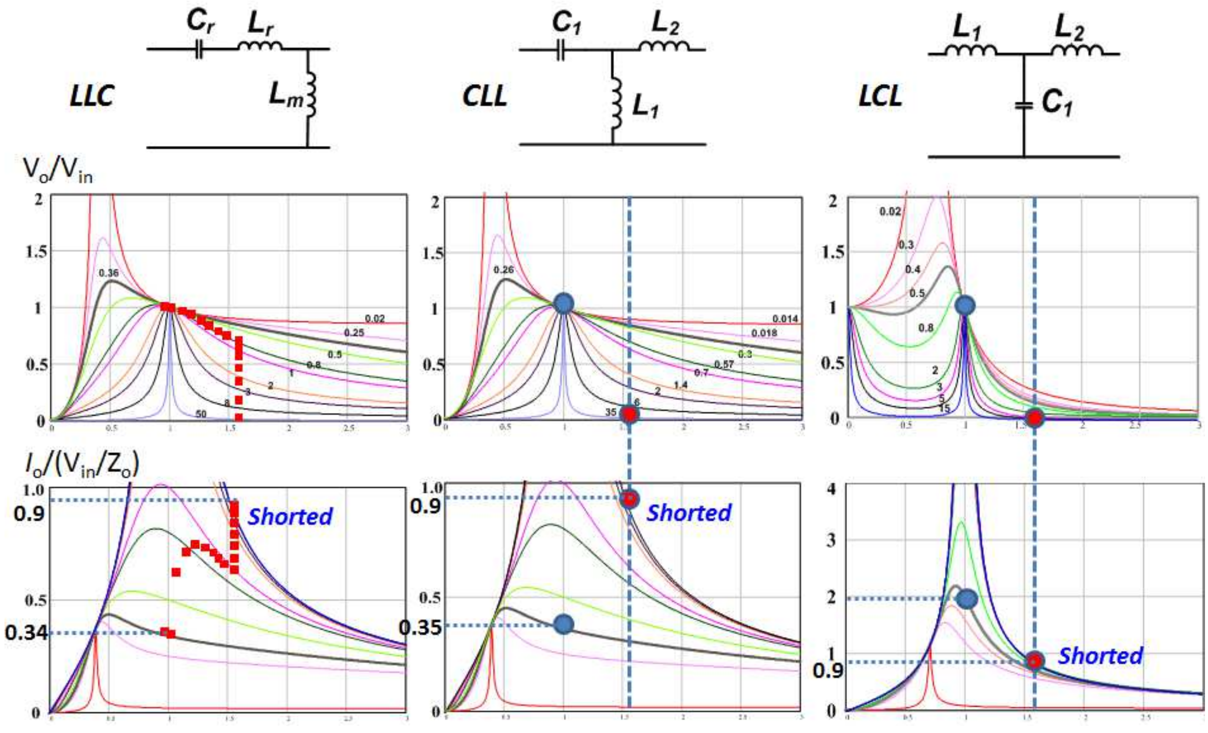

Fig. 3.32Startup Comparison of LLC, CLL & LCL Resonant Converters

The accurate synchronous rectifier drive is very critical in high output application for resonant converters. Utilizing primary side current of transformer is very easy way to get precise SR drive signal.

The LLC resonant converter normally integrates the magnetizing inductance into the transformer. The magnetizing current will give phase shift between primary and secondary current. That is the reason LLC resonant converter cannot use primary side current for SR drive. In another side, LLC can use primary side current without integrate L_m and L_r, which cause power density suffers.

CLL and LCL resonant converter is different as shown in Fig. 3.33. Both of them can integrate the leakage inductance without suffer SR drive.

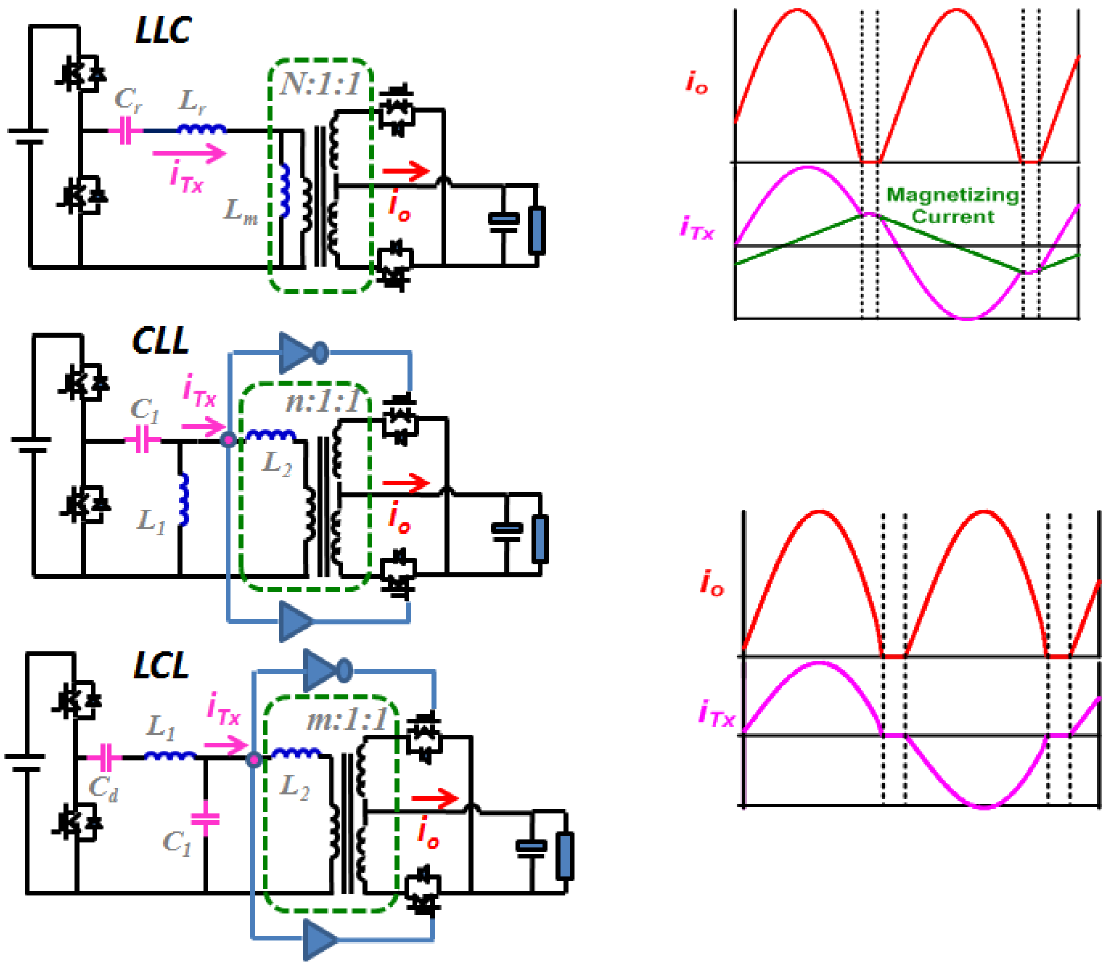

Fig. 3.33SR drive Comparison of LLC, CLL & LCL Resonant Converters

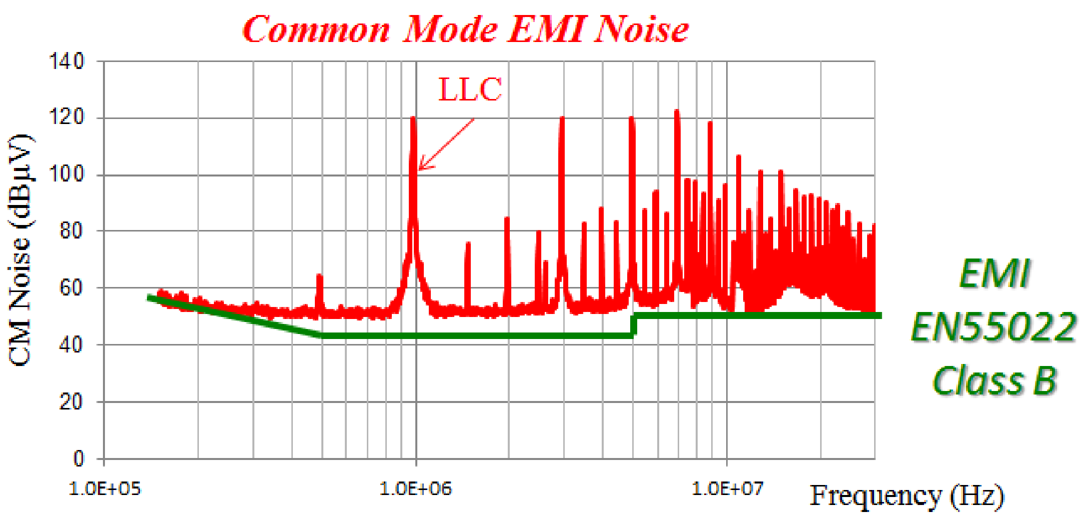

Fig. 3.34CM noise spectrum of LLC Resonant Converter

LLC resonant converter has high common mode noise at and beyond switching frequency. One example is shown in Fig. 3.34compared with EMI standard. The common mode noise path is given in Fig. 3.35.

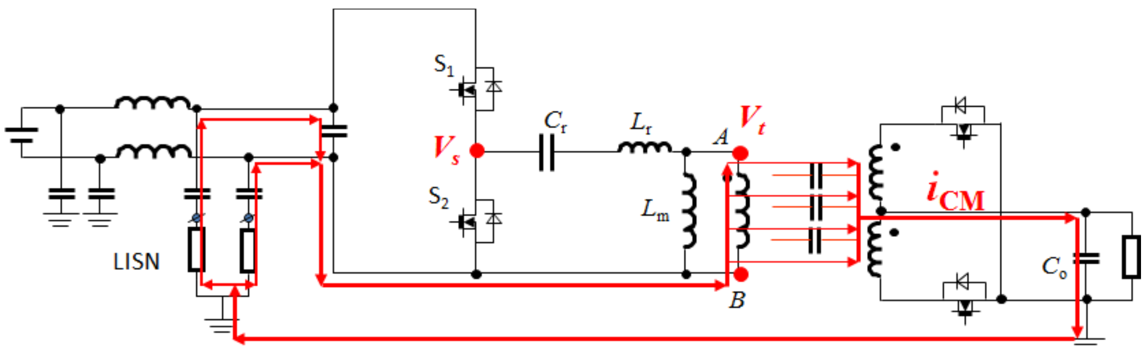

Fig. 3.35CM noise path of LLC Resonant Converter

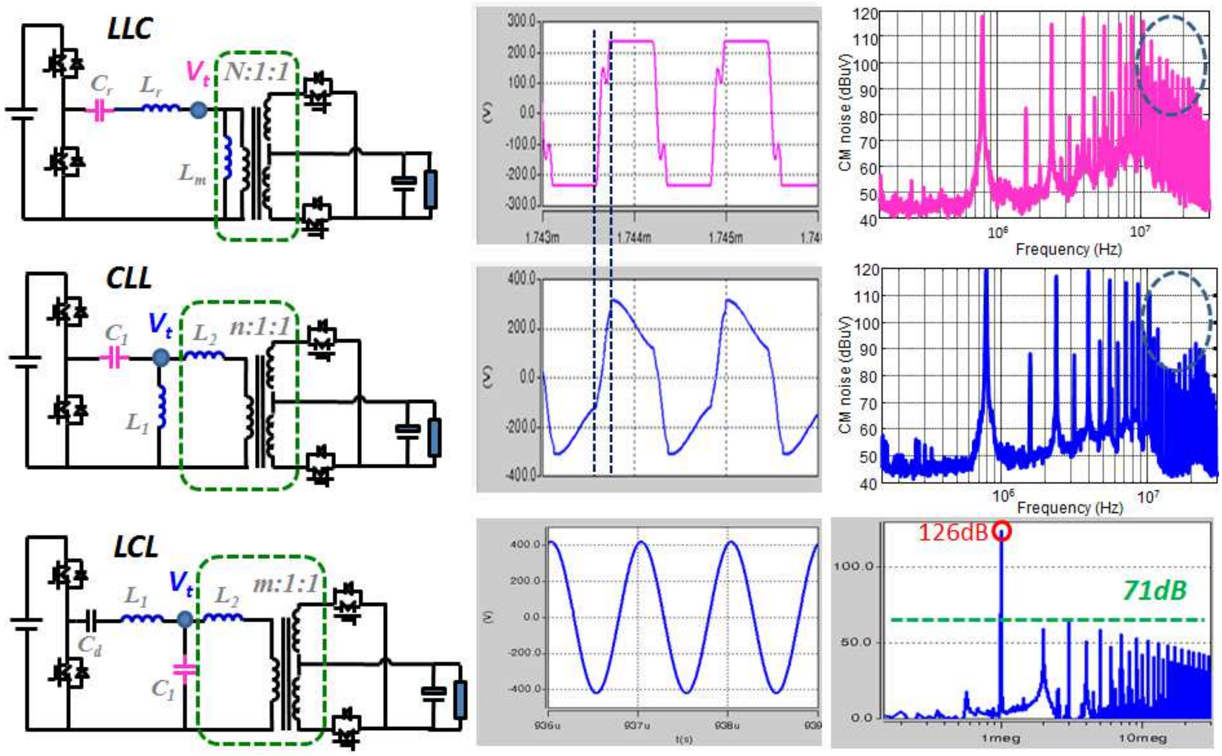

Fig. 3.36CM noise spectrum of LLC, CLL & LCL Resonant Converters

Compare with LLC, CLL has lower CM noise at very high frequency spectrum due to soft voltage edge. The LCL resonant converter has very different EMI characteristics. The voltage cross transformer is like sinusoidal, thus, there is high peak at switching frequency but very low for higher frequencies. Fig. 3.36 shows the CM noise spectrum comparison.

Fig. 3.37shows the comparison results of all three resonant converters.

	LLC	CLL	LCL
V & I Stress	Low	Low	High
Start-up (short circuit protection)	Hard	Hard	Easy
Synchronous Rectifier	Hard	Easy	Easy
CM Noise	High	High	Good@ f>f_s

Fig. 3.37CM noise spectrum of LLC, CLL & LCL Resonant Converters

3.5 Conclusion

A method based on state-plane is proposed to help evaluate the performance of resonant converters. Based on it, the voltage stress, current stresses and apparent power of resonant converters are easy to compare. This method can help select suitable circuit topology for certain application. Meanwhile, it also can help resonant converters' design.

Chapter 4. Integrated System Design for High Current Application

In this chapter, LLC resonant converter with matrix transformer is introduced. Flux cancellation method is utilized to reduce core size and loss. Synchronous Rectifier (SR) devices and output capacitors are integrated into secondary windings to eliminate termination related winding losses, via loss and reduce leakage inductance.

4.1 Introduction

As mentioned before, LLC type resonant converters are excel in both of efficiency and power density [D.1]-[D.8]. Firstly, it has ZVS capability for zero to full load range. Then, low turn off current is achievable for primary side switches. At the same time, synchronous rectifier (SR) devices are zero-current-switching (ZCS). At the end, it gets voltage gain boost capability without efficiency deterioration at normal condition, suitable for application with hold-up time requirement. In comparison with soft switching PWM converters, LLC resonant converters can achieve higher frequency and higher power density with better efficiency.

High switching frequency introduces high power density. However, the switching loss and magnetic components losses are increased. The emerging GaN devices [D.9]-[D.11] give the opportunity to diminish the switching related loss. Hence, the magnetic design becomes very critical.

The isolated high output current DC/DC applications, like server, suffer very high conduction loss, especially for the transformer and SR devices [D.12], [D.13]. Paralleling SR devices are required to reduce device conduction loss. For winding loss, matrix transformer is good candidate for its high current capability [D.14]. However, the price paid for matrix transformer is multiple cores. Reference [D.15] uses flux cancellation method to reduce the core number for less core volume and core loss. The drawbacks are expensive 12 layers PCB transformer and the large conduction loss from alternative current through vias among PCB layers.

To eliminate the AC conduction loss among layers, one effective way is mounting MOSFET device on PCB board [D.17], [D.16]. This structure can help reduce conduction loss between layers dramatically. Both transformer structures have litz wires for primary side windings and PCB board for secondary side windings. Nevertheless, its primary winding is complicated and hard to manufacture.

High termination losses are the third concern. Due to the proximity effect and skin effect, the currents in adjacent terminals with opposite directions attract each other. Thus, very high losses and hot spots are generated. This termination loss deteriorates efficiency significantly. For the conventional design, all SRs are placed on the motherboard. Physically speaking, a large loop of the secondary side rectifiers is inevitable. Consequently, a large distribution loss will be generated. In addition, for large number of SR devices, it is extremely difficult to achieve a symmetrical layout for each SR. Hence, current-sharing of the SR is a severe problem.

For high frequency high step down LLC resonant converters, the transformer loss dominates the whole converter loss [D.12]-[D.16], thus, the transformer design is very critical.

For conventional wired transformer, the primary side windings are solid or multi-strand wires for low switching frequency and low cost design. At high frequency, litz wires are chosen for lower conduction loss. For off-line dc-dc converters, the secondary side current is much higher than the primary side. Therefore, copper foils are selected for the secondary side winding. To alleviate ac winding loss, the primary side and the secondary side windings are interleaved as a sandwich structure. Mostly, the secondary side windings are connected with the motherboard via copper poles. However, this structure suffers high termination losses. Due to proximity effect, the current surges in ac connection terminals. Meanwhile, very little current goes through the center of the terminals because of the skin effect. Thus, very high losses and hot spot are generated [D.17].

In reference [D.16], the secondary side windings are integrated with the SR devices on PCB board, as shown in Fig.4.1. Virtually, termination is achieved at dc output. Thus, the termination loss can be reduced considerably. However, there are some limitations. The primary side windings are interleaved with the secondary side windings as one. For each cell, the primary side winding is connected in series. To finish the whole transformer, multiple cells are connected in parallel. As a result, this structure becomes very complicated. In addition, since all primary side and secondary side windings are paralleled, current sharing between windings might be a potential issue for some circumstances, especially for high current applications.

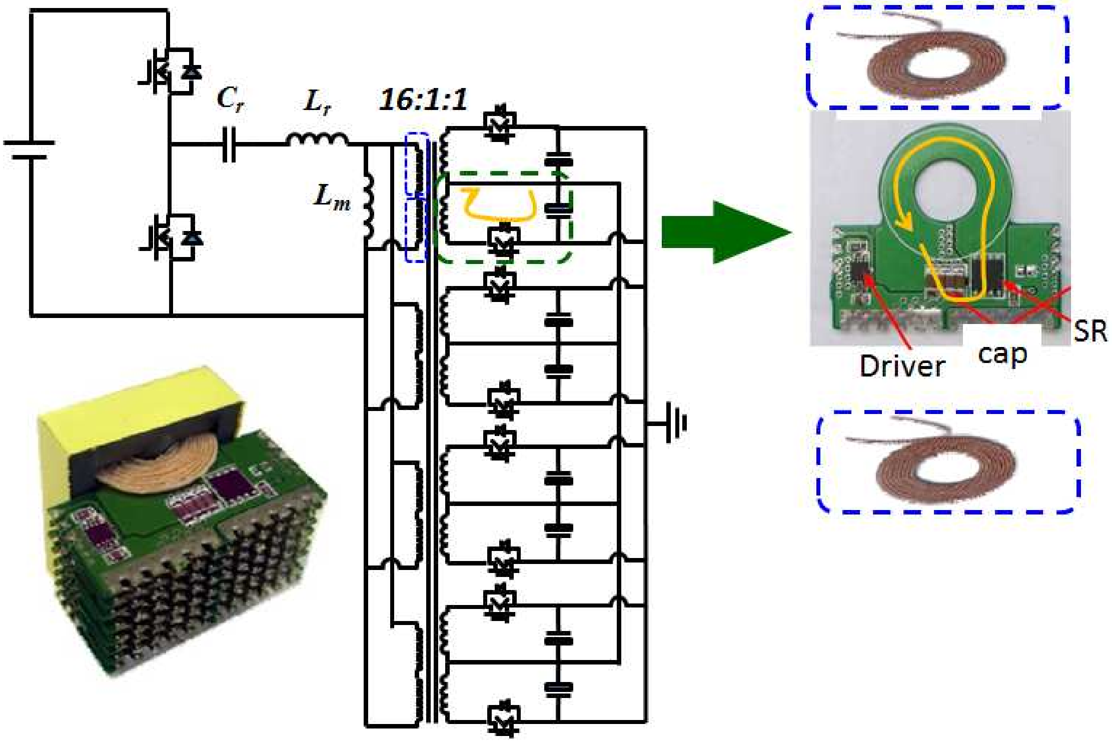

Fig.4.1 Circuit schematic of the transformer and SR in [D.16].

This transformer structure is simplified by [D.17]. The primary side winding are placed in series, and secondary windings in parallel, as shown in Fig.4.2. However, the manufacture process is still complicated for half litz wires half PCB board transformer. The current sharing of paralleled secondary side windings is not guaranteed neither.

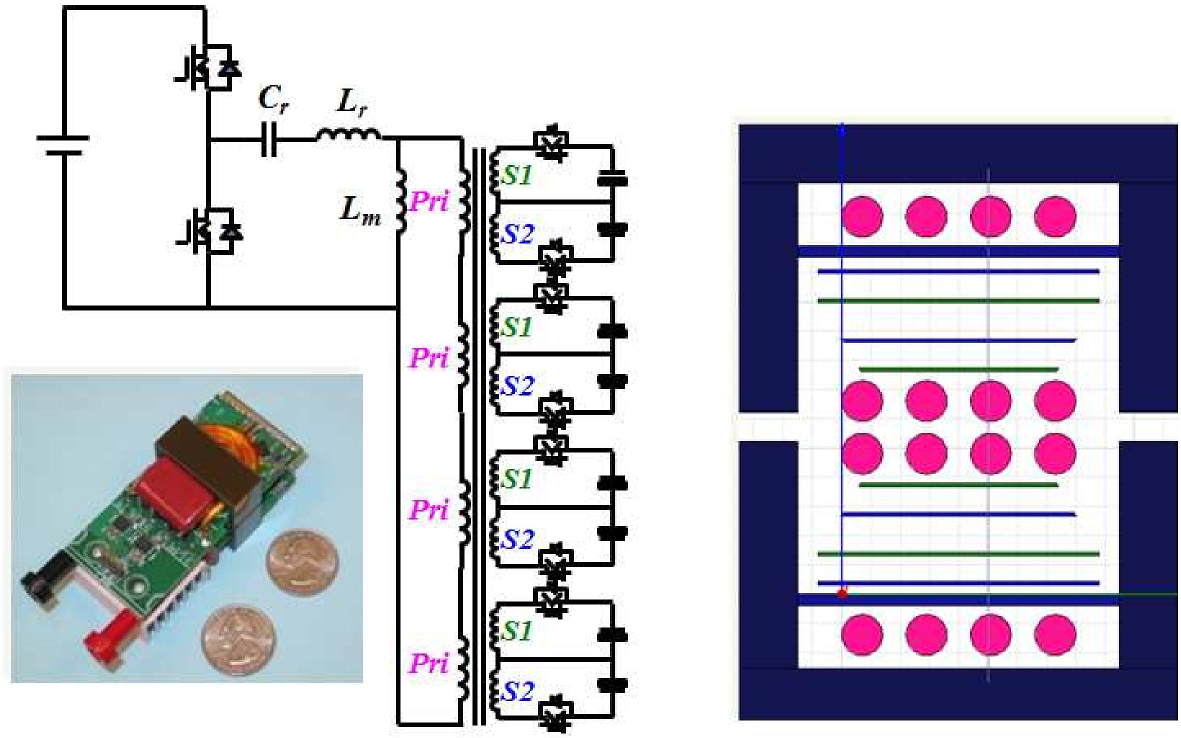

Fig.4.2 Circuit schematic and transformer structure in [D.17].

The planar transformer is easy to be adapted to an automatic manufacturing process [D.13]. It can achieve high power density and low profile. Mostly, multi-layer PCB board is used as planar transformer windings. The primary side and secondary side windings interleaves as sandwich structure. Nevertheless, it is hard to integrate SR devices on secondary side windings inside PCB board.

The state-of-art industry product is Vicor BCM series, as shown in Fig.4.3. By the soft-switching topology called Sine Amplitude Converter (SAC), which is very similar as LLC, the module can achieve ZVS-ZCS operation. Thus, high efficiency and power density is achievable. There are two half bridge stacked together at primary side, thus low voltage device can be utilized. Two core transformer structure is used to help split secondary side current. The secondary side conduction loss is reduced. The typical power density of this series is about 1000W/in^3, while the peak efficiency is around 95.5%. However, this module utilizes 12 MOSEFTs, 14 layers PCB board to achieve this performance.

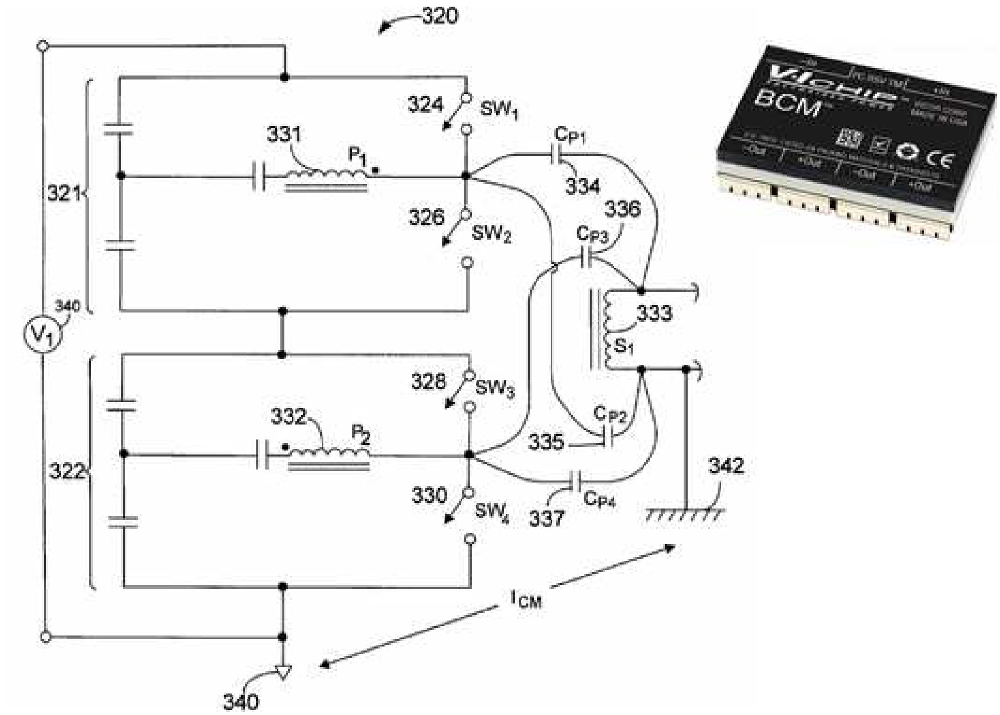

Fig.4.3Vicor BCM series.

Thus, how to improve the efficiency and power density of high step-down dc/dc converter is the key issue for the whole performance of datacenter.

4.2 Matrix Transformer with Flux Cancellation

The matrix transformer could help to fix the dilemma. The matrix transformer is defined as an array of elements interwired so that the whole functions as a single transformer [D.14]. Each element being a single transformer that contains a set turns ratio, i.e. 1:1, 2:1 ….n:1. The desired turns ratio is obtained by connecting the primary windings of the elements in series or parallel and the secondary's in series or parallel. For the high output current cases only a single turn secondary will be considered. The benefits of the matrix transformer are that it can split current between secondary windings connected in parallel, reduce leakage inductance by lowering the N2 value of the secondary loop inductance, and improve thermal performance by distributing the power loss throughout the elements. On the other hand, the matrix transformer structure also can effectively reduce MMF (magnetomotive force) of windings, especially for PCB winding. That also means leakage inductance and winding AC resistance reduction.

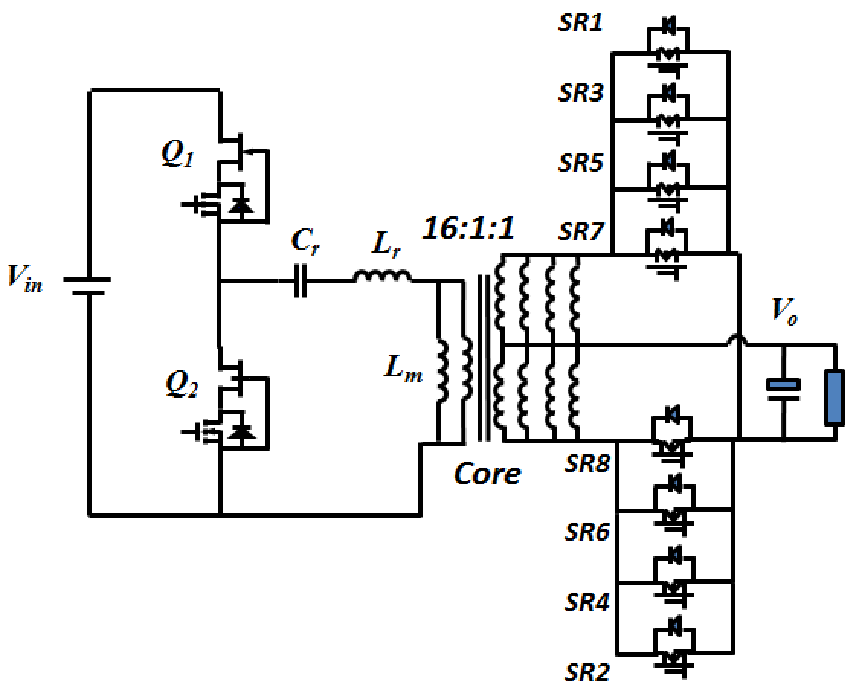

Fig. 4.4LLC resonant converter with four sets output

Fig. 4.4 shows one typical example of 400V/12V 1kW LLC resonant converter. The GaN HFETs Q_1 and Q_2 are primary devices. SR1, SR2, etc are synchronous rectifier (SR) devices.

The resonant capacitor is C_r. L_r is the leakage inductance of transformer, while L_m is the magnetizing inductance. The transformer turns ratio is 16:1:1. Based on optimized loss of synchronous rectifier devices, four sets of center-tap output are chosen. The detail reasons are discussed in [D.18].

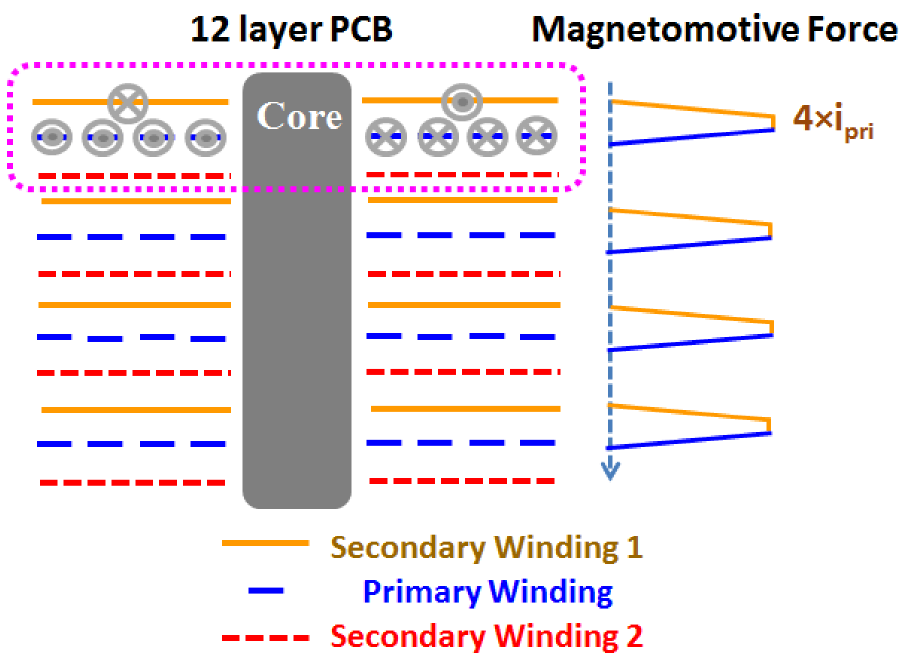

Fig. 4.512 layer PCB structure with one core and its MMF

Fig. 4.5 shows the planar transformer structure employing Fig. 4.4 circuit by one core structure and 12 layer PCB board as transformer windings. The primary side winding is in series, and secondary side in parallel. All the windings are wrapped around the single core. 12 layer PCB windings can be divided into 4 sections. Each section has three PCB layers with two layers for secondary winding and the center one for primary side. As indicated in Fig. 4.5, when secondary winding 1 conducts, the secondary winding 2 does not conduct due to center-tap structure. The current direction for first and second layer PCB board is marked. The other sections are similar. The magnetomotive force (MMF) between primary and secondary windings is four times of primary side current, as shown Fig. 4.5.

Fig. 4.6 shows the PCB winding structure employing matrix transformer concept. The current direction for the first three PCB layers are shown, other layers are similar. The primary and secondary windings wrap on two cores. The MMF between primary and secondary windings are only twice of primary current, as indicated in Fig. 4.6. Low MMF means low leakage inductance and low AC resistance of windings.

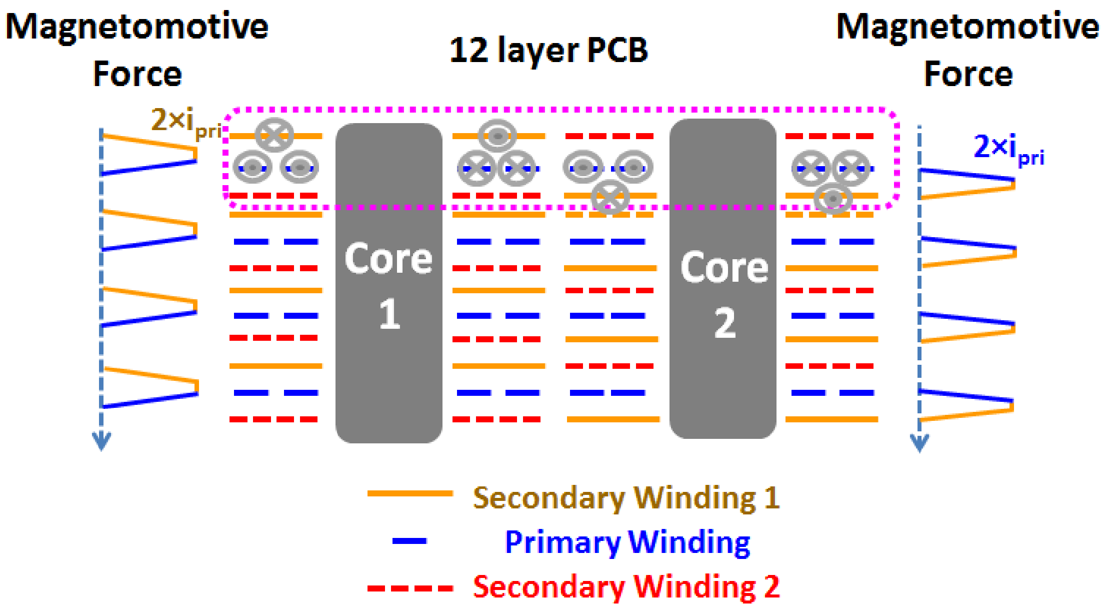

Fig. 4.612 layer PCB structure with two cores and its MMF

However, 12 layers PCB board is seldom used in most front end applications, like server, telecom, etc. Four layer PCB board is widely employed. Thus, matrix transformer based on 4 layer PCB board is adopted. The whole transformer is split into four small transformers, whose primary side are in series and secondary side in parallel. Each small transformer has four turns primary windings and two turns center-tap secondary windings as indicated in Fig. 4.7. As shown in Fig. 4.8, two PCB layers are taken for primary windings at top and bottom, and the inner two layers for secondary windings. At this instant, the secondary winding 1 and primary windings are conducted. The MMF between primary and secondary windings are only twice of primary current, that is very similar as the MMF of 12 layer structure in Fig. 4.6. Consequently, low MMF means low AC winding resistance and low leakage inductance of transformer. At the same time, the current sharing among secondary side are automatically achieved by the structure of primary winding in series and secondary winding in parallel.

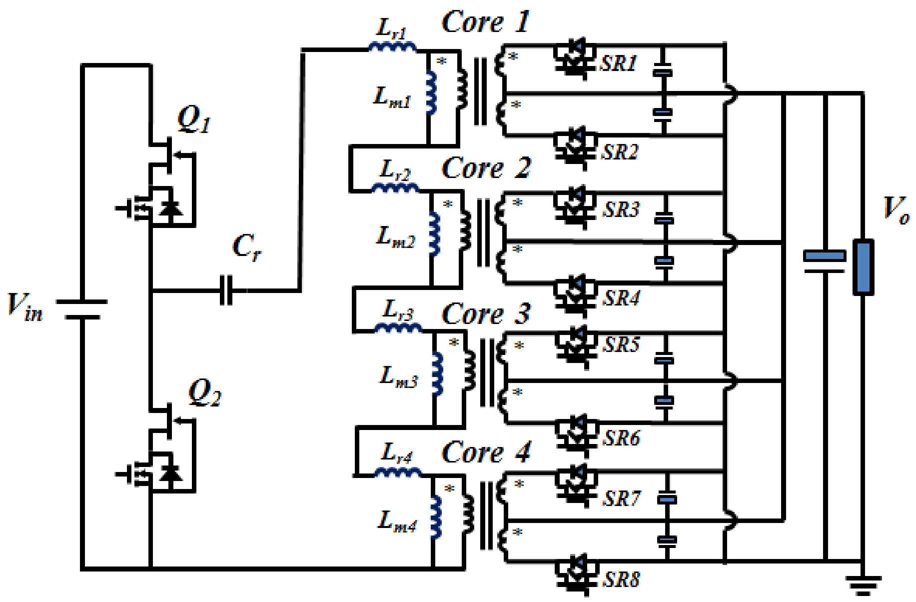

Fig. 4.7LLC Resonant Converter with Matrix Transformer Structure

When low MMF is achieved, the core loss is increased because of multiple cores. The flux excursion for each transformer core is the same in each matrix element as the traditional transformer as mentioned in Fig. 4.5. The primary winding pattern with four magnetic cores in

Fig. 4.8 is shown in Fig. 4.9. Just one of two primary winding layers is shown for simplicity. The other layer winding pattern is similar.

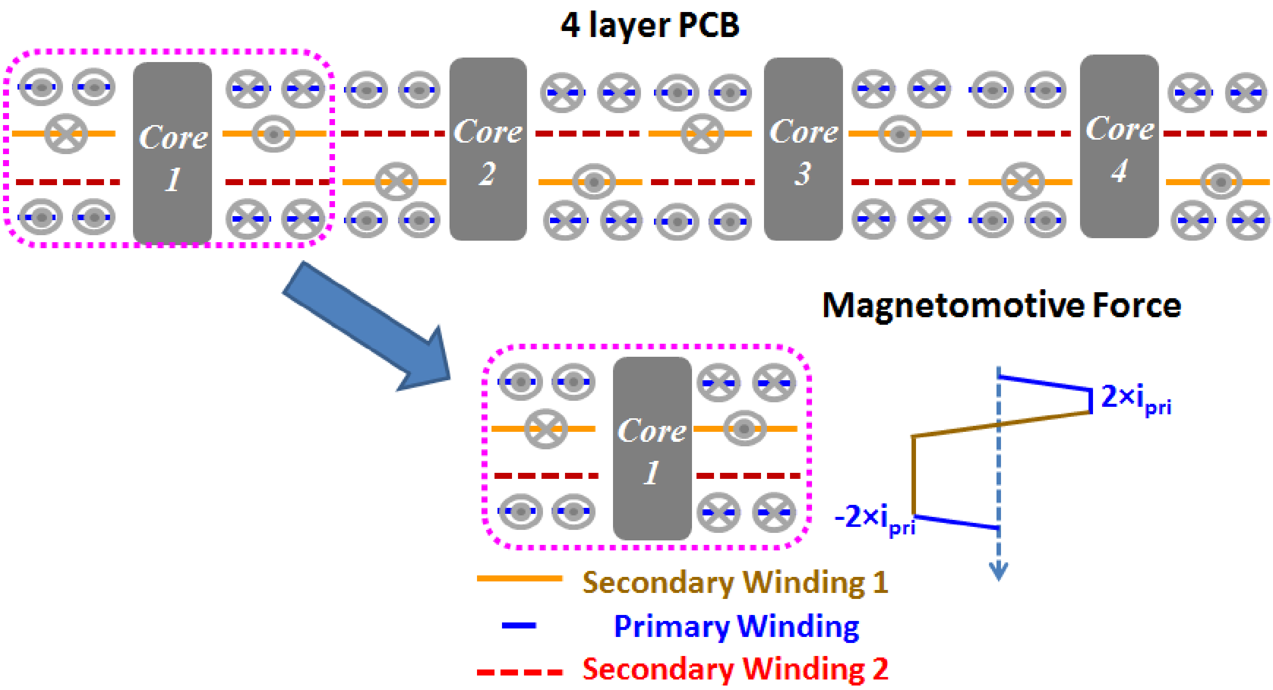

Fig. 4.8Four layer PCB structure with four cores and its MMF

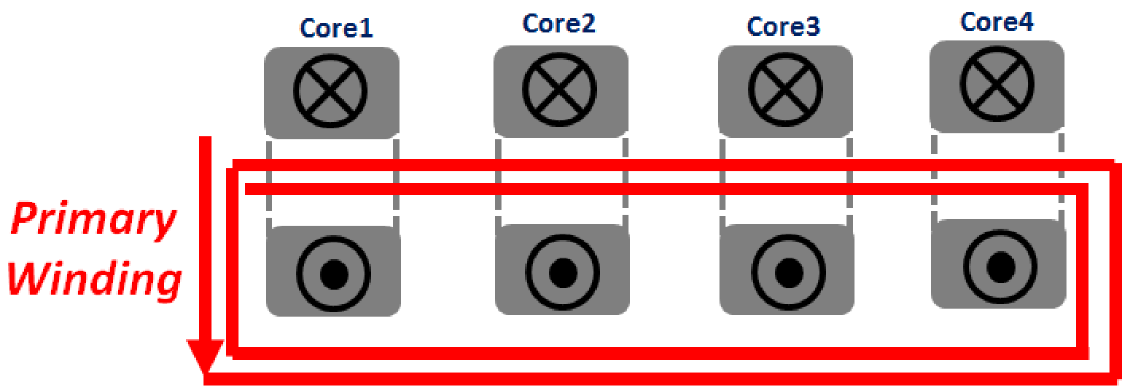

Fig. 4.9 Primary side winding pattern with four U-I cores matrix transformer

It has been known that using integrated magnetic structures can allow for flux cancellation [D.15]. The matrix transformer configuration offers an ideal case for magnetic integration as a result of the cores being excited with identical voltage-second generating the same flux in each core. This allows for almost complete flux cancellation if designed properly. This can decrease overall size and core loss.

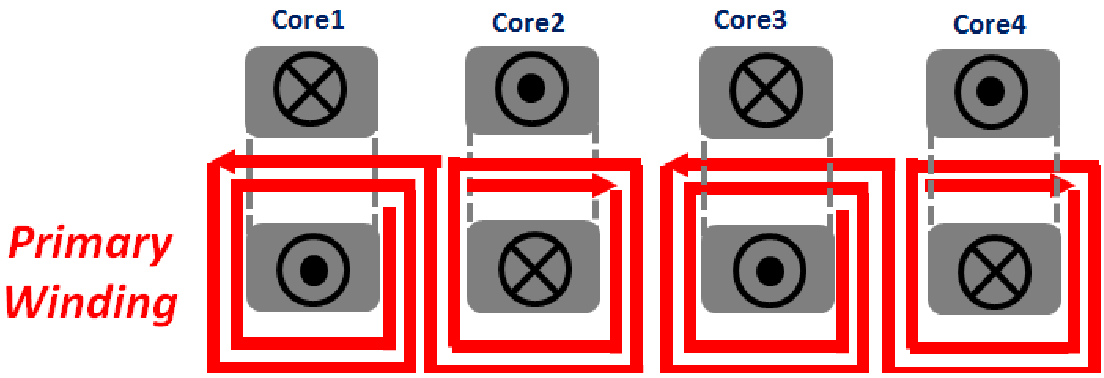

Fig. 4.10 Rearranged primary side winding pattern with four U-I cores

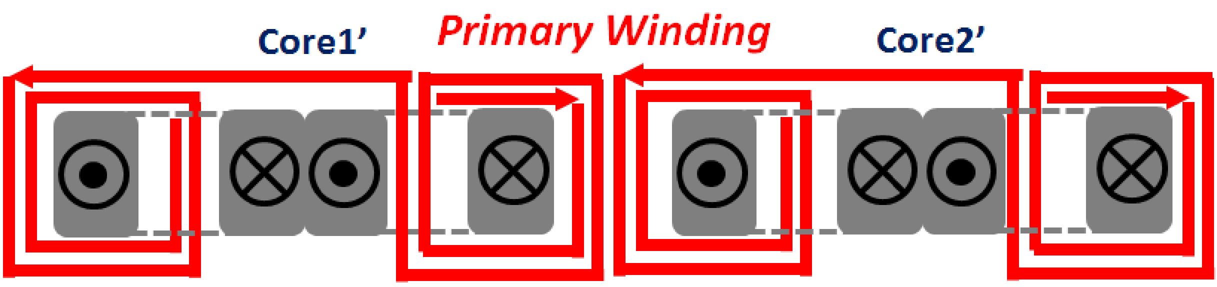

Fig. 4.11Primary side winding pattern for two E-I core matrix transformer

The primary side winding rearranged to reverse flux direction of core 2 and core 4 inFig. 4.10. Hence, the U-I core 1 and core 2 can both turn 90 degree and merge into E-I core 1’, while core 3 and core 4 can do into core 2’ as shown inFig. 4.11. The flux density in each core is the same due to same voltage-second, the magnetic flux in center leg of core 1’ can be cancelled, so can core 2'. Thus, the flux density in the center leg is nearly zero. The center leg of two E-I cores actually can be reaped, so two U-I cores are gotten, as pictured inFig. 4.12. By flux cancellation, four U-I cores of matrix transformer can be reduced to two U-I cores. The core loss and core size can be reduced into half. Then, the whole circuit is shown inFig. 4.13.

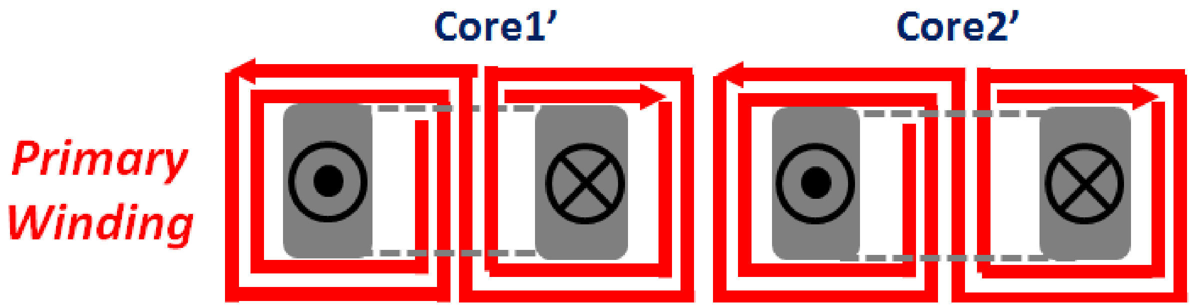

Fig. 4.12Primary side winding pattern for two core matrix transformer with flux cancellation

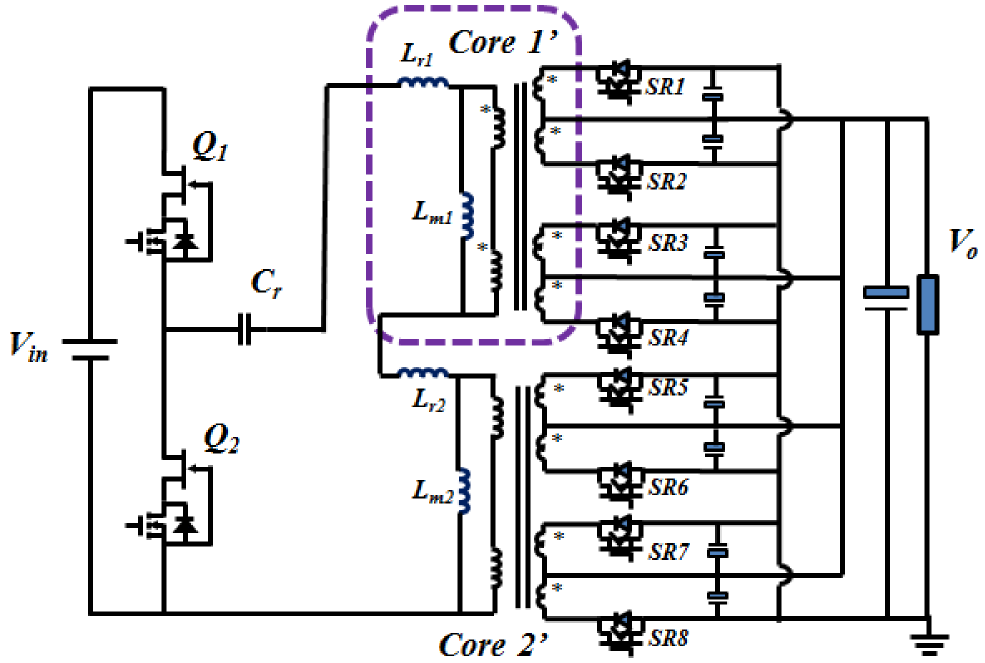

Fig. 4.13LLC resonant converter with proposed transformer structure

4.3 Winding Structure Integrated with Synchronous Rectifier Devices

As mentioned above, the planar matrix transformer has only four layer PCB board as windings, and easy manufacture. It also can effectively reduce leakage inductance and winding AC resistance with low MMF compared to the traditional single transformer design. Meanwhile, flux cancellation method will help reduce magnetic cores' size and loss.

For better efficiency, the transformer winding structure needs more improvement. In [D.15] and [D.17], we know the termination of secondary side windings introduces large AC conduction loss. To eliminate the AC loss introduced by termination, SR devices need be integrated into secondary side windings [D.16]. However, [D.16] did not givethe detail loss analysis and optimal winding design. The following discussion gives insight analysis and optimal transformer design of previous proposed matrix transformer structure.

The matrix transformer structure shown in Fig. 4.8has two parts. Each part has 8 turns primary windings in series, two sets center-taped secondary windings in parallel and one set of U-I core. These two parts are also in series at primary side and in parallel at secondary side. There are two options for winding arrangement.

The first one shown in Fig. 4.13has good interleaving structure. The winding structure of one U-I core indicated in dashed box is shown in Fig. 4.14andFig. 4.15. The top view is in Fig. 4.14, and the side view in Fig. 4.15. Primary windings locate top and bottom side of PCB board. For one half circle of switching period, primary winding conducts current, when secondary winding 1 (Sec1) conducts and secondary winding 2 (Sec2) does not. The magenetomotive force

(MMF) of this structure is given in Fig. 4.15. However, the secondary windings need vias and external terminal to connect the SR devices on top and bottom layers, as indicated in Fig. 4.14.

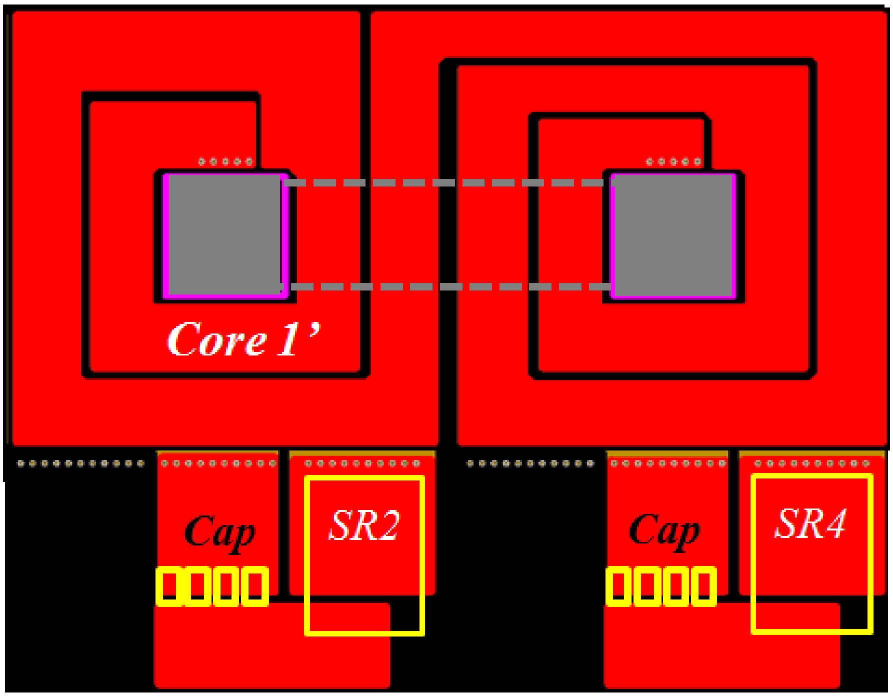

Fig. 4.14 Top view of 1st winding arrangement

The Maxwell 3D Finite Element Analysis (FEA) simulation is applied to estimate the leakage inductance and AC resistance of transformer windings. Fig. 4.16 shows the FEA simulation results of AC current distribution for secondary side of transformer. The dash arrows express the AC current direction. It is clear that there is severe current crowding along the terminal connecting SR device and capacitors. The reason is that the termination does not interleave with primary winding, thus, the AC currents in opposite direction will attract each other along the edge. The doted box is where vias connecting the middle layer secondary windings and the top layer. The current through vias is not even either.

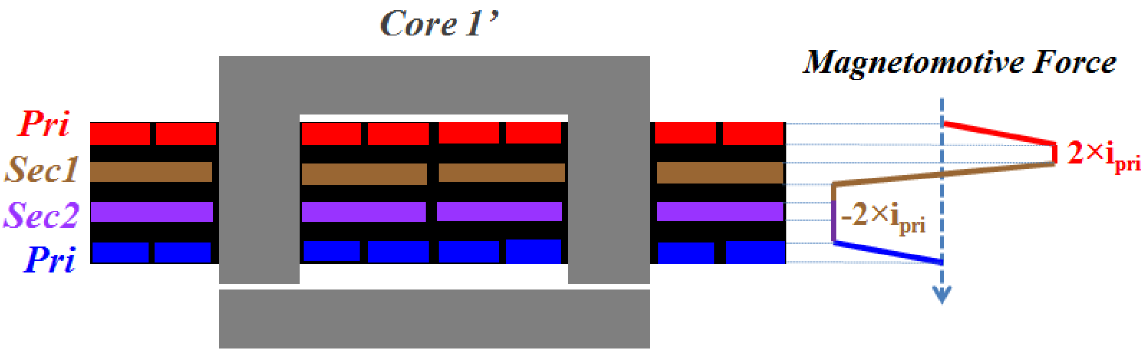

Fig. 4.15Cross view of the first winding arrangement and its MMF

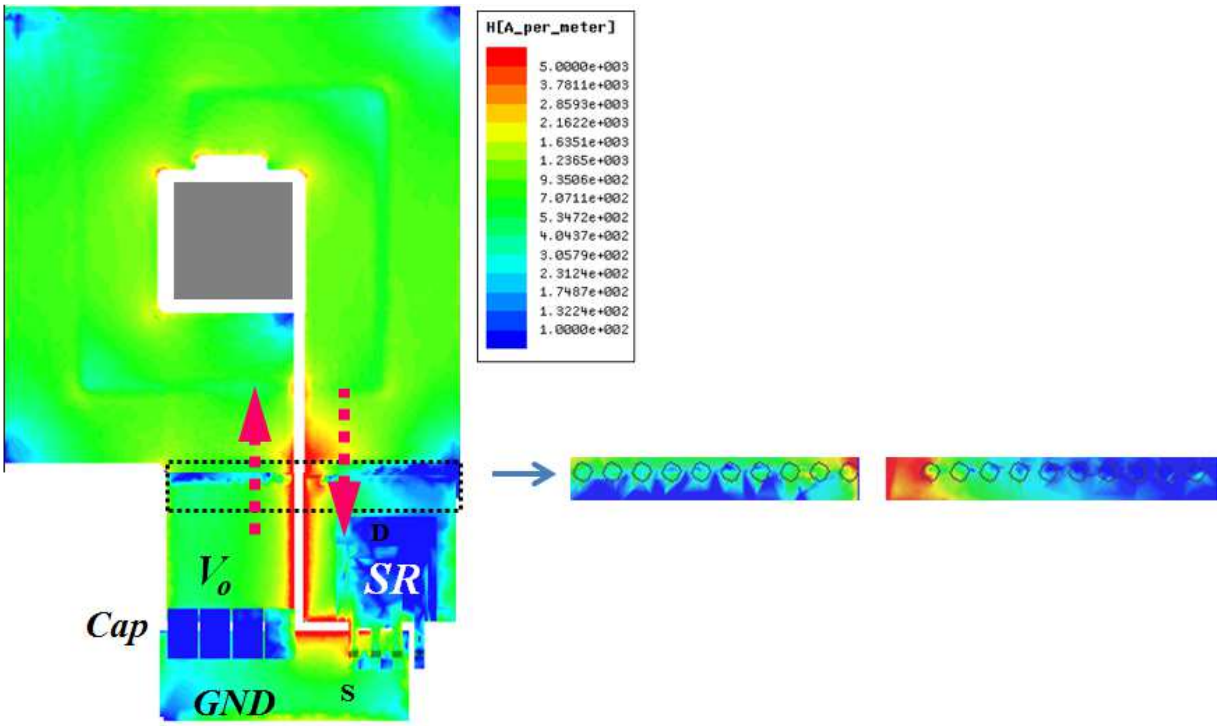

Fig. 4.16 AC current distribution for secondary winding of the first winding arrangement

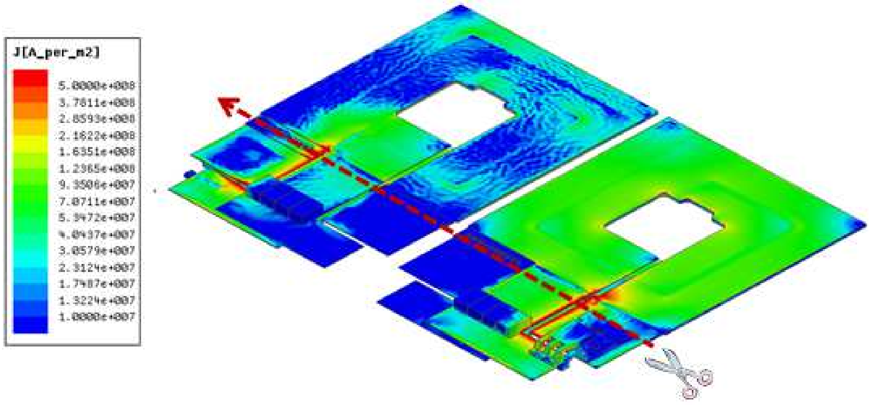

(a) Current Density Distribution

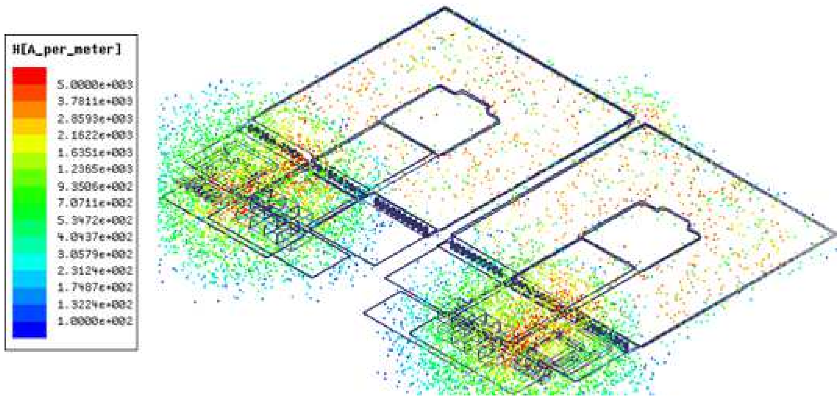

(b) Magnetic Field Intensity Plot

Fig. 4.17 FEA simulation for the first winding arrangement

The simulation result of one U-I core transformer is given in Fig. 4.17. The secondary side AC resistance including termination is R_{sec}=6.81mΩ, and the leakage inductance is L_k = 176.4nH.

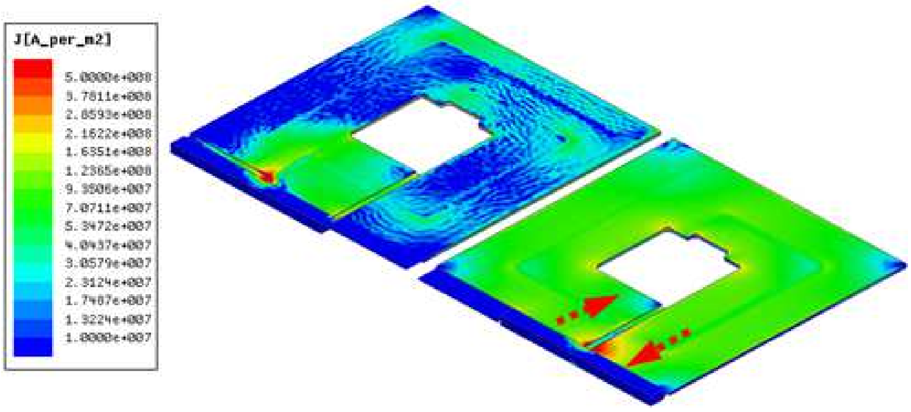

(a) Current Density Distribution

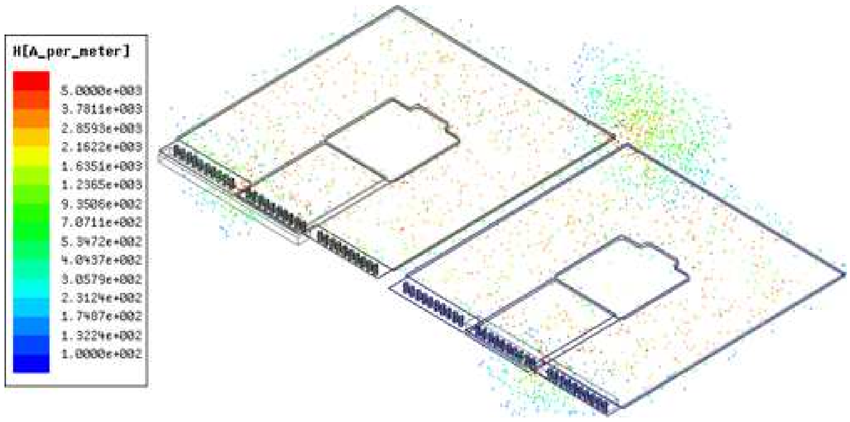

(b) Magnetic Field Intensity Plot

Fig. 4.18 FEA simulation for the first winding arrangement with output shorted

If the transformer secondary side is cut off as dash line indicated in Fig. 4.17(a), and shorted by copper bar at the cut port. Fig. 4.18is the simulation result. The secondary side AC resistance is R_{sec}=3.35mΩ, and the leakage inductance L_k = 58.0nH. This phenomenon means the AC resistance of termination including via is 3.46 mΩ, and the leakage inductance 118.4nH. However, there are opposite direction currents flow in and out the shorted port, which will also cause current crowding.

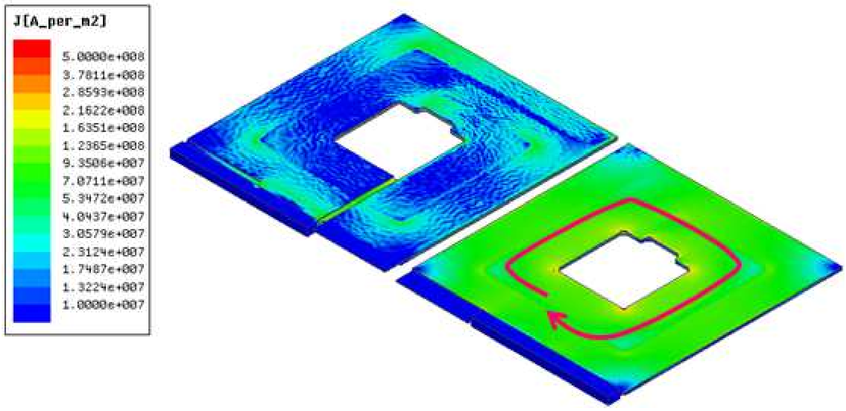

(a) Current Density Distribution

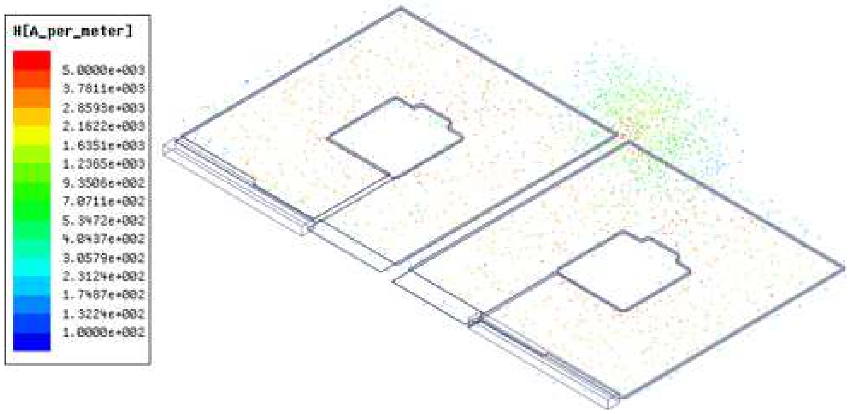

(b) Magnetic Field Intensity Plot

Fig. 4.19 FEA simulation for the first winding arrangement with secondary winding shorted

Fig. 4.19is the simulation result for the secondary winding totally shorted, that means no AC current flow out and in secondary winding, and no termination loss. The AC current direction is shown in solid line in Fig. 4.19. The AC resistance is R_{sec}=1.37mΩ, and the leakage inductance L_k=36.6nH. Compared with Fig. 4.17, the AC resistance of secondary winding with termination is 4 times larger than the one without termination.

Based on previous analysis, the lossy parts of the first winding arrangement are the terminal and the vias which connect the secondary windings, SR devices and output capacitors. To eliminate this termination related loss, the second winding arrangement is proposed whose SR devices and output capacitors are integrated into secondary windings. For this one, no extra terminal needed for devices and capacitors connection. The devices and capacitors are naturally part of secondary side windings. The AC current loop of secondary winding is exactly matching those of primary side winding. There is no AC current flowing out and in secondary side windings, thus no extra AC current loss is introduced.

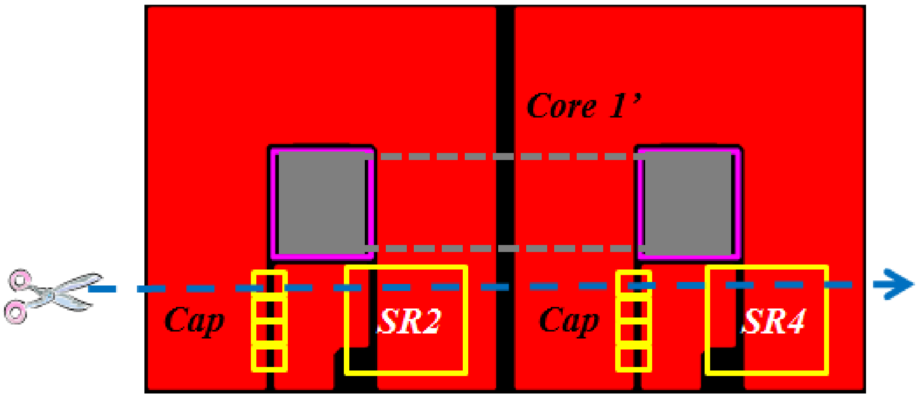

Fig. 4.20 Top view of the second winding arrangement

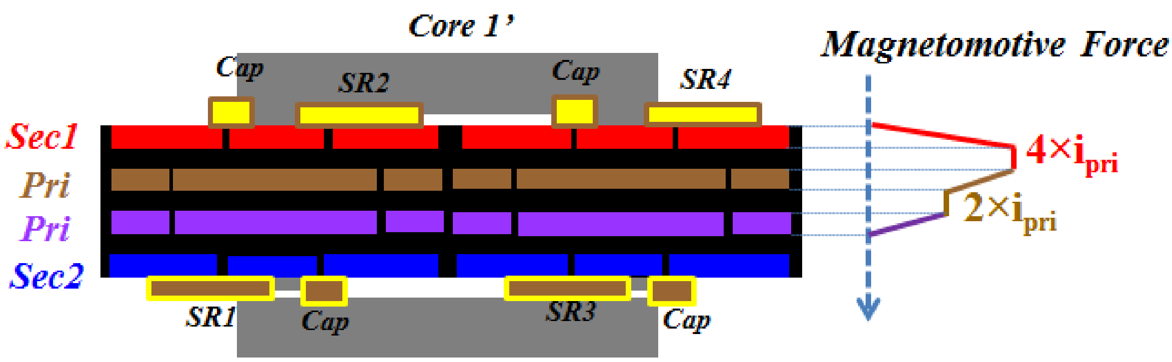

Fig. 4.21 Cross view of the second winding arrangement

The second winding arrangement is proposed in Fig. 4.20 and Fig. 4.21. The secondary windings locate top and bottom side of PCB board. The SR MOSFETs and output capacitors are part of secondary windings. In Fig. 4.21, the MMF between windings is higher than that of the first winding arrangement in Fig. 4.15, which means this winding structure has worse interleaving.

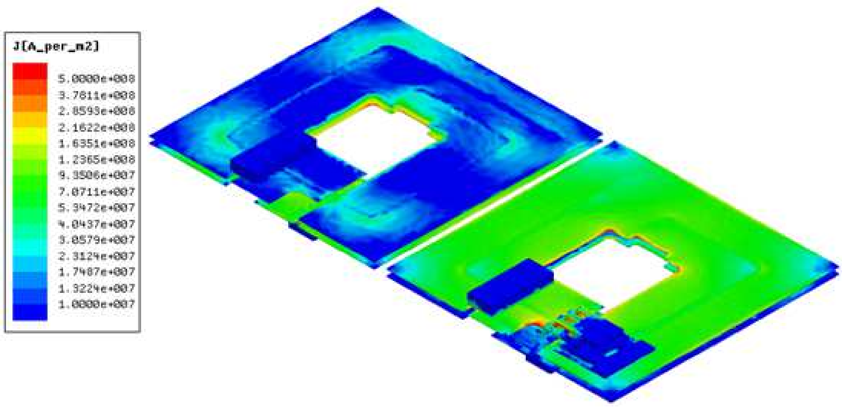

(a) Current Density Distribution

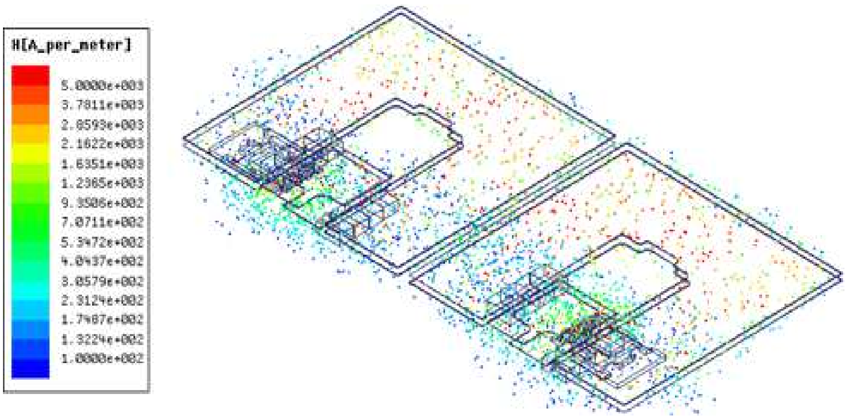

(b) Magnetic Field Intensity Plot

Fig. 4.22 FEA simulation for the second winding arrangement

The FEA simulation results are given in Fig. 4.22. The secondary side AC resistance is R_{sec}=2.08mΩ, and the leakage inductance L_k = 63.4nH.Although the first winding arrangement has better interleaving, its AC resistance and leakage inductance are much higher than the second one. That means the termination loss is much larger than the loss saved by better interleaving structure.

In the first winding arrangement, SR devices connect secondary side winding byvias and external connection, which cause huge AC conduction loss. The second reason is that its primary winding and secondary winding are not exactly match each other. When the windings are not overlapped very well, the leakage flux induced by those parts will force the current crowded to the edge of windings. In the second winding arrangement, the SR devices are integrated into secondary windings, thus, there is no termination loss. The primary and secondary windings are exactly overlapped, thus, there is nearly no current crowding anywhere in this case as shown in Fig. 4.22(a). Only little crowding current is induced by SR device package.

4.4 Matrix Transformer Design Procedure

At the beginning of detail transformer design, the transformer width is constrained by the dimension of synchronous rectifier devices. For this case, we choose Infineon device SuperSO8 package, the minimal width of whole transformer is 70mm. Then, 1 MHz is picked as the switching frequency. The core material 3F45 is chosen based on performance factor [B.25]. Then, the loss density is shown in Fig. 4.23. As the cross area increases, the core loss drops dramatically. The curve is reach diminishing returns around shadow area. One point (Ae=44mm^2) is chosen in shadow area based on the tradeoff of core size and loss.

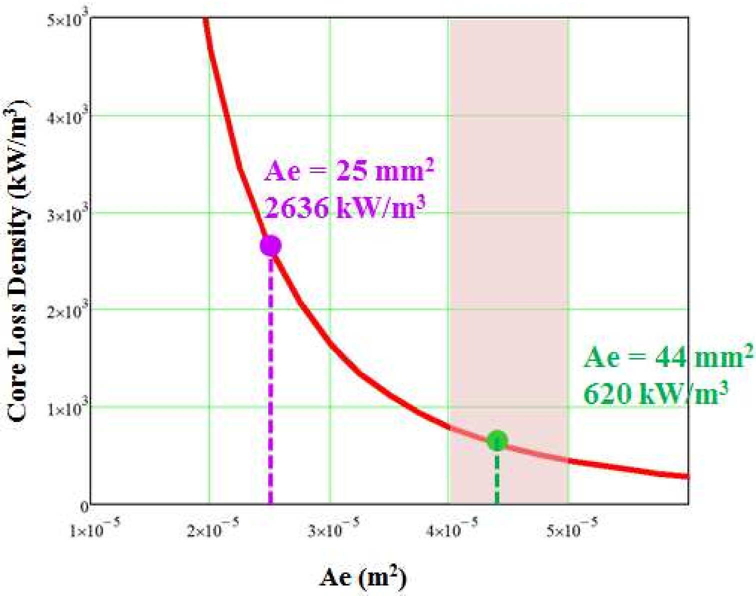

Fig. 4.23 Loss density vs. Cross area.

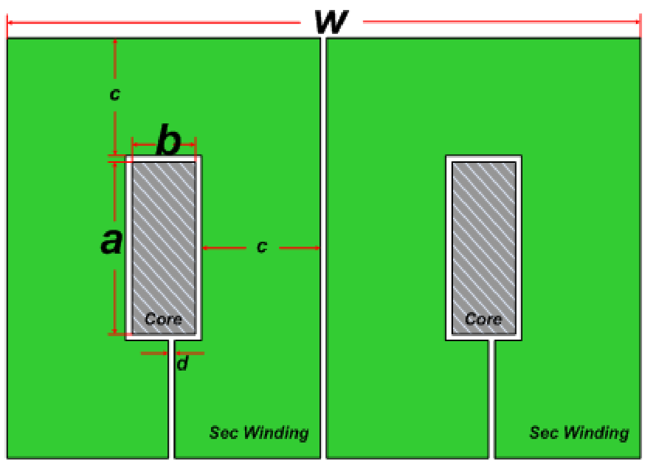

Fig. 4.24 Core and winding dimensions

As shown in Fig. 4.24, the core shape does not only influence the core loss but also winding loss. Because the transformer width is determined, we can only change the a and b value of core to get the minimal winding loss. Fig. 4.25 and Fig. 4.26 show the trend of AC and DC resistance of secondary winding and primary winding, which changes as a and b ratio changes. At last, we can choose the a and b values based on minimal resistance.

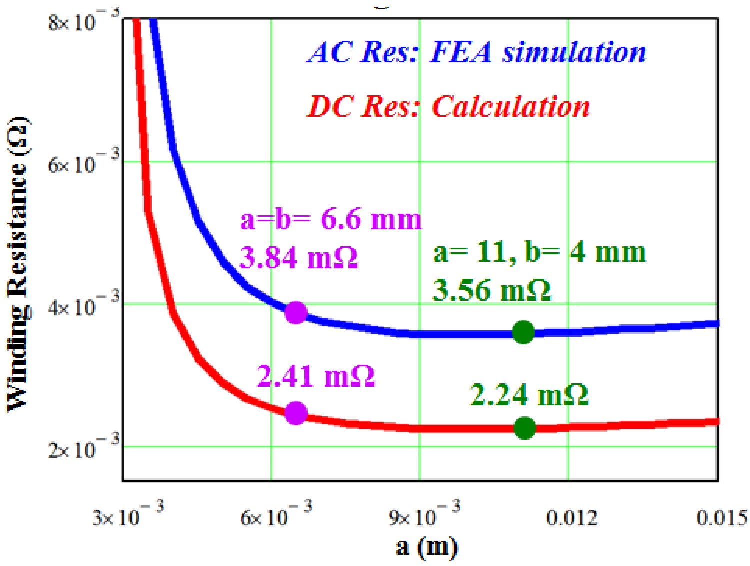

Fig. 4.25 AC & DC resistance of Sec winding.

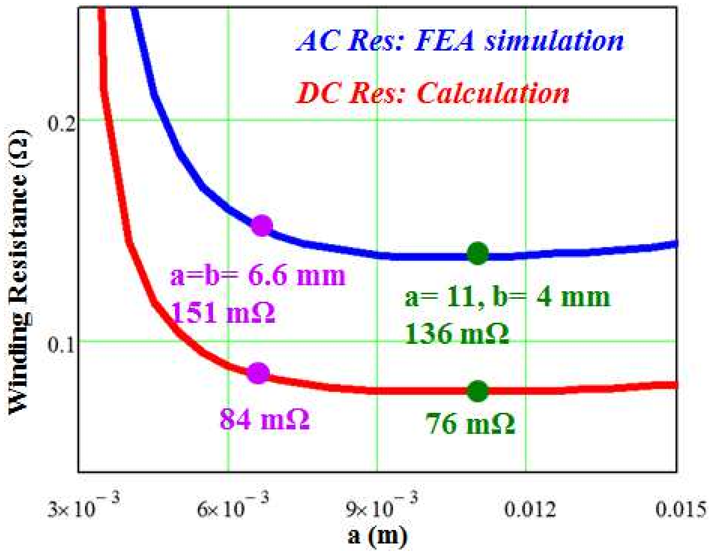

Fig. 4.26 AC & DC resistance of Pri winding.

The last step is chosen suitable winding thickness. The simulation results are given in Table 2.1. The skin depth at 1 MHz is around 66um. However, the results show the optimal thickness is around 3 oz copper. 4 oz copper is chosen for better efficiency.

Table 4.1The AC resistance of pri and sec windings vs. thickness

Copper Thickness	2 oZ (70 um)	3 oZ (105 um)	4 oZ (140 um)
Pri AC Resistance (mΩ)	90	69.2	68.2
Sec AC Resistance (mΩ)	2.59	1.98	1.78

4.5 Experimental Results

An 1MHz 390V/12V 1kW LLC resonant converter prototype with proposed matrix transformer structure is built. The second winding arrangement is applied. The circuit is given in Fig. 4.27, while the hardware picture is shown in Fig. 4.28.

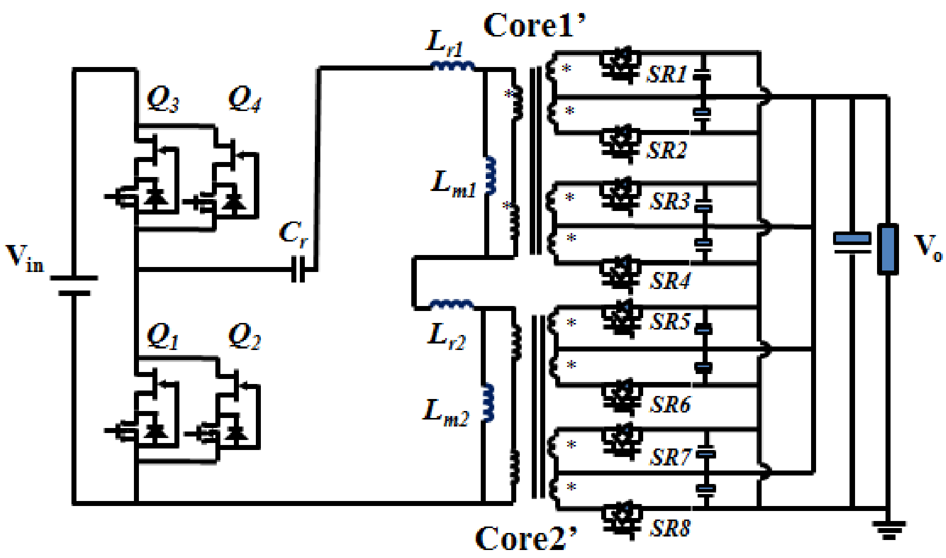

Fig. 4.27The circuit of 1kW, 400V/12V LLC resonant converter prototype

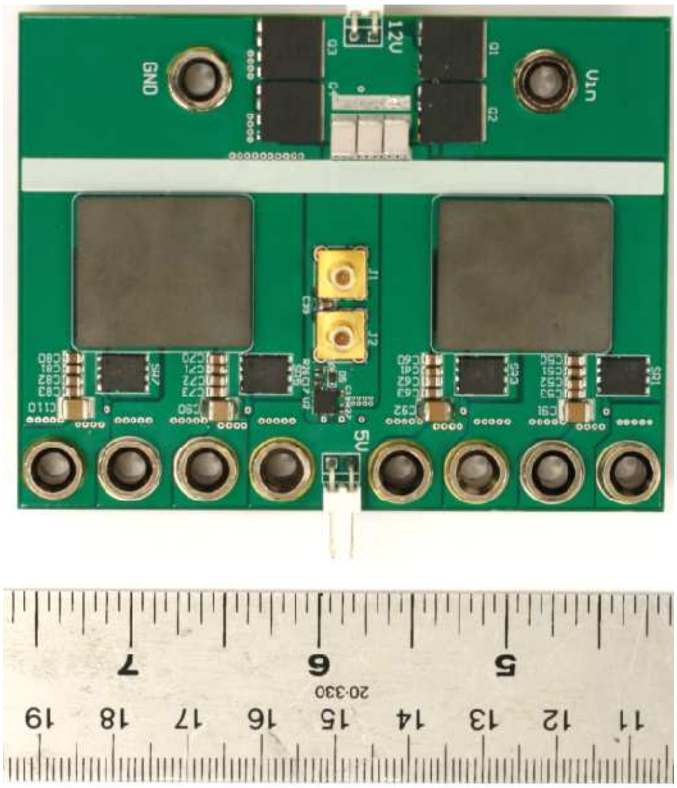

Fig. 4.28The prototype of 1kW, 400V/12V LLC resonant converter

The primary devices are Transphorm GaN HEMTs. For better efficiency, two GaN devices is paralleled. Thus, there are four devices at primary side. SR devices are BSC010N04LSI from Infineon. The core material is 3F45.The magnetizing and leakage inductances are used as resonant elements, which are integrated into matrix transformer. The leakage inductance of matrix transformer is 220nH, while the magnetizing inductance is 17.6uH. The resonant capacitor is70nF.The power density of power stage is around 830W/in^3.

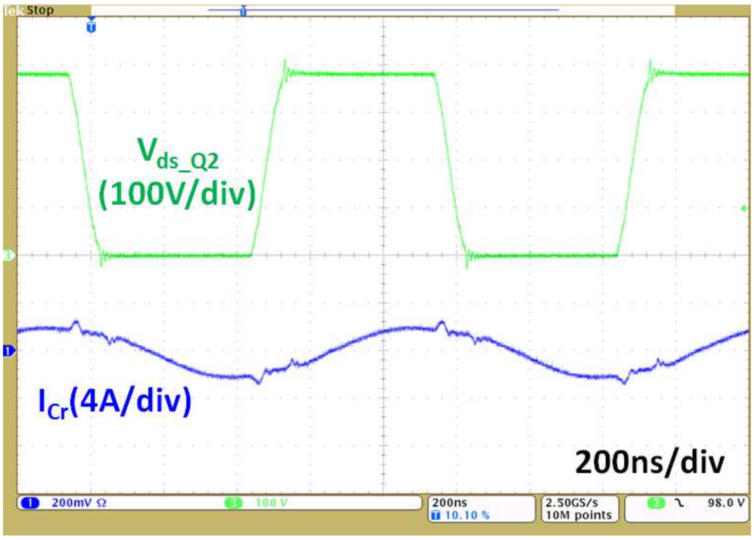

Fig. 4.29Experimental waveforms for 15% load condition

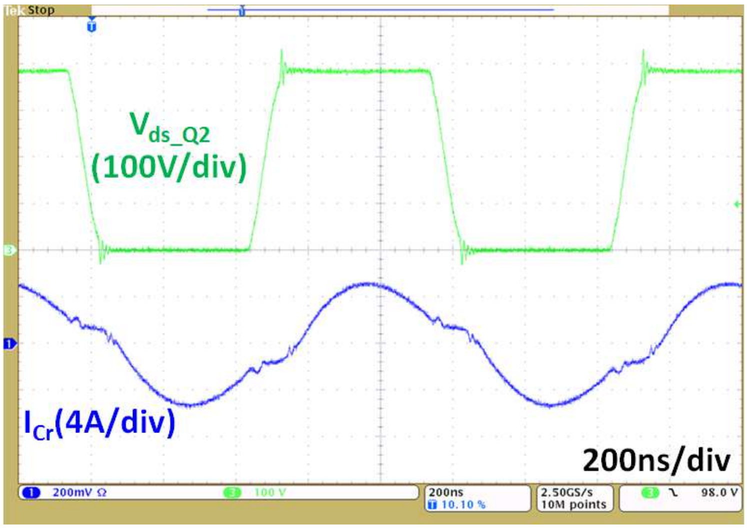

Fig. 4.30Experimental waveforms for 50% load condition

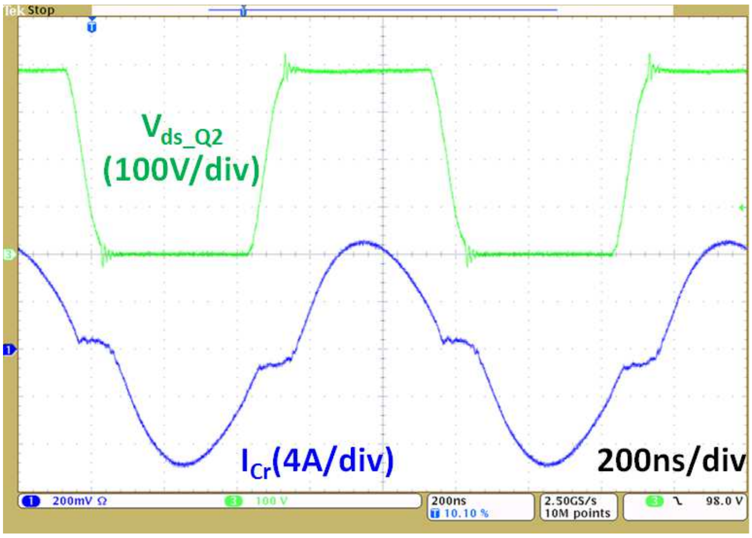

Fig. 4.31 Experimental waveforms for 100% load condition

Fig. 4.29, Fig. 4.30 and Fig. 4.31show the waveforms under 15%, 50% and 100% load. V_{ds_Q2} is the drain-source voltage waveform of primary device Q_2. I_{Cr} is the current through resonant capacitor C_r. Even as high as 1 MHz switching frequency, the primary side devices can easy achieve Zero-Voltage-Switching (ZVS). The oscillation during dead time is caused by the leakage inductance and secondary rectifier's junction capacitance. The turnoff current is as low as 2A.

One of the best industry products on market is Vicor module, whose power density is around 1050W/in^3. To achieve the efficiency and power density, it has 14 layer PCB board, 12 MOSFETs for 300W output power. Compared with this product, our prototype just has 4 layer PCB and 12 devices for 1kW to reach similar power density and efficiency. The prototype efficiency can reach as high as 95.4%. The efficiency comparison is shown in Fig. 4.32.

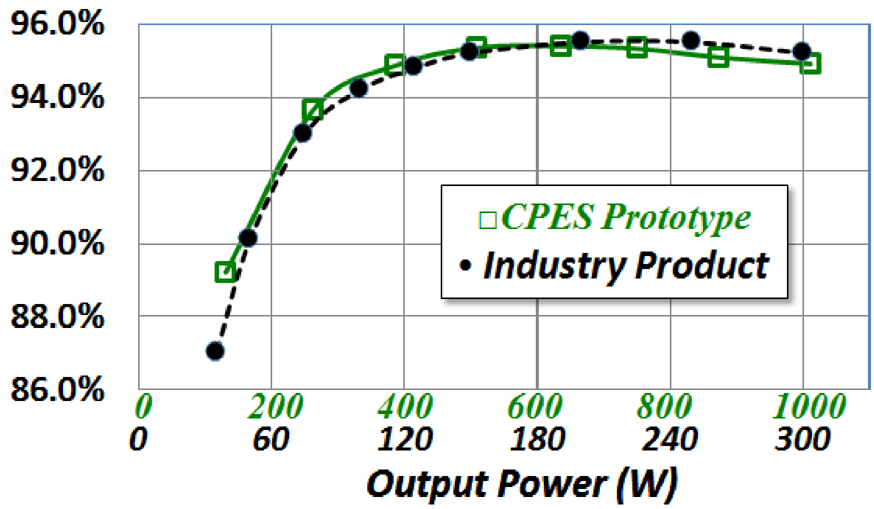

Fig. 4.32The efficiency comparison for CPES prototype and industry product

One more thing needs to clarify is that the advantage of GaN devices is smaller C_{oss} compared with Si MOSFET having the same R_{dson}. That will result in lower turn off current which help achieve zero-voltage switching. Lower turn off current means less circulating energy in the circuit. Thus, the major loss reduction parts caused by GaN device are the conduction loss and driving loss of primary devices, the conduction loss of primary winding of transformer. While the major loss saved by new transformer structure is secondary side winding conduction loss and termination loss. The detail analysis for GaN device benefits is described in [D.20].

Table 4.2 Loss breakdown of prototype under 100% load

Loss	Value (*W*)
Primary MOSFET Conduction Loss	*8.2*
Primary MOSFET Turnoff Loss	*2.2*
Primary MOSFET Driving Loss	*0.6*
Resonant Capacitor (C_r) Loss	*0.46*
Transformer Core Loss	*5.10*
Transformer Primary Winding Loss	***4.49***
Transformer Secondary Winding Loss	***7.24***

Secondary MOS Conduction Loss	***6.6***
Secondary MOS Driving Loss	***3.6***
Secondary MOS Body Diode Loss	***2.53***
Output Capacitor Loss	*1.95*
Connection, Trace & Solder Loss	*3.56*
Calculated Total Loss	*46.53*
Measured Total Loss	*51*

Table 4.3 Loss breakdown of prototype under 15% load

Loss	Value (*W*)
Primary MOSFET Conduction Loss	*0.27*
Primary MOSFET Turnoff Loss	***2.2***
Primary MOSFET Driving Loss	*0.6*
Resonant Capacitor (C_r) Loss	*0.015*
Transformer Core Loss	***5.10***
Transformer Primary Winding Loss	*0.15*
Transformer Secondary Winding Loss	*0*
Secondary MOS Conduction Loss	*0*
Secondary MOS Driving Loss	***3.6***
Secondary MOS Body Diode Loss	*0*
Output Capacitor Loss	*0*
Connection, Trace & Solder Loss	*0.24*
Calculated Total Loss	*12.17*
Measured Total Loss	*15.75*

Based on previous Maxwell 3D simulation, the new winding structure can save more than 60% secondary side winding loss under full load. More than 20% of total loss is reduced. The detail loss breakdown for 100% load and 15% load are given in Table 4.2 and Table 4.3. It is clear to see the major loss is distributed around transformer and secondary rectifier devices at full load.

4.6 Conclusion

To deal with the high output current applications, matrix transformer structure help reduce the leakage inductance and winding AC resistance of transformer. The price is the rising of cores loss and volume due to multiple magnetic cores. Flux cancellation reduces core size and core loss. Then, SR devices and output capacitors are integrated into secondary side windings to eliminate the termination loss. A high efficiency high power density matrix transformer structure based on previous discussion is proposed.

Chapter 5. Design Considerations for Passive Integration

In this chapter, the multi-elements resonant converters' characteristics are reviewed. The voltage and current stresses of all resonant elements are examined. Based on stress, the principles of choosing suitable passive components for integration are proposed. Then, the magnetic integration method is shown based on multi-winding transformer structure. The basic principles of passive integration are discussed. A novel passive integration method is proposed for multi-elements resonant converters. A 1000 W, 800 kHz, 400 V/48 V test board for resonant tanks is built to verify the proposed method.

5.1 Introduction

To make practical use of LLC and CLL resonant converters, the over current protection has to be fulfilled, especially for startup and over load conditions. The purpose of over current protection is to limit the current stress in the system during over load or short circuit condition, also to limit the inrush current during start up so that the power converter can be protected from destructive damage. Multi-element resonant converters were proposed to solve this issue [E.1]-[E.2]with more passive components added to the resonant tank. However, the additional passive components impose the demand for integration efforts in order to alleviate their impact on converter size.

At a high switching frequency, the passive components' volume can be reduced. However, in the state-of-the-art resonant converters, the discrete passive components and the heat sink still occupy more than 80% of the total system volume [E.3]. To reduce the volume of the magnetic components, magnetic integration has been proposed. However, the passive components still have large profile. To further reduce the overall volume, passive integration technology is applied to integrate the resonant inductor (L_r) and capacitor (C_r), the magnetizing inductor (L_m), and the transformer (T_x) (L-L-C-T) into one module [E.4]-[E.10]. There is still a challenge to employ passive integration techniques in multi-elements resonant converters. This paper proposes a novel passive integration method to solve this problem.

5.2 Basic Characteristics of Multi-elements resonant converters

The LLC resonant tank can be considered as a band pass filter which includes series resonant frequency (SRF) and parallel resonant frequency (PRF), as shown in Fig. 5.1 and Fig. 5.2. The series resonant frequency is created by L_r and C_r, black dot in Fig. 5.2. It is the optimal point at nominal operation. The fundamental component of input energy can be delivered from the source to the load very efficiently. Therefore, high efficiency can be achieved. The hold-up time capability is given by the parallel resonant frequency, dash line oval in Fig. 5.2. This resonant frequency is determined by L_r, L_m and C_r.

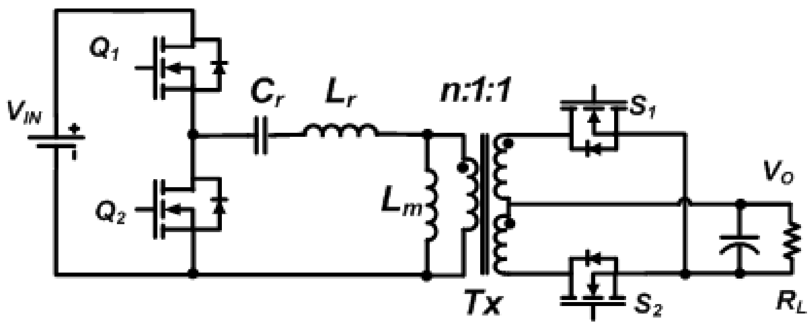

Fig. 5.1LLC resonant converter

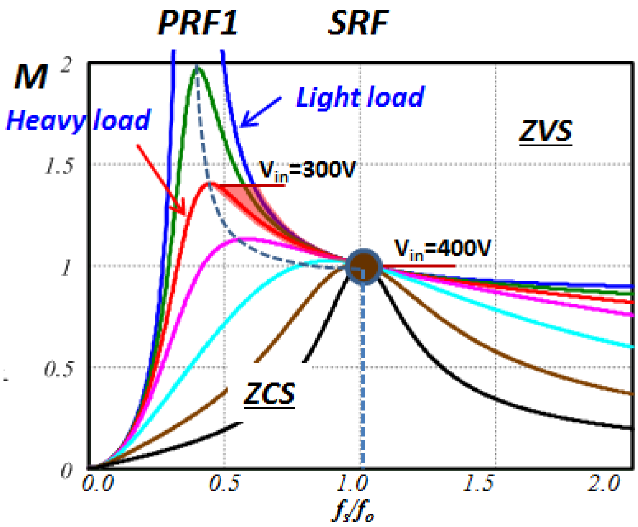

Fig. 5.2Circuit and voltage gains of LLC resonant converter

However, with poor frequency selectivity, namely, very wide bandwidth, the frequency has to be increased very high to achieve enough damping effect. To improve the characteristics of LLC resonant converters, additional resonant elements are needed. With additional resonant element component, a multi-element resonant tank, which combines band pass filter and notch filter, is proposed to solve the current protection issues. One of these resonant converters is depicted in Fig. 5.3. The notch filter section is created with L_p and C_p. The band pass filter section consists of L_p, C_r and C_p.

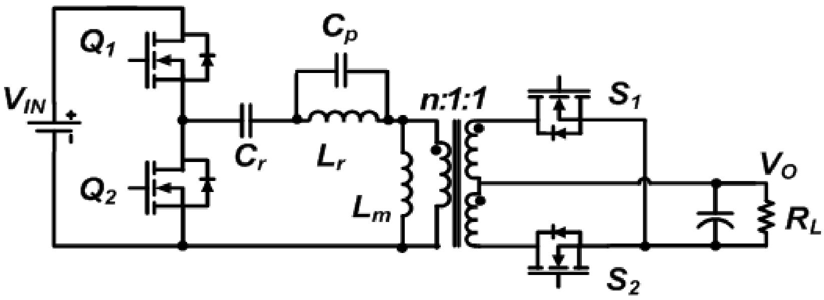

Fig. 5.3One example of selected 4-elements resonant converters

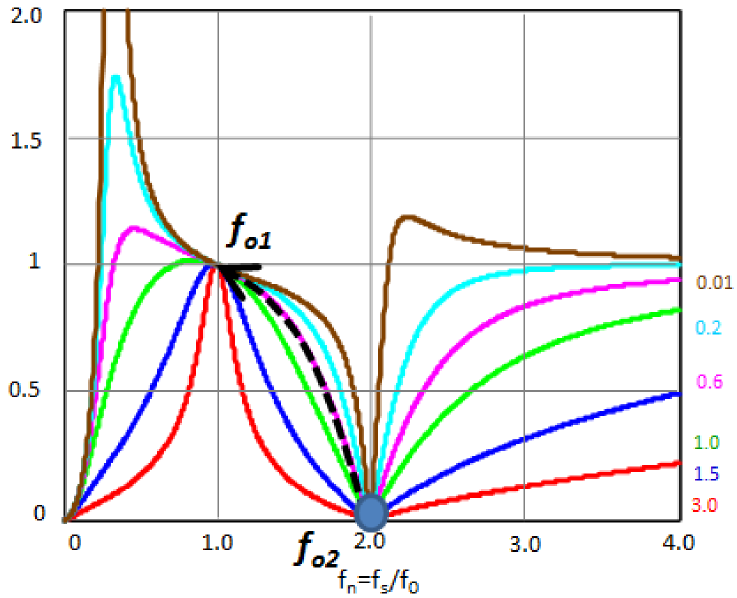

Fig. 5.4Gain Curves of selected 4-elements resonant converter

The voltage gain of this four-element resonant tank is illustrated in Fig. 5.4. The resonant tank with notch filter characteristic can create zero voltage gain. Conceptually, infinite impedance can be created when frequency operates at the resonant frequency f_{02} of the notch filter. As a result, if overload or even shorted output condition occurs, the current can be limited inherently by the resonant tank characteristic. The notch filter center frequency f_{02} can be designed to achieve the over load protection.

In general, with variable frequency control, the resonant tank input voltage is excited as a square waveform. According to the Fourier analysis, the voltage excitation only consists of odd harmonics. Therefore, to avoid circulating energy at nominal condition, notch filter resonant frequency f_{02}should be designed at even times of nominal resonantfrequencyf_{01}. Meanwhile, f_{02} is preferred close to f_{01}.Thus, $f_{02} = 2f_{01}$ is a good choice.

As shown in Fig. 5.5, the voltage and current stresses of LLC and proposed 4-element resonant converter are very similar.

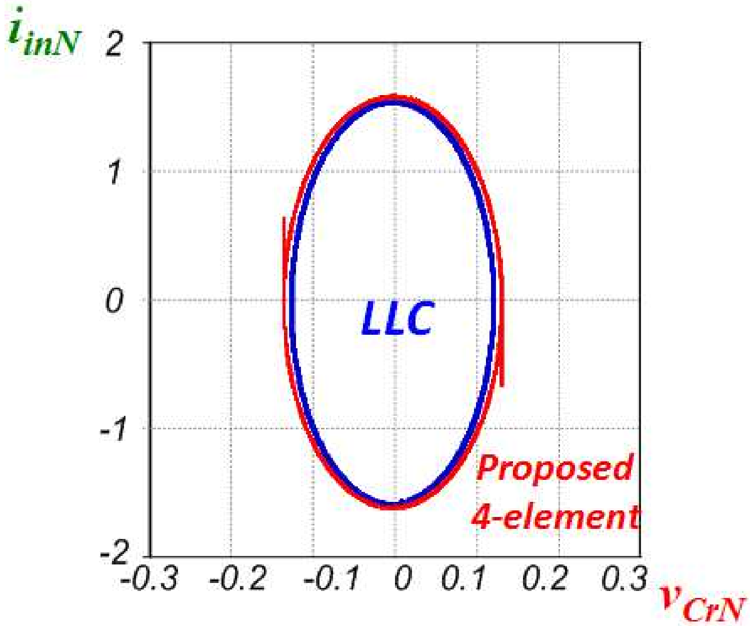

Fig. 5.5 V-I stresses of LLC and 4-element resonant converters

When converter operates at f_{01}, the notch filter represents inductive. The impedance of C_p is much larger than L_p. The major part of primary side current flows through L_p, not C_p. The current stress on C_p is much less than C_r.

With leakage inductance L_r, a second band pass filter is created. A 5-elements resonant tank is given as an example, shown in Fig. 5.6. The second band pass filter is designed at the three times of the nominal frequency. The third order harmonics energy of primary side can be delivered through this band pass filter. Obviously, the power delivery is more efficient.

However, there are 6 passive components in resonant tank. The high number of passive components might increase the size considerably. It is very desirable to integrate the passive components. Hence, higher power density can be achieved.

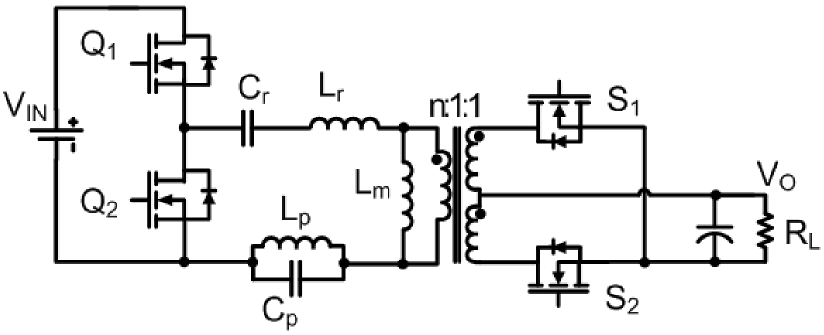

Fig. 5.6One example of 5-element resonant converters

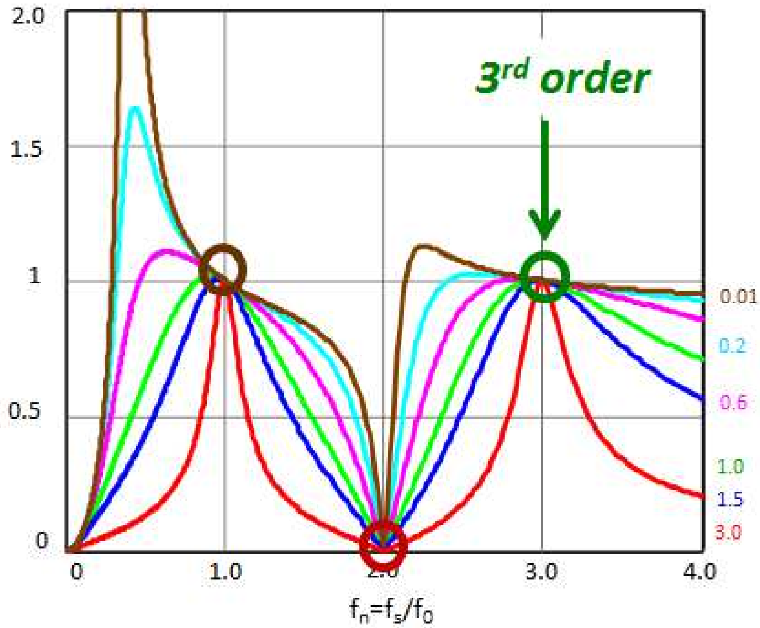

Fig. 5.7Gain Curves of selected 5-elements resonant converter

5.3 Magnetic integration for multi-elements resonant converters

To improve the power density, the magnetic integration method is widely applied in resonant converters. For LLC resonant converters, L_r is the leakage inductance, and L_m is the magnetizing inductance, as shown inFig. 5.1.

For 5-elements resonant converters, there are four magnetic components: L_r, L_p, L_m, and transformer. It is hard to integrate all components into one module by traditional transformer structure. The transformer structure needs to be modified.

In this section, a different transformer structure is proposed to integrate all magnetic components into one.

As mentioned in [E.9], cantilever model is suited for multiple-winding magnetic model. Fig. 5.8(a) gives the cantilever model for LLC center-tap transformer. Winding 1 is the primary side winding, and winding 2, 3 are two secondary side windings. The effective leakage inductance l_{12}, l_{13}, l_{23} represent the couple relationship between winding 1, 2, and 3. n_2, n_3 represent the effective turns ratio of winding 2, 3 with winding 1.

Normally, the two secondary side windings are very close, and have same turns (n_2=n_3), thus, l_{23} is negligible. Thus, l_{12}, l_{13} can be combined as l_{123}, as shown in Fig. 5.8 (b). Then, this model can be transferred into equivalent model in Fig. 5.8(c).Here, $\boldsymbol{L_{11}^2/(L_{11}+l_{123})}$represents the magnetizing inductance (L_m), sodoes $(L_{11}\times l_{123})/(L_{11}+l_{123})$ the leakage inductance (L_r).

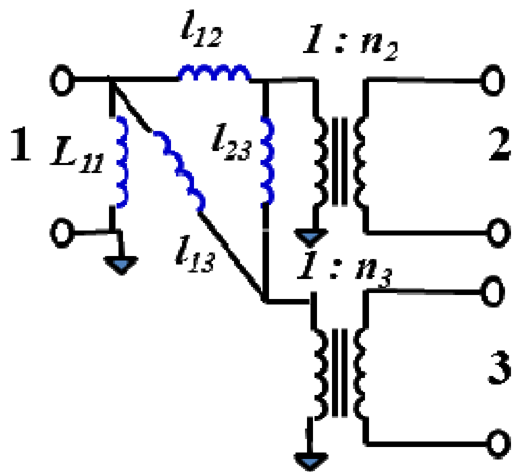

(a) Cantilever model for LLC transformer

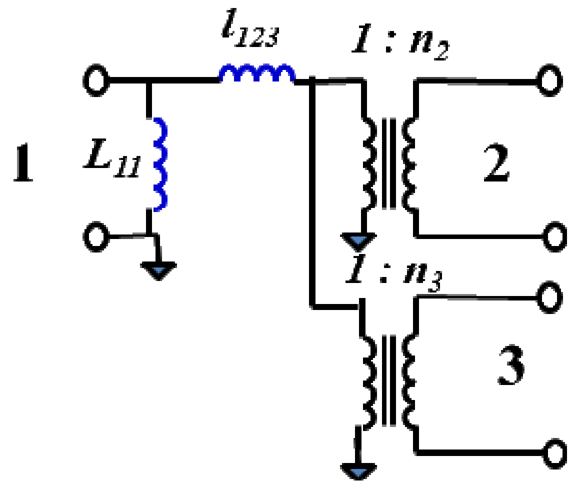

(b) Simplified model for LLC transformer

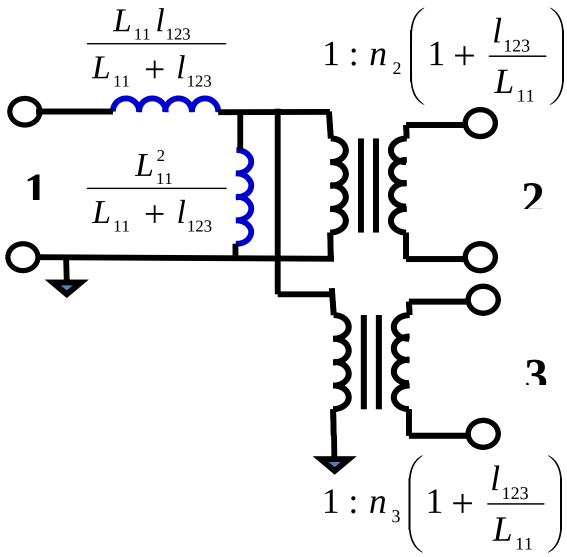

(c) Equivalent model for LLC transformer

Fig. 5.8Cantilever model for LLC transformer

With traditional transformer structure, only series resonant inductor and magnetizing inductor can be integrated. To integrate the third resonant inductor, one more winding (winding 4) is added into transformer.

The effective leakage inductance l_{14}, l_{24}, l_{34} represent the couple relationship between winding 1, 2, 3 and 4. n_4 represent the turns ratio of winding 4 with winding 1. The cantilever model is shown in Fig. 5.9.

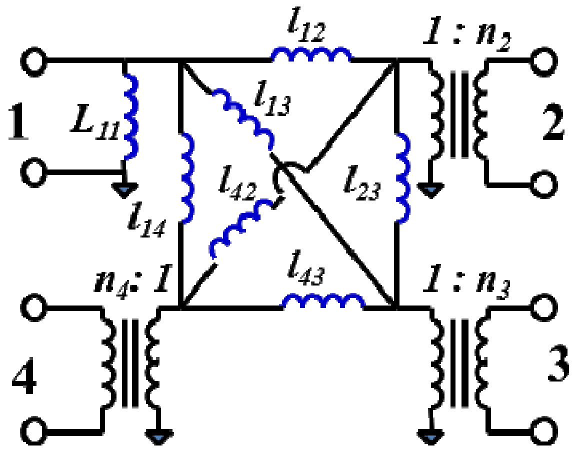

Fig. 5.9Cantilever model for proposed transformer

As mentioned above, l_{23} is small enough to be negligible, and l_{12}, l_{13} can be combined as l_{123}. If winding 4 is not coupled tightly with winding 2 and 3, l_{42} and l_{42} would be large enough to be ignored. The equivalent circuit is in Fig. 5.10.

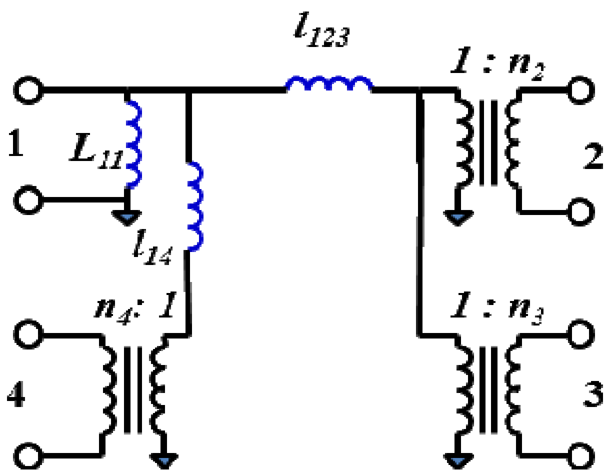

Fig. 5.10Simplified model for proposed transformer

The resonant tank connection is shown in Fig. 5.11 (a). The dash lines are the connecting wires among integration module and discrete capacitors C_r and C_p. The winding 1 and 4 share the same ground. When $n_4=1$, the node A and B have the same electrical potential, so they can be treated as virtually shorted as in Fig. 5.11 (b). Thus, the final resonant tank is Fig. 5.11 (c). The leakage inductance between winding 1 and 4 (l_{14}) creates L_p.

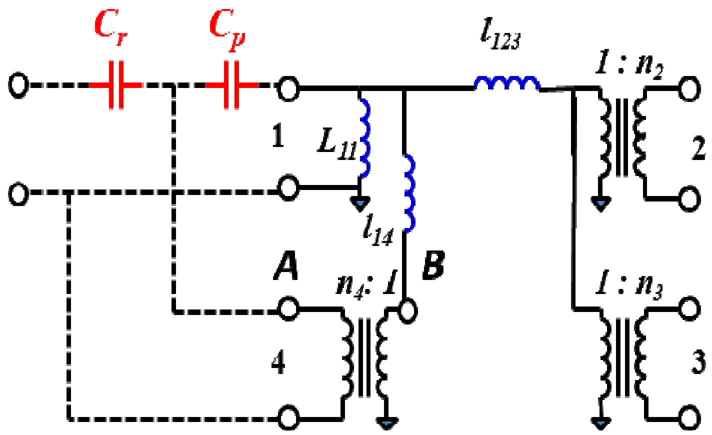

(a) Connection for discrete Cr, Cp and integrated magnetics

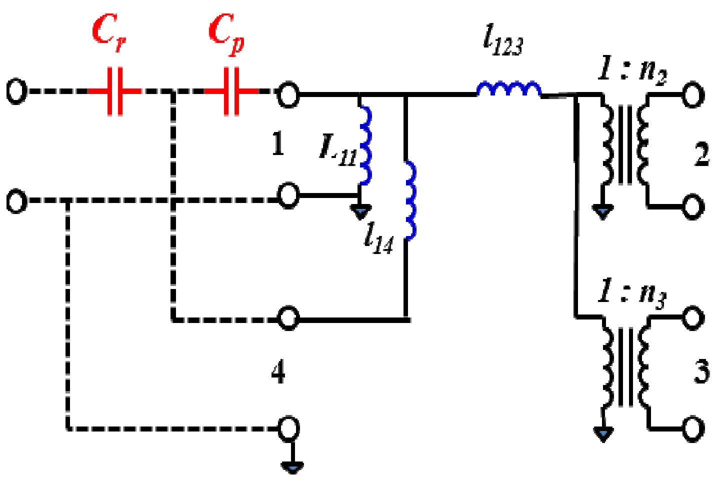

(b) Equivalent circuit when $n_4=1$

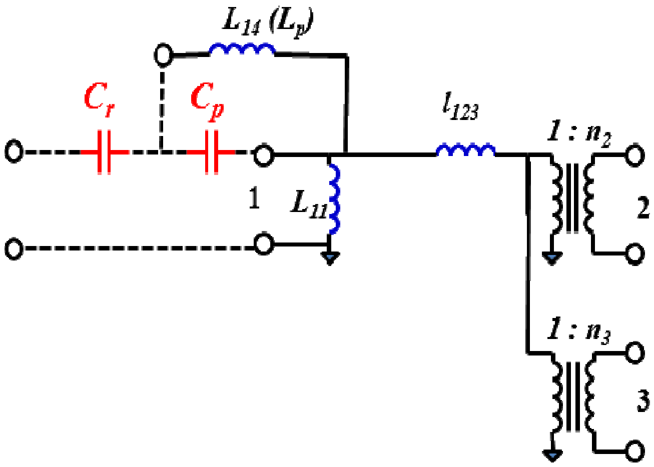

(c) Modified equivalent circuit when n_4=1

Fig. 5.11 Equivalent circuit for discrete C_r, C_p and integrated magnetics

The gain curves for this multi-element resonant converter are shown in Fig. 5.12, which is very similar as Fig. 5.9. Namely, superior merits, full load range ZVS, good frequency controllability for current limit and voltage gain, can be successfully obtained.

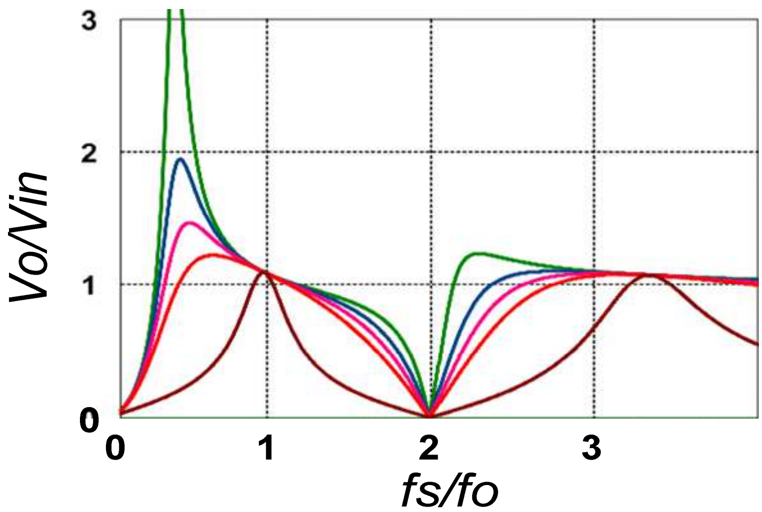

Fig. 5.12The gain curves of passive integration model

Each parameter of the cantilever model can be directly measured. All magnetic components in resonant tank are integrated in one transformer module.

For simplification, an easy way to understanding the integration method is based on the magnetic relationship between windings. Fig. 5.13 (a) shows the integrated magnetic module which includes transformer (T_x), magnetizing inductance (L_m), leakage inductance (L_r) and L_p. The equivalent circuit is given in Fig. 5.13 (b). L_r is the leakage inductance indicating the magnetic decoupling of winding 2, 3 and winding 1, 4. L_p is the leakage inductance indicating the magnetic decoupling of winding 1 and winding 4. Magnetizing inductance (L_m) is determined by the air gap.

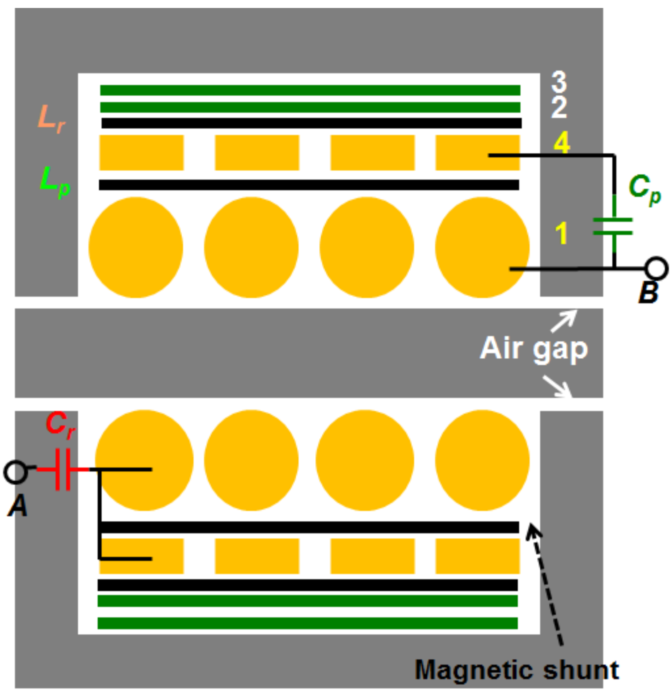

(a) Crossview of integrated magnetics

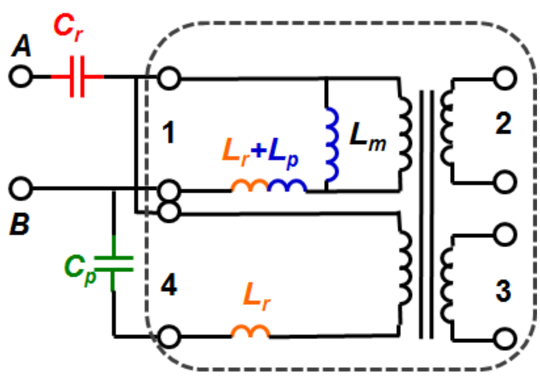

(b) Equivalent circuit

Fig. 5.13The realization of magnetic integration module

The turns of winding 1 and winding 4 is the same, and these two windings are connected at one terminal. Thus, we can transform Fig. 5.13 (b) to Fig. 5.14 (a). While Lr is determined by the distance between primary winding (1,4) and secondary winding (2, 3), so Fig. 5.14 (a) can be transferred into Fig. 5.14 (b), which is similar as the resonant tank in Fig. 5.6.

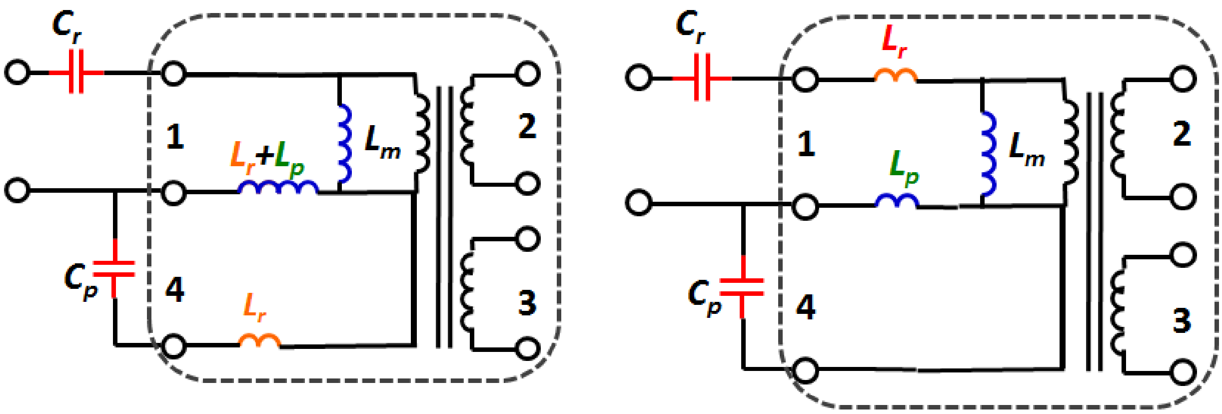

(a) Transformation 1 (b) Transformation 2

Fig. 5.14The transformation of equivalent circuit

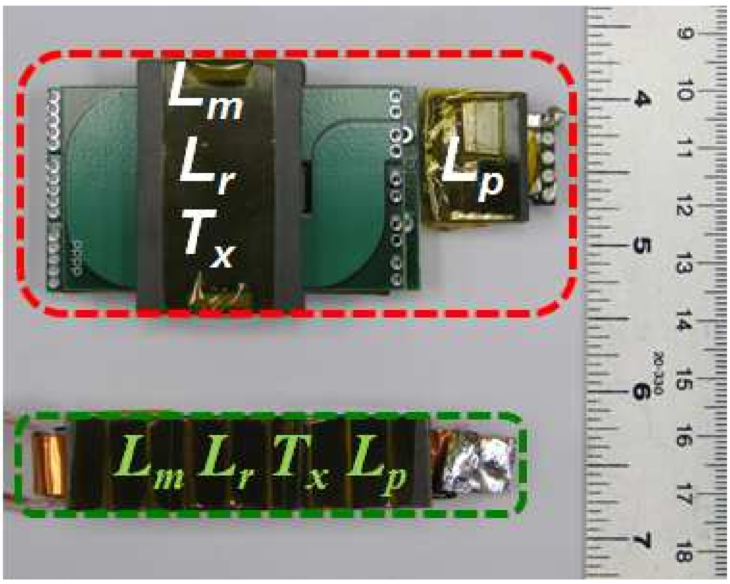

Fig. 5.15 Volume comparison of proposed and traditional magnetic integration method

One magnetic module is built to verify the volume improvement. The previous magnetic integration method utilizing magnetizing inductance and leakage inductance of transformer, but cannot integrate L_p. The proposed method can integrate all the magnetic components. The previous magnetic components volume is $39.73cm^3$. The new magnetic module is $16.23cm^3$.

The experimental waveforms are provided in Fig. 5.16 (a). It is clear that the fundamental go through winding 1 and the 3rd harmonic through winding 4. For fundamental, the impedance of C_p and L_r is very high, while L_p and L_r is relative low. Thus, major part of fundamental flew through winding 1. For 3rd harmonic, the impedance of C_p and L_r is very low, while L_p and L_r is relative high. Thus, major part of 3rd harmonic flew through winding 4.

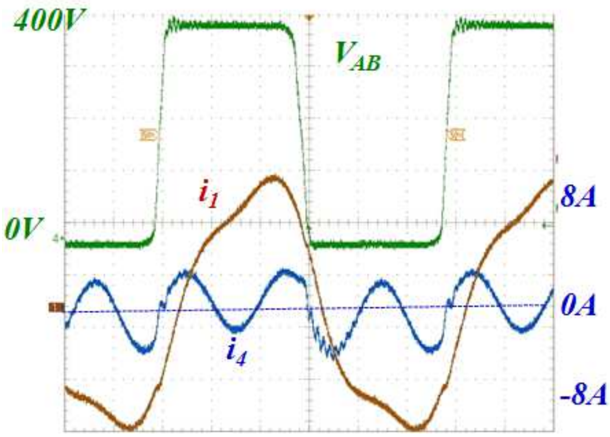

(a) Experiment results for winding stresses

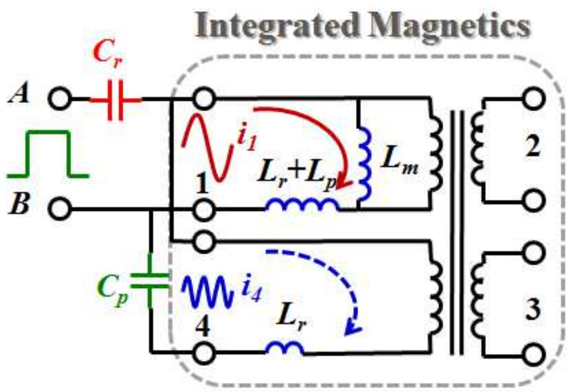

(b) Equivalent circuit

Fig. 5.16 Stress comparison for integrated magnetic module

5.4 Passive Integration for Multi-element Resonant Converters

In order to further improve the power density, passive integrationincluding the resonant capacitors is required.

Firstly, there are two resonant capacitors (C_r and C_p) in the resonant tank. Which capacitor integrated into module should be chosen carefully. Voltage and current stresses are very critical to capacitor's lifetime. High voltage stress or high current stress will cause short life time of capacitors, in other words, short life of whole converter. Thus, low stress resonant capacitor should be picked.

Based on the analysis of Fig. 5.16, we can see all current including fundamental and 3rd harmonic flow through C_r, only small 3rd harmonic through C_p. For half bridge structure, there is half DC input voltage cross C_r, while no DC voltage bias on C_p. It is obvious that C_p has much less stress than C_r. Thus, C_p should be taken into integrated module.

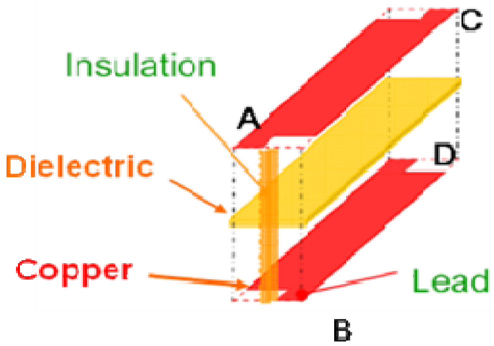

(a) Physical structure of LC cell

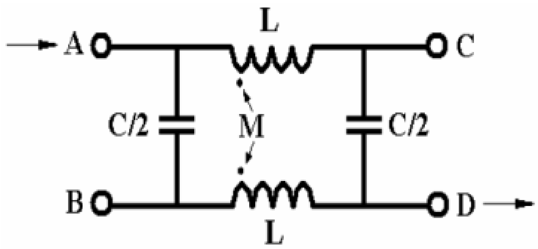

(b) Lossless symmetric model

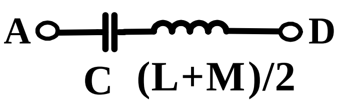

(c) 1st order model for fundamental design

Fig. 5.17LC cell structure and equivalent circuit

LC cell is the basic element in passive integration. Its structure is shown in Fig. 5.17(a). The dielectric layer is covered by copper layers at the both side. The lossless symmetric model of this structure is given in Fig. 5.17(b). C is the capacitance of LC cell, while L is the self-inductance of one side copper strip and M is the mutual inductance. Its equivalent circuit measured between terminal A and D is a series of inductor and capacitor, as shown in Fig. 5.17(c).The value of inductance and capacitance can be controlled by cascading LC cells, as shown in Fig. 5.18. The equivalent capacitors are in parallel and the equivalent inductors are in series.

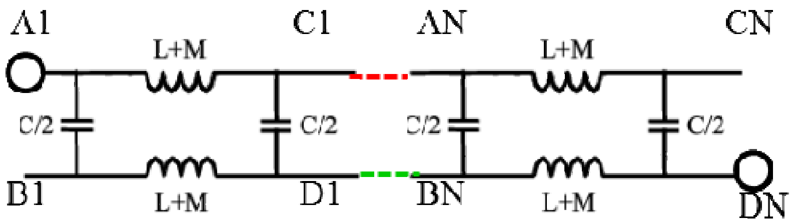

Fig. 5.18Interconnection of LC cells

The capacitance of each LC cell can be calculated by following formula.

$$C = \frac{\varepsilon_0 \cdot \varepsilon_r \cdot A_{cu}}{T_{di}} \tag{5.1}$$

C is the capacitance. A_{cu} is the area of each plate. ε_r is the relative static permittivity (dielectric constant) of the material between the plates. ε_0 is the permittivity of free space. T_{di} is the separation between the plates.

The passive integration with a stacked structure for resonant converters has been proposed to integrate the LLCT module to achieve high power density. Fig. 5.19gives the winding structure of LLCT module. The exploded view of an LLCT module with the stacked structure is shown in Fig. 5.20. Two sets of C core and I core constitute the two winding windows. The secondary winding is made of thin copper strips. The primary winding is implemented with cascading LC cells in order to integrate the resonant capacitor in to the transformer. The cells are connected at the terminals through the interconnections on the vertical surface at the two ends of the module as shown in Fig. 5.20. The cell dimensions and the properties of the dielectric substrate determine the resonant capacitance (C_r). The magnetizing inductance (L_m) can be adjusted by changing the length of the air gap. By inserting leakage layer between the primary and secondary windings, the leakage inductance (L_r) can also be controlled.

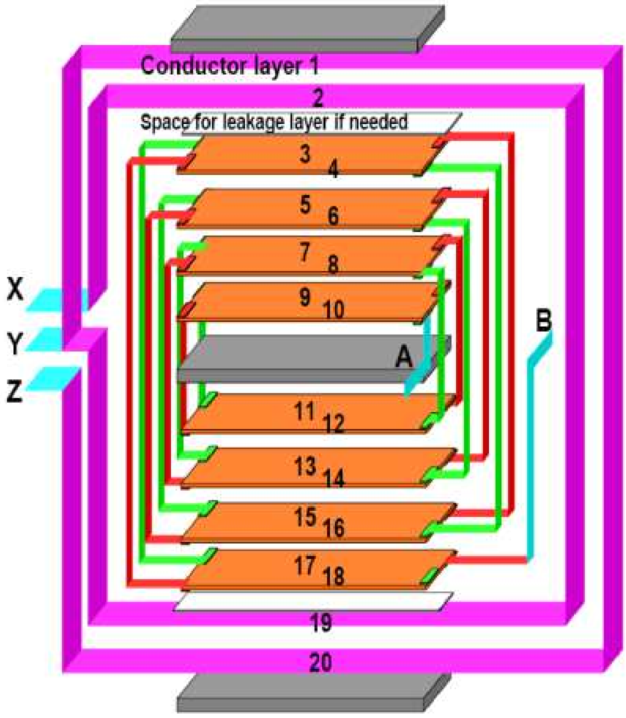

Fig. 5.19Interconnections and winding structure of an integrated LLCT module

For the 5-element resonant tank, it is difficult to integrate both capacitors. The choice of capacitor to be integrated is determined by the consideration of reliability. Large voltage and current stress will cause short life time of capacitor. In this particular topology, C_r has very high

DC voltage bias while C_p only has small AC voltage. Moreover, C_r carries all the primary current while C_p only carries the third order harmonics as discussed before. Thus, C_r has much higher voltage and current stress than C_p, in other words, less reliable. Thus, C_p is chosen to be integrated into the transformer.

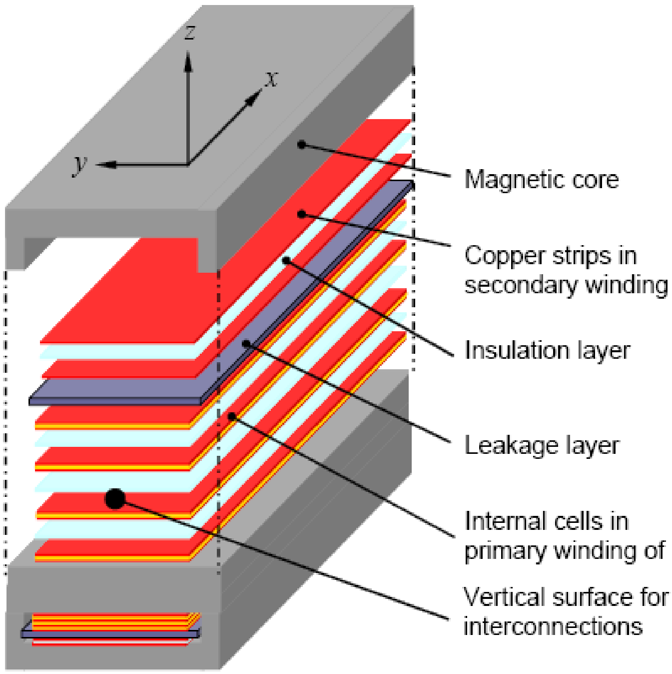

Fig. 5.20Exploded view of an LLCT module with the stacked structure

The integrated transformer structure for L_p,L_r,L_m,C_p, and transformer is similar to the integration technique for magnetic integration except that one winding (winding 1) is replaced by LC cell, the connection is shown in Fig. 5.21(a). It is a 4-winding structure and the cantilever model is introduced to derive its equivalent circuit. Winding 1 and 4 are primary windings constructed by LC cell and copper wire, respectively. The LC cell interconnection is like Fig. 14. That means the equivalent capacitor of LC cell is in series of parasitic inductance of winding 1, like Fig. 5.21(b). Winding 2 and 3 are secondary side windings. L_{11} is the self-inductance of winding 1. The effective leakage inductance l_{12}, l_{13}, l_{14}, l_{23}, l_{24}, l_{34} represent the couple relationship between winding 1, 2, 3 and 4. n_2, n_3, n_4 represent the turns ratio of winding 2, 3, 4 with winding 1, as shown in Fig. 5.21(c).

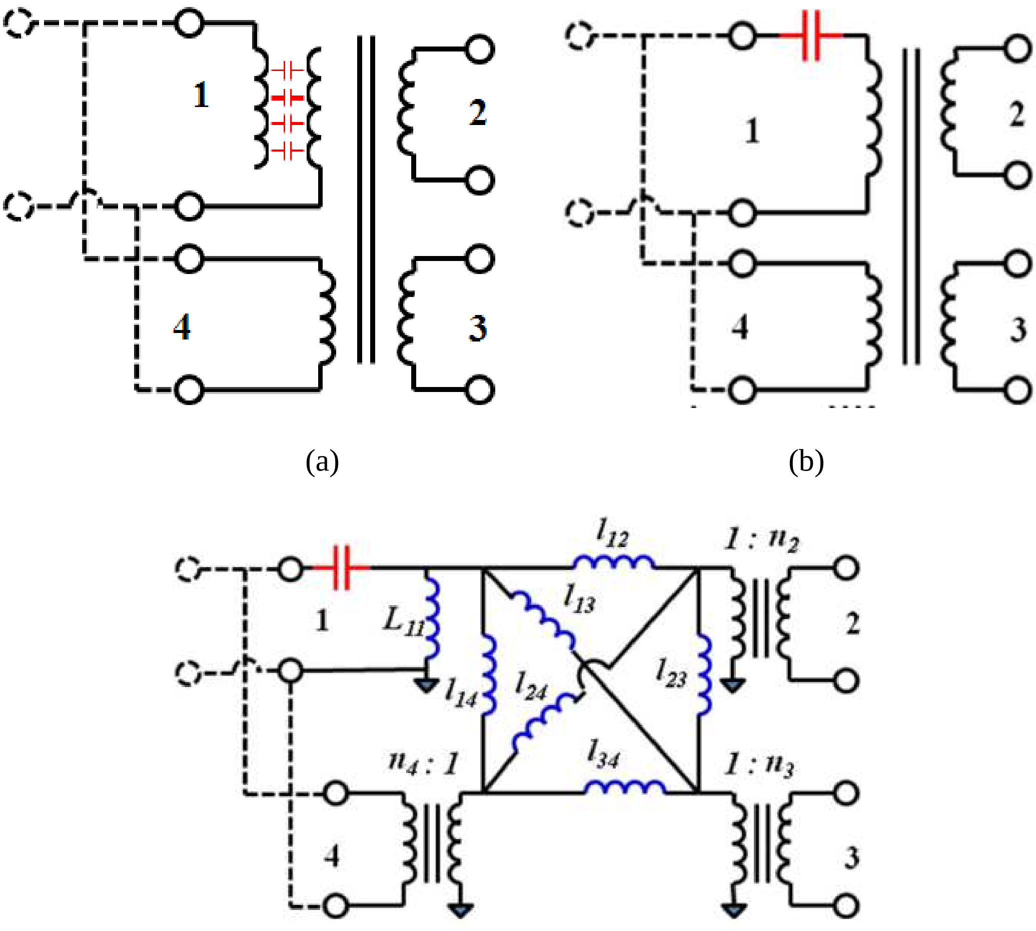

(a) (b)

(c)

Fig. 5.21Winding model for 4-winding transformer

Normally, the two secondary side windings are very close, and have same turns (n_2=n_3), thus, l_{23} is negligible. Thus, l_{12}, l_{13} can be combined as l_{123}, so can l_{24}, l_{34} as l_{423}, as shown in Fig. 5.22. The dash lines represent connection wire between integration module and C_r. If winding 4 is not coupled tightly with winding 2 and 3, l_{423} would be large enough to be ignored. Then, it is the same topology as in Fig. 5.12 (a). Thus, it also can be modified as the resonant tank in Fig. 5.12(c). They are also have the same gain curves.

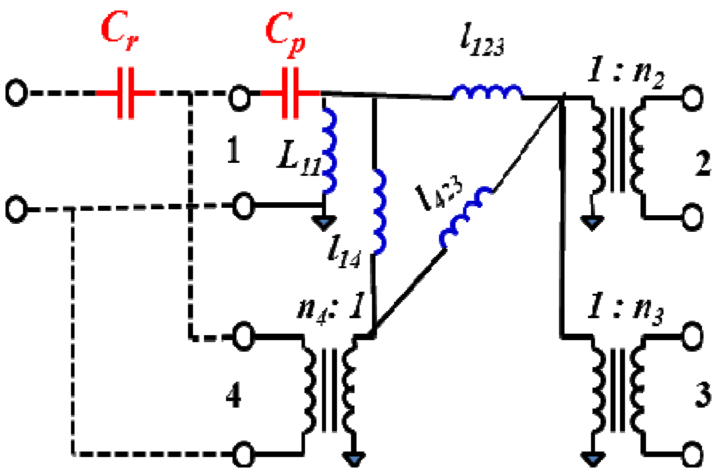

Fig. 5.22The passive integration model

Thus, all passive components are integrated except C_r (the high stress component). All the leakage inductance can be tuned by adjusting the distance between windings or with magnetic shunt. L_{11} can be controlled by air gap.

The transformer structure in Fig. 5.23is given for example. C_p is determined by LC cell in winding 1. L_{11} is controlled by air gap. l_{14} (L_p) is controlled by magnetic shunt between winding 1 and 4. l_{123} (L_r) is controlled by magnetic shunt between winding 1 and 2. Winding 4 can be either round copper wire or copper strips.

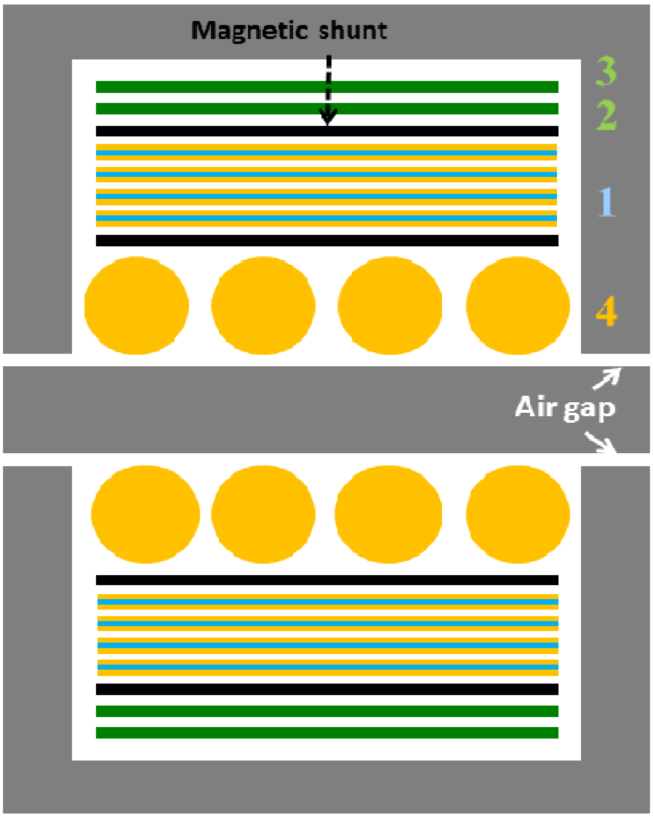

Fig. 5.23Transformer structure for integration

5.5 Measurement of Transformer parameters

Different with the transformer module before, passive integrated transformer including LC cell is not suited to use the same measure method. The capacitance of LC cells makes the measurement method invalid. A new measure method is proposed based on cantilever model.

The transformer model of proposed passive integration structure is shown in Fig. 5.24.

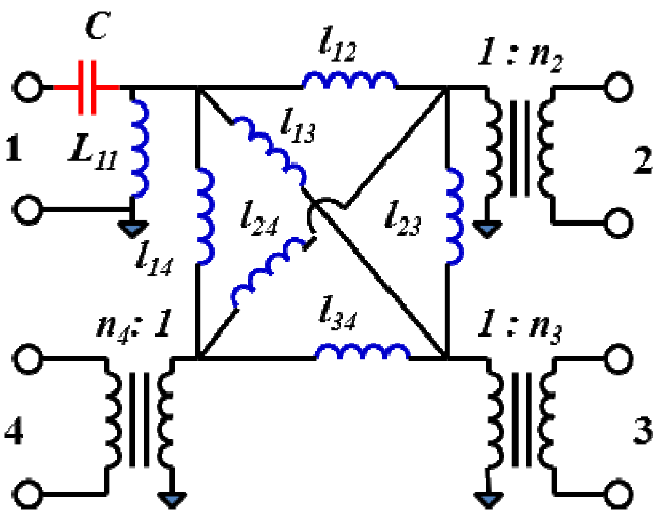

Fig. 5.24Transformer model of proposed structure

First, the self-inductance $L_{11}$and capacitance C are measured based on impedance analyzer (***Agilent 4294A***), by open-circuiting windings 1, 2 and 3.

To measure the effective turns ratios n_2, n_3,...,n_k, and AC voltage $V_1$is applied to winding 1, with the other windings open circuited. The effective turns ratio n_k, is given by

$$n_k = \frac{V_k}{V_1}\frac{\frac{1}{j\omega C} + j\omega L_{11}}{j\omega L_{11}} = \frac{V_k}{V_1}\frac{\omega^2 L_{11}C - 1}{\omega^2 L_{11}C} \tag{5.2}$$

V_k is the measured voltage of winding k. ω is the angular frequency of AC voltage applied to winding 1. A negative value of n_k indicates that the winding polarity marks should be reversed.

Direct measurement is hard for this transformer structure due to LC cell. All the inductance can be calculated based on impedance measurement. Six measurement cases are needed for effective leakage inductance calculation.

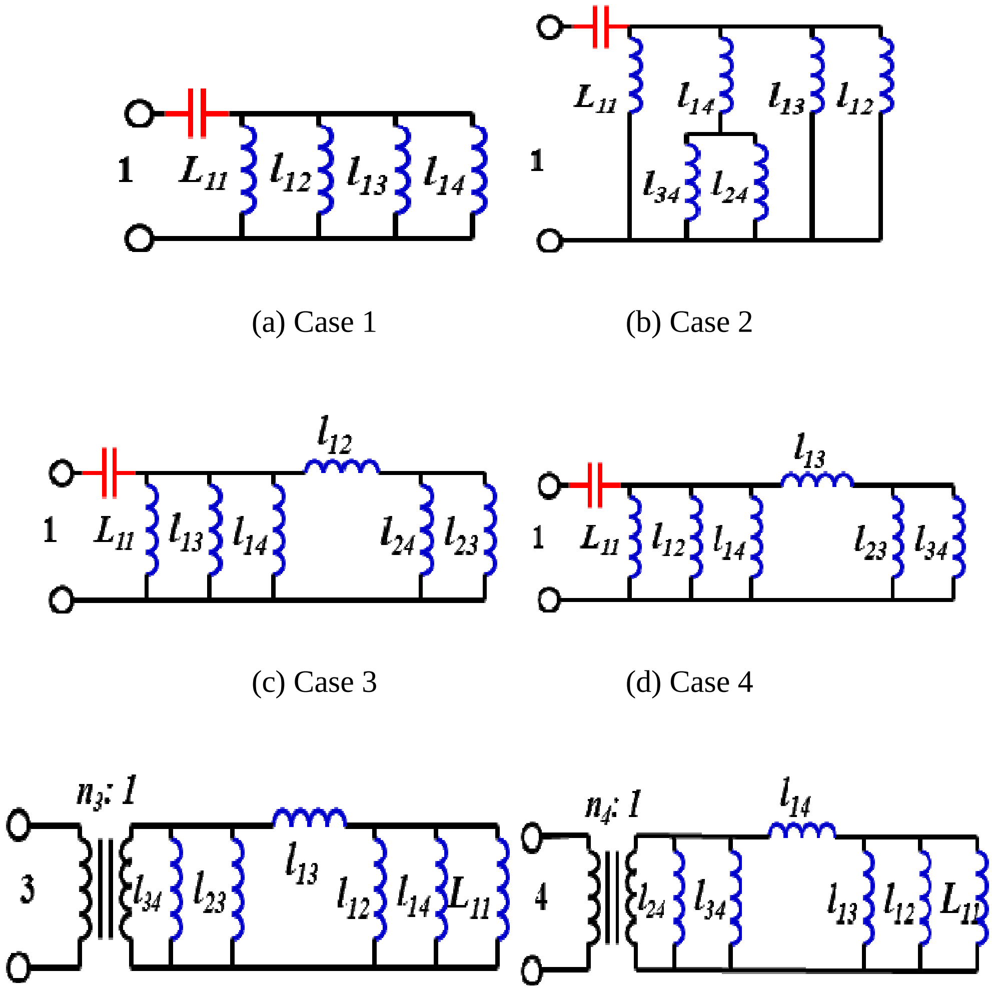

(a) Case 1 (b) Case 2

(c) Case 3 (d) Case 4

(e) Case 5 (f) Case 6

Fig. 5.25. Equivalent circuits for 6 cases

Case 1 is measuring the impedance of winding 1 port by shorting winding 2, 3 and 4. The equivalent circuit is shown in Fig. 5.25(a).

Case 2 is measuring the impedance of winding 1 port by shorting winding 2, 3 and opening winding 4. The equivalent circuit is shown in Fig. 5.25 (b).

Case 3 is measuring the impedance of winding 1 port by shorting winding 3, 4 and opening winding 2. The equivalent circuit is shown in Fig. 5.25 (c).

Case 4 is measuring the impedance of winding 1 port by shorting winding 2, 4 and opening winding 3. The equivalent circuit is shown in Fig. 5.25 (d).

Case 5 is measuring the impedance of winding 4 port by shorting winding 2, 3 and opening winding 1. The equivalent circuit is shown in Fig. 5.25 (f).

Based on above 6 cases, all effective leakage inductances can be calculated. The calculated results based on real integrated module are shown in Fig. 5.26.

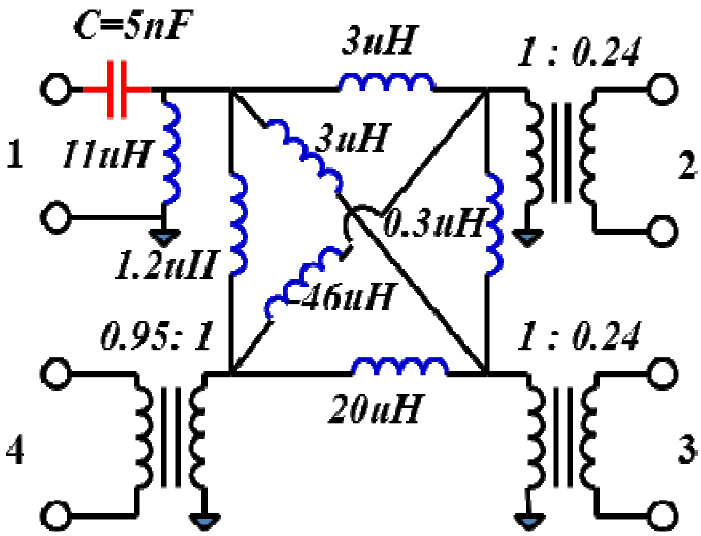

Fig. 5.26Calculated results of integrated transformer module

The final parameters of integrated module after simplified are shown in Fig. 5.27.

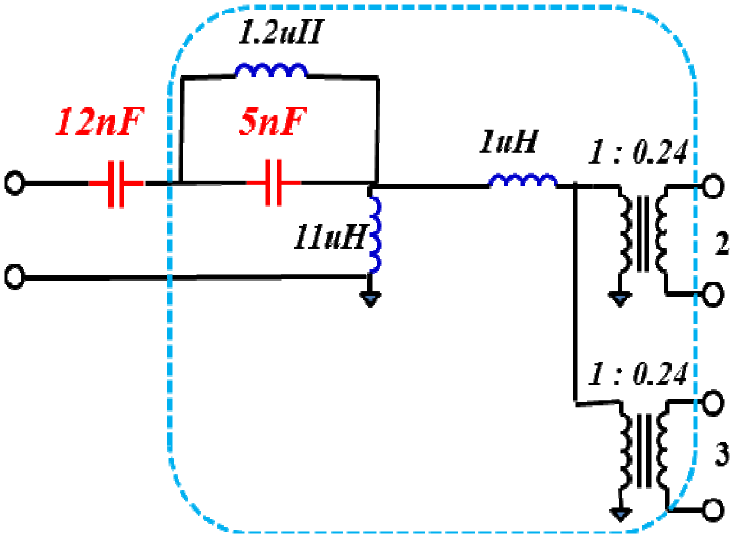

Fig. 5.27 The final parameters of integrated transformer module

The volume comparison is given inFig. 5.28. The volume of previous magnetic components and C_p is $40.48cm^3$. The passive integration module is $16.79cm^3$.

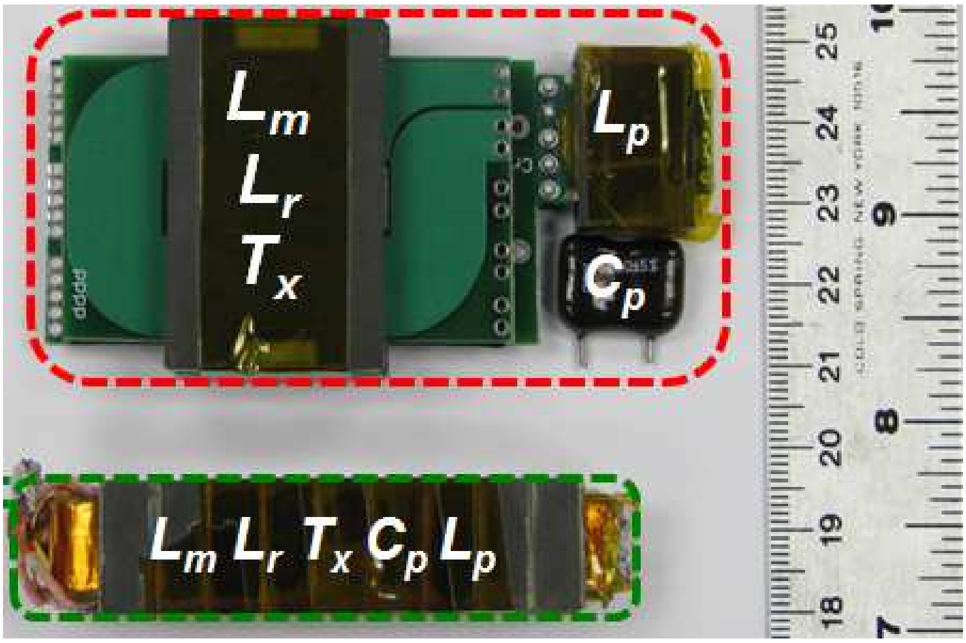

Fig. 5.28 The volume comparison of passive module and discrete components

5.6 Thermal Improvement by Heat Extractor

Associated with the increasing power density, loss density increases. Although the loss density in the passive component is much lower than that in power semiconductor devices, the lower thermal conductivities of most materials applied in passive components leads to high temperature gradient inside the component. The thermal issues limit the increase of power density. The maximum allowed temperature inside an integrated module is one of the most important design criteria.

Although the surface temperature of a passive module can be controlled by the external cooling conditions, the temperature rise inside the module is determined by the loss distribution, the material properties and the structure. For a practical design, the structure is basically determined by the considerations of electromagnetic function, and the materials are generally selected for their electromagnetic characteristics to meet the required parameter values. When the structure and materials are fixed, the loss distribution is determined by the circuit operation, which is normally also fixed. Thus, itis difficult to improve the thermal performance of an existing design without changing the structure or materials. The most common approach to reduce the inside temperature gradient is to increase the dimensions, which reduces the loss density and increase the heat dissipation area, however, sacrifices the power density. It is clear that in cases where the thermal constraint is the dominant design criterion, the heat dissipating ability of a module is directly related to the power density. In other words, by improving the heat dissipating ability, the power density can be improved. Being aware of this, the heat extraction technology is developed[E.12].

To apply heat extractors in power electronics module, the heat extractor plate should be parallel to the magnetic flux to avoid influencing the electromagnetic performance. The structure shown in Fig. 5.29can embed heat extractors without change the electromagnetic performance, but the inside filed distribution changes due to the redistribution of the magnetic flux. The induced fringing effect may even influence the conduction loss. If the heat extractors occupy a small relative volume, the change of the magnetic field is neglected.

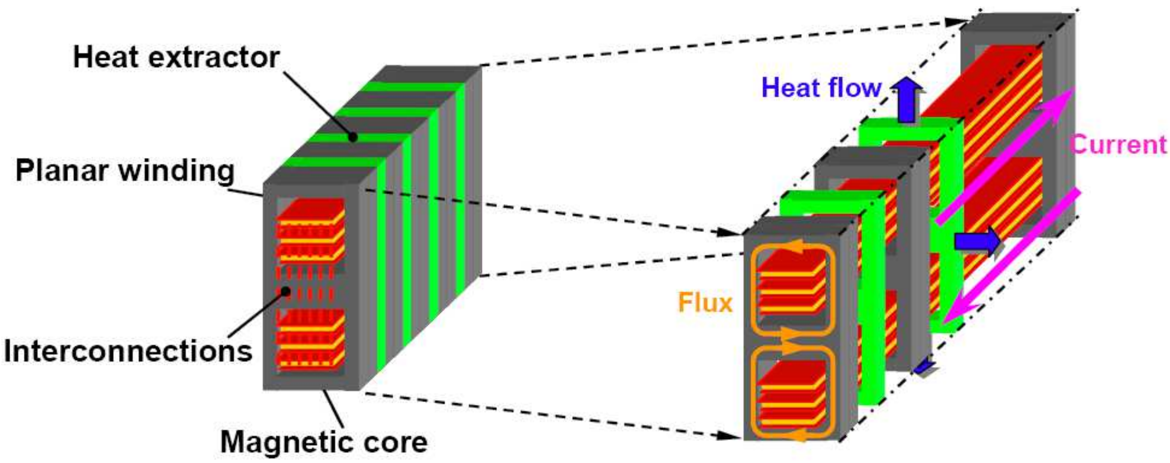

Fig. 5.29Integrated passive module with heat extractors

The embedding of heat extractors also changes the distribution of the thermal field. Originally regarded as a uniform heat source, the core is now several individual heat sources with higher heat generation.

In the integrated module, there are two heat sources: the winding block and the magnetic core. By applying the superposition principle, the amounts of heat flux generated by these two heat sources can be studied separately, and the results can be combined linearly. For the heat generated inside the winding block, both the core and heat extractors are conduction channels, through which heat can be conducted to the heat sink. The internal and external thermal contact resistance and the equivalent thermal resistance of the combination of the core and heat extractors are the barriers on this heat path.

For heat generated in the core, the winding block functions as a conductor connecting the core and heat extractors. The internal thermal contact resistance functions twice on one of the heat paths. Because of the different heat distribution, the equivalent thermal resistance of the combination of core and heat extractors is different from that for heat coming from inside the winding block.

The equivalent structures of both cases are shown in Fig. 5.30, where the core and the winding block are replaced by equivalent spot heat sources, and the corresponding equivalent thermal resistance is applied. Here, the thermal conductivity of core material (MnZn ferrites) is about (3.5~5.0) x 10^{-3}K·m·W^{-1}, while the thermal conductivity of heat extractor (aluminum nitride), is about 170~190 K·m·W^{-1}. The thermal conductivity of heat extractor is much larger than core material. Thus, large portion of heat generated by windings and cores would pass through heat extractor to the heatsink.

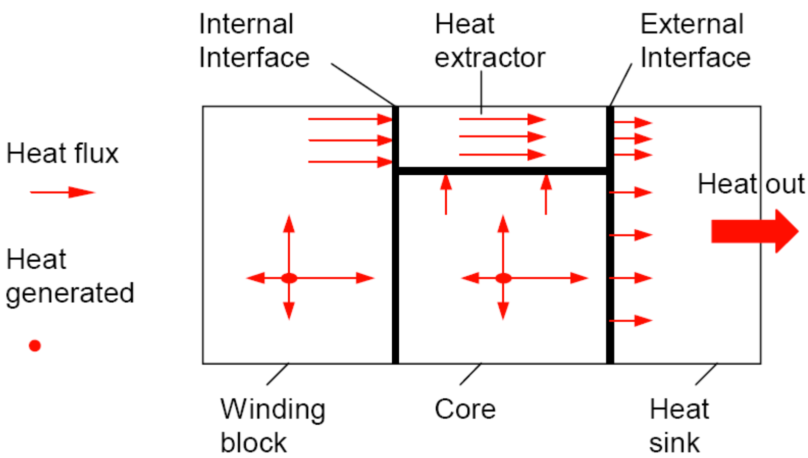

Fig. 5.30 Diagram of heat paths on cross section

The core dimension is given by Fig. 5.31, while the heat extractors are made of 0.5mm aluminum nitride substrates and have the same cross-sectional dimensions with the core. The core material is 3F4. The whole core is combined by 9 pieces of 3F4 ferrite and 8 pieces of heat extractor. The real picture is shown in Fig. 5.32.

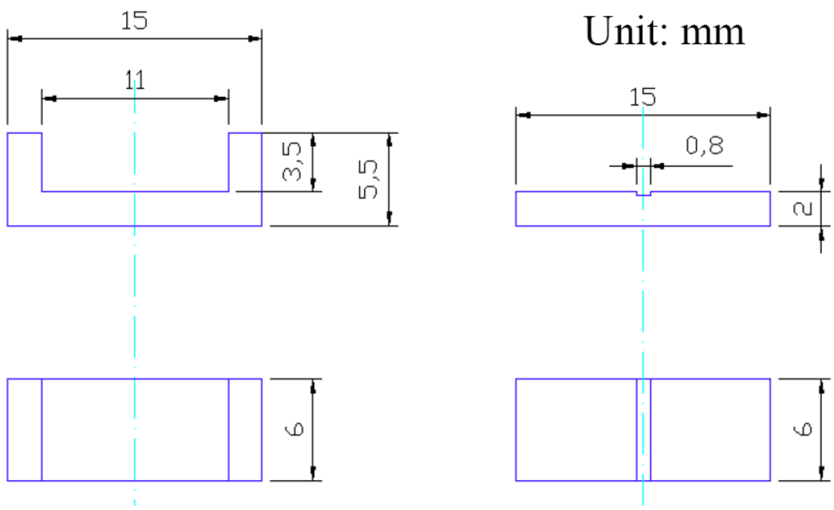

Fig. 5.31Core dimensions

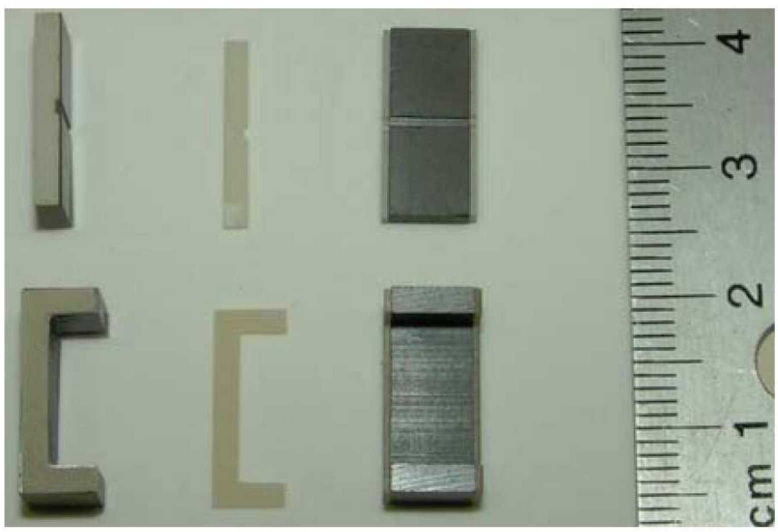

Fig. 5.32Picture of cores and heat extractors

The volume comparison after adding heat extractor is given in Fig. 5.33.

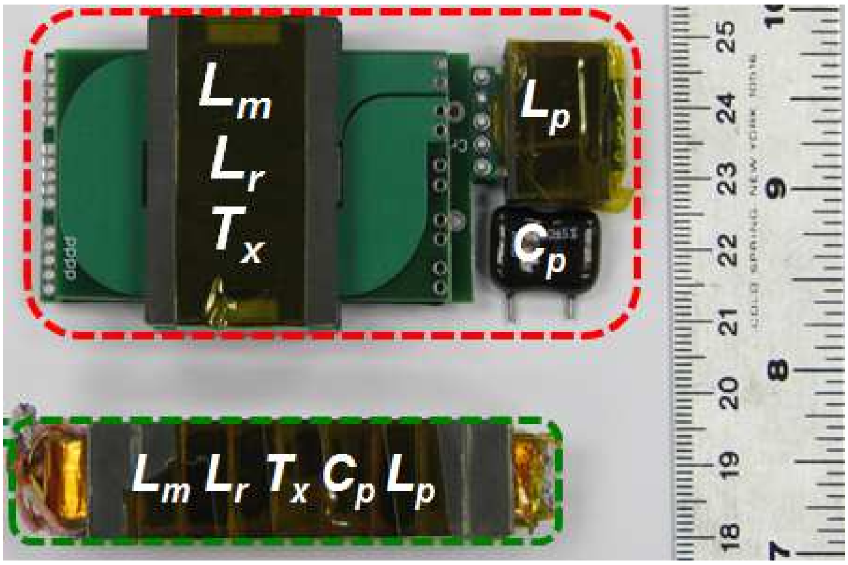

Fig. 5.33 The volume comparison of passive module and discrete components

5.7 Experimental Results

An 800 kHz 1.2kW 400V/48V five-element integration prototype is shown in Fig. 5.34 (a). The parameters in resonant tank are $C_r=12nF$, $C_p=5nF$, $L_p=1.2uH$, $L_r=0.9uH$, $L_m=10uH$. The turns ratio is 4:1:1. The no load and 50% load waveforms are shown in Fig. 5.34 (b), (c). The waveforms for secondary side short-circuit is given in Fig. 5.34 (d). The output current is suppressed to 20A at 1.6 times of resonant frequency, which is less than full load current. The power density is nearly 171W/inch^3.

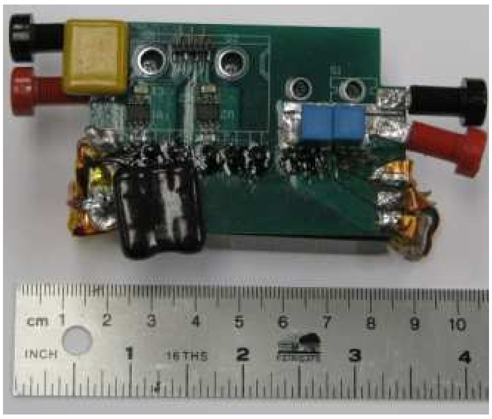

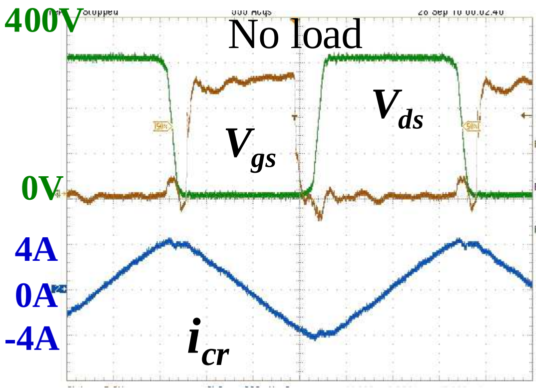

(a) Power stage (b) No load waveform

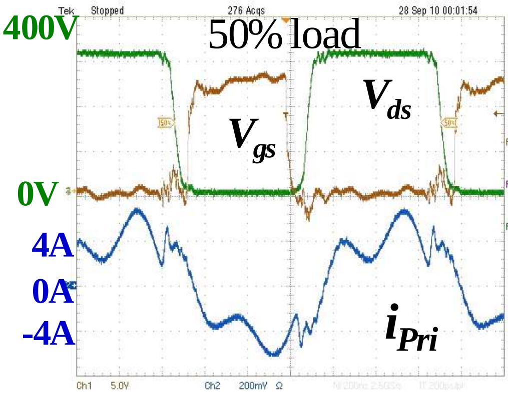

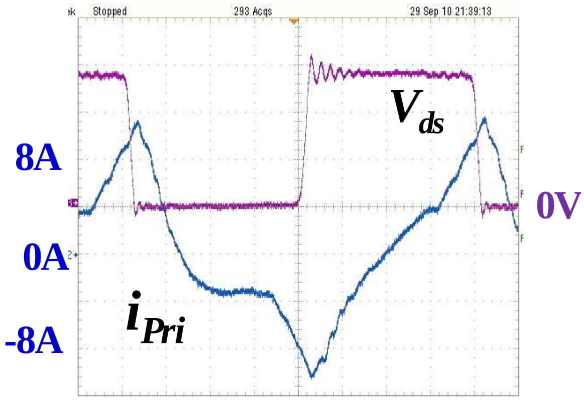

(c) 50% load waveform (d) Short-circuit waveform

Fig. 5.34Experimental results for five-element resonant converter with passive integration module

5.8 Conclusion

A novel passive integration method is proposed for multi-element resonant converters. Based on this method, the passive integration for 3-element, or higher order elements resonant converters are achievable. Most of passive components (capacitors, inductors and transformer) are integrated into one module to achieve high power density. The proposed multi-winding transformer structure with integrated inductor and capacitor are analyzed with a detailed cantilever model. Design guidelines are summarized for the control of the component values. One prototype of 1.2kW, 800 kHz 400V/48V 5-element resonant converter is built and tested to verify the proposed structure. The power density can be achieved as high as 171W/inch^3.

Chapter 6. Conclusion and Future Work

6.1 Conclusion

The LLC resonant converter exhibits higher efficiency and higher power density than conventional PWM converters. Thus, it has been widely adopted as a desirable power supply for telecoms, servers, desktops, laptops, flat-panel TVs, LED lighting, etc. To further improve the LLC performance, several novel concepts and techniques have been developed in this dissertation.

The high switching frequency is needed recently for high power density requirement. However, LLC resonant converter suffers high transformer loss. Matrix transformer is introduced to reduce winding loss and total volume. Flux cancellation method is utilized to reduce core size and loss. Synchronous Rectifier (SR) devices and output capacitors are integrated into secondary windings to eliminate termination related winding losses, via loss and reduce leakage inductance.

To solve the inherent issues, like start-up and short-circuit protection, SR driving and EMI, etc., a systematic method is proposed to find the similar resonant topologies like LLC. Based on this method, lots of high order resonant converters are found to solve the issues LLC type resonant converters cannot handle.

To evaluate the performance of found valuable topologies, a general evaluation system is proposed. State-plane analysis with new normalization factors is utilized. Based on it, the voltage stress, current stresses and apparent power of resonant converters are easy to compare. This method can help select suitable circuit topology for certain application. Meanwhile, it also can help resonant converters' design. The important performance factors, like start-up, short-circuit protection, SR driving and EMI, are also taken into account for the whole evaluation system.

The passive integration is necessary for high power density resonant converter, especially for high order system. Based on stress, suitable passive components are chosen for integration. Then, the magnetic integration method is shown based on multi-winding transformer structure. The passive integration principles are discussed. A novel passive integration method is proposed for multi-elements resonant converters.

In conclusion, this work is focus on the topology analysis and integration of resonant converters. Searching the suitable topologies for certain application, and evaluate the performance of them. Then, improve the system power density by integration techniques.

6.2 Future Work

All of these novel implementations proposed in this work will help find valuable resonant converters and evaluate their performance. Following this research, there are still some remaining works can be done:

1. The proposed matrix transformer is high power density and high efficiency, but its EMI performance is unknown. The continuous work may study the EMI noise reduction for matrix transformer.

2. By passive integration, the power density of five-element resonant converter is improved a lot. If passive integration techniques cooperates with matrix transformer, how this impact the efficiency and power density of whole system is interesting for future study.

3. The state-plane with new normalization can be extent to not only resonant converters, but also can be used for PWM converters.

References

A. Introduction

[A.1] W. A. Tabisz, M. M. Jovanovic, and F. C. Lee, "Present and future of distribution power systems", in Proc. APEC 1992, pp. 11-18.

[A.2] G. C. Hua, W. A., Tabisz, C. S. Leu, N. Dai, R. Watson, F. C. Lee, “Development Of a dc distributed power system,” in Proc. IEEE APEC 1994, vol.2, pp. 763 -769.

[A.3] F.C. Lee, P. Barbosa, P. Xu, J. Zhang, B. Yang, F. Canales, “Topologies and design considerations for distributed power system applications,” in Proc. of the IEEE, Volume 89 Issue: 6, June 2001, pp: 93 –950.

[A.4] S. K. Mazumder, K. Shenai, “On the reliability of distributed power systems: a macro- to micro- level overview using a parallel DC-DC converter,” in Proc. IEEE PESC, 2002, pp. 809-814.

[A.5] M. M. Jovanovic, "Technology drivers and trends in power supplies for computer/telecom," APEC 2006, Plenary session presentation.

[A.6] A. Pratt, P. Kumar, T. V. Aldridge, “Evaluation of 400V DC distribution in telco and data centers to improve energy efficiency,” in Proc. IEEE INTELEC, 2007, pp. 32-39.

[A.7] M. Ton, B. Fortenbery, and W. Tschudi, “DC power for improved data center efficiency," [Online]. Available: http://hightech.lbl.gov/dc-powering/about.html, Jan. 2007.

[A.8] D. J. Becker, "400Vdc power distribution: Overcoming the challenges," in Proc. IEEE INTELEC, 2010, pp. 1-10.

[A.9] 80Plus Program [Online]. Available: http://www.80plus.org.

[A.10] Energy Start Program [Online]. Available: http://www.energystar.gov, 2012.

[A.11] Climate Savers Computing Initiative [Online]. Available: http://www.climatesavers computing.org, 2012.

[A.12] Texas Instruments User’s Guide (Nov. 2009). UCC28810EVM-003 110W multiple string

LED driver with universal line input and PFC [Online]. Available: http://www.ti.com /lit/ug/sluu380b/ sluu380b.pdf.

[A.13] H. Chiu, Y. Lo, J. Chen, S. Cheng, “A high-efficiency dimmable LED driver for low-power lighting applications,” IEEE Trans. on Industrial Electronics, vol. 57, Issue 2, pp. 735-1743, Feb. 2010.

[A.14] Q. Hu, R. Zane, “LED driver circuit with series-input-connected converter cells operating in continuous conduction mode,” IEEE Trans. on Power Electronics, vol. 25, Issue 3, pp. 574-582, Mar. 2010.

[A.15] H. Wu, S. Ji, F. C. Lee, X. Wu, “Multi-channel constant current (MC3) LLC resonant LED driver,” in Proc. IEEE ECCE’11, pp. 2568- 2575, 2011.

[A.16] D. Reusch, F. C. Lee, D. Gilham, Y. Su, "Optimization of a high density gallium nitride based non-isolated point of load module", in Proc. IEEE ECCE 2012, pp. 2914-2920.

[A.17] X. Huang, Z. Liu, Q. Li, F.C. Lee, "Evaluation and application of 600V GaN HEMT in cascode structure," in Proc. IEEE APEC 2013.

[A.18] S. Ji, D. Reusch, F. C. Lee, "High-frequency high power density 3-D integrated gallium-nitride based point of load module design," IEEE Trans. on Power Electronics, vol. 28, Issue 9, pp. 4216-4226, Sep. 2013.

[A.19] Y. Su, Q. Li, F. C. Lee, "Design and evaluation of a high-frequency LTCC inductor substrate for a three-dimensional integrated DC/DC converter," IEEE Trans. on Power Electronics, vol. 28, Issue 9, pp. 4354-4355, Sep. 2013.

[A.20] W. Chen, F.C. Lee, M.M. Jovanovic, J.A. Sabate, “A Comparative Study of A Class of Full Bridge Zero Voltage Switched PWM Converters,” Proc. IEEE APEC, 1995, pp. 893-899.

[A.21] A.W. Lotfi, Q. Chen, F.C. Lee, “A Nonlinear Optimization Tool For The Full Bridge Zero Voltage Switched DC-DC Converter,” Proc. IEEE PESC ‘92, 1992, pp. 1301-1309.

[A.22] Xinbo Ruan; Yangguang Yan, “Soft-Switching Techniques for PWM Full Bridge Converters,” Proc. IEEE PESC ’00, 2000, pp. 634 -639 vol.2.

[A.23] J.G. Cho, J.A. Sabate, G. Hua, and F.C. Lee, “Zero Voltage and Zero Current Switching Full Bridge PWM Converter for High Power Applications,” Proc. IEEE PESC ’94, 1994.

[A.24] J.H. Liang, Po-chueh Wang, Kuo-chien Huang, Cern-Lin Chen, Yi-Hsin Leu, Tsuo-Min chen, “ Design Optimization For Asymmetrical Half Bridge Converters,” Proc. IEEE APEC ’01, 2001, pp. 697-702, vol.2.

[A.25] Y. Leu, C. Chen, “Analysis and Design of Two-Transformer Asymmetrical Half-Bridge Converter,” Proc. IEEE PESC ’02, 2002, 943-948.

[A.26] S. Korotkov, V. Meleshin, R. Miftahutdinov, S. Fraidlin, “Soft Switched Asymmetrical Half Bridge DC/DC Converter: Steady State Analysis. Analysis of Switching Process,” Proc. Telescon ’97,. 1997, pp. 177-184.

[A.27] L. Krupskiy, V. Meleshine, A. Nemchinov, “Unified Model of Asymmetrical Half Bridge for Three Important Topological Variations,” Proc. IEEE INTELEC ’99, 1999, pp.8.

[A.28] W. Chen, P. Xu, F.C. Lee, “The Optimization Of Asymmetrical Half Bridge Converter,” Proc. IEEE APEC ’01, 2001, pp. 603-707, vol.2.

[A.29] Bo Yang, “Topology Investigation for Front End DC-DC Power Conversion for Distributed Power System," PhD Dissertation, Dept. ECE., Virginia Tech, 2003.

[A.30] Intel Corporation, NEC Corporation, Dell Computer Corporation, Data General a division of EMC Corporation, Compaq Computer Corporation, Silicon Graphics Inc., and International Business Machines Corporation, “A server system infrastructure (SSI) specification for entry chassis power supplies," 1998.

[A.31] R. Oruganti and F.C. Lee, “Effect of Parasitic Losses on the Performance of Series Resonant Converters,” Proc. IEEE IAS, ’85, 1985.

[A.32] R. Oruganti, J. Yang, and F.C. Lee, “Implementation of Optimal Trajectory Control of Series Resonant Converters,” Proc. IEEE PESC ’87, 1987.

[A.33] A.K.S. Bhat, “Analysis and Design of a Modified Series Resonant Converter,” IEEE Trans. on Power Electronics, 1993, pp. 423-430.

[A.34] J.T. Yang and F.C. Lee, “Computer Aided Design and Analysis of Series Resonant Converters,” Proc. IEEE IAS ’87, 1987.

[A.35] V. Vorperian and S. Cuk, “A Complete DC Analysis of the Series Resonant Converter,” Proc. IEEE PESC’82, 1982.

[A.36] F.S. Tsai, and F.C. Lee, “A Complete DC Characterization of a Constant- Frequency, Clamped-Mode, Series Resonant Converter,” Proc IEEE PESC’88, 1988.

[A.37] R. Oruganti, J. Yang, and F.C. Lee, “State Plane Analysis of Parallel Resonant Converters,” Proc. IEEE PESC ’85, 1985.

[A.38] R. Liu, I. Batarseh, C.Q. Lee, “Comparison of Capacitively and Inductively Coupled Parallel Resonant Converters,” IEEE Trans. On Power Electronics, 1993, pp. 445-454, vol.8, issue 4.

[A.39] M. Emsermann, “An Approximate Steady State and Small Signal Analysis of the Parallel Resonant Converter Running Above Resonance,” Proc. Power Electronics and Variable Speed Drives ’91, 1991, pp. 9-14.

[A.40] Y.G. Kang, A.K. Upadhyay, D. Stephens, “Analysis and Design of a Half Bridge Parallel Resonant Converter Operating Above Resonance,” Proc. IEEE IAS ’98, 1998, pp. 827-836.

[A.41] A.K.S. Bhat, “Analysis and design of LCL-type series resonant converter,” in Proc. IEEE INTELEC, 1990, pp: 172 - 178.

[A.42] B. Yang, F.C. Lee, A.J. Zhang and G. Huang, “LLC Resonant Converter For Front End DC-DC Conversion,” in Proc. IEEE APEC, 2002, vol. 2, pp. 1108-1112.

[A.43] B. Lu, W. Liu, Y. Liang, F. C. Lee, and J. D. van Wyk, “Optimal Design Methodology for LLC Resonant Converter,” in Proc. IEEE APEC, 2006, pp. 533–538.

[A.44] D. Fu; Y. Liu; F.C. Lee, M. Xu, “A Novel Driving Scheme for Synchronous Rectifiers in LLC Resonant Converters,” IEEE Trans. on power electron. vol. 24, iss. 5, pp: 1321 – 1329, May 2009.

[A.45] H. Groot, E. Janssen, R. Pagano, and K. Schetters , “Design of a 1-MHz LLC Resonant Converter Based on a DSP-Driven SOI Half-Bridge Power MOS Module”, IEEE Trans. on power electron., vol. 22, no. 6, pp. 2307-2320, Nov. 2007.

[A.46] X. Xie, J. Zhang, C. Zhao, Z. Zhao, and Z. Qian, “Analysis and Optimization of LLC Resonant Converter with a Novel Over-Current Protection Circuit”, IEEE Trans. on power electron., vol. 22, no. 2, pp. 435-443, Mar, 2007.

[A.47] Y. Gu, Z. Lu, L. Hang, Z. Qian, and G. Huang, “Three-Level LLC Series Resonant DC-

DC Converter,” IEEE Trans. on power electron. vol. 20, no. 4, pp. 781–789, Jul. 2005.

[A.48] K. Yi, G. Moon, “Novel Two-Phase Interleaved LLC Series-Resonant Converter Using a Phase of the Resonant Capacitor,” IEEE Trans. on Ind. Electron., vol. 56, iss. 5, pp: 1815 – 1819, May 2009.

[A.49] On Semiconductor, "NCP1395LLCGEVB: 240W LLC evaluation board," [online], available:http://www.onsemi.com/PowerSolutions/evalBoard.do?id=NCP1395LLCGEVB, Feb, 2006.

[A.50] Texas Instrument, "UCC25600EVM: LLC resonant half bridge converter 300 W evaluation module," [online], available: http://www.ti.com/lit/ug/sluu361/sluu361.pdf, Apr, 2009.

[A.51] STMicroelectronics, "STEVAL-ISA018V1 demonstration board based on resonant half-bridge SMPS for industrial applications," [online], available: http://www.st.com/internet/com/TECHNICAL_RESOURCES/TECHNICAL_LITERATURE/USER_MANUAL/CD00238992.pdf, May, 2010.

[A.52] Power Integration, "Reference design report for a 150 W LLC high-voltage DC-DC resonant converter using hiperLCSTM LCS702HG," [online], available: http://www.powerint. com/sites/default/files/PDFFiles/rdr239.pdf, Sep, 2011.

[A.53] Infineon, "ICE2HS01G: High performance resonant mode controler," [online], available:http://www.infineon.com/dgdl/Design+Guide+for+LLC+Converter+with+ICE2HS01G+05072011.pdf?folderId=db3a304412b407950112b408e8c90004&fileId=db3a304330f68606013103ebd94f3e98, May, 2011.

[A.54] NXP Semiconductors, "TEA1713T: Resonant power supply control IC with PFC," [online], available: http://www.nxp.com/documents/data_sheet/TEA1713T.pdf, Feb, 2011.

[A.55] Fairchild Semiconductor, "FAN7621: PFM controller for half-bridge resonant converters," [online], available: http://www.fairchildsemi.com/ds/FA/FAN7621.pdf, July, 2010.

[A.56] Vishay Siliconix ,” Application notes 833: Switching Analysis of Synchronous Rectifier MOSFETs With Phase-Shifted Full-Bridge Converter and Current Doubler, ”[online], available: http://www.vishay.com/docs/69747/answitch.pdf, Oct, 2007

[A.57] X. Xie, J. Liu, F.N.K. Poon, M. Pong, "A novel high frequency current-driven SR applicable to most switching topologies", IEEE Trans. on Power Electronics, vol. 16, issue. 5, 2001, pp. 635-648.

[A.58] X. Wu, G. Hua, J. Zhang, Z. Qian, "A new current-driven synchronous rectifier for series–parallel resonant (LLC) DC-DC converter", IEEE Trans. on Industrial Electronics, vol. 58, issue. 1, 2011, pp. 289-297.

[A.59] International Rectifier, "IR11672AS: Advanced smart rectifier control IC" [Online]. Available: http://www.irf.com/product-info/datasheets/data/ir11672aspbf.pdf.

[A.60] D. Fu, Y. Liu, F. C. Lee and M. Xu, "A Novel Driving Scheme for Synchronous Rectifiers in LLC Resonant Converters," IEEE Trans. Power Electron., vol. 24, no. 5, pp. 1321–1329, May 2009.

[A.61] Dianbo Fu; Pengju Kong; Shuo Wang; Lee, F.C.; Ming Xu, "Analysis and suppression of conducted EMI emissions for front-end LLC resonant DC/DC converters," Power Electronics Specialists Conference, 2008. PESC 2008. IEEE , vol., no., pp.1144,1150, 15-19 June 2008

[A.62] R. P. Severns, "Topologies for three-element resonant converters," IEEE Trans. Power Electron., vol. 7, no. 1, pp. 89–98, Jan. 1992.

[A.63] I. Batarseh, "Resonant converter topologies with three and four energy storage elements," IEEE Trans. Power Electron., vol. 9, no. 1, pp. 64–73, Jan. 1994.

[A.64] Dianbo Fu; Lee, F.C.; Ya Liu; Ming Xu, "Novel multi-element resonant converters for front-end dc/dc converters," Power Electronics Specialists Conference, 2008. PESC 2008. IEEE , vol., no., pp.250,256, 15-19 June 2008

[A.65] Vicor Corporation, "High-voltage DC distribution is key to increased systemefficiency and renewable-energy opportunities, " [online], available: http://www.vicr.com/documents/whitepapers/wp-High-voltage-DC-istribution.pdf

[A.66] IBM, "A New Redundancy Strategy for High-Availability Power System," [online], available: http://www-03.ibm.com/procurement/proweb.nsf/7a84535a0acd580885256b3f000e250a/3a70bbaee228048085257ac20066b558/$FILE/8-A%20New%20Redundancy%20Strategy%20for%20High-Availability%20Power%20Systems%20(Covi).pdf

[A.67] Vicor Corporation, "From 48 V direct to Intel VR12.0: Saving 'Big Data' $500,000 per datacenter, per year, "[online]

[A.68] C. Prasantanakorn, "Current sharing method for resonant DC-DC transformers," Master thesis in Virginia Tech, 2011.

[A.69] U. K. Mishra, P. Parikh, and Y. Wu, “AlGaN/GaN HEMTs – an overview of device operation and applications,” Proceedings of the IEEE, vol. 90, no. 6, pp.1022-1031, Jun. 2002.

[A.70] M. A. Khan, G. Simin, S. G. Pytel, A. Monti, E. Santi, and J. L. Hudgins, “New developments in gallium nitride and the impact on power electronics,” in proc. IEEE Power Electronics Specialists Conference, 2005, pp. 15-26.

[A.71] N. Kaminski, “State of the art and the future of wide band-gap devices,” in Proc. IEEE Power Electronics and Applications, 2009, pp. 1–9.

[A.72] Y. Wu, M. J. Mitos, M. Moore, and S. Heikman, “A 97.8% Efficient GaN HEMT boost converter with 300W output power at 1 MHz,” IEEE Electron Device Letters, vol. 29, no. 8, pp. 824–826, Aug. 2008.

[A.73] W. Saito, T. Nitta, Y. Kakiuchi, Y. Saito, K. Tsuda, I. Omura, and M. Yamaguchi, “A 120-W boost converter operation using a high-voltage GaN-HEMT,”IEEE Electron Device Letters, vol. 29, no. 1, pp. 8–10, Jan. 2008.

[A.74] W. Saito, T. Domon, I. Omura, T. Nitta, Y. Kakiuchi, K. Tsuda, and M. Yamaguchi, “Demonstration of resonant inverter circuit for electrodeless fluorescent lamps using high voltage GaN-HEMT,” in proc. IEEE Power Electronics Specialists Conference, 2008, pp. 3324-3329.

[A.75] W. Chen, K. Wong, and K. J. Chen, “Single-chip boost converter using monolithically integrated AlGaN/GaN lateral field-effect rectifier and normally off HEMT, ” IEEE Electron Device Letters, vol. 30, no. 5, pp. 430–432, May. 2009.

[A.76] D. Costinett, H. Nguyen; R. Zane, and D. Maksimovic, “GaN-FET based dual active bridge DC-DC converter,” in proc. IEEE Applied Power Electronics Conference, 2010, pp 1425-1432.

[A.77] M. J. Scott, K. Zou, J. Wang, C. Chen, M. Su, and L. Chen, “A Gallium-Nitride switched-capacitor circuit using synchronous rectification," in proc. IEEE Energy Conversion Congress and Exposition, 2011, pp 2501-2505.

[A.78] B. Hughes, Y. Y. Yoon, D. M. Zehnder, and K. S. Boutros, " A 95% efficient normally-off GaN-on-Si HEMT hybrid-IC boost converter with 425-W output power at 1MHz," in proc. IEEE Compound Semiconductor Integrated Circuit Symposium, 2011, pp 1-3.

[A.79] B. Hughes, J. Lazar, S. Hulsey, D. Zehnder, D. Matic, and K. Boutros, "GaN HFET Switching Characteristics at 350V-20A and Synchronous Boost Converter Performance at 1MHz," in proc.IEEE Applied Power Electronics Conference, 2012, pp 2506-2508.

[A.80] J. Delaine, P. Olivier, D. Frey, and K. Guepratte, "High frequency DC-DC converter using GaN device," in proc. IEEE Applied Power Electronics Conference, 2012, pp 1754-1761.

B.Synthesis of Multi-Element Resonant Converters

[B.1] V. Vorperian ,etc , "A complete DC analysis of the series resonant converter, " Proc of PESC, 1982, page 85-100

[B.2] Steigerwald, R.L, "A comparison of half-bridge resonant converter topologies," Trans of IEEE, Vol 3, issue 2, 1988, page 174-182

[B.3] J. Chen, etc, "Load Independent AC/DC Power Supply for Higher Frequencies with Sine-Wave Output," IEEE Trans. Indus Application, Vol IA-19, Issue 2, 1983, page 223-227

[B.4] Bo Yang, "Topology Investigation for Front End DC-DC Power Conversion for Distributed Power System," PhD Dissertation, Dept. ECE. Virginia Tech, 2003.

[B.5] G. Huang, A. J. Zhang, and Y. Gu, "LLC Series Resonant DC-to-DC Converter," U.S. Patent 6 344 979, Feb. 5, 2002.

[B.6] B. Yang, F. C. Lee, and M. Cancannon, "Over current protection methods for LLC resonant converter," in Proc. IEEE APEC, 2003, pp. 605–609.

[B.7] B. Yang, F. C. Lee, A. J. Zhang, and G. Huang, "LLC resonant converter for front end dc-dc conversion," in Proc. IEEE APEC, 2002, pp. 1108–1112.

[B.8] B. Yang, Y. Ren, and F. C. Lee, “Integrated magnetic for LLC resonant converter,” in Proc. IEEE APEC, 2002, pp. 346–351.

[B.9] Bo Yang, “Topology Investigation for Front End DC-DC Power Conversion for Distributed Power System," PhD Dissertation, Dept. ECE., Virginia Tech, 2003.

[B.10] Y. Gu, Z. Lu, L. Hang, Z. Qian, and G. Huang, “Three-level LLC series resonant DC-DC converter,” IEEE Trans. Power Electron., vol. 20, no. 4, pp. 781–789, Jul. 2005.

[B.11] R. P. Severns, “Topologies for three-element resonant converters,” IEEE Trans. Power Electron., vol. 7, no. 1, pp. 89–98, Jan. 1992.

[B.12] Daocheng Huang; Dianbo Fu; Lee, F.C.; , "High switching frequency, high efficiency CLL resonant converter with synchronous rectifier," ECCE 2009. IEEE , vol., no., pp.804-809, 20-24 Sept. 2009

[B.13] Weiyi Feng; Lee, F.C., "Optimal Trajectory Control of LLC Resonant Converters for Soft Start-Up," Power Electronics, IEEE Transactions on , vol.29, no.3, pp.1461,1468, March 2014

[B.14] Dianbo Fu; Lee, F.C.; Ya Liu; Ming Xu; , "Novel multi-element resonant converters for front-end dc/dc converters," PESC 2008. IEEE , vol., no., pp.250-256, 15-19 June 2008

[B.15] I. Batarseh, “Resonant converter topologies with three and four energy storage elements,” IEEE Trans. Power Electron., vol. 9, no. 1, pp. 64–73,Jan. 1994.

[B.16] Steigerwald, R.L.; , "A comparison of half-bridge resonant converter topologies," Power Electronics, IEEE Transactions on , vol.3, no.2, pp.174-182, Apr 1988

[B.17] Dianbo Fu; Ya Liu; Lee, F.C.; Ming Xu; , "A Novel Driving Scheme for Synchronous Rectifiers in LLC Resonant Converters," Power Electronics, IEEE Transactions on , vol.24, no.5, pp.1321-1329, May 2009

[B.18] Feng, Weiyi; Huang, Daocheng; Mattavelli, Paolo; Fu, Dianbo; Lee, Fred C.; , "Digital implementation of driving scheme for synchronous rectification in LLC resonant converter," ECCE 2010, vol., no., pp.256-263, 12-16 Sept. 2010

C. Evaluation System for Resonant Converters

[C.1] E. X. Yang, F. C. Lee, and M. M. Jovanovic, "Small-signal modeling of LCC resonant converter," in Proc. IEEE-PESC'92, pp.167-178, 1992.

[C.2] B. Yang and F. C. Lee, "Small-signal analysis for LLC resonant converter," in CPES Seminar, 2003, S7.3, pp.144-149, 2003.

[C.3] H.de. Groot, E. Janssen, R. Pagano, K. Schetters, "Design of a 1-MHz LLC resonant converter based on a DSP-driven SOI half-bridge power MOS module," IEEE Trans. on Power Electronics, vol.22, Issue.6, pp. 2307 - 2320, 2007.

[C.4] L. Hang; Z. Lu; Z. Qian, "Research of digital control strategy for multi-resonant LLC converter," in Proc. IEEE Industrial Electronics, 2007, pp. 479 - 484, 2007.

[C.5] J. Jang, M. Joung, B, Choi, and H. Kim, "Dynamic analysis and control design of optocoupler isolated LLC series resonant converters with wide input and load variations," in Proc. IEEE-ECCE'09, pp.758-765, 2009

[C.6] J. Jang, M. Joung, S. Choi, Y. Choi, and B. Choi, "Current mode control for LLC series resonant DC-to-DC converters," in Proc. IEEE-APEC'11, pp.21-27, 2011.

[C.7] R. Oruganti, and F.C. Lee, "Resonant power processors, Part I- state plane analysis", IEEE Trans. on Industry Application, vol.IA-21, Issue 6, pp. 1453-1460, 1985.

[C.8] R. Oruganti, and F.C. Lee, "Resonant power processors, Part II- methods of control", IEEE Trans. on Industry Application, vol.IA-21, Issue 6, pp. 1461-1471, 1985.

[C.9] R. Oruganti, "State-Plane Analysis of Resonant Converters," PhD dissertation in Virginia Tech, 1987.

[C.10] R. Oruganti, J.J. Yang, and F.C. Lee, "Implementation of optimal trajectory control or series resonant converter", IEEE Trans. on Power Electronics, vol. 3, Issue 3, pp. 318-327, 1988.

D. Integrated System Design for High Current Application

[D.1] G. Huang, A. J. Zhang, and Y. Gu, "LLC Series Resonant DC-to-DC Converter," U.S.

Patent 6 344 979, Feb. 5, 2002.

[D.2] B. Yang, F. C. Lee, A. J. Zhang, and G. Huang, “LLC resonant converter for front end dc/dc conversion,” in Proc. IEEE APEC 2002, pp. 1108–1112.

[D.3] B. Yang, Y. Ren, and F. C. Lee, “Integrated magnetic for LLC resonant converter,” in Proc. IEEE APEC, 2002, pp. 346–351.

[D.4] Bo Yang, “Topology Investigation for Front End DC/DC Power Conversion for Distributed Power System," PhD Dissertation, Dept. ECE., Virginia Tech, 2003.

[D.5] Y. Gu, Z. Lu, L. Hang, Z. Qian, and G. Huang, “Three-level LLC series resonant DC/DC converter,” IEEE Trans. Power Electron., vol. 20, no. 4, pp. 781–789, Jul. 2005.

[D.6] D. Fu, Y. Liu, F. C. Lee and M. Xu, “A Novel Driving Scheme for Synchronous Rectifiers in LLC Resonant Converters,” IEEE Trans. Power Electron., vol. 24, no. 5, pp. 1321–1329, May. 2009.

[D.7] D. Huang; D. Fu; F.C. Lee and P. Kong; , "High-Frequency High-Efficiency CLL Resonant Converters With Synchronous Rectifiers," , IEEE Trans. Industrial Electronics , vol.58, no.8, pp.3461-3470, Aug. 2011

[D.8] D. Huang; F.C. Le; D. Fu; , "Classification and selection methodology for multi-element resonant converters," in Proc. IEEE APEC 2011, pp.558-565, 6-11 March 2011

[D.9] “GaNpowIR – An Introduction”, IRF.com. Feb 2010

[D.10] International Recitifier. “iP2010PbF- High Frequency GaN-Based Integrated Power Stage”. www.IRF.com

[D.11] Efficient Power Conversion. “EPC1015- Enhancement Mode Power Transistor”. www.EPC.com

[D.12] Prieto, R.; Cobos, J.A.; Garcia, O.; Alou, P.; Uceda, J., "Taking into account all the parasitic effects in the design of magnetic components," Applied Power Electronics Conference and Exposition, 1998. APEC '98. Conference Proceedings 1998., Thirteenth Annual , vol.1, no., pp.400,406 vol.1, 15-19 Feb 1998

[D.13] Dai, N.; Lee, F. C., "Edge effect analysis in a high-frequency transformer," Power Electronics Specialists Conference, PESC '94 Record., 25th Annual IEEE , vol., no., pp.850,855 vol.2, 20-25 Jun 1994

[D.14] Edward Herbert, “Design and Application of Matrix Transformers and Symmetrical Converters,” a tutorial presented at the High Frequency Power Conversion Conference '90, Santa Clara, CA, May 11, 1990.

[D.15] Reusch, D.; Lee, F.C.; , "High frequency bus converter with low loss integrated matrix transformer," Proc. IEEE APEC 2012, pp.1392-1397, 5-9 Feb. 2012

[D.16] Chao Yan; Fan Li; Jianhong Zeng; Teng Liu; Jianping Ying; , "A Novel Transformer Structure for High power, High Frequency converter," PESC 2007. IEEE , vol., no., pp.214-218, 17-21 June 2007

[D.17] Fu, D.; Lee, F.C.; Shuo Wang; , "Investigation on transformer design of high frequency high efficiency dc-dc converters," Proc. IEEE APEC 2010, pp.940-947, 21-25 Feb. 2010

[D.18] Dianbo Fu, PhD Dissertation, “Topology Investigation and System Optimization of Resonant Converters”

[D.19] Ferroxcube Data Handbook 2009

[D.20] Huang, X.; Li, Q.; Liu, Z.; Lee, F.C., "Analytical loss model of high voltage GaN HEMT in cascode configuration," Power Electronics, IEEE Transactions on , vol.PP, no.99

E. Passive Integration of Multi-element Resonant Converters

[E.1] Dianbo Fu; Lee, F.C.; Ya Liu; Ming Xu; , "Novel multi-element resonant converters for front-end dc/dc converters," PESC 2008. IEEE , vol., no., pp.250-256, 15-19 June 2008

[E.2] Daocheng Huang; Lee, F.C.; Dianbo Fu; , "Classification and selection methodology for multi-element resonant converters," APEC 2011 IEEE , vol., no., pp.558-565, 6-11 March 2011

[E.3] B. Yang, R. Chen and F. C. Lee “ Integrated Magnetic for LLC Resonant Converter,” Applied Power Electronics Conference and Exposition, APEC‘OZ, vol. 1, pp. 346 - 351.

[E.4] R. Chen, J. T. Strydom and J. D. van Wyk, “Design of Planar Integrated Passive Module for Zero-Voltage- Switched Asymmetrical Half-Bridge PWM Converter,” Industry

Applications, IEEE Transactions, vol. 39, No. 6, pp. 1648-1655

[E.5] R. Chen, J. T. Strydom and J. D. van Wyk, “Second Order Approximation Lumped Parameter Model for Planar Integrated L-L-C-T Module,” Industry Application Conference, IAS’02, vol 4, pp. 2419-2424.

[E.6] J. T. Strydomm, and J. D. van Wyk, “Electromagnetic Design Optimization of Planar Integrated Power Passive Modules,” Power Electronics Specialists Conference, PESC’02, vol. 2, pp. 573-578.

[E.7] W. Liu, J. D. van Wyk and W. G. Odendaal, “Design and Evaluation of Integrated Electromagnetic Power Passives with Vertical Surface Interconnections,” Applied Power Electronics Conference and Exposition, APEC ’04, vol. 2, pp. 958-963.

[E.8] L. Zhao, “Generalized Frequency Plane Model of Integrated Electromagnetic Power Passives,” Ph.D. Dissertation, Virginia Polytechnic Institute and State University, 2004.

[E.9] W. Liu, J. D. van Wyk and W. G. Odendaal, “High Density Integrated Electromagnetic Power Passives with Vertical Interconnect and Stacked Structure,” Power Electronics Specialist, PESC’03, vol. 1, pp.442-447.

[E.10] Erickson, R.W.; Maksimovic, D.; , "A multiple-winding magnetics model having directly measurable parameters," PESC 98, vol.2, no., pp.1472-1478 vol.2, 17-22 May 1998

[E.11] Mogilevsky, B.M.; Shirn, G.A.; , "Accelerated life tests of ceramic capacitors," Components, Hybrids, and Manufacturing Technology, IEEE Transactions on , vol.11, no.4, pp.351-357, Dec 1988

[E.12] Wenduo Liu; Dirker, J.; van Wyk, J.D., "Power Density Improvement in Integrated Electromagnetic Passive Modules With Embedded Heat Extractors," Power Electronics, IEEE Transactions on , vol.23, no.6, pp.3142,3150, Nov. 2008

[E.13] Mogilevski, B.M.; Shirn, G.A.; , "Accelerated life tests of ceramic capacitors," Electronics Components Conference, 1988., Proceedings of the 38th , vol., no., pp.362-370, 9-11 May 1988